Ab Initio Molecular Dynamics

A Virtual Laboratory

by

Milad Hobbi Mobarhan

Thesis

for the degree of

Master of Science

Faculty of Mathematics and Natural Sciences
University of Oslo

June 2014

Abstract

In this thesis, we perform ab initio molecular dynamics (MD) simulations at the Hartree-Fock level, where the forces are computed on-the-fly using the Born-Oppenheimer approximation. The theory behind the Hartree-Fock method is discussed in detail and an implementation of this method based on Gaussian basis functions is explained. We also demonstrate how to calculate the analytic energy derivatives needed for obtaining the forces acting on the nuclei. Hartree-Fock calculations on the ground state energy, dipole moment, ionization potential, and population analysis are done for H_2, N_2, FH, CO, NH_3, H_2O, and CH_4. These results are in perfect agreement with the literature. Ab initio MD calculations with different Gaussian basis sets, are performed on the diatomic systems H_2, N_2, F_2, FH, and CO, for equilibrium bond length and vibration frequency analysis. Finally, a study on the reaction dynamics of the nucleophilic substitution reaction $H^- + CH_4 \longrightarrow CH_4 + H^-$ is done, illustrating the importance of the initial vibrational energy of the methane molecule for the reaction to occur.

To my parents, sister and her husband.

For their endless love, support and encouragement.

Acknowledgements

I would like to thank my main supervisor, Morten Hjorth-Jensen, and second supervisor, Anders Malthe-Sørenssen, for everything they have taught me, and for always being so motivating. I appreciate the great amount of freedom they gave me during the course of this project. They have also given me valuable and constructive suggestions during the planning and development of this thesis, and at same time let me explore the aspects of my thesis that interested me the most.

In my daily work, I have been blessed with a friendly group of fellow students. Svenn-Arne Dragly and Henrik Mathias Eiding, whom I shared my office with, deserve a special thanks for close cooperation and many lively and encouraging discussions. I am lucky to have made such great friends.

Additionally, I would like to thank everybody at the Computational Physics research group, especially Jørgen Høgberget, Sigve Bøe Skattum and Anders Hafreager for always being supportive. Thank you so much for everything!

Collaboration Details

All code developed for this thesis have been written from scratch by the author. The Hartree-Fock code has, however, been developed in parallel with two similar codes, written by Dragly [1] and Eiding [2]. There has been close collaboration during the development of these codes. Therefore, the overall structure of the codes, as well as some functions, have ended up to be quite similar.

Milad H. Mobarhan
Oslo, June 2014

Contents

List of Symbols

$\mathcal{A}$ Antisymmetrizing operator 22, 25, 26, 182, 183

φ Atomic orbital 15, 17, 35–38, 40, 41, 43–46, 59, 148

$\mathcal{J}$ Coulomb operator 27, 28, 31, 34, 37

m_e Electron mass 10, 11, 13, 82, 83, 86, 88, 181, 182

$\mathcal{K}$ Exchange operator 27, 28, 31, 34, 37

$\mathcal{F}$ Fock operator 30, 34, 36, 40, 41, 90, 92

$\mathcal{H}$ Hamiltonian 10–13, 17–19, 24–26, 47, 82–87, 89–92, 95, 182, 183

$\mathcal{L}$ Lagrangian 27, 28, 90–92

ϕ Molecular orbital 15, 17–23, 32–37, 39, 40, 43–46, 55, 147

$\hbar$ One-particle kinetic and nuclear attraction operator 18, 19, 24–28, 31, 33, 34, 36, 37, 40

ξ Spin function 21, 23

β Spin down function 20, 21, 32–34, 39–41, 43, 44, 153

ψ Spin orbital 21–23, 25–34, 39, 43–45, 90, 143, 182

α Spin up function 20, 21, 32–34, 39–41, 43, 44, 153

$\mathcal{g}$ Two-particle electron interaction operator 24–28, 36

Ψ Total wave function 10–13, 20, 83–89, 91, 95

Ψ_{H} Hartree wave function 22, 25, 26, 182, 183

Φ_{H} Spatial Hartree wave function 18, 19

χ Nuclear wave function 83–86, 88, 89

Ψ_{SD} Slater determinant wave function 21–23, 25, 26, 90, 92

Chapter 1

Introduction

Classical molecular dynamics (MD) is a well-established tool that highlights the dynamical nature of molecular interactions. Its applications range from biological folding processes [3] to material formation mechanisms [4]. At this level of theory, the evolution of the system is followed by solving the classical equations of motion for all the particles in the system. The interatomic interactions are described by a predefined potential based on empirical data and/or independent electronic structure calculations. The potential is represented by a specific functional form and is typically broken up into two-body and many-body contributions, long-range and short-range terms, electrostatic and non-electrostatic interactions, etc. [5]. Predefined potentials lead to tremendous computational simplifications, but finding them is a nontrivial task. This is due to the large variety of interatomic interactions that exist between different atoms and molecules. These interactions are determined by the electronic structure of the system.

An alternative to traditional MD is to perform quantum mechanical calculations to determine the interatomic interactions. In this approach the forces acting on the nuclei are computed on-the-fly using electronic structure calculations, as the atomic trajectories are generated. Thus, the electronic degrees of freedom are no longer represented by fixed interaction potentials, but are active during the dynamical simulations. The family of methods based on this approach are referred to as ab initio MD[1]. This extension of classical MD makes it possible to handle complex systems in which the electronic structure changes drastically during the simulation. These systems are generally very difficult to model by predefined potentials.

By basing computations on first principles quantum mechanics, it is possible to overcome the lack of experimental data to carry out accurate predictions with atomistic resolution. This would otherwise be impossible. Furthermore, quantum mechanics provides the fundamental information required to describe quantum effects, electronically excited states, as well as reaction paths and barrier heights involved in chemical reactions processes.

Putting MD onto an ab initio grounds implies that the approximation is shifted from the level of predefining an interaction potential, to the level of selecting a method

[1]Other common names are for instance first principles, on-the-fly, direct, extended Lagrangian, or just quantum molecular dynamics amongst others [5].

for solving the Schrödinger equation. It is a matter of course that a price has to be paid for performing calculations at a more fundamental level. The drawback in ab initio simulations is the limitations in length and time scale compared to what is doable with traditional methods. It is therefore necessary to have efficient theoretical and computational methods for being able to bridge the gap between quantum mechanical calculations and MD simulations.

An obvious candidate for electronic structure calculations in ab initio MD, is the Hartree-Fock method. Although this method is inadequate for accurate quantum mechanical studies, it is one of the few methods that can be applied to large molecular systems. Furthermore, the Hartree-Fock theory is a central starting point for more sophisticated and accurate many-body methods, such as Møller-Plesset perturbation theory and coupled-cluster methods [2, 6, 7].

The aim of this thesis is to implement an efficient and modular many-body quantum mechanics code. Our intention is to use this code in ab initio MD calculations and/or parameterization of predefined potentials. In particular, the focus is on the Hartree-Fock method. The implementation of this method is based on Gaussian basis functions for efficient computation of many-center molecular integrals [7]. Although this thesis focuses on the transition from quantum mechanics to MD, the code is written in a general way such that it can easily be used for pre-calculations in pure quantum mechanical studies. A possible application is to perform Hartree-Fock calculations to find optimal single-particle wave functions for quantum Monte-Carlo studies [8].

Thesis Structure

The thesis is structured in the following way:

- The first part, Chapters 2 to 5, presents the underlying theoretical models. In particular, Chapter 2 introduces the basic concepts of quantum mechanics and many-body theory with focus on the Hartree-Fock method. The reader is assumed to have a basic understanding of the most fundamental features of quantum mechanics and the Dirac notation [9]. Chapter 3 gives an introduction on the most used basis sets in many-body calculations, with focus on Gaussian basis sets. In Chapter 4, we present the techniques, provided by the McMurchie-Davidson scheme [7], for efficient evaluation of one- and two-electron molecular integrals. Finally in Chapter 5, the transition from quantum mechanics to MD is discussed. This chapter includes a derivation of classical MD, starting from the time-dependent Schrödinger equation.

- In the second part, Chapters 6 to 8, the implementation of the codes is presented, in addition to tools and software used during the development. The reader is assumed to have some background in programming and to be familiar with the programming languages C++ and Python.

- In the final part, the results from our calculations are presented. In Chapter 9, we present the Hartree-Fock results from calculations on various molecules, used to benchmark the code. These results include the ground state energy, dipole moments, ionization potentials, and population analysis. In this chapter,

some graphical models, obtained from Hartree-Fock calculations, are also discussed. In Chapter 10, the results from MD simulations are presented. These include equilibrium bond length calculations and vibrational frequency analysis, in addition to studies on dynamics of the nucleophilic substitution reaction $H^- + CH_4 \longrightarrow CH_4 + H^-$.

- Chapter 11 concludes this thesis and provides suggestions for possible extensions.

Part I

Theory

Chapter 2

Hartree-Fock Molecular Orbital Theory

In molecules, electrons are shared among the atoms to form chemical bonds. This determines the molecular structures. But electrons are quantum mechanical particles and must be treated by the laws of quantum mechanics. Therefore, in order to describe molecular structures, a theory where the quantum mechanical properties of the electrons are incorporated, is needed. Molecular orbital theory is one such theory. The fundamental idea is that the electrons are no longer deterministically given defined coordinates. Their position is described according to a probability distribution function, defining all the possible positions. Moreover, the electrons are not assigned to individual bonds between atoms. They are "smeared out" across the molecule.

The basis of molecular orbital theory is the Hartree-Fock method, which is the cornerstone of electronic structure theory [7]. The importance of this method cannot be overemphasized in quantum chemistry, and investigating it in detail will provide a good understanding of the many-electron problem. Hartree-Fock is also a central starting point for more sophisticated and accurate methods, such as the non-variational Møller-Plesset and coupled-cluster methods [2]. Although the Hartree-Fock method by itself is inadequate for accurate studies, it is still one of the few methods that can be applied to large molecular systems. Therefore, it is a natural method to use in ab initio molecular dynamics (MD) schemes.

In this chapter we will first give a brief overview of the fundamental features of quantum mechanics. We present how to handle the many-electron problem, using the Hartree method and later the Hartree-Fock method. The fundamental equations in Hartree-Fock theory, will be derived and discussed. In the final part of this chapter, the application on closed and open shell systems is discussed, using the restricted and unrestricted Hartree-Fock method.

The first part of this chapter is heavily influenced by Chapter 4 of Ref. [10]. The derivation of the Hartree-Fock equation is done in line with the derivation given in Chapter 4 of Ref. [11], while the discussion of restricted Hartree-Fock (RHF) and unrestricted Hartree-Fock (UHF) is inspired by Chapter 3 of Ref. [6]. For a more detailed description of quantum theory, the reader is referred to standard texts such as Refs. [9, 12].

2.1 Key Features of Quantum Mechanics

The foundations of quantum mechanics are the postulates. These are theoretical principles based on experimental observations which the applications of quantum mechanics are built on [10]. The fundamental idea in quantum theory is that any (physical) system can be described by a wave function, Ψ. Any measurable property of the system can be obtained by letting an appropriate operator act on the wave function. Mathematically this can be written as

$$\mathcal{O}\Psi = o\Psi, \tag{2.1}$$

where $\mathcal{O}$ is an operator and o is a scalar value for some property of the system. This equation is nothing but an eigenvalue problem, if we think of Ψ as an N-element column vector and $\mathcal{O}$ as an $N \times N$ square matrix. This analogy hints that linear algebra plays a central role in quantum mechanics. In fact, linear algebra is the mathematical language of quantum mechanics.

The physical interpretation of the wave function is as follows. The product with its complex conjugate (i.e. $|\Psi^*\Psi|$) represents the probability density for a system to be found within some region of a multi-dimensional space. The probability interpretation leads to the requirement that the wave function has to be normalizable, i.e. the integral of $|\Psi^*\Psi|$ over all space must be 1. Without this, the probability interpretation would not be possible. Additionally, Ψ has to be single valued and continuous [9].

As discussed in Ref. [10], the best description of Ψ at this point is that it is an oracle; when queried with questions by an operator, it returns answers. The exact form of the wave function is often not known, but there are, fortunately, several theories on how to approximate it for a many-body system. One such theory is Hartree-Fock.

2.1.1 Hamiltonian Operator

Associated with each measurable parameter in a system, is a quantum mechanical operator. The Hamiltonian operator, $\mathcal{H}$, is the most central one and returns the energy, E, of the system as an eigenvalue, when Eq. (2.1) holds;

$$\mathcal{H}\Psi = E\Psi. \tag{2.2}$$

This equation is the time-independent or stationary Schrödinger equation [12].

Hamiltonian for a system consisting of N_e electrons and N_n nuclei with charges Z_n reads

$$\begin{aligned}\mathcal{H} = &-\sum_{i=1}^{N_e}\frac{\hbar^2}{2m_e}\nabla_i^2 - \sum_{n=1}^{N_n}\frac{\hbar^2}{2M_n}\nabla_n^2 + \frac{1}{4\pi\epsilon_0}\frac{1}{2}\sum_{\substack{i,j=1\\ i\neq j}}^{N_e}\frac{e^2}{|\mathbf{r}_i - \mathbf{r}_j|} \\ &- \frac{1}{4\pi\epsilon_0}\sum_{n=1}^{N_n}\sum_{i=1}^{N_e}\frac{Z_n e^2}{|\mathbf{r}_i - \mathbf{R}_n|} - \frac{1}{4\pi\epsilon_0}\frac{1}{2}\sum_{\substack{n,m=1\\ n\neq m}}^{N_n}\frac{Z_n Z_m e^2}{|\mathbf{R}_n - \mathbf{R}_m|}.\end{aligned} \tag{2.3}$$

The indices i and j refer to the electrons, while n and m refer to the nuclei, m_e is the electron mass, and M_n is the mass of nucleus n. The first two terms represent the kinetic energy of the electrons and the nuclei, while the third and fourth terms represent the Coulomb repulsion between the electrons, and the Coulomb attraction between the electrons and nuclei, respectively. Finally, the last term contains the Coulomb repulsion between the nuclei. Note that this Hamiltonian depends on the set of positions $\{\mathbf{r}_i\}$ and $\{\mathbf{R}_n\}$ of the electrons and nuclei, respectively. Thus, we expect the wave function of the system to also depend on the positions of electrons and nuclei.

For a molecular system, the eigenvalue problem in Eq. (2.2) can in general have many solutions Ψ_i, each with an associated eigenvalue E_i. These solutions will form a complete basis, which we can, without loss of generality, assume to be orthonormal. Mathematically this means that

$$\int \Psi_i^* \Psi_j \, \mathrm{d}\mathbf{r} = \delta_{i,j}, \tag{2.4}$$

where the integral is taken over a generalized $3(N_e + N_n)-$dimensional volume element $\mathrm{d}\mathbf{r}$. Note that $\mathbf{r} = \mathbf{r}(\{\mathbf{r}_i\}, \{\mathbf{R}_n\})$, and must not be confused with the electronic coordinates $\mathbf{r}_i$.

The energy E_j associated with Ψ_j is found by considering Eq. (2.2) for a specific Ψ_j. By multiplying a general Ψ_i^* from left and integrate over the generalized space, we get

$$\int \Psi_i^* \mathcal{H} \Psi_j \, \mathrm{d}\mathbf{r} = E_j \delta_{i,j}. \tag{2.5}$$

When the wave function Ψ_j is known, we can find the associated eigenvalue E_j just by solving the integral on the left hand side with $i = j$. This recipe is quite straightforward, but solving the integral in Eq. (2.5) can be quite demanding.

2.1.2 The Variational Principle

An important element in several many-body theories is the variational principle [12], which will be used frequently in the rest of this thesis. A detailed description of this concept will therefore be given in the following.

We consider Ψ to be some appropriate wave function for a system, and define an arbitrary but complete set of orthonormal wave functions Ψ_i, which satisfy Eq. (2.2). Using this complete set, Ψ can be expressed as a linear combination, given by

$$\Psi = \sum_i c_i \Psi_i, \tag{2.6}$$

where c_i are unknown coefficients, which define how the basis functions combine to form Ψ. The normality of Ψ imposes a constraint on the coefficients, which is easily derived from

$$
\begin{aligned}
1 &= \int |\Psi^* \Psi| \, \mathrm{d}\mathbf{r} \\
&= \int \sum_i c_i^* \Psi_i^* \sum_j c_j \Psi_j \, \mathrm{d}\mathbf{r} \\
&= \sum_{i,j} c_i^* c_j \int \Psi_i^* \Psi_j \, \mathrm{d}\mathbf{r} \\
&= \sum_{i,j} c_i^* c_j \delta_{i,j} \\
&= \sum_i |c_i^* c_i|. \qquad (2.7)
\end{aligned}
$$

The element $|c_i^* c_i|$ is the probability that a measurement of the energy would yield the value E_i. It is therefore clear that the sum of these probabilities should be 1 as shown in Eq. (2.7). The interpretation of the coefficients becomes more clear by inserting Eq. (2.6) into Eq. (2.5), leading to

$$
\begin{aligned}
\int \Psi^* \mathcal{H} \Psi \, \mathrm{d}\mathbf{r} &= \int \left(\sum_i c_i^* \Psi_i^* \right) \mathcal{H} \left(\sum_j c_j \Psi_j \right) \mathrm{d}\mathbf{r} \\
&= \sum_{i,j} c_i^* c_j \int \Psi_i^* \mathcal{H} \Psi_j \, \mathrm{d}\mathbf{r} \\
&= \sum_{i,j} c_i^* c_j E_j \delta_{i,j} \\
&= \sum_i |c_i^* c_i| E_i. \qquad (2.8)
\end{aligned}
$$

Thus, the energy associated with the wave function Ψ can be determined from all the coefficients c_i and the eigenvalues E_i.

Now, we assume E_0 to be the lowest value in the set of energies. By combining the results from Eqs. (2.7) and (2.8), we can write

$$
\int \Psi^* \mathcal{H} \Psi \, \mathrm{d}\mathbf{r} - E_0 \int |\Psi^* \Psi| \, \mathrm{d}\mathbf{r} = \sum_i |c_i^* c_i| (E_i - E_0). \qquad (2.9)
$$

Since $|c_i^* c_i|$ is always real and positive and $(E_i - E_0) \geq 0$ by definition, the right hand side will always be greater or equal to zero. This means that we have

$$
\frac{\int \Psi^* \mathcal{H} \Psi \, \mathrm{d}\mathbf{r}}{\int |\Psi^* \Psi| \, \mathrm{d}\mathbf{r}} \geq E_0. \qquad (2.10)
$$

The last equation is the variational principle in mathematical notation. This principle gives us a way to judge the quality of an approximated wave function, which not

necessarily needs to be represented by a linear combination. Any variation in the trial wave function that lowers the approximated energy, is necessarily making the approximated energy closer to the exact answer, and the trial wave function closer to the true ground state wave function.

2.1.3 The Born-Oppenheimer Approximation

The molecular Hamiltonian, given in Eq. (2.3), contains of pairwise attraction and repulsion terms. This implies that no particle is moving independently of all the others. Because of this interdependency, the stationary Schrödinger equation may be quite demanding to solve. This problem can, however, be alleviated by the Born-Oppenheimer approximation [10].

The Born-Oppenheimer approximation consists of separating the degrees of freedom of the nuclei, from those of the electrons. This approximation is justified in most cases because of the high nuclear to electron mass ratio. It is therefore intuitively clear that the nuclei move much more slowly than the electrons and can be considered as fixed. This leads to a Hamiltonian for the electrons in the field generated by a static configuration of nuclei, and a separate equation for the nuclei in which the electronic energy enters as a potential.

We are mainly interested in the Hamiltonian for the electrons, which reads

$$\mathcal{H}_{el} = -\sum_{i=1}^{N_e} \frac{\hbar^2}{2m_e}\nabla_i^2 + \frac{1}{4\pi\epsilon_0}\frac{1}{2}\sum_{\substack{i,j=1\\ i\neq j}}^{N_e} \frac{e^2}{|\mathbf{r}_i - \mathbf{r}_j|} - \frac{1}{4\pi\epsilon_0}\sum_{n=1}^{N_n}\sum_{i=1}^{N_e} \frac{Z_n e^2}{|\mathbf{r}_i - \mathbf{R}_n|}. \tag{2.11}$$

Thus, the (stationary) electronic Schrödinger equation can be expressed as

$$\left(\mathcal{H}_{el} + V_N\right)\Psi_{el}\left(\{\mathbf{r}_i\};\{\mathbf{R}_n\}\right) = E_{el}\Psi_{el}\left(\{\mathbf{r}_i\};\{\mathbf{R}_n\}\right), \tag{2.12}$$

where V_N is the nuclear-nuclear potential energy term in Eq. (2.3). The subscript "el" emphasizes the use of the Born-Oppenheimer approximation. Note that the electronic wave function is a function of electronic degrees of freedom, but depends parametrically on the nuclear coordinates. This is the reason for using a semicolon instead of a comma in the variable list of Ψ_{el}. Moreover, V_N is constant for a given set of fixed nuclear coordinates. This means that we can solve Eq. (2.12) without including V_N, since the wave function is invariant with respect to the appearance of constant terms in the Hamiltonian [9].

The Born-Oppenheimer approximation is the foundation of the important concepts of potential energy surface (PES). The concept reflects the relationship between the energy of a molecule (or a collection of molecules) and its geometry, which is of great interest in many cases. However, without the Born-Oppenheimer approximation, this concept wouldn't be meaningful at all.

2.2 Construction of Trial Wave Functions

By applying the Born-Oppenheimer approximation, we can concentrate on solving the (stationary) electronic Schrödinger equation, given in Eq. (2.12). Solving this equation, however, is still a very demanding task and often not doable at all without further approximations. The difficulty lies in the pairwise repulsion term in the Hamiltonian, which implies that no electron moves independently of all other electrons. That is, the motion of the electrons is correlated[1]. Moreover, we also have a serious dimensionality problem. Solving Schrödinger's equation for a system consisting of N_e electrons, involves solving a partial differential equation in $3N_e$ dimensions. This quickly becomes unfeasible, as the number of particles increases, using any of the standard methods for solving partial differential equations.

From the discussion above, it seems quite hopeless to try to solve the electronic Schrödinger equation exactly. Instead of trying to solve this equation directly, one usually makes a guess on the wave function and uses the variational method to judge the quality of the guess. The wave function with the lowest energy eigenvalue, is believed to be closest to the ground state.

In the following, we will cover how one goes about constructing the trail wave function. We start by discussing a molecular system consisting of just one electron, and move thereafter to many-electron systems.

We will hereafter use lowercase Greek letters for one-electron wave functions and uppercase Greek letters for many-electron wave functions. We also drop the subscript "el" in Eq. (2.12), and unless otherwise specified, all wave functions are electronic wave functions, with a parametrical dependency on nuclear coordinates.

2.2.1 The Concept of an Orbital

Before we proceed, we need to define what we mean by an orbital. In essence an orbital is the (spatial) wave function of a single electron in an atomic or molecular system[2]. A simple picture used to describe molecular systems, is that the electrons occupy orbitals. That is, each electron takes an orbital as its wave function. As we will see shortly, these orbitals are combined either as a simple product or antisymmetrized products to form the total wave function. This picture is in reality an approximation. The true wave function will depend on the simultaneous coordinates of all the electrons. However, despite the huge simplification of the many-electron problem, the concept of an orbital turns out to be very useful, because it reduces the many-electron problem to the same number of one-electron problems.

To distinguish between orbitals in an atomic system and a molecular system, we will hereafter use the terms atomic orbitals (AOs) and molecular orbitals (MOs). The major difference between AOs and MOs, is that the latter will depend implicitly on the coordinates of more than one nucleus, while AOs only depend on the coordinates of one nucleus.

[1] The term correlation is central in quantum chemistry, and is used to describe the interdependency between the electrons, usually beyond what is described in the Hartree-Fock method.

[2] If we take electron spin into account, the term orbital can also be used for the spatial wave function of pair of electrons, with opposite spin function.

2.2.2 The LCAO Basis Set Approach

We consider a molecular system consisting of just one electron. The electronic wave function for this system depends on the fixed nuclear coordinates and the three Cartesian coordinates of the single electron. If our system had only one nucleus as well, we have the hydrogen atom, where Eq. (2.2) can be solved in closed form. The resulting eigenfunctions are the well-known hydrogenic AOs; 1s, 2s, 2p, 3s, 3p, 3d, etc. [12]. Our suggestion is that these orbitals may be useful, as functions, for constructing MOs in more complex systems. We may represent an MO ϕ, as a linear combination of AOs;

$$\phi = \sum_{i=1}^{M} c_i \varphi_i, \tag{2.13}$$

where each AO φ_i is multiplied by a corresponding coefficient c_i, reflecting the contribution to the MO. This representation is known as the linear combination of atomic orbitals (LCAO), which is a fundamental idea in molecular orbital theory. The AOs don't necessarily need to be the hydrogenic orbitals. We could use orbitals of multi-electron atoms, which are qualitatively similar to those of hydrogen. However, Eq. (2.2) cannot be solved in closed form for these systems, and numerical methods must be applied. Once we have found the AOs for the multi-electron system, we can use them to express MOs, according to Eq. (2.13).

An example on how AOs can be used to represent MOs is shown in Figure 2.1[3]. This figure shows the shape of the lowest MOs of H_2O. These are constructed from the available AOs of oxygen and hydrogen atoms. To be more specific, the figure shows an isosurface[4] of $|\varphi_i|^2$ for each AO, and the resulting MOs (more correctly $|\phi_j|^2$), constructed from the available AOs. Note that the number of MOs, is equal to the number of AOs used to represent them.

It is very important to consider the basis set with AOs just as *functions* used to construct MOs. We anticipate that AOs are efficient functions for representing MOs, but this should not restrict our mathematical flexibility. For example, imagine a molecular system consisting of several hydrogen atoms. From our knowledge about the ground state of a single Hydrogen atom, we could naively limit ourselves to just use the hydrogenic 1s function to represent MOs. But, from a mathematical standpoint, this idea definitely restricts us. Ultimately, we have a mathematical problem. We try to represent an arbitrary function by a combination of more convenient functions. More AOs will bring the basis closer to spanning the true MO space. It should also be emphasized that sometimes it may even be more efficient to use rather unusual types of functions to represent MOs[5]. The issues related to the choice of basis functions will be discussed in much more detail in the next chapter.

The distinction of atomic single particle states as orbitals (that is occupied by electrons) and as basis functions (not occupied by electrons) used to construct MOs,

[3] All orbitals in this figure were found by Hartree-Fock calculations. The visualizations are made by `cubeViz` (see Appendix B.1).

[4] An isosurface is a surface that represents points of a constant value.

[5] As we will see in the next chapter, Gaussian functions turn out to be good candidates for representing MOs.

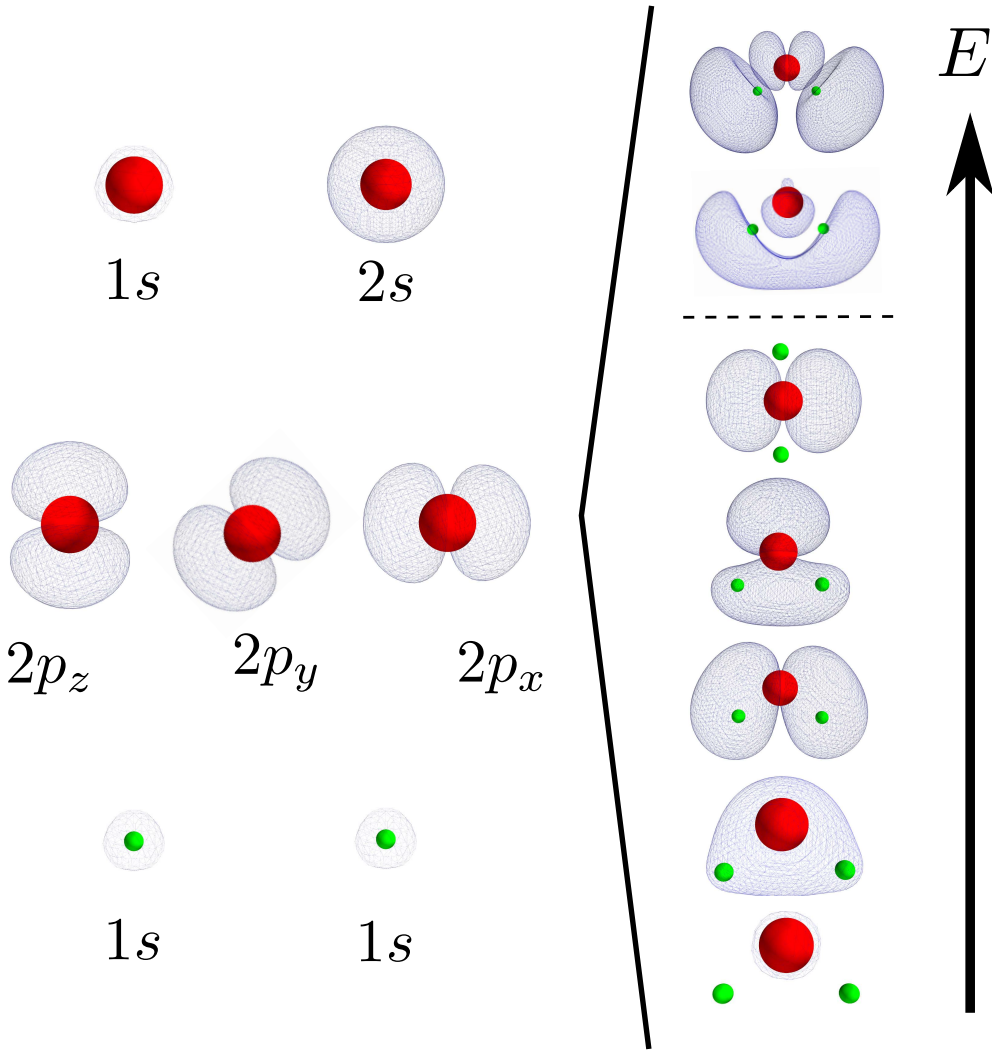

Figure 2.1: Molecular orbitals (MOs) of H_2O: combining seven atomic orbitals (AOs) (left) to form the same number of MOs (right) with increasing orbital energy. The oxygen atom (red) contributes with its 1s, 2s, $2p_x$, $2p_y$, and $2p_z$ orbitals, while the hydrogen atoms (green) contribute with their 1s orbital. The five lowest energy orbitals are doubly occupied, while the two highest orbitals are unoccupied.

is critical in molecular orbital theory and one should avoid conceptually mixing them. This is discussed in more detail in Ref. [10].

The secular equation

MOs can be constructed as a linear combination of AOs, as shown in Eq. (2.13). But the coefficients, reflecting the contribution of each AO to the MO, are not yet known. We will in the following give an recipe on how to find them.

Assuming real functions, we have from Eqs. (2.10) and (2.13);

$$
\begin{aligned}
E &= \frac{\int \left(\sum_i c_i\varphi_i\right) \mathcal{H} \left(\sum_j c_j\varphi_j\right) \mathrm{d}\mathbf{r}}{\int \left(\sum_i c_i\varphi_i\right) \left(\sum_j c_j\varphi_j\right) \mathrm{d}\mathbf{r}} \\
&= \frac{\sum_{i,j} c_i c_j \int \varphi_i \mathcal{H} \varphi_j \,\mathrm{d}\mathbf{r}}{\sum_{i,j} c_i c_j \int \varphi_i \varphi_j \,\mathrm{d}\mathbf{r}} \\
&= \frac{\sum_{i,j} c_i c_j H_{ij}}{\sum_{i,j} c_i c_j S_{ij}},
\end{aligned} \tag{2.14}
$$

where we have introduced the shorthand notation H_{ij} and S_{ij} for the integrals. These are often referred to as matrix elements, but are also known as "resonance integral" and "overlap integral", respectively.

We are interested in the coefficients that minimize the energy, so we require the derivative of the energy with respect to each of the coefficients to be zero;

$$
\frac{\partial E}{\partial c_k} = 0, \qquad \forall k. \tag{2.15}
$$

This gives rise to M equations that can be solved to find the M coefficients $\{c_i\}$. After performing the differentiation, these equations read

$$
\sum_i^M c_i(H_{ki} - ES_{ki}) = 0, \qquad \forall k. \tag{2.16}
$$

This is a linear algebra problem, which has a non-trivial solution, if and only if, $\det(H - ES) = 0$, i.e.

$$
\begin{vmatrix}
H_{11} - ES_{11} & H_{12} - ES_{12} & \dots & H_{1M} - ES_{1M} \\
H_{21} - ES_{21} & H_{22} - ES_{22} & \dots & H_{2M} - ES_{2M} \\
\vdots & \vdots & \ddots & \vdots \\
H_{M1} - ES_{M1} & H_{M2} - ES_{M2} & \dots & H_{MM} - ES_{MM}
\end{vmatrix} = 0. \tag{2.17}
$$

This equation is called the secular equation and has in general M roots, E_j. Each of these gives rise to a different set of coefficients $\{c_{ij}\}$ (by solving Eq. (2.16)), which will represent the MO ϕ_j as

$$
\phi_j = \sum_{i=1}^{M} c_{ij}\varphi_i. \tag{2.18}
$$

Here, index j is used for the MOs and index i for AOs. The set of coefficients which gives the lowest energy eigenvalue, defines the ground state MO, and higher energies define excited states.

2.3 Many-electron Wave Functions

In the previous section, we discussed how the wave function for a one-electron molecular system can be constructed. We will now take the next step and show how the wave function for a many-electron system can be approximated. We will do this in several stages and increase the quality of the trail wave function gradually. As we will see, the wave function will be based on the one-electron MOs, so that we can benefit from the experience we have gained by studying the one-electron system.

2.3.1 Hartree Wave Function

The motion of one electron in many-electron systems, depends on the motion of all the other electrons. This is due to the repulsion term in the Hamiltonian, given in Eq. (2.11). We say that the electrons are correlated. We will for the moment, totally ignore the interaction between electrons and simply drop the repulsion term. The Hamiltonian in this case is separable and can be expressed as

$$\mathcal{H}_0 = \sum_{i=1}^{N_e} \hbar_i, \tag{2.19}$$

where N_e is the total number of electrons, and $\hbar_i$ is the one-electron Hamiltonian, defined as (in atomic units, see Appendix A.1)

$$\hbar_i = -\frac{1}{2}\nabla_i^2 - \sum_{n=1}^{N_n} \frac{Z_n}{|\mathbf{r}_i - \mathbf{R}_n|}. \tag{2.20}$$

The eigenfunctions of $\mathcal{H}_0$ can be expressed as a product of eigenfunctions of $\{\hbar_i\}$. That is, the product

$$\Phi_{\mathrm{H}} = \phi_1\phi_2 \ldots \phi_N, \tag{2.21}$$

is an eigenfunction of $\mathcal{H}_0$, where the set $\{\phi_i\}$ are eigenfunctions of their respective operator $\{\hbar_i\}$. This can easily be shown by

$$\begin{aligned}
\mathcal{H}_0\Phi_{\mathrm{H}} &= \mathcal{H}_0\phi_1\phi_2\dots\phi_N \\
&= \sum_{i=1}^{N_e} \hbar_i\phi_1\phi_2\dots\phi_N \\
&= (\hbar_1\phi_1)\phi_2\dots\phi_N + \phi_1(\hbar_2\phi_2)\dots\phi_N + \dots + \phi_1\phi_2\dots(\hbar_N\phi_N) \\
&= (\epsilon_1\phi_1)\phi_2\dots\phi_N + \phi_1(\epsilon_2\phi_2)\dots\phi_N + \dots + \phi_1\phi_2\dots(\epsilon_N\phi_N) \\
&= \sum_{i=1}^{N_e} \epsilon_i\phi_1\phi_2\dots\phi_N \\
&= \left(\sum_{i=1}^{N_e} \epsilon_i\right)\Phi_{\mathrm{H}}\,,
\end{aligned} \tag{2.22}$$

where we have used that

$$\hbar_i\phi_i = \epsilon_i\phi_i, \tag{2.23}$$

with ϵ_i as the energy eigenvalue of ϕ_i. Thus, the energy eigenvalue of Φ_{H} is simply given as the sum of the one-electron energy eigenvalues. The approximated wave function in Eq. (2.21) is known as the Hartree product, thereby the subscript "H", and is one of the simplest trail wave functions for a many-body system.

What we have done so far is simple and straightforward, but also not correct since the interactions between the electrons are totally ignored. We will now include the electron repulsion term in the molecular Hamiltonian and see if we can improve the quality of the Hartree product. One option is to use the one-electron functions $\{\phi_i\}$, that minimize the expectation value of the Hamiltonian. This can in practice be done by applying variational calculus, which is described in details in Section 2.4.1. It turns out that each of the optimal functions are eigenfunctions of their own operator $\hbar_i$, given as

$$\hbar_i = -\frac{1}{2}\nabla^2 - \sum_{n=1}^{N_n}\frac{Z_n}{|\mathbf{r}-\mathbf{R}_n|} + V_i^H\{j\}, \tag{2.24}$$

where the last term represent the interaction with all other electrons, occupying orbitals $\{j\}$ and is given by

$$V_i^{\mathrm{H}}\{j\} = \sum_{i\neq j}\int \frac{|\phi_j|^2}{|\mathbf{r}-\mathbf{r}'|}\,\mathrm{d}\mathbf{r}'. \tag{2.25}$$

This term is known as the Hartree potential, and is very much like the second term in $\hbar_i$, but it involves an integration. This is because electrons are treated as wave functions. Their charge will therefore be spread out, so integration over all space is needed.

Now, Eq. (2.23) can be solved with the improved operators in Eq. (2.24) to find optimal one-electron functions. These functions can thereafter be used in the Hartree

product. However, due to the interaction term, the one-electron Hamiltonians depend on the eigenfunctions themselves. Therefore, we need to apply the Self-Consistent Field (SCF) procedure. In this scheme, we make a first guess on all $\{\phi_i\}$, which are used to construct the one-electron operators. We thereafter solve Eq. (2.23) to obtain a new set of functions $\{\phi_i\}$. Intuitively, we expect this new set to be closer to the true optimal set, and hence it makes sense to repeat the calculations with the new set. We can keep doing this procedure, until the change in the calculated energy eigenvalues are less than some chosen threshold criterion.

Instead of totally ignoring the repulsion term in the electronic Hamiltonian, we have added an effective interaction potential, which we hope describes some of the correlations between the electrons. This is indeed a better approximation, compared to just dropping the repulsion term, but the Hartree-potential is still defective and corresponds to a "non-interacting" system. This doesn't mean that the electrons do not see each other—they indeed do—but the interaction is just included in an average way, and hence their interaction is not accounted for instantaneously.

In addition to our simplified Hamiltonian, the wave function we have been using is also very simplified, and usually referred to as the uncorrelated or independent-particle wave function. From a statistical point of view, this approximation of the wave function is analogous to saying that the probability $P(A, B)$ for the event A and B is equal to probability of event A multiplied with the probability of event B. This would, of course, be true if events A and B were independent, but not otherwise.

2.3.2 Electron Spin and Antisymmetry

One very important thing we have totally ignored so far in this chapter, is the fact that electrons are identical fermions. This impacts the form of the wave function, due to the Pauli antisymmetry principle. The later states that the total wave function, including spin, for identical fermions must be antisymmetric with respect to exchange of the particles [9]. Mathematically, this can be written as

$$\begin{aligned}\mathcal{P}_{ij}\Psi\left(\mathbf{q}_1,\ldots,\mathbf{q}_i,\ldots,\mathbf{q}_j,\ldots,\mathbf{q}_N\right)\\ &= \Psi\left(\mathbf{q}_1,\ldots,\mathbf{q}_j,\ldots,\mathbf{q}_i,\ldots,\mathbf{q}_N\right)\\ &= -\Psi\left(\mathbf{q}_1,\ldots,\mathbf{q}_i,\ldots,\mathbf{q}_j,\ldots,\mathbf{q}_N\right),\end{aligned} \tag{2.26}$$

where $\mathcal{P}_{ij}$ is the permutation operator, which interchanges the coordinates of particle i and j. Note that $\mathbf{q}$ includes not only the three Cartesian coordinates, but also the spin, i.e. $\mathbf{q}_i = (\mathbf{r}_i, s_i)$, where s_i is the spin coordinate of particle i.

The spin coordinate is an additional degree of freedom, but it differs from the spatial degrees of freedom, in the sense that it is not continuous. The spin coordinate of the electrons takes only two values; $\frac{1}{2}$ or $-\frac{1}{2}$. In order to span the spin space we only need two functions; $\alpha(s)$ and $\beta(s)$, with functional form;

$$\alpha\left(\frac{1}{2}\right) = 1, \qquad \alpha\left(-\frac{1}{2}\right) = 0,$$
$$\beta\left(\frac{1}{2}\right) = 0, \qquad \beta\left(-\frac{1}{2}\right) = 1, \tag{2.27}$$

where $\alpha(s)$ denotes spin up and $\beta(s)$ denotes spin down. These functions are by definition orthonormal;

$$\int \alpha^*(s)\,\alpha(s)\,\mathrm{d}s = \int \beta^*(s)\,\beta(s)\,\mathrm{d}s = 1,$$
$$\int \alpha^*(s)\,\beta(s)\,\mathrm{d}s = \int \beta^*(s)\,\alpha(s)\,\mathrm{d}s = 0, \tag{2.28}$$

Note that integration in spin space is a summation over two discrete values of s, i.e.

$$\sum_s \xi(s) = \xi\left(\frac{1}{2}\right) + \xi\left(\frac{1}{2}\right). \tag{2.29}$$

Therefore, integration with respect to $\mathbf{q}$, denotes a summation over s and an integral over the spatial degrees of freedom;

$$\int \mathrm{d}\mathbf{q} \quad \Rightarrow \quad \sum_s \int \mathrm{d}\mathbf{r}. \tag{2.30}$$

2.3.3 Slater Determinant

The quality of the trail wave function increases if it is antisymmetric. This is because it then provides a more complete description of the system. In the following we will discuss how we can construct an antisymmetric trial wave function in terms of one-electron MOs. This can be achieved by representing the wave function as a Slater determinant;

$$\Psi_{\mathrm{SD}} = \frac{1}{\sqrt{N!}} \begin{vmatrix} \psi_1(\mathbf{q}_1) & \psi_2(\mathbf{q}_1) & \cdots & \psi_{N_e}(\mathbf{q}_1) \\ \psi_1(\mathbf{q}_2) & \psi_2(\mathbf{q}_2) & \cdots & \psi_{N_e}(\mathbf{q}_2) \\ \vdots & \vdots & \ddots & \vdots \\ \psi_1(\mathbf{q}_{N_e}) & \psi_2(\mathbf{q}_{N_e}) & \cdots & \psi_{N_e}(\mathbf{q}_{N_e}) \end{vmatrix}, \tag{2.31}$$

where N_e is the total number of electrons, and $\psi_i(\mathbf{q}_j)$ is molecular spin orbital i, occupied by electron j. Each element is a product of a spatial orbital (MO) and an electron spin eigenfunction:

$$\psi_i(\mathbf{q}_j) = \phi_i(\mathbf{r}_j)\xi_i(s_j), \tag{2.32}$$

where ϕ_i is a pure spatial function, and ξ_i is a spin function (either spin up (α) or spin down (β)). In some cases it is more convenient to write the Slater determinant in terms of the antisymmetrization operator (see Appendix A.2), defined as

$$\mathcal{A} \equiv \frac{1}{N!} \sum_{P} (-1)^{P_n} \mathcal{P}, \tag{2.33}$$

where P_n is the number of pair interchanges, and the sum goes over all permutations $\mathcal{P}$. The latter permutes the coordinates of the spin orbitals only, and not their label. By using the antisymmetrization operator we can express the Slater determinant simply as

$$\Psi_{\mathrm{SD}} = \sqrt{N!}\, \mathcal{A} \Psi_{\mathrm{H}}, \tag{2.34}$$

where $\Psi_{\mathrm{H}} = \psi_1(\mathbf{q}_1)\psi_2(\mathbf{q}_2)\dots\psi_N(\mathbf{q}_N)$ is the well-known Hartree product wave function.

A more compact notation for the Slater determinant is

$$|\Psi_{\mathrm{SD}}\rangle = |\psi_1\psi_2\psi_3\dots\psi_N\rangle\,, \tag{2.35}$$

where the prefactor $(N!)^{-1/2}$ is implicit. Moreover, if two spin orbitals, say ψ_1 and ψ_2, have the same orbital function but different spin function, we can write

$$|\Psi_{\mathrm{SD}}\rangle = |\phi_1^2\psi_3\dots\psi_N\rangle\,, \tag{2.36}$$

where ϕ_1 represents a pure spatial function and the subscript "2" indicates that this orbital is doubly occupied.

A nice property of determinants is that they change sign when any two rows (or columns) are interchanged, which is equivalent to interchanging the coordinates of two electrons. As a result, exchange of any two particle's coordinates changes the sign of the wave function. Furthermore, if two spin orbitals are equal, say $\psi_1 = \psi_2$, then the Slater determinant will vanish. This is in agreement with Pauli's exclusion principle, stating that two electrons cannot occupy the same quantum mechanical state [9].

In a Slater determinant, every spin orbital is evaluated for all electronic coordinates. That is, every electron is associated to every spin orbital. This is an attempt to include the indistinguishability of the electrons, which is an important feature of quantum mechanics. In a Hartree product, in contrast, the electrons are distinguishable. Here, each electron is associated with only their own spin orbital; electron i occupies spin orbital i, electron $i+1$ occupies spin orbital $i+1$ and so on.

Exchange hole

In a Slater determinant, the electrons are no longer uncorrelated, in contrast to the Hartree product. To see how the correlation arises, we consider the probability density for finding one electron with coordinates $\mathbf{q}_1$ and another with $\mathbf{q}_2$, simultaneously. To make the algebra easier, we consider a two-electron determinant given as

$$\Psi_{\mathrm{SD}}(\mathbf{q}_1, \mathbf{q}_2) = |\psi_1\psi_2\rangle\,. \tag{2.37}$$

The desired probability density with this wave function, is found by expanding the Slater determinant;

$$\begin{aligned}\rho(\mathbf{q}_1,\mathbf{q}_2) &= |\Psi_{\mathrm{SD}}|^2 \\ &= \frac{1}{2}\left|\psi_1(\mathbf{q}_1)\psi_2(\mathbf{q}_2) - \psi_1(\mathbf{q}_2)\psi_2(\mathbf{q}_1)\right|^2 \\ &= \frac{1}{2}\Big[|\psi_1(\mathbf{q}_1)|^2|\psi_2(\mathbf{q}_2)|^2 + |\psi_1(\mathbf{q}_2)|^2|\psi_2(\mathbf{q}_1)|^2 \\ &- \psi_1^*(\mathbf{q}_1)\psi_2(\mathbf{q}_1)\psi_2^*(\mathbf{q}_2)\psi_1(\mathbf{q}_2) - \psi_1(\mathbf{q}_1)\psi_2^*(\mathbf{q}_1)\psi_2(\mathbf{q}_2)\psi_1^*(\mathbf{q}_2)\Big]. \qquad (2.38)\end{aligned}$$

In the uncorrelated case (that is, with Hartree product), the same probability density is given by

$$\rho(\mathbf{q}_1,\mathbf{q}_2) = |\psi_1(\mathbf{q}_1)|^2|\psi_2(\mathbf{q}_2)|^2. \qquad (2.39)$$

We see already at this point the inclusion of correlations in a Slater determinant compared to Hartree product. In the latter the probability density is simplified to be the product of the one-electron probability densities.

The probability density for finding one electron with coordinates $\mathbf{r}_1$ and another with $\mathbf{r}_2$, simultaneously, is given by (after integration of spin degrees of freedom):

$$\begin{aligned}\rho(\mathbf{r}_1,\mathbf{r}_2) = \frac{1}{2}\Big[&|\phi_1(\mathbf{r}_1)|^2|\phi_2(\mathbf{r}_2)|^2 + |\phi_1(\mathbf{r}_2)|^2|\phi_2(\mathbf{r}_1)|^2 \\ &- \phi_1^*(\mathbf{r}_1)\phi_1(\mathbf{r}_2)\phi_2^*(\mathbf{r}_2)\phi_2(\mathbf{r}_1)\delta_{\xi_1\xi_2}\delta_{\xi_1\xi_2} \\ &- \phi_1(\mathbf{r}_1)\phi_2^*(\mathbf{r}_1)\phi_2(\mathbf{r}_2)\phi_1^*(\mathbf{r}_2)\delta_{\xi_1\xi_2}\delta_{\xi_1\xi_2}\Big]. \qquad (2.40)\end{aligned}$$

Now, if ψ_1 and ψ_2 have opposite spin, the two last terms on the right hand side vanish. Thus, opposite spin orbitals are still uncorrelated. This becomes particularly apparent if we consider the case where $\phi_1 = \phi_2$[6]:

$$\rho(\mathbf{r}_1,\mathbf{r}_2) = |\phi_1(\mathbf{q}_1)|^2|\phi_1(\mathbf{q}_2)|^2, \qquad (2.41)$$

which is exactly the result from the uncorrelated case[7].

But if ψ_1 and ψ_2 have same spin ($\delta_{\xi_1\xi_2} = 1$), the two last terms in Eq. (2.40) will not disappear. In this case, when $\mathbf{r}_1 = \mathbf{r}_2$, the terms on the right hand side will cancel and the probability density will be zero. This indicates that electron pairs with parallel spin are kept apart, which is a correlation effect. One can imagine that every electron is surrounded by an "exchange hole", where other electrons with the same spin are hardly found. Electrons with opposite spin, on the other hand, are not affected by the

[6]The electrons are allowed to have the same spatial orbital in this case, since they have opposite spins.

[7]Note that when $\phi_1 \neq \phi_2$, the probability density is given as an average, in contract to Eq. (2.39). This is a consequence of the indistinguishability of the electrons, which is not respected in the Hartree product.

exchange hole. It is important to realize that the occurrence of exchange holes, has nothing to do with the electron-electron repulsion, but is rather a consequence of the antisymmetric nature of the wave function. This phenomena will, however, as we will see shortly, have a direct effect on the energy of the system.

Note that we have referred to exchange hole as a correlation effect, but usually the term "correlation effects" is reserved for all correlations apart from exchange, and it is in this sense, we are going to use this term from now on. Also, note that, since the motion of electrons with opposite spin remains uncorrelated, it is customary to refer to a single determinant wave function as an uncorrelated wave function. In fact, every trial wave function, which at most includes exchange effects, is referred to as an uncorrelated wave function [10].

2.4 The Hartree-Fock Theory

Earlier in this chapter, we saw that optimal one-electron functions in a Hartree product can be found as eigenfunctions of a set of one-electron operators. These operators (Eq. (2.24)) occurred as a result of applying variational calculus to minimize the expectation value of the Hamiltonian, given in Eq. (2.11). We will in this section follow the same strategy, but use one single Slater determinant as wave function, instead of the Hartree product. In other words, we wish to find optimal spin orbitals in the Slater determinant, by invoking the variational method. This is the basic philosophy behind the Hartree-Fock method, which is a natural extension of the Hartree's SCF procedure.

In the following subsections we will describe the Hartree-Fock method in detail and derive the so-called Hartree-Fock equation. We will first give a formal derivation of this equation, and thereafter discuss the physical meaning of it in its general form. The derivations in this section are based on Chapter 4 of Ref. [11].

2.4.1 Derivation of the Hartree-Fock Equation

In this section we will derive the Hartree-Fock equation in its general spin orbital form, by minimizing the energy expression for a single Slater determinant, and without making any assumptions on the spin orbitals. Later in this chapter, we will discuss restricted and unrestricted spin orbitals and derive the corresponding equations for each case.

The derivation of Eq. (2.24) is analogous, but in that case, we use the Hartree product as wave function instead of Slater determinant.

Expectation value of the energy

We start by rewriting the Hamiltonian in Eq. (2.11) as

$$\mathcal{H} = \sum_{i=1}^{N_e} \mathcal{h}_i + \frac{1}{2} \sum_{\substack{i,j=1 \\ i \neq j}}^{N_e} \mathcal{g}_{ij}, \tag{2.42}$$

with

$$\hbar_i = -\frac{1}{2}\nabla_i^2 - \sum_{n=1}^{N_n} \frac{Z_n}{|\mathbf{r}_i - \mathbf{R}_n|}, \tag{2.43}$$

$$g_{ij} = \frac{1}{|\mathbf{r}_i - \mathbf{r}_j|}, \tag{2.44}$$

where N_e and N_n are the number of electrons and nuclei (with charge Z_n), respectively. Wee see immediately that $\hbar_i$ is a one-particle operator, since it depends only on $\mathbf{r}_i$, while g_{ij} is a two-particle operator and depends on both $\mathbf{r}_i$ and $\mathbf{r}_j$. In order to find the expectation value of the energy, we need to know the expectation value of both $\hbar_i$ and g_{ij}.

The expectation value of the one-particle operator $\hbar_i$ is found by integrating over both spatial and spin degrees of freedom:

$$\begin{aligned}\langle \Psi_{\mathrm{SD}} | \sum_{i=1}^{N_e} \hbar_i | \Psi_{\mathrm{SD}} \rangle &= N! \int [\mathcal{A}\Psi_{\mathrm{H}}]^\dagger \left(\sum_{i=1}^{N_e} \hbar_i \right) [\mathcal{A}\Psi_{\mathrm{H}}] \, \mathrm{d}\mathbf{q} \\ &= N! \sum_{i=1}^{N_e} \int {\Psi_{\mathrm{H}}}^* \left(\hbar_i \mathcal{A} \right) \Psi_{\mathrm{H}} \, \mathrm{d}\mathbf{q}\end{aligned} \tag{2.45}$$

where we have used that $\mathcal{A}^\dagger\mathcal{A} = \mathcal{A}^2 = \mathcal{A}$, and that $\mathcal{A}$ commutes with $\mathcal{H}$ and thereby with all $\hbar_i$ as well (see Appendix A.2). Now, any permutation of electron coordinates will make the integral zero because of the orthonormality of the spin orbitals. Therefore, the only nonzero contribution is when there is no permutation of coordinates;

$$\begin{aligned}\langle \Psi_{\mathrm{SD}} | \sum_{i=1}^{N_e} \hbar_i | \Psi_{\mathrm{SD}} \rangle &= \int {\Psi_{\mathrm{H}}}^* \left(\sum_{i=1}^{N_e} \hbar_i \right) \Psi_{\mathrm{H}} \, \mathrm{d}\mathbf{q} \\ &= \left(\int \psi_1^* \hbar_1 \psi_1 \, \mathrm{d}\mathbf{q}_1 \right) + \left(\int \psi_2^* \hbar_2 \psi_2 \, \mathrm{d}\mathbf{q}_2 \right) + \cdots + \left(\int \psi_N^* \hbar_N \psi_N \, \mathrm{d}\mathbf{q}_N \right) \\ &= \sum_{k=1}^{N_{so}} \langle \psi_k | \, \hbar \, | \psi_k \rangle \, .\end{aligned} \tag{2.46}$$

Note that we have dropped the subscript on $\hbar$, since this term has the same form for all i (i.e. for all electrons), which is not surprising since electrons are indistinguishable. We have also changed the summation index from i to k, to clearly indicate that we are summing over spin orbitals and not electrons, although the number of each is the same ($N_e = N_{so}$).

The expectation value of the two-particle integral g_{ij} is found in the same way;

$$\langle \Psi_{\mathrm{SD}} | \sum_{\substack{i,j=1 \\ i \neq j}}^{N_e} \mathcal{g}_{ij} | \Psi_{\mathrm{SD}} \rangle = N! \int [\mathcal{A}\Psi_{\mathrm{H}}]^\dagger \left(\sum_{\substack{i,j=1 \\ i \neq j}}^{N_e} \mathcal{g}_{ij} \right) [\mathcal{A}\Psi_{\mathrm{H}}] \, \mathrm{d}\mathbf{q}$$
$$= N! \sum_{\substack{i,j=1 \\ i \neq j}}^{N_e} \int {\Psi_{\mathrm{H}}}^* \left(\mathcal{g}_{ij} \mathcal{A} \right) \Psi_{\mathrm{H}} \, \mathrm{d}\mathbf{q}. \tag{2.47}$$

In this case, we will get a nonzero contribution when i and j are interchanged on one side, in addition to the contribution from zero permutation;

$$\begin{aligned}
\langle \Psi_{\mathrm{SD}} | \sum_{\substack{i,j=1 \\ i \neq j}}^{N_e} \mathcal{g}_{ij} | \Psi_{\mathrm{SD}} \rangle &= \left(\int \psi_1^*(\mathbf{q}_1) \psi_2^*(\mathbf{q}_2) \, \mathcal{g}_{12} \, \psi_1(\mathbf{q}_1) \psi_2(\mathbf{q}_2) \, \mathrm{d}\mathbf{q}_1 \, \mathrm{d}\mathbf{q}_2 \right) + \ldots \\
&+ \left(\int \psi_{N-1}^*(\mathbf{q}_{N-1}) \psi_N^*(\mathbf{q}_N) \, \mathcal{g}_{N-1,N} \, \psi_{N-1}(\mathbf{q}_{N-1}) \psi_N(\mathbf{q}_N) \, \mathrm{d}\mathbf{q}_{N-1} \, \mathrm{d}\mathbf{q}_N \right) \\
&- \left(\int \psi_1^*(\mathbf{q}_1) \psi_2^*(\mathbf{q}_2) \, \mathcal{g}_{12} \, \psi_2(\mathbf{q}_1) \psi_1(\mathbf{q}_2) \, \mathrm{d}\mathbf{q}_1 \, \mathrm{d}\mathbf{q}_2 \right) - \ldots \\
&- \left(\int \psi_{N-1}^*(\mathbf{q}_{N-1}) \psi_N^*(\mathbf{q}_N) \, \mathcal{g}_{N-1,N} \, \psi_N(\mathbf{q}_{N-1}) \psi_{N-1}(\mathbf{q}_N) \, \mathrm{d}\mathbf{q}_{N-1} \, \mathrm{d}\mathbf{q}_N \right) \\
&= \sum_{k,l=1}^{N_{so}} \langle \psi_k \psi_l | \, \mathcal{g} \, | \psi_k \psi_l \rangle - \langle \psi_k \psi_l | \, \mathcal{g} \, | \psi_l \psi_k \rangle \, ,
\end{aligned} \tag{2.48}$$

where we have used the following notation in the last step:

$$\langle \psi_k \psi_l | \, \mathcal{g} \, | \psi_m \psi_n \rangle = \int \psi_k^*(\mathbf{q}) \psi_l^*(\mathbf{q}') \, \frac{1}{|\mathbf{r} - \mathbf{r}'|} \, \psi_m(\mathbf{q}) \psi_n(\mathbf{q}') \, \mathrm{d}\mathbf{q} \, \mathrm{d}\mathbf{q}'. \tag{2.49}$$

The negative sign in front of the second term in Eq. (2.48) arises because all permutations which yield a single interchange of electron coordinates will be generated by an odd power of the permutation operator (P_n in Eq. (2.33) is odd).

Note that we have dropped the indices on $\mathcal{g}$ and changed the summation indices, for the same reason as before; electrons are indistinguishable. Moreover, the restriction in summation is ignored, since

$$\langle \psi_k \psi_l | \, \mathcal{g} \, | \psi_k \psi_l \rangle - \langle \psi_k \psi_l | \, \mathcal{g} \, | \psi_l \psi_k \rangle = 0,$$

when $k = l$. We are therefore allowed to sum freely.

By combining Eqs. (2.46) and (2.48), the expectation value of the energy can be expressed as

$$\begin{aligned}
E &= \langle \Psi_{\mathrm{SD}} | \, \mathcal{H} \, | \Psi_{\mathrm{SD}} \rangle \\
&= \sum_{k=1}^{N_{so}} \langle \psi_k | \, \mathcal{h} \, | \psi_k \rangle + \frac{1}{2} \sum_{k,l=1}^{N_{so}} \langle \psi_k \psi_l | \, \mathcal{g} \, | \psi_k \psi_l \rangle - \langle \psi_k \psi_l | \, \mathcal{g} \, | \psi_l \psi_k \rangle \, ,
\end{aligned} \tag{2.50}$$

where the electron coordinate indices on $\hbar$ and $\mathcal{g}$ operator are not needed, due to the indistinguishability of electrons. We can rewrite this expression in a more compact form, if we introduce the following operators;

$$J_l\psi(\mathbf{q}) = \int \frac{\psi_l^*(\mathbf{q}')\psi_l(\mathbf{q}')}{|\mathbf{r}-\mathbf{r}'|}\,\mathrm{d}\mathbf{q}'\;\psi(\mathbf{q}), \tag{2.51a}$$

$$K_l\psi(\mathbf{q}) = \int \frac{\psi_l^*(\mathbf{q}')\psi(\mathbf{q}')}{|\mathbf{r}-\mathbf{r}'|}\,\mathrm{d}\mathbf{q}'\;\psi_l(\mathbf{q}), \tag{2.51b}$$

and further

$$\mathcal{J} = \sum_l J_l, \qquad \mathcal{K} = \sum_l K_l, \tag{2.52}$$

which are known as the Coulomb and exchange operator, respectively. Using these operators we can rewrite Eq. (2.50) as

$$E = \sum_{k=1}^{N_{so}} \langle\psi_k|\,\hbar + \frac{1}{2}(\mathcal{J}-\mathcal{K})\,|\psi_k\rangle\,. \tag{2.53}$$

If we were to use a Hartree product as a trail wave function instead of a Slater determinant, the expectation value of the energy is almost the same as the expression above, but without the exchange term and with the constraint $k \neq l$ in the summation over l in $\mathcal{J}$. This is because the Coulomb part doesn't cancel without the exchange term, in the case $k = l$.

Variational method

In order to find optimal spin orbitals, we can apply the standard techniques of calculus of variations. This is, we seek for an optimal set of single-particle states that makes the energy functional in Eq. (2.53) stationary under infinitesimal changes; $|\psi_m\rangle \rightarrow |\psi_m\rangle + |\delta\psi_m\rangle$. The variation in spin orbitals is, however, not completely arbitrary and has to satisfy the orthonormality requirement;

$$\langle\psi_k|\psi_l\rangle = \int \psi_k^*\psi_l\,\mathrm{d}\mathbf{r} = \delta_{kl}. \tag{2.54}$$

By introducing the Lagrange multipliers Λ_{kl} [13], we can set up the Lagrange functional, which we wish to minimize;

$$\mathcal{L}[\psi_1,\psi_2,\ldots,\psi_{N_{so}}] = E - \sum_{kl}\Lambda_{kl}\left(\langle\psi_k|\psi_l\rangle - \delta_{kl}\right) \tag{2.55}$$

By applying an arbitrary change on one arbitrary spin orbital in this functional, and require

$$\delta\mathcal{L} = \mathcal{L}[\psi_1,\psi_2,\ldots,\psi_m+\delta\psi_m,\ldots\psi_{N_{so}}] - \mathcal{L}[\psi_1,\psi_2,\ldots,\psi_m,\ldots\psi_{N_{so}}] \equiv 0,$$

we obtain (by considering only first order terms of variation)

$$\begin{aligned} 0 \equiv \delta\mathcal{L} &= \delta E - \delta \sum_{kl} \Lambda_{kl} \langle \psi_k | \psi_l \rangle \\ &= \delta E - \left[\sum_{l} \Lambda_{ml} \langle \delta\psi_m | \psi_l \rangle + \sum_{k} \Lambda_{km} \langle \psi_k | \delta\psi_m \rangle \right] \\ &= \delta E - \sum_{k} \left[\Lambda_{mk} \langle \delta\psi_m | \psi_k \rangle + \Lambda_{km} \langle \psi_k | \delta\psi_m \rangle \right] \\ &= \delta E - \sum_{k} \left[\Lambda_{mk} \langle \delta\psi_m | \psi_k \rangle + \Lambda_{km} \langle \delta\psi_m | \psi_k \rangle^* \right], \end{aligned} \tag{2.56}$$

with

$$\begin{aligned} \delta E &= \langle \delta\psi_m | \, \hbar \, | \psi_m \rangle + \text{complex conj.} \\ &+ \frac{1}{2} \sum_{k} \Big(\langle \delta\psi_m \psi_k | \, \mathcal{g} \, | \psi_m \psi_k \rangle + \langle \psi_k \delta\psi_m | \, \mathcal{g} \, | \psi_k \psi_m \rangle \\ &- \langle \delta\psi_m \psi_k | \, \mathcal{g} \, | \psi_k \psi_m \rangle - \langle \psi_k \delta\psi_m | \, \mathcal{g} \, | \psi_m \psi_k \rangle \Big) + \text{complex conj.} \\ &= \langle \delta\psi_m | \, \hbar \, | \psi_m \rangle + \text{complex conj.} \\ &+ \sum_{k} \Big(\langle \delta\psi_m \psi_k | \, \mathcal{g} \, | \psi_m \psi_k \rangle - \langle \delta\psi_m \psi_k | \, \mathcal{g} \, | \psi_k \psi_m \rangle \Big) + \text{complex conj.}, \end{aligned} \tag{2.57}$$

where we have used

$$\langle \psi_k | \delta\psi_m \rangle = \langle \delta\psi_m | \psi_k \rangle^*, \tag{2.58a}$$

$$\langle \psi_m | \, \hbar \, | \delta\psi_m \rangle = \langle \delta\psi_m | \, \hbar \, | \psi_m \rangle^*, \tag{2.58b}$$

$$\langle \psi_m \psi_k | \, \mathcal{g} \, | \delta\psi_m \psi_k \rangle = \langle \delta\psi_m \psi_k | \, \mathcal{g} \, | \psi_m \psi_k \rangle^*, \tag{2.58c}$$

etc., which follow from the definition of the integrals, in addition to the symmetry property of the two-electron element;

$$\langle \psi_k \psi_l | \, \mathcal{g} \, | \psi_m \psi_n \rangle = \langle \psi_l \psi_k | \, \mathcal{g} \, | \psi_n \psi_m \rangle. \tag{2.59}$$

By introducing the Fock operator, defined as

$$\mathcal{F} = \hbar + \mathcal{J} - \mathcal{K}, \tag{2.60}$$

we can rewrite Eq. (2.56) to

$$\langle \delta\psi_m | \, \mathcal{F} \, | \psi_m \rangle + \text{complex conj.} = \sum_{k} \left[\Lambda_{mk} \langle \delta\psi_m | \psi_k \rangle + \Lambda_{km} \langle \delta\psi_m | \psi_k \rangle^* \right]. \tag{2.61}$$

Since the variations $\delta\psi^*$ and $\delta\psi$ are arbitrary and independent, Eq. (2.61) will lead to two equations;

$$\mathcal{F}\psi_m = \sum_k \Lambda_{mk}\psi_k, \tag{2.62a}$$

$$\mathcal{F}^*\psi_m^* = \sum_k \Lambda_{km}\psi_k^*. \tag{2.62b}$$

These two equations can be combined, by taking the complex conjugate of the last one and subtract from the first one, to give

$$\sum_k (\Lambda_{mk} - \Lambda_{km}^*)\psi_k = 0. \tag{2.63}$$

Now, since the spin orbitals are orthogonal, they are linearly independent, which means that the vector equation

$$\sum_k c_k\psi_k = 0, \tag{2.64}$$

has only the trivial solution (all c_k are zero). Therefore will Eq. (2.63) be true only if

$$\Lambda_{mk} = \Lambda_{km}^*.$$

Thus the Lagrange multipliers are elements of an hermitian matrix, and the two equations in Eq. (2.62) are simply the complex conjugate of each other and therefore equivalent. By using these observations, we can formulate the minimization condition as

$$\mathcal{F}\psi_m = \sum_k \Lambda_{mk}\psi_k. \tag{2.65}$$

Since the the varied spin orbital ψ_m is chosen arbitrary, an identical equation will appear for each spin orbital in the set $\{\psi_l\}$, resulting in N_{so} identical equations. The constraint on the solutions of these equations is that they should be orthogonal, and the Lagrange parameters must, therefore, be chosen such that this is the case. One option is to set $\Lambda_{mk} = \delta_{mk}\epsilon_m$, leading to

$$\mathcal{F}\psi_m = \epsilon_m\psi_m, \tag{2.66}$$

which is an eigenvalue equation, with ψ_m as an eigenfunction of $\mathcal{F}$. The solutions of this equation form an orthonormal set and by taking this set as our spin orbitals, the constraint equation (2.54) will be satisfied automatically.

Eq. (2.66) is known as the Hartree-Fock equation, which can be solved to find optimal spin orbitals that minimize the energy expression for a single Slater determinant. However, because of the nonlinear nature of this equation, a SCF iterative procedure, must be applied. The philosophy is the same as before; make a first guess on all the one-electron wave functions $\{\psi_l\}$ to construct the Fock operator, and thereafter solve

Eq. (2.66) to obtain a new set of one-electron functions $\{\psi_l\}$, which we expect to be closer to the true optimal set. We solve the same equation with the new set, and repeat this procedure until self-consistency is reached, i.e. until spin orbitals used to construct $\mathcal{F}$ are the same as its eigenfunctions. Note that in principle, the Hartree-Fock equation has infinite number of solutions, but in practice only the N_{so} lowest eigenfunctions are used to construct the Slater determinant. These solutions are usually referred to as occupied spin orbitals, while the remaining solutions are referred to as hole or virtual spin orbitals.

2.4.2 Hartree-Fock Equation - Physical Picture

By taking antisymmetry into account, the one-electron Hamiltonian in Eq. (2.24) can be extended to

$$\mathcal{F} = -\frac{1}{2}\nabla^2 - \sum_{n=1}^{N_n} \frac{Z_n}{|\mathbf{r} - \mathbf{R}_n|} + V^{HF}, \tag{2.67}$$

where the last term is the interaction potential operator, and can be expressed in terms of its action on an arbitrary state $\psi_k(\mathbf{q})$;

$$V^{\mathrm{HF}}\psi_k(\mathbf{q}) = \sum_l \left[\int \frac{\psi_l^*(\mathbf{q}')\psi_l(\mathbf{q}')}{|\mathbf{r} - \mathbf{r}'|}\, \mathrm{d}\mathbf{q}'\, \psi_k(\mathbf{q}) - \int \frac{\psi_l^*(\mathbf{q}')\psi_k(\mathbf{q}')}{|\mathbf{r} - \mathbf{r}'|}\, \mathrm{d}\mathbf{q}'\, \psi_l(\mathbf{q}) \right]. \tag{2.68}$$

These two terms are known as the direct term (or Coulomb term) and exchange term, respectively. If we exclude $l = k$ in summation, the direct term is nothing but the Hartree potential given in Eq. (2.25). The latter describes the total averaged potential acting on an electron in spin orbital ψ_k, arising from other electrons in other spin orbitals. However unlike Eq. (2.25), the direct term contains coupling between orbital k and itself, since we don't have any restriction in summation over l. This is of course unphysical, since an electron does not interact with itself. But, fortunately, this term is canceled by the exchange term, so we can nevertheless sum freely over l.

The exchange term looks much like the direct term, except that it is nonlocal. This means that when acting on ψ_k its value at $\mathbf{q}$ is determined by the value assumed by ψ_k at all possible positions $\mathbf{q}'$. The occurrence of this term is a direct consequence of the antisymmetric form of the wave function, which lowers the Coulomb interaction between the electrons with same spin. This is because these electrons are kept apart (due to exchange hole), and therefore will their interaction be reduced. As mentioned earlier, it is important to realize that this behavior has nothing to do with the electron-electron repulsion, and is a direct consequence of the antisymmetric nature of the wave function. But it does keep the electrons with parallel spin apart, and therefore reduces their Coulombic interaction, which effect the energy of the system.

The Hartree-Fock equation (Eq. (2.66)) has the form of an ordinary Schrödinger equation, although $\{\epsilon_k\}$ are primarily identified as Lagrange multipliers, and not energies. But they are, however, related to the total energy by

$$E = \sum_{k=1}^{N_{so}} \langle \psi_k | \, \hbar + \frac{1}{2}(\mathcal{J} - \mathcal{K}) \, | \psi_k \rangle = \sum_{k=1}^{N_{so}} \epsilon_k - \frac{1}{2} \langle \psi_k | \, \mathcal{J} - \mathcal{K} \, | \psi_k \rangle \, . \tag{2.69}$$

It is thus apparent, that the total energy is not simply the sum of all ϵ_k, which is due to the double counting of electron-electron interaction between pairs of electrons in $\sum_k \epsilon_k$. We must therefore compensate for this by subtracting $\frac{1}{2} \langle \psi_k | \, \mathcal{J} - \mathcal{K} \, | \psi_k \rangle$. In the literature, $\{\epsilon_k\}$ are often referred to as orbital energies, and attached physical significance through Koopmans' theorem [11].

Solving the Hartree-Fock equation yields a set $\{\psi_k\}$ of orthonormal spin orbitals with orbital energies $\{\epsilon_k\}$. In principle, the set consists of an infinite number of solutions, leading to an infinite Hartree-Fock spectrum. For a system consisting of N_e electrons, the ground state is approximated by taking the N_e lowest eigenstates of this spectrum as spin orbitals of the electrons (see Figure 2.2). It is, however, not a clear a priori that the the ground state is found by filling the lowest eigenstates, since the energy is not simply the sum of spin orbital energies. But in practical applications this turns out to be the case anyway [11].

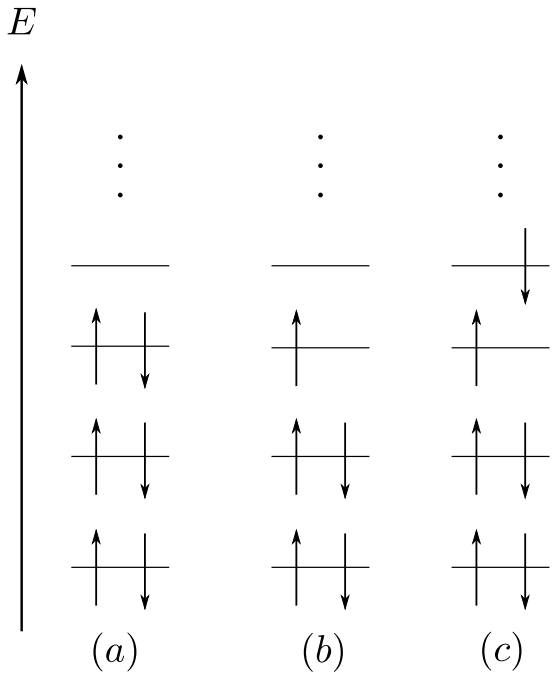

Figure 2.2: Hartree-Fock spectrum: schematic representation of how the levels are filled for (a): the ground state of an even number of electrons, (b): the ground state of an odd number of electrons and (c): an exited spectrum of an even number of electrons.

2.5 Closed- and Open-shell Systems

We have so far discussed the Hartree-Fock equation in a formal way, without specifying the explicit form of the spin orbitals. In order to do actual calculations using the Hartree-Fock method, we most be more specific about the form of the spin orbitals. Depending on the choice of spin orbitals we can formulate two different versions of Hartree-Fock; restricted Hartree-Fock (RHF) and unrestricted Hartree-Fock (UHF). In RHF, the spin orbitals have the same spatial part for different spin function, and is usually used to describe closed-shell systems, where all levels are doubly occupied. To describe open-shell systems, where there are partially filled levels containing only one electron, it is more common to use the UHF formalism[8]. In this case the spin orbitals have different spatial functions for different spin functions. In Figure 2.3 both restricted and unrestricted configurations are shown.

Note that a system with even number of electrons is not necessarily a closed-shell system, because of the possibility of degenerate levels. In addition, we may also consider an exited state where an electron is exited to a higher level. In this case two levels will be partially filled and we are therefore dealing with an open-shell system, although the number of electrons is even. A system with odd number of electrons will always be an open-shell system.

We will in the following sections describe both RHF and UHF, where we restrict the discussion about RHF to just closed-shell systems, although the formalism also can be applied to open-shell systems [6]. To describe open-shell systems the UHF formalism is usually used.

2.5.1 Restricted Hartree-Fock

In RHF, the spin orbitals are grouped in pairs with the same spatial wave function, but opposite spin;

$$\begin{aligned} \psi_{2k}(\mathbf{q}) &= \phi_k(\mathbf{r})\alpha(s), \\ \psi_{2k-1}(\mathbf{q}) &= \phi_k(\mathbf{r})\beta(s), \qquad k = 1, \ldots, N/2, \end{aligned} \tag{2.70}$$

where N is the total number of spin orbitals. Using these spin orbitals, we can express the ground state as

$$|\Psi_{\mathrm{RHF}}\rangle = |\psi_1\psi_2\psi_3\ldots\psi_N\rangle = |\phi_1^2\phi_2^2\ldots\phi_{N/2}^2\rangle\,, \tag{2.71}$$

where the subscript "2" indicates doubly occupied spatial orbitals. We now want to replace the general spin orbital Hartree-Fock equation in Eq. (2.66), with a pure spatial eigenvalue equation, by integrating out the spin degrees of freedom. Our starting point is naturally, the general spin orbital Hartree-Fock equation:

[8]The unrestricted formulation is sometimes also applied on systems that are normally thought as closed-shell systems, since it gives a better description than the restricted formalism does. One example is the dissociation problem discussed in Ref. [6].

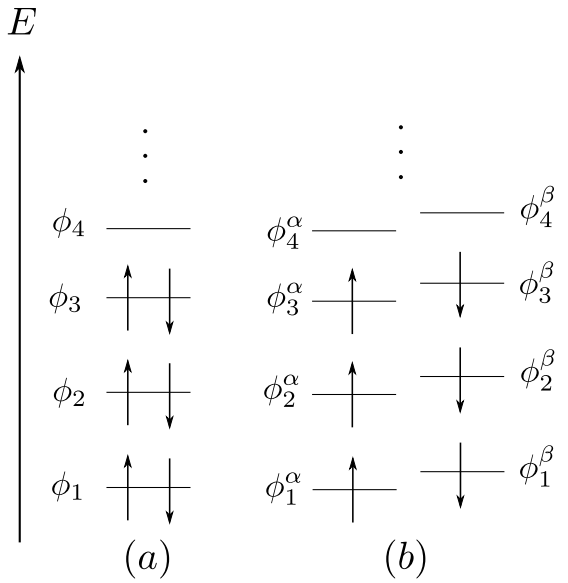

Figure 2.3: Restricted and unrestricted spectrum: schematic representation of (a): spin-restricted configuration and (b): spin-unrestricted configuration.

$$\mathcal{F}\psi_k(\mathbf{q}) = \epsilon_k \psi_k(\mathbf{q}), \tag{2.72}$$

where ψ_k can either have spin α or spin β function. We will assume that ψ_k has spin α function, but identical results will be obtained with spin β function;

$$\mathcal{F}\,\phi_k(\mathbf{r})\alpha(s) = \epsilon_k\,\phi_k(\mathbf{r})\alpha(s). \tag{2.73}$$

By multiplying $\alpha^*(s)$ from left, and integrating over spin, we obtain

$$\hbar\phi_k(\mathbf{r}) + \sum_{l=1}^{N} \int \alpha^*(s)\,(J_l - K_l)\,\phi_k(\mathbf{r})\alpha(s)\,\mathrm{d}s = \epsilon_k\,\phi_k(\mathbf{r}), \tag{2.74}$$

where $\hbar$ remains the same since it has no spin-dependency. Now, in a closed-shell system the sum over spin orbitals includes a sum over those with spin α function and a sum over those with spin β function;

$$\sum_{l=1}^{N} \quad \rightarrow \quad \sum_{l_\alpha=1}^{N/2} + \sum_{l_\beta=1}^{N/2},$$

so we can rewrite the integral in last equation as

$$\sum_{l=1}^{N} \int \alpha^*(s) \left(J_l - K_l\right) \phi_k(\mathbf{r}) \alpha(s) \, \mathrm{d}s = \sum_{l_\alpha=1}^{N/2} \int \alpha^*(s) \left(J_{l_\alpha} - K_{l_\alpha}\right) \phi_k(\mathbf{r}) \alpha(s) \, \mathrm{d}s + \sum_{l_\beta=1}^{N/2} \int \alpha^*(s) \left(J_{l_\beta} - K_{l_\beta}\right) \phi_k(\mathbf{r}) \alpha(s) \, \mathrm{d}s = \sum_{l=1}^{N/2} 2J_l(\mathbf{r}) - K_l(\mathbf{r}), \tag{2.75}$$

where $J_l(\mathbf{r})$ and $K_l(\mathbf{r})$ are analogous to definitions in Eq. (2.51), but in terms of spatial orbitals only;

$$J_l \phi(\mathbf{r}) = \int \frac{\phi_l^*(\mathbf{r}') \phi_l(\mathbf{r}')}{|\mathbf{r} - \mathbf{r}'|} \, \mathrm{d}\mathbf{r}' \; \phi(\mathbf{r}), \tag{2.76a}$$

$$K_l \phi(\mathbf{r}) = \int \frac{\phi_l^*(\mathbf{r}') \phi(\mathbf{r}')}{|\mathbf{r} - \mathbf{r}'|} \, \mathrm{d}\mathbf{r}' \; \phi_l(\mathbf{r}). \tag{2.76b}$$

The factor two in front of J_l arises, because the Coulomb terms are equal for spin α and β, while the exchange term for spin β vanishes due to spin orthogonality.

The closed-shell Fock operator can thus be written as

$$\mathcal{F}_{\text{spatial}} = \mathcal{h} + 2\mathcal{J}_{\text{spatial}} - \mathcal{K}_{\text{spatial}}, \tag{2.77}$$

where

$$\mathcal{J}_{\text{spatial}} = \sum_{l=1}^{N/2} J_l(\mathbf{r}), \tag{2.78}$$

$$\mathcal{K}_{\text{spatial}} = \sum_{l=1}^{N/2} K_l(\mathbf{r}). \tag{2.79}$$

The corresponding energy functional is given by

$$E = \sum_{k=1}^{N/2} \langle \phi_k | \, 2\mathcal{h} + 2\mathcal{J}_{\text{spatial}} - \mathcal{K}_{\text{spatial}} \, | \phi_k \rangle \, . \tag{2.80}$$

Note that the energy is a functional of spatial orbitals $\{\phi_k\}$, and not spin orbitals $\{\psi_k\}$, as it was in Eq. (2.53). From now on, we will drop the subscript "spatial" on operators in Eqs. (2.77) and (2.80), and instead specify the spatial form of the Fock operator by $\mathcal{F}(\mathbf{r})$. The original form of the Fock operator including spin will be specified as $\mathcal{F}(\mathbf{q})$. The operators $\mathcal{J}$ and $\mathcal{K}$, will be specified in the same way.

2.5.2 Introduction of a Basis: The Roothaan Equation

By eliminating the spin, we are left with a spatial eigenvalue problem;

$$\mathcal{F}(\mathbf{r})\phi_k(\mathbf{r}) = \epsilon_k\phi_k(\mathbf{r}), \qquad k = 1, \ldots, N/2, \tag{2.81}$$

where N is the total number of spin orbitals. This equation is in practice solved by introducing a set of known basis functions $\{\varphi_p\}$, which expand the unknown spatial wave functions (MOs);

$$\phi_k(\mathbf{r}) = \sum_{p=1}^{M} C_{pk}\varphi_p(\mathbf{r}), \tag{2.82}$$

where the expansion coefficients C_{pk} are not yet known. This is analogous to what we did earlier in this chapter, when we discussed the LCAO basis set approach (see Section 2.2.2). Although the basis functions are assumed to be normalized and linearly independent, they are not in general orthogonal. Orthogonality is required among the MOs, but not among the basis functions representing the MOs. If the set $\{\varphi_p\}$ was complete, we could represent the MOs exact, but in practice we are limited to use a finite set of M basis functions, because of computational reasons. Since we are limited to finite basis sets, it is important to choose a basis that describe the MOs efficient. In the next chapter, we will discuss the questions involved in the choice of a basis set in detail, but for now we will assume that the set $\{\varphi_p\}$ is some known basis set.

By inserting the expansion in Eq. (2.82), into the Hartree-Fock equation, we obtain

$$\mathcal{F}(\mathbf{r})\sum_{q=1}^{M} C_{qk}\varphi_q(\mathbf{r}) = \epsilon_k\sum_{q=1}^{M} C_{qk}\varphi_q(\mathbf{r}), \tag{2.83}$$

which can be converted to a matrix equation by multiplying $\varphi_p^*(\mathbf{r})$ from left and integrating;

$$\sum_{q=1}^{M} C_{qk}\int \varphi_p^*(\mathbf{r})\mathcal{F}(\mathbf{r})\varphi_q(\mathbf{r})\,\mathrm{d}\mathbf{r} \;= \epsilon_k\sum_{q=1}^{M} C_{qk}\int \varphi_p^*(\mathbf{r})\varphi_q(\mathbf{r})\,\mathrm{d}\mathbf{r}. \tag{2.84}$$

This equation can be rewritten if we introduce the overlap and Fock matrix with elements;

$$S_{pq} = \int \varphi_p^*(\mathbf{r})\varphi_q(\mathbf{r})\,\mathrm{d}\mathbf{r}, \tag{2.85a}$$

$$F_{pq} = \int \varphi_p^*(\mathbf{r})\mathcal{F}(\mathbf{r})\varphi_q(\mathbf{r})\,\mathrm{d}\mathbf{r}. \tag{2.85b}$$

Using these, we can rewrite the Hartree-Fock equation as

$$\sum_{q=1}^{M} F_{pq}C_{qk} \;= \epsilon_k\sum_{q=1}^{M} S_{pq}C_{qk}, \tag{2.86}$$

which also is known as the Roothaan equation. This equation can be written more compactly as

$$\mathbf{FC} = \mathbf{SC}\boldsymbol{\epsilon}, \tag{2.87}$$

where $\mathbf{C}$ is an $M \times N/2$ matrix;

$$\mathbf{C} = \begin{pmatrix} C_{1,1} & C_{1,2} & \cdots & C_{1,N/2} \\ C_{2,1} & C_{2,2} & \cdots & C_{2,N/2} \\ \vdots & \vdots & \ddots & \vdots \\ C_{M,1} & C_{M,2} & \cdots & C_{M,N/2} \end{pmatrix}, \tag{2.88}$$

and $\boldsymbol{\epsilon}$ is a rectangular diagonal matrix of the orbital energies ϵ_k;

$$\boldsymbol{\epsilon} = \begin{pmatrix} \epsilon_1 & & & \\ & \epsilon_2 & & \mathbf{0} \\ & & \ddots & \\ \mathbf{0} & & & \end{pmatrix}. \tag{2.89}$$

Note that it is the columns of $\mathbf{C}$ that describe the MOs, i.e. the first column in $\mathbf{C}$ are the coefficients of ϕ_1, the second column are the the coefficients of ϕ_2 and so on.

The matrix representation of the Fock operator

$$\mathcal{F}(\mathbf{r}) = \hbar + \sum_{l=1}^{N/2} 2J_l(\mathbf{r}) - K_l(\mathbf{r}), \tag{2.90}$$

in the basis $\{\varphi_p\}$ is given by

$$\begin{aligned} F_{pq} &= \int \varphi_p^*(\mathbf{r}) \left[\hbar + \sum_{l=1}^{N/2} 2J_l(\mathbf{r}) - K_l(\mathbf{r}) \right] \varphi_q(\mathbf{r})\, \mathrm{d}\mathbf{r} \\ &= h_{pq} + \sum_{l=1}^{N/2} \sum_{r,s=1}^{M} C_{rl}^* C_{sl} \Big(2g_{prqs} - g_{prsq} \Big), \end{aligned} \tag{2.91}$$

where

$$h_{pq} = \langle p | \, \hbar \, | q \rangle = \int \varphi_p^*(\mathbf{r}) \hbar \varphi_q(\mathbf{r})\, \mathrm{d}\mathbf{r}, \tag{2.92}$$

and

$$g_{prqs} = \langle pr | \, g \, | qs \rangle = \int \varphi_p^*(\mathbf{r}) \varphi_r^*(\mathbf{r}') \, \frac{1}{|\mathbf{r} - \mathbf{r}'|} \, \varphi_q(\mathbf{r}) \varphi_s(\mathbf{r}')\, \mathrm{d}\mathbf{r}\, \mathrm{d}\mathbf{r}'. \tag{2.93}$$

Note that l labels the MOs $\{\phi_l\}$, while p, q, r and s label the basis functions $\{\varphi_p\}$. By defining the density matrix;

$$P_{pq} = 2\sum_{l=1}^{N/2} C_{pl}C_{ql}^{*}, \tag{2.94}$$

we can rewrite the Fock matrix as

$$F_{pq} = h_{pq} + \frac{1}{2}\sum_{r,s=1}^{M} P_{rs}\Big(2g_{prqs} - g_{prsq}\Big). \tag{2.95}$$

By inserting the expansion in Eq. (2.82) into the energy expression in Eq. (2.80), we can express the energy in terms of the density matrix as well;

$$\begin{aligned} E &= \sum_{k=1}^{N/2} \langle\phi_k|\, 2\hat{h} + 2\mathcal{J}(\mathbf{r}) - \mathcal{K}(\mathbf{r})\,|\phi_k\rangle \\ &= \sum_{pq}^{M} P_{pq}h_{pq} + \frac{1}{2}\sum_{pqrs}^{M} P_{pq}P_{rs}\Big(g_{prqs} - \frac{1}{2}g_{prsq}\Big) \\ &= \frac{1}{2}\sum_{pq}^{M} P_{pq}(h_{pq} + F_{pq}). \end{aligned} \tag{2.96}$$

The density matrix is directly related to the charge density, as it is shown in Ref. [6], and can be used to characterize the Hartree-Fock results. In practice when using the SCF procedure, we make a guess on the density matrix (or equivalently on the coefficients C_{pk}), which is equivalent to make a guess on the charge density. With our guess we construct the Fock matrix and solve Eq. (2.87), to obtain a new and better set of coefficients, which can be used to calculate a new density matrix. This procedure can be repeated until self-consistency, as described earlier in this chapter.

2.5.3 Orthogonalization of the Basis

As mentioned in the last section, a basis set used to represent MOs is not required to be orthogonal. The only requirement is that the basis functions are normalized. The consequence of using a non-orthogonal basis set, is the occurrence of the overlap matrix $\mathbf{S}$ in Eq. (2.87), which is a generalized eigenvalue equation. Of course, if the basis set is an orthonormal set, then the overlap matrix is just the identity matrix, and we are left with an ordinary eigenvalue equation, which can be solved by standard methods in linear algebra.

The generalized eigenvalue problem in Eq. (2.87) can be transformed to an ordinary eigenvalue problem by performing a basis transformation that orthogonalizes the basis. This basis transformation involves finding a transformation matrix $\mathbf{V}$ that makes a transformed set of functions $\{\varphi'_q\}$ given by

$$\varphi'_q = \sum_{p} V_{pq}\varphi_p, \tag{2.97}$$

orthonormal, i.e.

$$\int \mathrm{d}\mathbf{r}\ \varphi_p'^*(\mathbf{r})\varphi_q'(\mathbf{r}) = \delta_{pq}. \tag{2.98}$$

To investigate the properties of the transformation matrix $\mathbf{V}$, we can insert the transformation in Eq. (2.97) into the last equation to get

$$\begin{aligned}\int \mathrm{d}\mathbf{r}\ \varphi_p'^*(\mathbf{r})\varphi_q'(\mathbf{r}) &= \int \mathrm{d}\mathbf{r}\ \left[\sum_r V_{rp}^*\varphi_r^*(\mathbf{r})\right]\left[\sum_s V_{sq}\varphi_s(\mathbf{r})\right] \\ &= \sum_{rs} V_{rp}^* S_{rs} V_{sq} = \delta_{pq},\end{aligned} \tag{2.99}$$

where the last line can be written as

$$\mathbf{V}^\dagger\mathbf{S}\mathbf{V} = \mathbf{1}. \tag{2.100}$$

By using the relation above, we can rewrite the generalized eigenvalue equation

$$\begin{aligned}\mathbf{F}\mathbf{C} &= \mathbf{S}\mathbf{C}\boldsymbol{\epsilon} \\ \mathbf{V}^\dagger\mathbf{F}\mathbf{V}\mathbf{V}^{-1}\mathbf{C} &= \mathbf{V}^\dagger\mathbf{S}\mathbf{V}\mathbf{V}^{-1}\mathbf{C}\boldsymbol{\epsilon} \\ \mathbf{F}'\mathbf{C}' &= \mathbf{C}'\boldsymbol{\epsilon},\end{aligned} \tag{2.101}$$

where $\mathbf{F}' = \mathbf{V}^\dagger\mathbf{F}\mathbf{V}$ and $\mathbf{C}' = \mathbf{V}^{-1}\mathbf{C}$. This equation is an ordinary eigenvalue equation which can be solved for $\mathbf{C}'$ and thereafter transformed back to the original coefficient matrix $\mathbf{C}$ by $\mathbf{V}\mathbf{C}'$.

The remaining problem is to find the transformation matrix $\mathbf{V}$ which brings $\mathbf{S}$ to unit form according to Eq. (2.100). One alternative, known as symmetric orthogonalization [6], is to define the transformation matrix as

$$\mathbf{V} \equiv \mathbf{U}\mathbf{s}^{-1/2}\mathbf{U}^\dagger, \tag{2.102}$$

where $\mathbf{s}$ is a diagonal matrix of the eigenvalues of $\mathbf{S}$, and $\mathbf{U}$ is a unitary matrix that diagonalizes the overlap matrix, i.e.

$$\mathbf{U}^\dagger\mathbf{S}\mathbf{U} = \mathbf{s}. \tag{2.103}$$

This unitary matrix exists because of the Hermitian nature of $\mathbf{S}$. Moreover, the eigenvalues of the overlap matrix are all positive, which follows directly from its definition. Therefore there is no difficulty in Eq. (2.102) of taking the square roots. Inserting the definition of the transformation matrix into Eq. (2.100), we obtain

$$\begin{aligned}(\mathbf{U}\mathbf{s}^{-1/2}\mathbf{U}^\dagger)^\dagger\mathbf{S}(\mathbf{U}\mathbf{s}^{-1/2}\mathbf{U}^\dagger) &= (\mathbf{U}\mathbf{s}^{-1/2}\mathbf{U}^\dagger)(\mathbf{U}\mathbf{s}\mathbf{U}^\dagger)(\mathbf{U}\mathbf{s}^{-1/2}\mathbf{U}^\dagger) \\ &= \mathbf{U}\mathbf{s}^{-1/2}\mathbf{s}\mathbf{s}^{-1/2}\mathbf{U}^\dagger = \mathbf{1},\end{aligned} \tag{2.104}$$

which shows that $\mathbf{V}$ indeed has the desired property.

A second alternative to orthogonalize the basis set, known as canonical orthogonalization [6], is to define the transformation matrix as

$$\mathbf{V} \equiv \mathbf{U}\mathbf{s}^{-1/2}, \tag{2.105}$$

which also is an orthogonalizing transformation matrix;

$$(\mathbf{U}\mathbf{s}^{-1/2})^{\dagger}\mathbf{S}\mathbf{U}\mathbf{s}^{-1/2} = \mathbf{s}^{-1/2}\mathbf{U}^{\dagger}\mathbf{S}\mathbf{U}\mathbf{s}^{-1/2} = \mathbf{s}^{-1/2}\mathbf{s}\mathbf{s}^{1/2} = \mathbf{1}. \tag{2.106}$$

2.5.4 Unrestricted Hartree-Fock

Adding an electron to a closed-shell system will turn the system into an open-shell system, where the new electron will interact differently with spin-up and spin-down electrons present in the system. This is because exchange is felt by parallel spins only. In such a case, using restricted spin orbitals is limiting, and it turns out that the energy is lowered when the spin orbitals have different spatial function for different spins. This motivates the introduction of unrestricted spin orbitals defined as

$$\psi_k(\mathbf{q}) = \begin{cases} \phi_k^{\alpha}(\mathbf{r})\alpha(s), \\ \quad \text{or} \\ \phi_k^{\beta}(\mathbf{r})\beta(s). \end{cases} \tag{2.107}$$

That is, electrons with spin α are described by a set of spatial orbitals $\{\phi_k^{\alpha}\}$, while electrons with spin β are described by a different set $\{\phi_k^{\beta}\}$.

To derive the unrestricted, spatial form of the Hartree-Fock equation, we need to insert the definition in Eq. (2.107) into Eq. (2.72), resulting in

$$\mathcal{F}(\mathbf{q})\psi_k(\mathbf{q}) = \epsilon_k\psi_k(\mathbf{q}) \quad \Rightarrow \quad \begin{aligned} \mathcal{F}(\mathbf{r})\phi_k^{\alpha}(\mathbf{r})\alpha(s) &= \epsilon_k^{\alpha}\phi_k^{\alpha}(\mathbf{r})\alpha(s), \\ \mathcal{F}(\mathbf{r})\phi_k^{\beta}(\mathbf{r})\beta(s) &= \epsilon_k^{\beta}\phi_k^{\beta}(\mathbf{r})\beta(s), \end{aligned} \tag{2.108}$$

where we have made distinction between the orbital energies ϵ_k^{α} and ϵ_k^{β}, since corresponding spatial orbitals are different. The next step in derivation, is the same as for the restricted spin orbitals; multiplying from left by $\alpha^*(s)$ or $\beta^*(s)$ (depending on if we are considering the equation for ϕ_k^{α} or ϕ_k^{β}), and integrating out the spin degrees of freedom. This leads to

$$\int \alpha^*(s)\mathcal{F}(\mathbf{r})\alpha(s)\ \mathrm{d}s\phi_k^{\alpha}(\mathbf{r}) = \epsilon_k^{\alpha}\phi_k^{\alpha}(\mathbf{r}), \tag{2.109a}$$

$$\int \beta^*(s)\mathcal{F}(\mathbf{r})\beta(s)\ \mathrm{d}s\phi_k^{\beta}(\mathbf{r}) = \epsilon_k^{\beta}\phi_k^{\beta}(\mathbf{r}). \tag{2.109b}$$

Now, an electron with spin α will have an effective interaction, consisting of Coulomb and exchange interaction with all spin α electrons, and only Coulomb interaction with

spin β electrons. An analogous argument can be used for electrons of spin β. Thus, the integrals on the left hand side can be written as

$$\mathcal{F}^{\alpha}(\mathbf{r}) = \int \alpha^*(s)\mathcal{F}(\mathbf{r})\alpha(s)\,\mathrm{d}s = \hbar + \sum_{l=1}^{N_\alpha} J_l^{\alpha}(\mathbf{r}) - K_l^{\alpha}(\mathbf{r}) + \sum_{l=1}^{N_\beta} J_l^{\beta}(\mathbf{r}), \tag{2.110a}$$

$$\mathcal{F}^{\beta}(\mathbf{r}) = \int \beta^*(s)\mathcal{F}(\mathbf{r})\beta(s)\,\mathrm{d}s = \hbar + \sum_{l=1}^{N_\beta} J_l^{\beta}(\mathbf{r}) - K_l^{\beta}(\mathbf{r}) + \sum_{l=1}^{N_\alpha} J_l^{\alpha}(\mathbf{r}), \tag{2.110b}$$

where the exchange and Coulomb operators are defined in analogy to our previous definitions in Eq. (2.76)

$$J_l^{\alpha}\phi^{\alpha}(\mathbf{r}) = \int \frac{\phi_l^{\alpha *}(\mathbf{r}')\phi_l^{\alpha}(\mathbf{r}')}{|\mathbf{r}-\mathbf{r}'|}\,\mathrm{d}\mathbf{r}'\ \phi^{\alpha}(\mathbf{r}), \tag{2.111a}$$

$$K_l^{\alpha}\phi^{\alpha}(\mathbf{r}) = \int \frac{\phi_l^{\alpha *}(\mathbf{r}')\phi^{\alpha}(\mathbf{r}')}{|\mathbf{r}-\mathbf{r}'|}\,\mathrm{d}\mathbf{r}'\ \phi_l^{\alpha}(\mathbf{r}). \tag{2.111b}$$

The definitions of J_l^{β} and K_l^{β} are analogous. Note that the self-interaction is eliminated in both $\mathcal{F}^{\alpha}$ and $\mathcal{F}^{\beta}$, since

$$[J_l^{\alpha} - K_l^{\alpha}]\phi_l^{\alpha}(\mathbf{r}) = [J_l^{\beta} - K_l^{\beta}]\phi_l^{\beta}(\mathbf{r}) = 0. \tag{2.112}$$

Thus, we can now define the Hartree-Fock equations for unrestricted spin orbitals as

$$\mathcal{F}^{\alpha}(\mathbf{r})\phi_k^{\alpha}(\mathbf{r}) = \epsilon_k^{\alpha}\phi_k^{\alpha}(\mathbf{r}), \tag{2.113a}$$

$$\mathcal{F}^{\beta}(\mathbf{r})\phi_k^{\beta}(\mathbf{r}) = \epsilon_k^{\beta}\phi_k^{\beta}(\mathbf{r}). \tag{2.113b}$$

These equations are, however, coupled and cannot be solved independently. This is because $\mathcal{F}^{\alpha}$ depends on β orbitals through J_l^{β}, while $\mathcal{F}^{\beta}$ depends on α orbitals through J_l^{α}.

2.5.5 Introduction of a Basis: Pople-Nesbet Equations

In order to solve the unrestricted Hartree-Fock equations (2.113), we use the same philosophy as we used to derive the Roothaan equation; we introduce some known basis set and convert the unrestricted Hartree-Fock equations to matrix equations. More specific, we expand ϕ^{α} and ϕ^{β} in terms of a set $\{\varphi_p\}$;

$$\phi_k^{\alpha}(\mathbf{r}) = \sum_{q=1}^{M} C_{qk}^{\alpha}\varphi_q(\mathbf{r}), \qquad k = 1, \ldots, N_\alpha, \tag{2.114a}$$

$$\phi_k^{\beta}(\mathbf{r}) = \sum_{q=1}^{M} C_{qk}^{\beta}\varphi_q(\mathbf{r}), \qquad k = 1, \ldots, N_\beta. \tag{2.114b}$$

Substituting these expansions in the corresponding equations, multiplying with $\varphi_p^*(\mathbf{r})$ and integrating over coordinate $\mathbf{r}$, gives us the so-called Pople-Nesbet equations;

$$\sum_{q=1}^{M} F_{pq}^{\alpha} C_{qk}^{\alpha} = \epsilon_k^{\alpha} \sum_{q=1}^{M} S_{pq} C_{qk}^{\alpha}, \tag{2.115a}$$

$$\sum_{q=1}^{M} F_{pq}^{\beta} C_{qk} = \epsilon_k^{\beta} \sum_{q=1}^{M} S_{pq} C_{qk}^{\beta}, \tag{2.115b}$$

or more compactly

$$\mathbf{F}^{\alpha}\mathbf{C}^{\alpha} = \mathbf{S}\mathbf{C}^{\alpha}\boldsymbol{\epsilon}^{\alpha}, \tag{2.116a}$$

$$\mathbf{F}^{\beta}\mathbf{C}^{\beta} = \mathbf{S}\mathbf{C}^{\beta}\boldsymbol{\epsilon}^{\beta}, \tag{2.116b}$$

where $\mathbf{F}^{\alpha}$ and $\mathbf{F}^{\beta}$ are the matrix representation of $\mathcal{F}^{\alpha}$ and $\mathcal{F}^{\beta}$ operators, $\mathbf{C}^{\alpha}$ and $\mathbf{C}^{\beta}$ are the coefficient matrices with dimensions $M \times N_{\alpha}$ and $M \times N_{\beta}$ respectively, $\mathbf{S}$ is the overlap matrix, and finally $\boldsymbol{\epsilon}^{\alpha}$ and $\boldsymbol{\epsilon}^{\beta}$ are the rectangular diagonal matrices of orbital energies for the α and β orbitals.

By defining the density matrices

$$P_{pq}^{\alpha} = \sum_{l}^{N_{\alpha}} C_{pl}^{\alpha} (C_{ql}^{\alpha})^*, \tag{2.117a}$$

$$P_{pq}^{\beta} = \sum_{l}^{N_{\beta}} C_{pl}^{\beta} (C_{ql}^{\alpha})^*, \tag{2.117b}$$

we can express the Fock matrix elements as[9]

$$F_{pq}^{\alpha} = h_{pq} + \sum_{rs}^{M} P_{rs}^{\alpha} \Big(g_{prqs} - g_{prsq} \Big) + \sum_{rs}^{M} P_{rs}^{\beta} g_{prqs}, \tag{2.118a}$$

$$F_{pq}^{\beta} = h_{pq} + \sum_{rs}^{M} P_{rs}^{\beta} \Big(g_{prqs} - g_{prsq} \Big) + \sum_{rs}^{M} P_{rs}^{\alpha} g_{prqs}, \tag{2.118b}$$

and the energy functional as

$$E = \frac{1}{2} \sum_{pq}^{M} \Big[(P_{pq}^{\alpha} + P_{pq}^{\beta}) h_{pq} + P_{pq}^{\alpha} F_{pq}^{\alpha} + P_{pq}^{\beta} F_{pq}^{\beta} \Big]. \tag{2.119}$$

In order to solve the matrix eigenvalue problems in Eq. (2.116), we must orthonormalize the basis set, diagonalize the Fock matrix in the new orthonormal basis, and thereafter transform the resulting coefficient matrices back to the old basis, just as described in Section 2.5.3.

[9] For more detailed derivation see Section 3.8 in Ref. [6].

Chapter 3

Atomic Basis Functions for Molecular Hartree-Fock Calculations

In Hartree-Fock theory, the exact electronic wave function of a physical system is approximated by a single Slater determinant formed from one-electron spin orbitals ψ_k. Each spin orbital is in most applications expressed as a product of a spatial function and a spin function, where the former is expressed as a linear combination in some known basis set (see Figure 3.1);

$$\phi_k(\mathbf{r}) = \sum_p C_{pk}\varphi_p(\mathbf{r}). \tag{3.1}$$

The basis functions φ_p, along with the spin functions α and β, are the core elements in the Hartree-Fock wave function. The quality of the wave function is fully determined by the form of the spatial basis functions. By incorporating the physical characteristics of the electronic system in our basis, we will improve the quality of the total wave function. Thus, the choice of basis for expanding the spatial orbitals, is extremely important, and an enormous amount of effort has gone into developing mathematical and computational techniques to construct suitable basis sets.

In this chapter, the mathematical properties of the most common basis sets, used in molecular orbital calculations, are investigated with focus on the Gaussian basis sets. The material in this chapter is based on Chapter 6 of Ref. [10], Chapter 2 of Ref. [6], and Chapter 6 of Ref. [7].

3.1 Basis Sets

An enormous amount of effort has gone into developing computational and mathematical models to reach the Hartree-Fock limit (HF limit), which is to say to solve the Hartree-Fock equation with the equivalent of an infinite basis set [10]. At this limit, the error in energy (correlation energy) associated with the Hartree-Fock approximation is given as

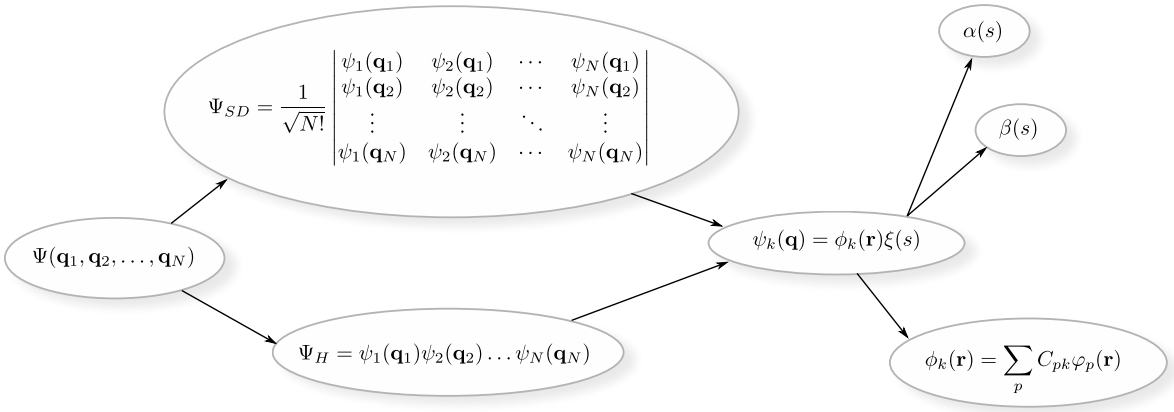

Figure 3.1: The structure of the Hartree and Hartree-Fock wave function. The coordinates $\mathbf{q}$ include both spatial and spin coordinates. ψ_k is spin orbital k, $\alpha(s)$ and $\beta(s)$ are spin functions, ϕ_k is the spatial part of spin orbital k, expanded in a set of spatial functions $\{\varphi_p\}$.

$$E_{\text{corr}} = E - E_{\text{HF}}, \tag{3.2}$$

where E is the true energy, and E_{HF} is the energy of the system at the HF limit. In practice, we are restricted to work with finite basis sets, generally leading to a solution which is not at the HF limit. The best we can do is to use basis functions that allow for an efficient and systematic extension towards the HF limit. A lot of work has therefore been done to identify such basis functions. Ideally, a suitable set of basis functions satisfy two other requirements, in addition to allow for a systematic extension towards completeness. Firstly, the basis should allow for a rapid convergence to any atomic or molecular electronic state, requiring only a few terms for a reasonably accurate description of the electronic distribution [7]. Secondly, the basis functions should have a closed-form that makes integral evaluations, required in Self-Consistent Field (SCF) calculations, easy and efficient. It should be mentioned that, although keeping the number of basis functions to a minimum is desired, sometimes it may be better to use larger basis sets if the integral evaluations can be carried out faster than for a smaller basis set.

3.1.1 Many-center Expansions

In the Born-Oppenheimer approximation (see Section 2.1.3), the electrons move in a field generated by a static configuration of the nuclei. As a result, the electronic wave function depends implicitly on the coordinates of the nuclei. Within this approximation, the most obvious difference between the wave function of an atomic system and a molecular system, is that the wave function of the latter depends (implicitly) on the coordinates of more than one nucleus. An atomic wave function, in contrast, depends only on the coordinates of the single nucleus. This difference has, of course, important consequences for the expansion of the spatial orbitals. While atomic orbitals (AOs) can

simply be represented by one-center expansions (the basis functions are centered on the single nucleus), there is often no simple way to do the same in the representation of molecular orbitals (MOs).

One way to represent MOs, is to use the linear combination of atomic orbitals (LCAO) (see Section 2.2.2) approach *with* many-center expansions. This involves introducing a separate basis for each atom in the molecule. To illustrate this type of construction, we consider the representation of MOs for the water molecule (H_2O). In this system all electrons have to deal with three nucleus; two hydrogen nuclei and one oxygen nucleus. Using the many-center expansion we can express the MO ϕ_k as

$$\begin{aligned}\phi_k\left(\mathbf{r};\mathbf{R}_{\mathrm{H}^1},\mathbf{R}_{\mathrm{H}^2},\mathbf{R}_{\mathrm{O}}\right) = &\sum_p C_{pk}^{\mathrm{H}^1}\varphi_p^{\mathrm{H}}(\mathbf{r};\mathbf{R}_{\mathrm{H}^1}) \\ &+ \sum_p C_{pk}^{\mathrm{H}^2}\varphi_p^{\mathrm{H}}(\mathbf{r};\mathbf{R}_{\mathrm{H}^2}) \\ &+ \sum_p C_{pk}^{\mathrm{O}}\varphi_p^{\mathrm{O}}(\mathbf{r};\mathbf{R}_{\mathrm{O}}),\end{aligned} \tag{3.3}$$

where $\mathbf{R}_{\mathrm{H}^1}$, $\mathbf{R}_{\mathrm{H}^2}$ and $\mathbf{R}_{\mathrm{O}}$ are the coordinates of the hydrogen nuclei and the oxygen nucleus, respectively. The first two terms are linear combinations of AOs associated with the hydrogen atoms, centered around the nuclei H^1 and H^2, respectively. The last term is a linear combination of AOs associated with the oxygen atom, centered around the oxygen nucleus. In this description all AOs, regardless of the atom they belong to, serve simply as basis functions. Note the use of ";" instead of a comma in the variable list of the functions, to clearly show the implicit dependency on nuclear coordinates. It is important to be aware that since the dependency on nuclear coordinates is just implicit, the basis functions $\varphi_p^{\mathrm{H}}(\mathbf{r};\mathbf{R}_{\mathrm{H}^1})$ and $\varphi_p^{\mathrm{H}}(\mathbf{r};\mathbf{R}_{\mathrm{H}^2})$ are considered as different functions, although the form of the functions are identical. Furthermore, the centering of basis functions on the nuclei is just a choice we make, and certainly not a requirement. This is just part of the many-center procedure of the MOs. Indeed, our intuition suggests that they should be centered on the nuclei, but this should not limit our mathematical flexibility. Ultimately, what we are trying is to express some unknown function (MO ψ_k) in terms of a set of known functions. This is a mathematical problem, without any requirements on the centering of the basis functions.

The idea of representing MOs by nucleus-centered AOs (Eq. (3.3)), must be applied carefully and any additional functions that may be needed to describe the physical characteristics of the molecular system, must be included as well. The main advantage of using many-center expansions, is that the physical characteristics of the atomic systems can be incorporated in the basis, and we can in a systematic way combine AOs to set up the wave function of polyatomic molecules. The drawback of many-center expansions is the lost of the analytic relationships such as orthogonality and recurrence relations.

3.1.2 Construction of Atomic Orbitals

With the exception of the hydrogen atom, where the exact form of its orbitals can be found, numerical methods must be applied to find the AOs associated with other atoms. In such cases, a numerical calculation with high precision is performed to find the numerical orbitals. These numerical orbitals are thereafter approximated by a least-square expansion of some convenient set of functions $\{\tilde{\varphi}_a\}$. In mathematical notation this means

$$\varphi_p = \sum_a d_{ap}\tilde{\varphi}_a, \tag{3.4}$$

where the coefficients d_{ap} most be chosen such that the expansion fits the AO φ_p in an optimal way. The expansion functions $\tilde{\varphi}_a$ are typically hydrogenic functions, Slater-type functions or Gaussian-type functions. Today, we have good least-square expansions for AOs associated with a large number of atoms, which are specially designed for orbitals of various atoms. Note that the coefficients d_{ap} are fixed in the course of a molecular SCF calculation and are not allowed to change. The variation in molecular SCF calculations is done on the coefficients C_{pk}.

As an extension to Figure 3.1, all the different elements used to represent MOs in a polyatomic molecule, are shown in Figure 3.2. The simple representation of an MO given in Eq. (3.1), is first separated into sums over AOs associated with the different atoms. Further, the AOs themselves are represented by an expansion over convenient functions, such as hydrogenic functions, Slater-type functions or Gaussian functions.

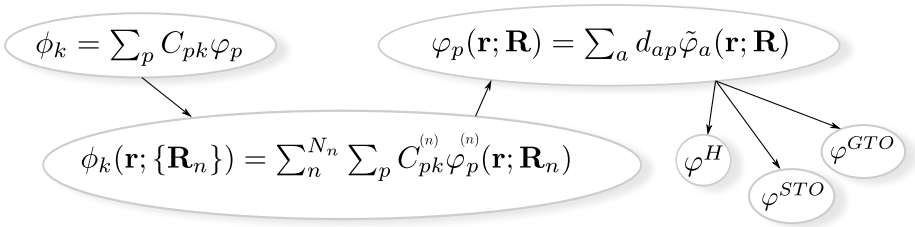

Figure 3.2: The many-center expansion of AOs to form a single MO. The MO ϕ_k depends parametrically on the coordinates of all nuclei, while the AOs $\varphi_{p,n}$ depend on the coordinates of their own nucleus only. N_n specifies the number of nuclei. Each AO is represented by a least-square expansion, specially designed for the specific AO, using well-known functions such as hydrogenic functions, Slater-type functions or Gaussian functions.

It should be emphasized once more that the hierarchy shown in Figure 3.2, is just one way to represent the MOs. There are no theoretical requirements, within the Hartree-Fock theory, whatsoever on how the MOs should be represented as long as they are orthogonal. However, the procedure represented here is the most usual way to represent MOs, and is widely used in molecular orbital theory.

3.2 Hydrogenic Functions

The one-electron hydrogenic system is one of very few systems where Schrödinger's equation can be solved exactly. The Hamiltonian for this system is given by

$$\mathcal{H} = -\frac{1}{2}\nabla^2 - \frac{Z}{r}, \tag{3.5}$$

where Z is the nuclear charge, and r is the distance between the electron and the nucleus. The eigenstates of this Hamiltonian can be written in a closed-form and it is natural to use them as basis functions to expand AOs of other atoms. The set of eigenstates can be written as a product of an angular part and a radial part [7];

$$\varphi^{\mathrm{H}}_{n\ell m_\ell} = R^{\mathrm{H}}_{n\ell}(r) Y_{\ell m_\ell}(\theta, \tau), \tag{3.6}$$

$$Y^{m_\ell}_\ell(\theta, \tau) = \sqrt{\frac{2\ell+1}{4\pi}\frac{(\ell-m_\ell)!}{(\ell+m_\ell)!}}\, P^{m_\ell}_\ell(\cos\theta)\, e^{i m_\ell \tau}, \tag{3.7}$$

$$R^{\mathrm{H}}_{nl}(r) = \left(\frac{2Z}{n}\right)^{3/2} \sqrt{\frac{(n-\ell-1)!}{2n(n+\ell)!}} \left(\frac{2Zr}{n}\right)^{\ell} L^{2\ell+1}_{n-\ell-1}\left(\frac{2Zr}{n}\right) \exp\left(-\frac{Zr}{n}\right), \tag{3.8}$$

where $P^{m_\ell}_\ell$ is the associated Legendre polynomial, $L^{2\ell+1}_{n-\ell-1}$ is the generalized Laguerre polynomial of degree $n-\ell-1$, n is the principal quantum number ($n > 0$), ℓ is the angular quantum number ($\ell < n$) and m_ℓ is the magnetic quantum number ($m_\ell \leq |l|$). These eigenfunctions are usually referred to as 1s, 2s, 2p, 3s, 3p, 3d, etc., depending on the quantum numbers n and ℓ. For example, $\varphi^{\mathrm{H}}_{200}$ is known as the 2s eigenfunction, while $\varphi^{\mathrm{H}}_{210}$ is a 2p eigenfunction. In Figure 3.3, the radial distribution function $(R^{\mathrm{H}}_{n\ell}\, r)^2$ is plotted for some of the hydrogenic functions with $Z = 1$. This quantity is the probability density of finding the electron in a thin spherical shell with radius r, divided by 4π.

The hydrogenic eigenfunctions are orthonormal, which follows directly from the fact that they are eigenfunctions of the Hermitian operator given in Eq. (3.5). This has the advantage of making the overlap matrix identical to the identity matrix. Furthermore, the presence of the exponential in $-Zr/n$, ensures that the wave function decays exponentially at large distances, which is a required property. However, the hydrogenic eigenfunctions have their disadvantages. In fact, they turns out to be not so useful as basis functions for many-electron systems. First, the unbound states must be supplemented by the continuum states [7], since they by themselves don't set up a complete basis, which of course is a disadvantage from a computational point of view. Second, because of the presence of the inverse quantum number n^{-1} in the exponential, they tend to spread out quickly with increasing principal quantum number n. In particular, this becomes clear in the expectation value of r;

$$\langle \varphi^{\mathrm{H}}_{n\ell m_\ell} |\, r\, | \varphi^{\mathrm{H}}_{n\ell m_\ell} \rangle = \frac{3n^2 - \ell(\ell+1)}{2Z}, \tag{3.9}$$

reflecting the diffuseness of the eigenfunctions. This behavior is problematic and we will in practice need a large number of functions to describe both the core- and valence regions of a many-electron system.

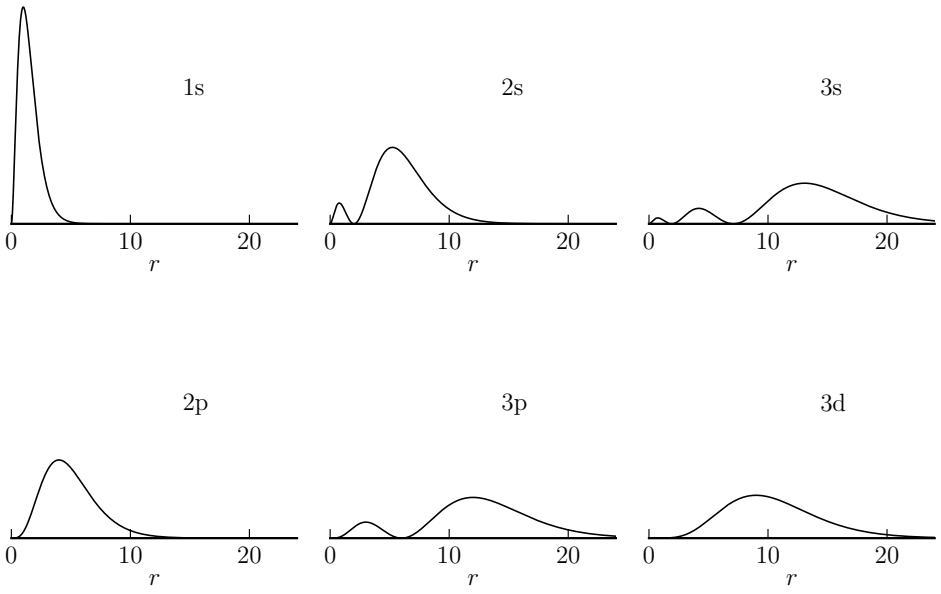

Figure 3.3: The radial distribution function $(R^{\mathrm{H}}_{n\ell}r)^2$ of hydrogenic functions for $Z = 1$. The scales are the same in all plots.

3.3 Slater-Type Orbitals

Another class of functions that often is used as a basis set, are the so-called Slater-type orbitals (STOs), which retain the exponential form of the hydrogenic functions, and at the same time avoid the problems associated with the use of continuum states. The mathematical form of these functions, for some exponent ζ, is given by

$$\varphi^{\mathrm{STO}}_{n\ell m_\ell} = R^{\mathrm{STO}}_n(r) Y^{m_\ell}_\ell(\theta, \tau), \tag{3.10}$$

$$R^{\mathrm{STO}}_n(r) = \frac{(2\zeta)^{3/2}}{\sqrt{(2n)!}} (2\zeta r)^{n-1} \exp\left(-\zeta r\right), \tag{3.11}$$

where the quantum numbers n, ℓ and m_ℓ take on the same values as in the hydrogenic case, and the nomenclature is also the same as for hydrogenic functions. For example, $\varphi^{\mathrm{STO}}_{200}$ is referred to as 2s STO (not the same as the 2s hydrogenic function!). For a fixed exponent ζ, the STOs are complete, but not orthogonal. They are, however, still very much attractive as basis functions, because of the flexibility they offer. This flexibility is reflected in the representation of the radial part of the one-electron space, where not only functions with different quantum numbers n can be used, but also functions with different exponents ζ_n are available. The reason for this becomes clear if we study where the maximum in the radial distribution curve occurs. This value is found by setting the derivative of the radial distribution function $(R^{\mathrm{STO}}_n r)^2$ equal to zero;

$$\frac{\mathrm{d}}{\mathrm{d}r}(R^{\mathrm{STO}}_n r)^2 = 0, \quad \Rightarrow \quad r^{\mathrm{STO}}_{\mathrm{max}} = \frac{n}{\zeta}. \tag{3.12}$$

Now, if we, for example, calculate the radial maximum $r_{\max}^{\mathrm{STO}}$ for 1s STO with exponents $\zeta_n = n^{-1}$, we will get the same radial maximum as we will get for 1s, 2s and 3s STOs with fixed exponent $\zeta = 1$ (see Figure 3.4). This hints to the possibility of using STOs with different exponents as an alternative to functions with different quantum numbers n.

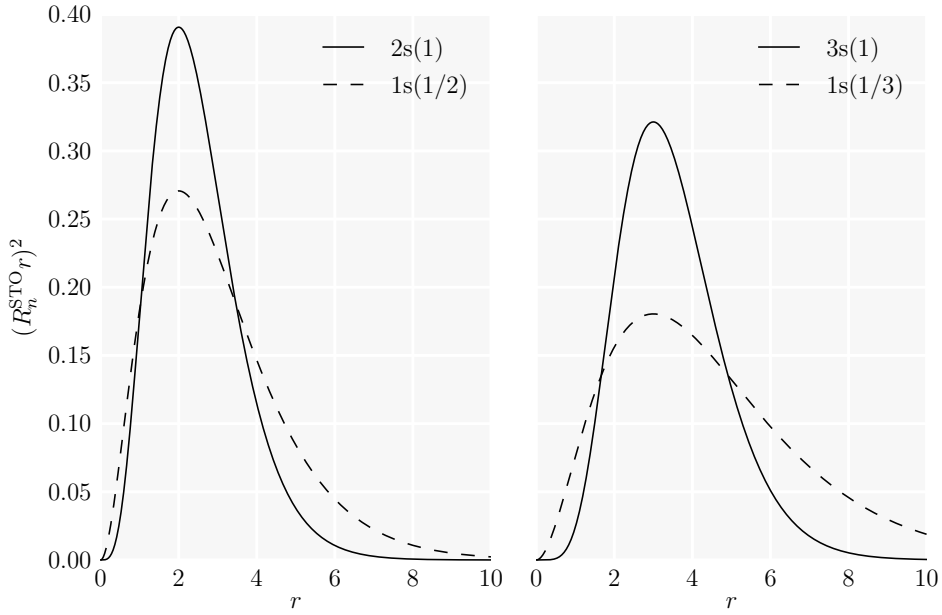

Figure 3.4: The radial distribution function $(R_n^{\mathrm{STO}} r)^2$, in atomic units, for 2s(1) and 1s(1/2) STOs (left), and for 3s(1) and 1s(1/3) STOs (right). The notation is $n\mathrm{s}(\zeta)$. The radial maximum is the same for STOs in each figure.

The remaining question is if it is possible to generate a complete set of functions by combining STOs with variable exponents. In particular, as discussed in Ref. [7], the basis of type $(1\mathrm{s}(\zeta_{1\mathrm{s}}),\ 1\mathrm{s}(\zeta_{2\mathrm{s}}), \dots)$, $(2\mathrm{p}(\zeta_{1\mathrm{p}}),\ 2\mathrm{p}(\zeta_{2\mathrm{p}}), \dots)$, etc., is complete. In this basis for each angular momentum ℓ, only the functions of the lowest principal quantum number n, are used. For example, to represent the numerically obtained 2s orbital of, let say, carbon, the following expansion can be used

$$\varphi_{2\mathrm{s}} = \sum_n d_n \varphi_{100}^{\mathrm{STO}}(\zeta_n), \tag{3.13}$$

where only the 1s STO (lowest n with $\ell = 0$) with variable exponent is used. An alternative to this type of basis, is to use a single, fixed exponent basis of type (1s, 2s, ...), (2p, 3p, ...), and so on, where the radial space is described by functions with different n, all with the same exponent ζ. Using this basis the 2s orbital of carbon can be represented as

$$\varphi_{2\mathrm{s}} = \sum_n d_n \varphi_{n00}^{\mathrm{STO}}(\zeta). \tag{3.14}$$

In practice, the best results are achieved when the one-electron space is expanded both in terms of principal quantum number and by means of variable exponents. For the *radial* 1s, 2s and 2p orbitals of the carbon atom, using a mix of these two basis types and only three STOs, the following least-square expansions are optimal[1]

$$\varphi_{1s}^{\text{radial}} = 0.998R_{1s}^{\text{STO}}(r,\zeta_{1s}) + 0.009R_{2s}^{\text{STO}}(r,\zeta_{2s}), \tag{3.15}$$

$$\varphi_{2s}^{\text{radial}} = -0.231R_{1s}^{\text{STO}}(r,\zeta_{1s}) + 1.024R_{2s}^{\text{STO}}(r,\zeta_{2s}), \tag{3.16}$$

$$\varphi_{2p}^{\text{radial}} = R_{2p}^{\text{STO}}(r,\zeta_{2p}), \tag{3.17}$$

where $\zeta_{1s} = 5.58$, $\zeta_{2s} = 1.57$ and $\zeta_{2p} = 1.46$. Note that since we only had one STO with p symmetry, $\varphi_{2p}^{\text{radial}}$ is fully represented by the R_{2p}^{STO}. The s orbitals, in contrast, are represented by STOs with different quantum numbers n and different exponents.

The STOs give quite remarkable results for atoms and diatomic molecules, but are much less convenient for other molecular systems. This is mainly because of the lack of efficient methods for calculating the many-center, two-electron STO integrals required for molecular calculations. In fact, the integral evaluations are so inefficient for molecular systems, that STOs are replaced with more convenient functions, namely the Gaussian-type orbitals.

3.4 Gaussian-Type Orbitals

In modern computational chemistry, Gaussian-type orbitals (GTOs) are the most used functions in molecular calculations. This is mainly due to the existence of efficient methods for the evaluation of many-center integrals required in molecular SCF calculations. In spherical coordinates, the nonorthogonal basis functions spanning a complete basis, known as the *spherical-harmonic Gaussian-type orbitals* (GTOs), are given by

$$\varphi_{n\ell m_\ell}^{\text{GTO}} = R_{n\ell}^{\text{GTO}}(r)Y_\ell^{m_\ell}(\theta,\tau) \tag{3.18}$$

$$R_{n\ell}^{\text{GTO}}(r) = \frac{2(2\alpha)^{3/4}}{\pi^{1/4}}\sqrt{\frac{(4\alpha)^{2n-\ell-2}}{(4n-2\ell-3)!!}}r^{2n-\ell-2}\exp\left(-\alpha r^2\right), \tag{3.19}$$

where the quantum numbers n, ℓ and m_ℓ take on the same values as STOs (and hydrogenic functions), and the nomenclature is the same as for STOs (and hydrogenic functions). As an example, $\varphi_{200}^{\text{GTO}}$ is referred to as 2s GTO. The exponent α is a positive number larger than zero, and determines the size or the diffuseness of the function; a large exponent implies a dense function, while a small exponent implies a diffuse function. The most important difference between STOs and GTOs is the decay term, which is an exponential in r^2 for GTOs, in contrast to STOs where the decay term is an exponential in r. Therefore, the GTOs will decay much more rapidly than the STOs (see Figure 3.5).

As for the STOs, GTOs with variable exponents can be used to describe the radial space. However, in contrast to STOs, the radial space is exclusively described by means

[1]The expansion coefficients and the exponents are taken from Ref. [7].

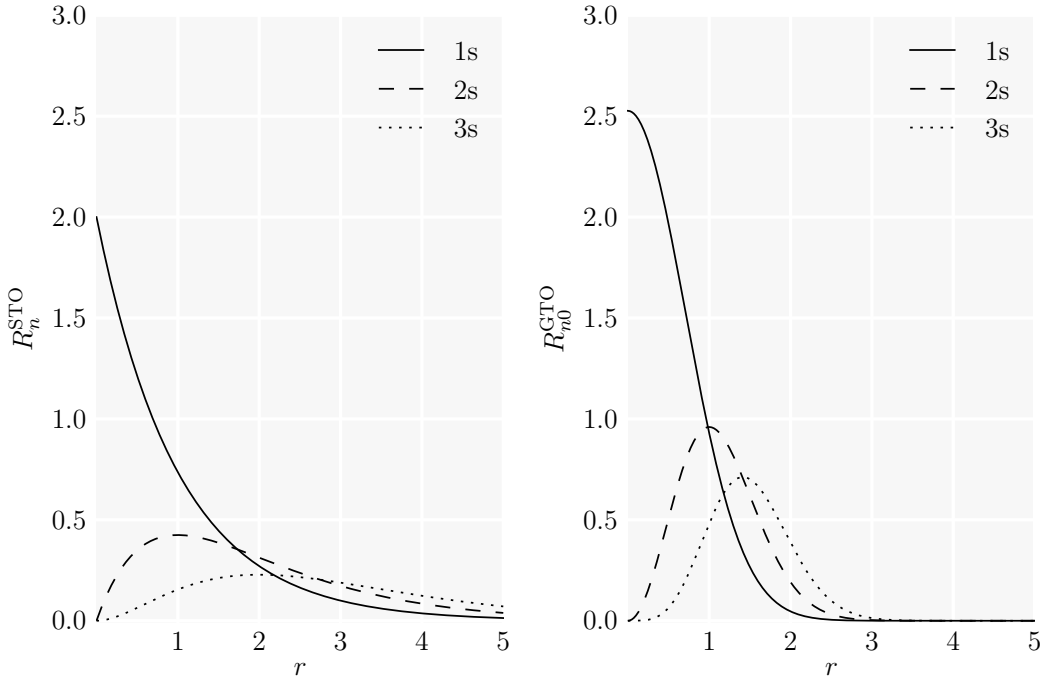

Figure 3.5: The radial forms R_n^{STO} of the STOs (left) and R_{n0}^{GTO} of the GTOs (right) for $\ell = 0$ with unit exponent.

of variable exponents, with the same quantum number $n = \ell + 1$. In practice, any basis function of s symmetry, for example 2s and 3s Slater functions, will be expanded in only 1s Gaussians (with variable exponent), any basis function of p symmetry, will be expanded in only 2p Gaussians (with variable exponent), and so on. The reason for just using functions with lowest quantum number n for each ℓ, is due to the simplifications that arise in the integral evaluations. These simplifications are not present for higher quantum numbers n [10]. In the case of variable exponent, we can rewrite Eq. (3.18) simply by inserting $\ell + 1$ for n, to arrive at the following complete set of spherical-harmonic GTOs

$$\varphi_{\alpha_n \ell m_\ell}^{\mathrm{GTO}} = R_{\alpha_n \ell}^{\mathrm{GTO}}(r) Y_\ell^{m_\ell}(\theta, \tau), \tag{3.20}$$

$$R_{\alpha_n \ell}^{\mathrm{GTO}}(r) = \frac{2(2\alpha_n)^{3/4}}{\pi^{1/4}} \sqrt{\frac{(4\alpha_n)^\ell}{(2\ell+1)!!}} r^\ell \exp\left(-\alpha_n r^2\right). \tag{3.21}$$

The completeness of this modified set is discussed in Ref. [7].

3.4.1 Cartesian Gaussian-Type Orbitals

A very important feature of the Gaussian distributions is their separability in Cartesian directions. This simplifies integral evaluations in SCF calculations significantly. The set of *Cartesian GTOs* are defined as

$$\varphi_{ijk}^{\mathrm{GTO}}(x,y,x) = \varphi_i^{\mathrm{GTO}}(x)\varphi_j^{\mathrm{GTO}}(y)\varphi_k^{\mathrm{GTO}}(z), \tag{3.22}$$

where the x component is given by

$$\varphi_i^{\mathrm{GTO}}(x) = \left(\frac{2\alpha}{\pi}\right)^{(1/4)} \sqrt{\frac{(4\alpha)^i}{(2i-1)!!}} x^i \exp(-\alpha x^2), \tag{3.23}$$

and similar for the y and z component. When all the non-negative integers i, j and k are zero, the GTO has the spherical symmetry and is called an s-type GTO. When one of the indices is one, the GTO has axial symmetry about a single axis and is called p-type GTO. In this case there are three possibilities, leading to p_x, p_y and p_z GTOs. Further, if the sum of indices is two, we have d-type GTO, where there are in total six possible combinations of i,j and k that sum up to two. The f-type GTOs, g-type GTOs, etc. can be defined in the same way.

3.4.2 Contracted Gaussian-Type Orbitals

Normally one would prefer to use STOs as basis functions in expansion of AOs instead of GTOs. This because the former describe more correctly the qualitative features of the electronic structure. A fewer number of functions would therefore be needed in the expansion for comparable results. The evaluation of many-center integrals with STOs is, however, extremely time consuming compared to GTOs, where all integrals can be evaluated rapidly and efficiently. As an attempt to combine the best feature of GTOs (computational efficiency) with that of STOs (proper radial shape), a fixed linear combination of Gaussian functions is used to represent AOs. This is equivalent to what we did with STOs, but linear combinations of Gaussian functions usually involve more terms compared to the corresponding linear combination of STOs. The linear combination of GTOs, known as contracted Gaussian-type orbitals (CGTOs), can in Cartesian coordinates be written as

$$\varphi_p^{\mathrm{CGTO}}(x,y,z;\{\alpha\}) = \sum_a d_{ap}\, \varphi_{ijk}^{\mathrm{GTO}}(x,y,z;\alpha_a), \tag{3.24}$$

where the contraction coefficients d_{ap} and the exponent α_a are chosen to optimize the description of the specific AO. The individual Gaussian functions $\varphi_{ijk}^{\mathrm{GTO}}$ are called primitive Gaussian-type orbitals (GTOs), and the total number of them used to form the CGTO is referred to as contraction length. Note that the contraction parameters are chosen in advance, and are not allowed to change in the course of an SCF calculations.

With a proper choice of parameters, the expansion in Eq. (3.24) can in principle be used to describe any function, such as Slater-type functions, atomic Hartree-Fock functions, etc. In this way we can avail ourselves of the efficient methods associated with integral evaluation of Gaussian functions, and at the same time have an acceptable description of the electronic structure. Indeed, the number of functions in the expansion of AOs is larger compared to STOs, but the integral evaluations are much more efficient when using GTOs.

3.4.3 Minimal Basis Sets

A minimum or single-zeta basis set is usually defined as a set with only one basis function for each occupied AO in the atom. This definition is, however, a bit imprecise. For example, a basis consisting of the basis functions[2] 1s, 2s, $2p_x$, $2p_y$, and $2p_z$ is considered as minimal for Li and Be, although the 2p orbitals are not occupied in these two atoms. The reason for why the term minimal is still used, is because one considers the occupation (partially or completely) of electron shells (2sp, 3sp, ..., etc.) in atoms, instead of orbitals, when using the term minimal basis. It doesn't matter if the shell is partially or completely filled, what matters is if any orbital in the shell is occupied. Thus the minimal basis for H and He consists of just one function, Li to Ne contain five functions, Na to Ar contain nine function, and so on.

Since the minimal basis set contains very few basis functions, these should, at least, have good quality, in order to compensate for the low number of functions in the set. From this perspective STOs should be used rather than GTOs, but then we will have efficiency issues in the integral evaluations. One way to get around this problem is to use GTOs to approximate STOs. This is the idea behind the most common minimal basis set used in molecular SCF calculations, namely STO-kG. Here, one uses a contraction of k primitive GTOs for each basis function, where the contraction parameters (coefficients and exponents) are chosen so that the basis functions approximate Slater functions. That is, each STO is approximated by one CGTO, made up of three primitive GTOs. In Figure 3.6, the 1s STO-kG functions for $k = 1, \ldots, 6$ with the corresponding 1s STO with unit exponent, is shown. It is clear that at least three Gaussian functions are needed to get an acceptable representation of the 1s STO. In fact, for minimal basis set calculations the STO-3G basis set is the most popular one for exploratory investigations. Figure 3.7 gives an overview of the STO-3G minimal basis for the first-row atoms, illustrating how the Gaussian functions are combined to construct basis functions.

One important aspect of the STO-kG basis sets, is the sharing of contraction exponents in 2sp, 3sp, ..., etc., shells. That is, the contracted basis functions corresponding to 2s and 2p have the same set of exponents (see Figure 3.7). Similarly the contracted basis functions corresponding to 3s and 3p have the same exponent, and so on. This constraint leads to a considerable efficiency in integral evaluations, since all integrals involving any sp shell can be treated together. This constraint is also used in other basis set types, as we will see shortly.

3.4.4 Split-Valence Basis Sets

A minimal basis set has limited flexibility, and is not capable of giving highly accurate result in molecular calculations. One way to introduce more flexibility in the representation of AOs, is to use split-valence basis sets. This approach is based on the observation that molecule formation has little impact on the shape of inner atomic shells. Intuitively, we may therefore expect that the contracted basis functions, fitted to core AOs of separated atoms, appears with the same contraction parameters when

[2]The basis functions can be hydrogenic, STOs or GTOs.

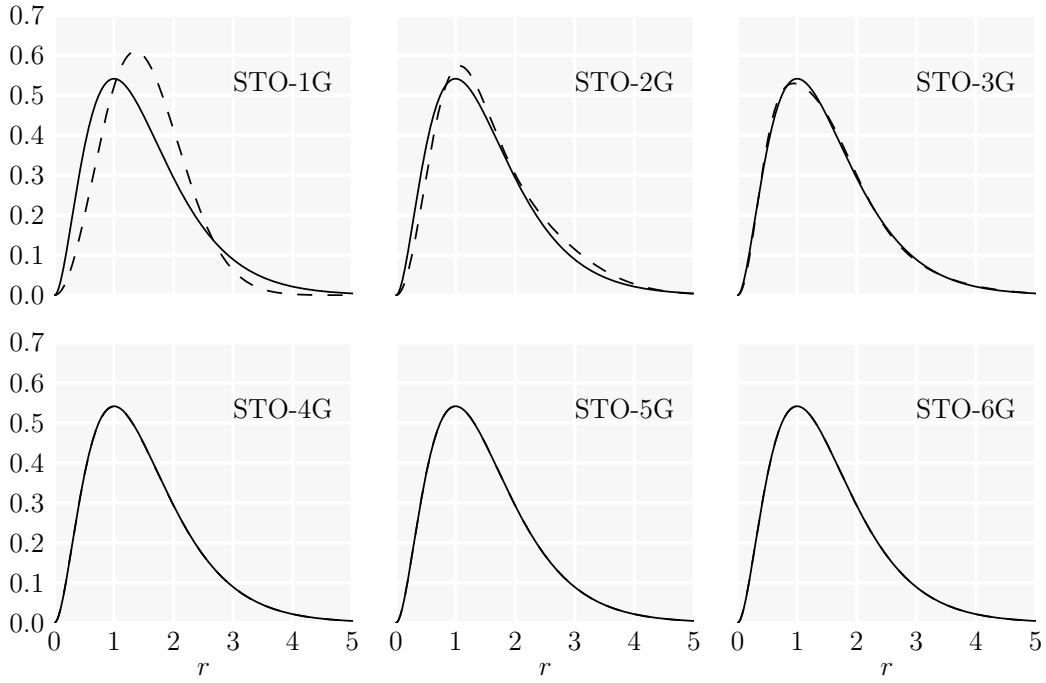

Figure 3.6: The radial distribution functions of the 1s STO-kG basis functions (dashed line) for $k = 1, \ldots, 6$, together with the 1s STO basis function (solid line) with $\zeta = 1$.

used to represent MOs. It is therefore reasonable to claim that more is gained by having flexibility in the valence basis functions than in the core. In split-valence basis sets, core orbitals continue to be represented by a single contracted basis function, while the valence orbitals are split into arbitrarily many functions (thereby the name split-valence), where each can be varied independently during construction of the MOs. The notation for these basis sets is typically $X - YZ$G, where X represents the number of primitive GTOs used in the contracted basis functions for each core AO. The letters Y and Z indicate that the valence orbitals are represented by two contracted basis functions each, the first one consisting of Y primitive Gaussians and the other one consisting of Z primitive Gaussians.

In Figure 3.8, an overview of the 3-21G basis is shown for the first-row atoms. As for the minimal basis sets, sharing of exponents between 2s and 2p CGTOs, is present but now the sharing is in $2s_I$-$2p_I$ and in $2s_{II}$-$2p_{II}$. In addition to that, the contraction coefficients are shared in $2p_I$'s p_x, p_y and p_z part, and similarly for $2p_{II}$. The valence AOs can of course be represented by more than two contracted basis functions, as it is the case in the basis set 6-311G, where the valence AOs are represented by three contracted basis functions consisting of three primitives, one primitive, and one primitive, respectively. The notation used for these types of sets is $X - YZW$G. The presence of three numbers after the hyphens implies that this basis set is a *split-valence triple-zeta* basis set. Using this terminology $X - YZ$G is a *split-valence double-zeta*

basis set, while $X-YZWV$G is a *split-valence quad-zeta* basis set.

As an example on how the flexibility in the $X-YZ$G basis is present in construction of MOs, we consider the expansion in Eq. (3.3) for the MOs of H_2O. Using the 3-21G basis this expansion can be written as

$$\begin{aligned}
\phi_k =& C_{1,k}\left(\sum_{a=1}^{2} d^{\mathrm{H}}_{1\mathrm{s}_I,a}\,\varphi^{\mathrm{GTO}}_{000}(\alpha^{\mathrm{H}}_{1\mathrm{s}_I,a};\mathbf{R}_{\mathrm{H}^1})\right) + C_{2,k}\left(d^{\mathrm{H}}_{1\mathrm{s}_{II}}\,\varphi^{\mathrm{GTO}}_{000}(\alpha^{\mathrm{H}}_{1\mathrm{s}_{II}};\mathbf{R}_{\mathrm{H}^1})\right)\\
&+C_{3,k}\left(\sum_{a=1}^{2} d^{\mathrm{H}}_{1\mathrm{s}_I,a}\,\varphi^{\mathrm{GTO}}_{000}(\alpha^{\mathrm{H}}_{1\mathrm{s}_I,a};\mathbf{R}_{\mathrm{H}^2})\right) + C_{4,k}\left(d^{\mathrm{H}}_{1\mathrm{s}_{II}}\,\varphi^{\mathrm{GTO}}_{000}(\alpha^{\mathrm{H}}_{1\mathrm{s}_{II}};\mathbf{R}_{\mathrm{H}^2})\right)\\
&+C_{5,k}\left(\sum_{a=1}^{3} d^{\mathrm{O}}_{1\mathrm{s},a}\,\varphi^{\mathrm{GTO}}_{000}(\alpha^{\mathrm{O}}_{1\mathrm{s},a};\mathbf{R}_{\mathrm{O}})\right)\\
&+C_{6,k}\left(\sum_{a=1}^{2} d^{\mathrm{O}}_{2\mathrm{s}_I,a}\,\varphi^{\mathrm{GTO}}_{000}(\alpha^{\mathrm{O}}_{2\mathrm{sp}_I,a};\mathbf{R}_{\mathrm{O}})\right) + C_{7,k}\left(d^{\mathrm{O}}_{2s_{II}}\,\varphi^{\mathrm{GTO}}_{000}(\alpha^{\mathrm{O}}_{2\mathrm{sp}_{II}};\mathbf{R}_{\mathrm{O}})\right)\\
&+C_{8,k}\left(\sum_{a=1}^{2} d^{\mathrm{O}}_{2\mathrm{p}_I,a}\,\varphi^{\mathrm{GTO}}_{100}(\alpha^{\mathrm{O}}_{2\mathrm{sp}_I,a};\mathbf{R}_{\mathrm{O}})\right) + C_{9,k}\left(d^{\mathrm{O}}_{2\mathrm{p}_{II}}\,\varphi^{\mathrm{GTO}}_{100}(\alpha^{\mathrm{O}}_{2\mathrm{sp}_{II}};\mathbf{R}_{\mathrm{O}})\right)\\
&+C_{10,k}\left(\sum_{a=1}^{2} d^{\mathrm{O}}_{2\mathrm{p}_I,a}\,\varphi^{\mathrm{GTO}}_{010}(\alpha^{\mathrm{O}}_{2\mathrm{sp}_I,a};\mathbf{R}_{\mathrm{O}})\right) + C_{11,k}\left(d^{\mathrm{O}}_{2\mathrm{p}_{II}}\,\varphi^{\mathrm{GTO}}_{010}(\alpha^{\mathrm{O}}_{2\mathrm{sp}_{II}};\mathbf{R}_{\mathrm{O}})\right)\\
&+C_{12,k}\left(\sum_{a=1}^{2} d^{\mathrm{O}}_{2\mathrm{p}_I,a}\,\varphi^{\mathrm{GTO}}_{001}(\alpha^{\mathrm{O}}_{2\mathrm{sp}_I,a};\mathbf{R}_{\mathrm{O}})\right) + C_{13,k}\left(d^{\mathrm{O}}_{2\mathrm{p}_{II}}\,\varphi^{\mathrm{GTO}}_{001}(\alpha^{\mathrm{O}}_{2\mathrm{sp}_{II}};\mathbf{R}_{\mathrm{O}})\right), \quad (3.25)
\end{aligned}$$

where the 1s AO of hydrogen atoms are represented by two CGTOs consisting of one and two primitives, respectively. The 1s oxygen AO is a core orbital, and is therefore represented by only one CGTO with three primitives. The valence orbitals of oxygen (2s, $2\mathrm{p}_x$, $2\mathrm{p}_y$, $2\mathrm{p}_z$) are represented by two CGTOs, with two and one primitives, respectively. We have in total 13 coefficients C_{pk} that can be varied independently during the construction of the MOs. For comparison, using the STO-3G basis, we will have just seven coefficients to vary.

One question that arises for split-valence basis sets, is how the contraction parameters are chosen. In the minimal basis set STO-kG, the parameters were found by fitting the CGTOs to STOs, but when using split-valence basis sets there is no point in doing this. Instead, the contraction parameters are optimized to fit the AOs directly. This is can be done by optimizing the parameters to minimize the energy for some test sets of atoms and/or molecules [10].

3.4.5 Polarization Functions

In the present chapter and last chapter, we have several times emphasized the distinction between AOs and basis functions. One example on why this distinction is so important is illustrated in the geometry calculations of ammonia NH_3. By doing a Hartree-Fock calculation on this molecule, using a basis consisting of only s and p

functions, we will find that the equilibrium geometry is planar, while NH_3 in reality has a trigonal pyramidal geometry. This is observed although the s and p functions describe the separate atoms hydrogen and nitrogen, reasonably well. The reason for this is simply because we don't have enough flexibility in our basis. Recall that the many-center expansions should be supplemented with any additional functions that may be needed to describe the physical characteristics of the molecular system. These additional functions are almost always added in the form of basis functions corresponding to one quantum number of higher angular momentum than the valence orbitals. So, for example, for NH_3, it means to include $d-$type functions, in addition to s and p. This gives the needed flexibility in our basis to obtain a more reasonable equilibrium geometry.

Adding basis functions corresponding to one quantum number of higher angular momentum than the valence orbitals, is referred to as polarization of basis, and the additional functions are called polarization functions. The polarization functions for H and He is p-type functions, d-type functions for first-row atoms, and so on. The notation used for polarized basis sets is characterized by the presence of the symbol "*". An example is the 6-31G* basis, which implies the addition of d functions, to polarize the valence p functions in 6-31G. A second star (e.g. 6-31G**) implies the polarization of s functions in H and He with p functions. A more explicit notation is of the form 6-31G(3d2fg,2pd), which indicates that first-row atoms are polarized by three sets of d functions, two sets of f functions, and a set of g functions, and H and He are polarized by two sets of p functions and one of d.

3.4.6 Diffuse Functions

In molecules with unshared pairs or anions, the electronic structure tends to be more spatially diffuse, since some of the electrons are barely bound. A basis without the flexibility to allow for weakly bound electrons far from the remaining density, can lead to significant errors in energy and other molecular properties. This type of flexibility is usually added to the basis, by additional s and p functions, with very small exponents (very diffuse functions). The presence of diffuse functions in the basis set is symbolized by the addition of a plus sign "++" (e.g. 6-31++G), which indicates the addition of diffuse p functions for first-row atoms. A second plus sign (e.g. 6-31++G) in the name indicates the presence of a diffuse s function for H and He, in addition to diffuse p functions. The more explicit notation of the from 6-311G(2df,2pd) is also much used. This notation indicates the addition of two sets of d functions and one set of f functions for first-row atoms, and addition of two sets of p functions and one set of d functions for H and He.

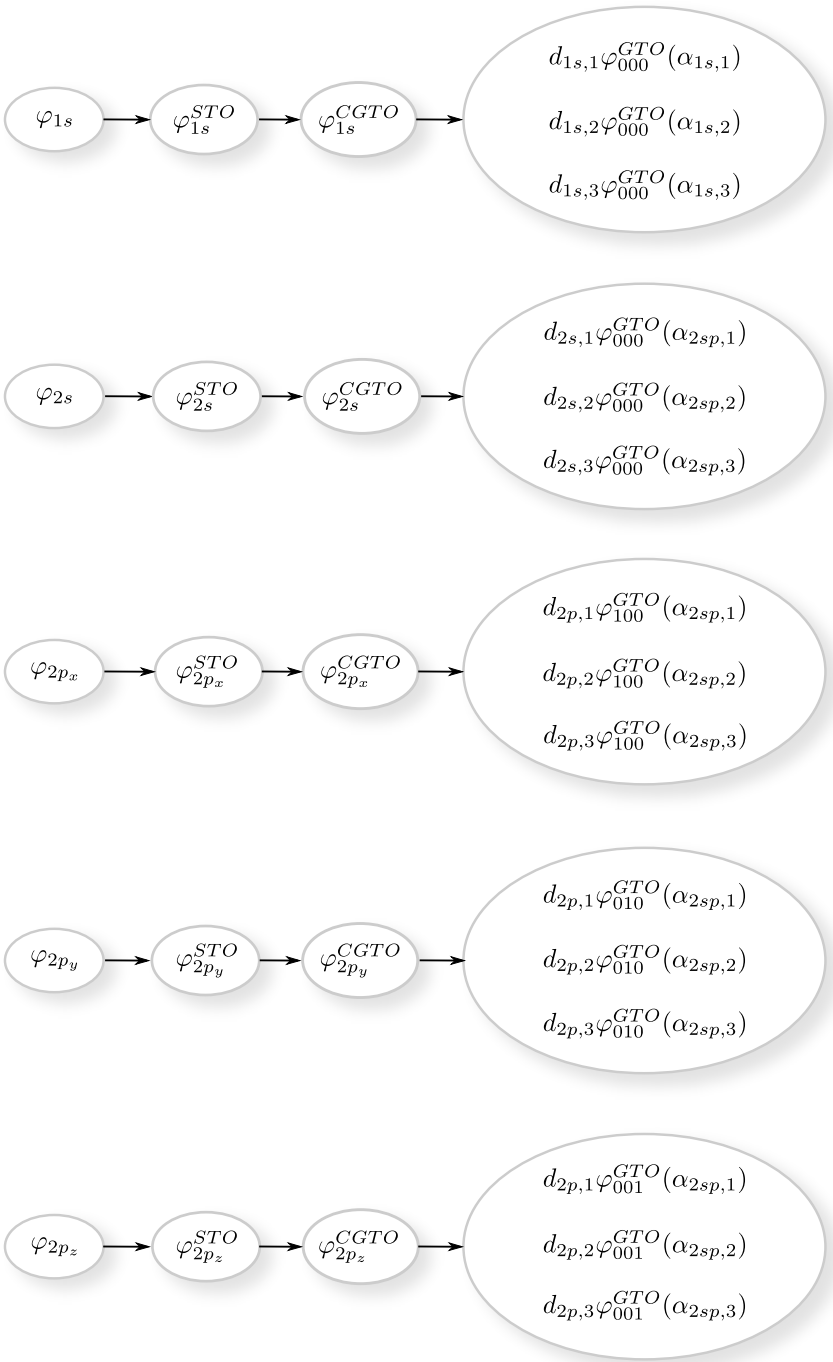

Figure 3.7: Overview of the minimal basis set STO-3G for first-row atoms (Li to Ne). Each AO φ_p is approximated by one STO φ_p^{STO}. The basis consists of five basis functions, where each is given in contracted form, consisting of three primitives each, optimized to fit STOs. Note the sharing of exponent α_{2sp} between the primitives in 2s and 2p CGTOs. The contraction coefficients are also the same for all 2p CGTOs.

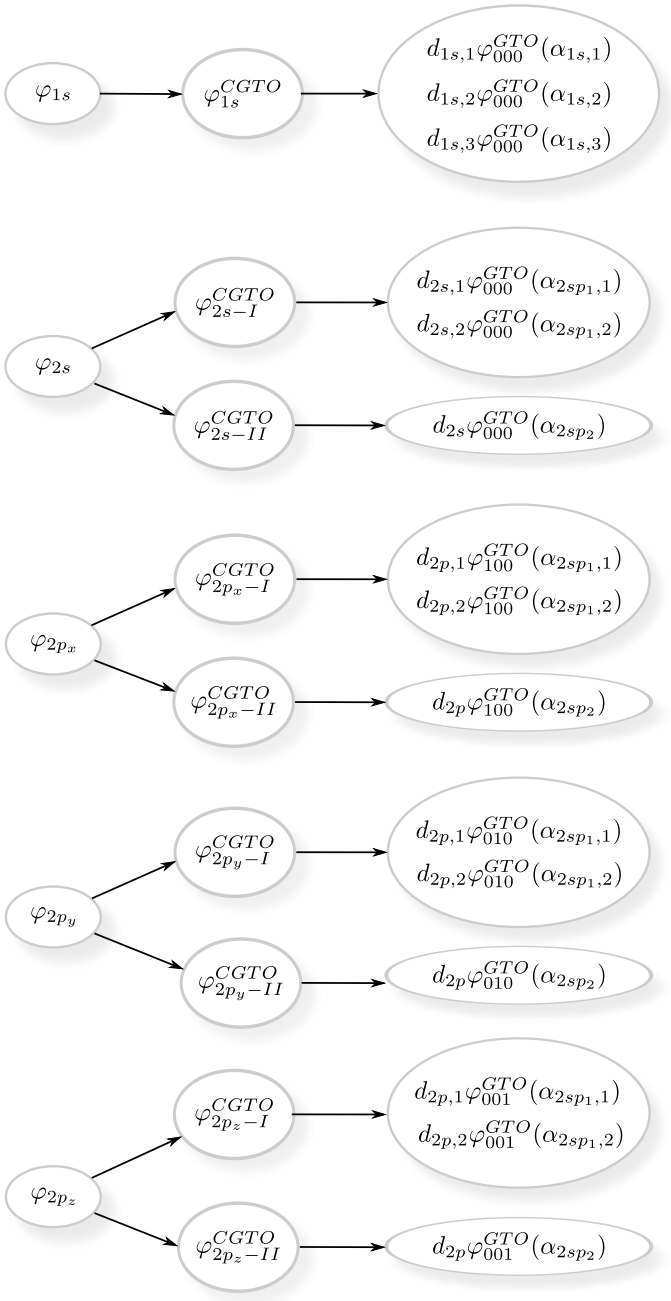

Figure 3.8: Overview of the 3-21G basis for first-row atoms (Li to Ne). The core 1s AO is represented by one CGTO, with three primitives. The valence AOs (2s and 2p) are each represented by two CGTOs, where the first one consist of two primitives, while the second one has one primitive. Note the sharing of exponents $\alpha_{2\mathrm{sp}_1}$ and $\alpha_{2\mathrm{sp}_2}$ in the 2s and 2p CGTOs, in addition to sharing of coefficients in $2\mathrm{p}_I$ CGTOs and $2\mathrm{p}_{II}$ CGTOs.

Chapter 4

Molecular Integral Evaluation

In computational chemistry, an enormous amount of effort has gone into developing mathematical and computational techniques to efficiently evaluate molecular integrals of the type

$$O_{pq} = \int \varphi_p^*(\mathbf{r}) O(\mathbf{r}) \varphi_q(\mathbf{r}) \, \mathrm{d}\mathbf{r}, \tag{4.1}$$

and

$$g_{prqs} = \int \varphi_p^*(\mathbf{r}) \varphi_r^*(\mathbf{r}') \, \frac{1}{|\mathbf{r} - \mathbf{r}'|} \, \varphi_q(\mathbf{r}) \varphi_s(\mathbf{r}') \, \mathrm{d}\mathbf{r} \, \mathrm{d}\mathbf{r}', \tag{4.2}$$

where $O(r)$ is a one-electron operator, $|\mathbf{r} - \mathbf{r}'|$ is the separation between the electrons, and φ_p belongs to a set of functions used to expand the molecular orbital (MO). The choice of basis is heavily affected by how efficient the integrals above can be evaluated. For many-center molecular calculations, the Gaussian functions are by far the most widely used, due to fast computation of the two-electron integral. The success of Gaussian basis sets in molecular calculations is closely related to the development of efficient recursive procedures for the calculations of molecular integrals. One such procedure is provided by the McMurchie-Davidson scheme [7], where an expansion in Hermite Gaussians is used to obtain efficient integral expressions.

This chapter presents the techniques provided by the McMurchie-Davidson scheme for evaluating of the one- and two-electron integrals. We will first investigate the properties of the Cartesian and Hermite Gaussians, before discussing the evaluation of simple one-electron integrals. Thereafter, the Coulomb integrals are considered, and the properties and evaluation of the nearly related function, known as the Boys function, are discussed. Finally, in the last part of this chapter, the calculation of integral derivatives is considered. The material in this chapter is adopted from Chapter 12 of Ref. [7] and Chapter 9 of Ref. [14].

4.1 Cartesian Gaussians

In last chapter we defined the normalized Cartesian Gaussians as

$$\varphi_{ijk}^{\mathrm{GTO}}(x, y, x) = \varphi_i^{\mathrm{GTO}}(x) \varphi_j^{\mathrm{GTO}}(y) \varphi_k^{\mathrm{GTO}}(z), \tag{4.3}$$

where the x component is given by

$$\varphi_i^{\mathrm{GTO}}(x) = \left(\frac{2\alpha}{\pi}\right)^{(1/4)} \sqrt{\frac{(4\alpha)^i}{(2i-1)!!}} x^i \exp(-\alpha x^2), \tag{4.4}$$

and similar for the y and z component. Since we in this chapter are exclusively concerned with Gaussian functions, it is desirable to extend this notation somewhat. We will therefore, hereafter, write a (non-normalized) Cartesian Gaussian as

$$\begin{aligned} G_a(\mathbf{r}) &= G_{ijk}(\mathbf{r}, a, \mathbf{A}) \\ &= (x - A_x)^i (y - A_y)^j (z - A_z)^k \exp(-a r_A^2) \\ &= x_A^i y_A^j z_A^k \exp(-a r_A^2), \end{aligned} \tag{4.5}$$

where a is the orbital exponent, $\mathbf{r}$ is the electronic coordinate, $\mathbf{A}$ is the origin of the Gaussian (nuclear position) and

$$\mathbf{r}_A = \mathbf{r} - \mathbf{A},$$

with total angular momentum quantum number $l = i + j + k \geq 0$. In a factorized form the Cartesian Gaussians can be written as

$$G_{ijk}(\mathbf{r}, a, \mathbf{A}) = G_i(x_A, a) G_j(y_A, a) G_k(z_A, a), \tag{4.6}$$

where for example

$$G_i(x_A, a) = x_A^i \exp(-a x_A^2). \tag{4.7}$$

The factorization is a very important feature of Cartesian Gaussians, and, as we shall see shortly, this feature simplifies the molecular integral evaluations significantly.

Another very important feature of Cartesian Gaussians is their differentiation property. Taking the first derivative of Eq. (4.7), we obtain

$$\frac{\partial G_i}{\partial A_x} = -\frac{\partial G_i}{\partial x} = 2a G_{i+1} - i G_{i-1}, \tag{4.8}$$

which is a linear combination of two undifferentiated Gaussians with incremented and decremented quantum numbers. More generally, using the notation

$$G_i^q = \frac{\partial^q G_i}{\partial A_x^q}, \tag{4.9}$$

we have the following recurrence relation for the derivatives

$$G_i^{q+1} = 2a G_{i+1}^q - i G_{i-1}^q, \tag{4.10}$$

which can be used to construct higher derivatives from those of lower order. We should also note the trivial recurrence

$$x_A G_i = G_{i+1}, \tag{4.11}$$

which is going to be used frequently in this chapter.

	Cartesian Gaussian	Hermite Gaussian
Definition:	$G_i = x_A^i \exp(-ax_A^2)$	$\Lambda_t = \left(\partial/\partial P_x\right)^t \exp(-px_P^2)$
Recurrence:	$x_A G_i = G_{i+1}$	$x_P \Lambda_t = \frac{1}{2p}\Lambda_{t+1} + t\Lambda_{t-1}$
Differentiation:	$\frac{\partial G_i}{\partial A_x} = 2aG_{i+1} - iG_{i-1}$	$\frac{\partial \Lambda}{\partial P_x} = \Lambda_{t+1}$

Table 4.1: Comparison of Cartesian and Hermite Gaussians.

4.2 Hermite Gaussians

Another class of Gaussian functions, which are useful in molecular integral evaluations, are the Hermite Gaussians. Although, these functions can be used as basis functions themselves, they are often used as intermediates in the calculation of integrals over Cartesian Gaussians. This is mainly due to their convenient form in terms of differentiation. The Hermite Gaussians of exponent p and centered on $\mathbf{P}$ are defined by

$$\Lambda_{tuv}(\mathbf{r}, p, \mathbf{P}) = \left(\partial/\partial P_x\right)^t \left(\partial/\partial P_y\right)^u \left(\partial/\partial P_z\right)^v \exp(-pr_P^2), \tag{4.12}$$

where

$$\mathbf{r}_P = \mathbf{r} - \mathbf{P}.$$

Like the Cartesian Gaussians, these function can be factorized as

$$\Lambda_t(x_P, a) = \left(\partial/\partial P_x\right)^t \exp(-px_P^2), \tag{4.13}$$

which only differs from the Cartesian Gaussian in the polynomial factors. Using the definition in Eq. (4.13) we obtain the simple relation:

$$\frac{\partial \Lambda}{\partial P_x} = -\frac{\partial \Lambda}{\partial x} = \Lambda_{t+1}. \tag{4.14}$$

Furthermore, we have the following recurrence relation

$$x_P \Lambda_t = \frac{1}{2p}\Lambda_{t+1} + t\Lambda_{t-1}, \tag{4.15}$$

which can be proved by combining

$$\Lambda_{t+1} = \left(\partial/\partial P_x\right)^t \frac{\partial \Lambda_0}{\partial P_x} = 2p \left(\partial/\partial P_x\right)^t x_p \Lambda_0, \tag{4.16}$$

with the commutator

$$\left[\left(\partial/\partial P_x\right)^t, x_p\right] = -t \left(\partial/\partial P_x\right)^{t-1}. \tag{4.17}$$

The relations in Eqs. (4.14) and (4.15) are compared to the corresponding relations for Cartesian Gaussians in Table 4.1.

A very useful result, which simplifies the calculation of one-electron integrals, is obtained by integrating the Hermite Gaussians over all space;

$$\begin{aligned}\int_{-\infty}^{\infty} \Lambda_t(x)dx &= \left(\partial/\partial P_x\right)^t \int_{-\infty}^{\infty} \exp(-px_P^2)\,\mathrm{d}x \\ &= \left(\partial/\partial P_x\right)^t \sqrt{\frac{\pi}{p}} \\ &= \delta_{t0}\sqrt{\frac{\pi}{p}}. \end{aligned} \tag{4.18}$$

This result illustrates an important technique which we shall use on several occasions, and involves taking the differential operators of Hermite Gaussians outside the integration sign. In this way, the integrals over Hermite Gaussians are replaced with differentiated integrals over "spherical" Gaussians, i.e. functions with no angular terms.

4.3 Overlap Distributions

The Gaussian product theorem states that the product of two Gaussians centered on two different centers **A** and **B**, is a finite sum of Gaussians centered on a point along the axis connecting them [7]. This theorem has a central role in molecular integral calculations since the integrals always occur in pairs. For simplicity consider the product of two s-type (spherical) Gaussians

$$\exp(-ax_A^2)\exp(-bx_B^2) = \exp(-qQ_x^2)\exp(-px_P^2), \tag{4.19}$$

where

$$p = a + b, \tag{4.20}$$

$$P_x = \frac{aA_x + bB_x}{p}, \tag{4.21}$$

$$Q_x = A_x - B_x, \tag{4.22}$$

$$q = \frac{ab}{a+b}. \tag{4.23}$$

The product in Eq. (4.19) consists of one term which depends on the electronic coordinate x, while the other term, known as the pre-exponential factor, is a constant and doesn't depend on x. The latter is small when the separation between the centers Q_x is large. Thus, an integral over two Gaussian functions (two-center integral) can be reduced to a one-center integral, and similarly a four-center integral can be reduced to a two-center integral. This simplifies the integral evaluations significantly. Figure 4.1 illustrates how the product of two Gaussians form a new Gaussian centered at a new point P_x.

The product of two general Gaussian functions is usually referred to as overlap distribution;

$$\begin{aligned}\Omega_{ij}(x) &= G_i(x_A, a)G_j(x_B, b) \\ &= K_{AB}^x x_A^i x_B^j \exp(-px_P^2), \end{aligned} \tag{4.24}$$

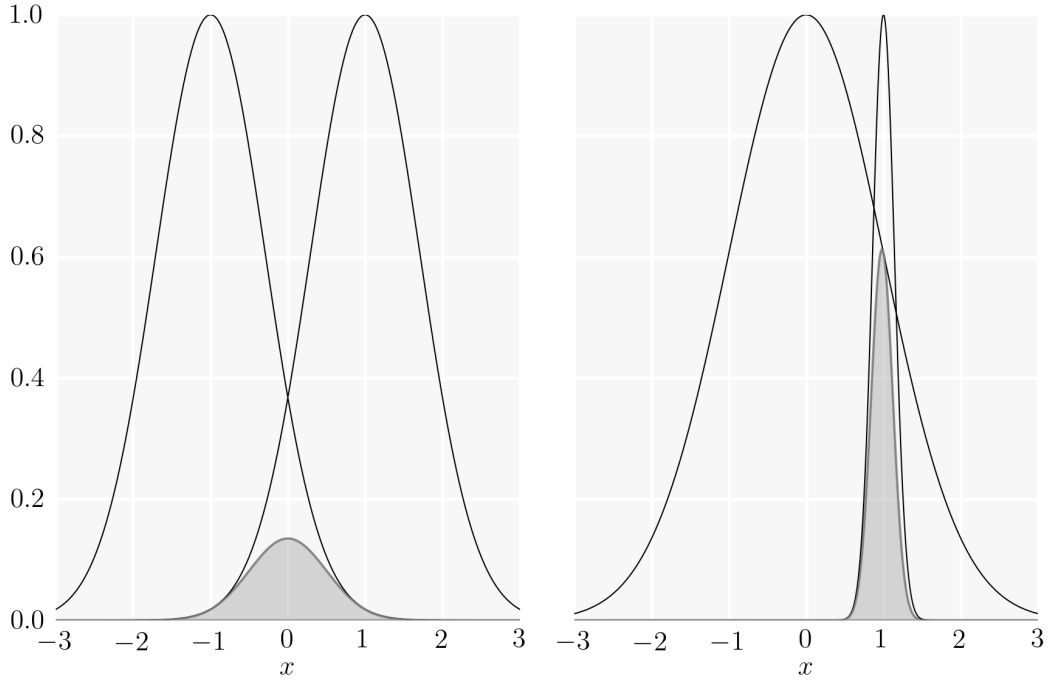

Figure 4.1: The Gaussian product rule: the shaded areas represent the product of two individual Gaussians. Left: the exponents are equal to 1 and the two Gaussians are centered at $x = \pm 1$. Right: the exponents are equal to $1/2$ and 25, and the two Gaussians are centered at $= 0$ and $x = 1$.

where the constant K^x_{AB} is the pre-exponential factor. For integral calculations, this form of the overlap distribution is, however, not so useful because it involves x^i_A and x^j_B. Hermite Gaussians on the other hand are much more suited for integration as we saw in last section, and one should therefore expand the Cartesian overlap distribution in Hermite Gaussians centered at $\mathbf{P}$. This is possible since any polynomial of degree $i + j$, as the one in Eq. (4.24), may be expanded in Hermite polynomials of degree $t \leq i + j$ [14]. We can therefore write

$$\Omega_{ij} = \sum_{t=0}^{i+j} E^{ij}_t \Lambda_t, \tag{4.25}$$

where the expansion coefficients E^{ij}_t are independent of electronic coordinates and therefore constants. The expansion coefficients are found through a set of recurrence relations. We consider the incremented distribution

$$\Omega_{i+1,j} = \sum_{t=0}^{i+j+1} E^{i+1,j}_t \Lambda_t. \tag{4.26}$$

To relate this expansion to that of $\Omega_{i,j}$ we consider an alternative Hermite expansion of $\Omega_{i+1,j}$, by using the relation $x_P \Lambda_t = \frac{1}{2p}\Lambda_{t+1} + t\Lambda_{t-1}$:

$$\begin{aligned}
\Omega_{i+1,j} &= x_A \Omega_{ij} \\
&= (x - A_x)\Omega_{ij} \\
&= (x - P_x)\Omega_{ij} + (P_x - A_x)\Omega_{ij} \\
&= x_p \Omega_{ij} - \frac{qQ_x}{a}\Omega_{ij} \\
&= \sum_{t=0}^{i+j} E_t^{ij} x_p \Lambda_t - \frac{qQ_x}{a} \sum_{t=0}^{i+j} E_t^{ij} \Lambda_t \\
&= \sum_{t=0}^{i+j} E_t^{ij} \left(\frac{1}{2p}\Lambda_{t+1} + t\Lambda_{t-1} - \frac{qQ_x}{a}\Lambda_t \right) \\
&= \sum_{t=0}^{i+j+1} \left(\frac{1}{2p} E_{t-1}^{ij} + (t+1) E_{t+1}^{ij} - \frac{qQ_x}{a} E_t^{ij} \right) \Lambda_t,
\end{aligned} \tag{4.27}$$

where the coefficients are taken to satisfy the relations

$$E_t^{ij} = 0, \qquad \text{for } t < 0 \text{ or } t > i + j. \tag{4.28}$$

A comparison of the expansions in Eqs. (4.26) and (4.27), yields the McMurchie-Davidson recurrence relations for the Hermite coefficients

$$E_t^{i+1,j} = \frac{1}{2p} E_{t-1}^{ij} - \frac{qQ_x}{a} E_t^{ij} + (t+1) E_{t+1}^{ij}, \tag{4.29}$$

and similarly it can be shown that

$$E_t^{i,j+1} = \frac{1}{2p} E_{t-1}^{ij} + \frac{qQ_x}{b} E_t^{ij} + (t+1) E_{t+1}^{ij}, \tag{4.30}$$

with starting coefficient

$$E_0^{00} = K_{AB}^x. \tag{4.31}$$

From these recurrence relations, the Hermite coefficients are easily generated and can be used to expand the overlap distribution in terms of Hermite Gaussians.

Note that the Hermite expansion coefficients are functions of $\mathbf{Q}$ but are independent of $\mathbf{P}$. Therefore, the derivatives of these coefficients with respect to $\mathbf{P}$ will vanish while the derivatives with respect to $\mathbf{Q}$ can be generated from the following equations [14]:

$$E_0^{00;\,n+1} = -2q \left[Q_x E_0^{00;\,n} + n E_0^{00;\,n-1} \right], \tag{4.32a}$$

$$E_t^{i+1,j;\,n} = \frac{1}{2p} E_{t-1}^{ij;\,n} - \frac{q}{a} \left[Q_x E_t^{ij;\,n} + n E_t^{ij;n-1} \right] + (t+1) E_{t+1}^{ij;\,n}, \tag{4.32b}$$

$$E_t^{i,j+1;\,n} = \frac{1}{2p} E_{t-1}^{ij;\,n} + \frac{q}{b} \left[Q_x E_t^{ij;\,n} + n E_t^{ij;\,n-1} \right] + (t+1) E_{t+1}^{ij;\,n}, \tag{4.32c}$$

where

$$E_t^{ij;\,n} = \frac{\partial^n E_t^{ij}}{\partial Q_x^n}. \tag{4.33}$$

These expressions become very useful in calculations of geometrical derivatives.

4.4 Simple One-Electron Integrals

From a computational point of view, molecular integrals can be divided into those that involve Coulomb interactions and those that do not. The reason for this division is due to numerical aspects, and is reflected in the way these integrals are found. While non-Coulomb integrals can be expressed in closed analytical form, the Coulomb integrals involve at some stage a numerical procedure. We will in the following first treat non-Coulomb integrals and thereafter the Coulomb integrals.

4.4.1 Multipole Moments

A general Cartesian multipole moment integral is given by

$$\begin{aligned} S_{ab}^{efg} &= \langle G_a |\, x_C^e y_C^f z_C^g \,| G_b \rangle \\ &= \int G_{ikm}(\mathbf{r}, a, \mathbf{A})\; [x_C^e y_C^f z_C^g]\; G_{jln}(\mathbf{r}, b, \mathbf{B})\; \mathrm{d}x\, \mathrm{d}y\, \mathrm{d}z. \end{aligned} \tag{4.34}$$

A special case of this integral is the overlap integral. Since the multipole integrals are separable in Cartesian directions, they may be calculated as

$$S_{ab}^{efg} = S_{ij}^e S_{kl}^f S_{mn}^g, \tag{4.35}$$

where for example

$$S_{ij}^e = \langle G_i |\, x_C^e \,| G_j \rangle = \int G_i(x_A, a)\; [x_C^e]\; G_j(x_B, b)\; \mathrm{d}x. \tag{4.36}$$

We can therefore consider one of the Cartesian directions in the following discussion. The other two are obtained in the same manner. Inserting the expanded overlap distribution in Eq. (4.25) into the last equation, we obtain

$$S_{ij}^e = \sum_{t=0}^{i+j} E_t^{ij} \int_{-\infty}^{\infty} x_C^e \Lambda_t \, \mathrm{d}x. \tag{4.37}$$

In the last equation, the Hermite coefficients can be found by recursion as already described. Here we will therefore focus on the Hermite integrals, given by

$$M_t^e = \int_{-\infty}^{\infty} x_C^e \Lambda_t \, \mathrm{d}x. \tag{4.38}$$

In the special case when $e = 0$, this integral is nothing but the integral in Eq. (4.18) and the result is simply

$$M_t^0 = \delta_{t0}\sqrt{\frac{\pi}{p}}. \tag{4.39}$$

The remaining integrals can be found by recursion. These are easily obtained by combining

$$M_t^{e+1} = \int_{-\infty}^{\infty} x_C^e x_C \Lambda_t \, \mathrm{d}x, \tag{4.40}$$

with the relation

$$x_C\Lambda_t = x_P\Lambda_t + X_{PC}\Lambda_t = \frac{1}{2p}\Lambda_{t+1} + t\Lambda_{t-1} + X_{PC}\Lambda_t, \tag{4.41}$$

to give

$$M_t^{e+1} = tM_{t-1}^e + X_{PC}M_t^e + \frac{1}{2p}M_{t+1}^e, \tag{4.42}$$

where $X_{PC} = P_x - C_x$. The final expression for the Cartesian multipole moment integrals, becomes

$$S_{ij}^e = \sum_{t=0}^{\min(i+j,e)} E_t^{ij} M_t^e, \tag{4.43}$$

where the Hermite coefficients are found from the recurrence relations in Eqs. (4.29)–(4.31), while the moments are found by using Eqs. (4.39) and (4.42). Note that the sum over t goes to $\min(i+j, e)$, since the Hermite multipole moment integrals vanish for $t > e$, as shown in Ref. [14].

The most important simple one-electron integral in the Self-Consistent Field (SCF) calculations is the overlap integral. By using the expressions above we can express this integral as

$$S_{ab}^{000} = E_0^{ij} E_0^{kl} E_0^{mn} \left(\frac{\pi}{p}\right)^{3/2}. \tag{4.44}$$

4.4.2 Momentum and Kinetic Energy Integrals

A general one-electron integral involving differential operators is given by

$$D_{ab}^{efg} = \langle G_a | \, (\partial/\partial x)^e (\partial/\partial y)^f (\partial/\partial z)^g \, | G_b \rangle \,, \tag{4.45}$$

which can be factorized in the same way as the multipole moment integrals

$$D_{ab}^{efg} = D_{ij}^e D_{kl}^f D_{mn}^g, \tag{4.46}$$

where for example

$$D_{ij}^e = \langle G_i | \, (\partial/\partial x)^e \, | G_j \rangle \,. \tag{4.47}$$

As shown earlier in this chapter, the differential operator on Gaussian functions, generates a linear combination of undifferentiated Gaussians. Therefore, will integrals like the one in Eq. (4.47), reduce to a combination of overlap integrals. Using the differentiation relation of Cartesian Gaussian shown in Table 4.1 we find that

$$D^0_{ij} = S^0_{ij}, \tag{4.48}$$

and

$$D^{e+1}_{ij} = jD^e_{i,j-1} - 2bD^e_{i,j+1}, \tag{4.49}$$

which can be used to generate differentiated integrals of arbitrary order. As an example we consider the kinetic energy integral:

$$\begin{aligned} T_{ab} &= -\frac{1}{2}\left[D^2_{ij}D^0_{kl}D^0_{mn} + D^0_{ij}D^2_{kl}D^0_{mn} + D^0_{ij}D^0_{kl}D^2_{mn}\right] \\ &= T_{ij}S^0_{kl}S^0_{mn} + S^0_{ij}T_{kl}S^0_{mn} + S^0_{ij}S^0_{kl}T_{mn}, \end{aligned} \tag{4.50}$$

where for example

$$T_{ij} = -\frac{1}{2}D^2_{ij} = -\frac{1}{2}\left[j(j-1)S^0_{i,j-2} - 2b(2j+1)S^0_{ij} + 4b^2S^0_{i,j+2}\right]. \tag{4.51}$$

Once the Hermite coefficients are computed, there is really not much work to do in order to find the overlap and kinetic integrals.

4.5 Coulomb Integrals

Unlike the multipole moment integrals and momentum integrals, the Coulomb integrals cannot be expressed in closed analytical form. They can, however, be reduced to one-dimensional integrals, which are relatively straightforward to compute. In the present section, we consider first the electrostatics of spherical Gaussian charge distributions, leading to an interaction potential described by the so-called Boys function. We thereafter show how Coulomb integrals over Hermite Gaussians can be obtained by differentiating the Boys function, and derive a set of recursion formulas for generating these derivatives. Finally, we will show how the Cartesian Coulomb integrals can be obtained from the corresponding integrals over Hermite Gaussians.

4.5.1 Electrostatics for Gaussian Charge Distributions

The Gaussian distribution of a unit charge of exponent p, centered at $\mathbf{P}$ is given by

$$\rho_p(\mathbf{r}_P) = \left(\frac{p}{\pi}\right)^{3/2} \exp(-pr^2_P). \tag{4.52}$$

We consider the electrostatic potential at $\mathbf{C}$ due to this charge distribution:

$$V_p(\mathbf{C}) = \int \frac{\rho_P(\mathbf{r}_P)}{r_C}\,\mathrm{d}\mathbf{r}, \tag{4.53}$$

and the energy of repulsion between two such distributions:

$$V_{pq} = \int \frac{\rho_P(\mathbf{r}_{1P})\rho_Q(\mathbf{r}_{2Q})}{r_{12}}\,\mathrm{d}\mathbf{r}_1\,\mathrm{d}\mathbf{r}_2, \tag{4.54}$$

where the second distribution $\rho_Q(\mathbf{r}_{2Q})$ of exponent q, is centered at $\mathbf{Q}$. For large separations of R_{PC} and R_{PQ}, these two expressions should, of course, reduce to the expression for point charges.

One-electron integral

In contrast to simple one-electron integrals discussed in the previous sections, the Coulomb integral in Eq. (4.53), cannot be factorized in Cartesian directions due to the inverse operator. The presence of r_C is avoided by the substitution

$$\frac{1}{r_C} = \frac{1}{\sqrt{\pi}} \int_{-\infty}^{\infty} \exp(-r_C^2 t^2)\,\mathrm{d}t, \tag{4.55}$$

yielding the four dimensional integral

$$V_p(\mathbf{C}) = \frac{p^{3/2}}{\pi^2} \int \exp(-pr_P^2) \left[\int_{-\infty}^{\infty} \exp(-r_C^2 t^2)\,\mathrm{d}t \right] \mathrm{d}\mathbf{r}. \tag{4.56}$$

The last expression can be rewritten by invoking the Gaussian product rule (Eq. (4.19)):

$$V_p(\mathbf{C}) = \frac{p^{3/2}}{\pi^2} \int_{-\infty}^{\infty} \left[\int \exp(-[p+t^2]r_S^2)\,\mathrm{d}\mathbf{r} \right] \exp\left(-\frac{pt^2}{p+t^2} R_{CP}^2 \right) \mathrm{d}t, \tag{4.57}$$

where $\mathbf{R}_{CP} = \mathbf{C} - \mathbf{P}$ and $\mathbf{S}$ is some point on the line connecting $\mathbf{C}$ and $\mathbf{P}$:

$$\mathbf{S} = \frac{p\mathbf{P} + t^2\mathbf{C}}{p+t^2}. \tag{4.58}$$

Integrating over the spatial coordinates now gives a one-dimensional integral

$$V_p(\mathbf{C}) = \frac{p^{3/2}}{\sqrt{\pi}} \int_{-\infty}^{\infty} (p+t^2)^{-3/2} \exp\left(-pR_{CP}^2 \frac{t^2}{p+t^2} \right) \mathrm{d}t, \tag{4.59}$$

which can be simplified even further by making the substitution

$$u^2 = \frac{t^2}{p+t^2}, \tag{4.60}$$

to obtain the final expression

$$V_p(\mathbf{C}) = \sqrt{\frac{4p}{\pi}} \int_0^1 \exp\left(-pR_{CP}^2 u^2 \right) \mathrm{d}u. \tag{4.61}$$

We have thus reduced a three-dimensional integral over all space (Eq. (4.53)) to a one-dimensional integral over $[0, 1]$. The integral in the last equation, is the (zeroth-order) Boys function, defined as

$$F_n(x) = \int_0^1 \exp\left(-xt^2\right) t^{2n}\,\mathrm{d}t, \qquad \text{with } n = 0. \tag{4.62}$$

We will discuss the nature of this function in detail shortly, but for the moment we note that the potential from the Gaussian charge distribution can be written in terms of the Boys function, by

$$V_p(\mathbf{C}) = \sqrt{\frac{4p}{\pi}}\, F_0(pR_{CP}^2). \tag{4.63}$$

Two-electron integral

The interaction between two Gaussian charge distributions can be expressed as the electrostatic energy of the second distribution in the potential due to the first distribution:

$$\begin{aligned} V_{pq} &= \int V_p(\mathbf{r}_2)\rho_Q(\mathbf{r}_{2Q})\,\mathrm{d}\mathbf{r}_2 \\ &= \sqrt{\frac{4p}{\pi}}\left(\frac{q}{\pi}\right)^{3/2} \int F_0(pr_{2P}^2)\exp(-qr_{2Q}^2)\,\mathrm{d}\mathbf{r}_2. \end{aligned} \tag{4.64}$$

Once again by invoking the Gaussian product rule and integrating over all space, we obtain

$$V_{pq} = \sqrt{\frac{4pq}{\pi}} \int_0^1 \frac{q}{(pt^2+q)^{3/2}} \exp\left(-\frac{pqt^2 R_{PQ}^2}{pt^2+q}\right) \mathrm{d}t. \tag{4.65}$$

If we now substitute

$$u^2 = \frac{p+q}{pt^2+q}t^2, \tag{4.66}$$

we obtain the final result

$$V_{pq} = \sqrt{\frac{4\alpha}{\pi}}\, F_0(\alpha R_{PQ}^2), \tag{4.67}$$

where the reduced exponent α is

$$\alpha = \frac{pq}{p+q}. \tag{4.68}$$

The two-electron integral for two spherical Gaussian distributions, may therefore be expressed in terms of the Boys function as well.

4.5.2 The Boys function

We have seen that the Coulomb integrals can be described by the Boys function $F_0(x)$, which simplifies the evaluations of Coulomb integrals significantly. In this section, we discuss in more detail the nature of this function. We will first present some of the most important properties of the Boys function and thereafter show how this function can be evaluated.

Properties

The Boys function of order n is defined by

$$F_n(x) = \int_0^1 \exp\left(-xt^2\right) t^{2n} \, \mathrm{d}t, \tag{4.69}$$

for $x \geq 0$.

- the Boys function is strictly positive since the integrand is positive:

$$F_n(x) > 0. \tag{4.70}$$

- The Boys function is strictly decreasing function since its derivatives are negative:

$$\frac{\mathrm{d}F_n(x)}{\mathrm{d}x} = -F_{n+1}(x) < 0. \tag{4.71}$$

- Since the integrand in

$$F_n(x) - F_{n+1}(x) = \int_0^1 \exp\left(-xt^2\right) t^{2n}(1-t^2) \, \mathrm{d}t, \tag{4.72}$$

  is positive within the integration range, we have that

$$F_n(x) > F_{n+1}(x), \tag{4.73}$$

  for all n.

- The values at $x = 0$ can be expressed in closed form as

$$F_n(0) = \int_0^1 t^{2n} \, \mathrm{d}t = \frac{1}{2n+1}, \tag{4.74}$$

  which implies

$$F_n(x) \leq \frac{1}{2n+1}, \tag{4.75}$$

  since the function is strictly decreasing.

- For large values of x, the Boys function can be approximated by

$$\begin{aligned} F_n(x) &= \int_0^1 \exp\left(-xt^2\right) t^{2n}\,\mathrm{d}t \\ &\approx \int_0^\infty \exp\left(-xt^2\right) t^{2n}\,\mathrm{d}t \\ &= \frac{(2n-1)!!}{2^{n+1}}\sqrt{\frac{\pi}{x^{2n+1}}}, \quad \text{(large } x\text{)}, \end{aligned} \tag{4.76}$$

  from which we conclude that the Boys function goes to zero as x goes to infinity.

- The zeroth-order boys function is related to the error function by

$$F_0(x) = \sqrt{\frac{\pi}{4\pi}}\mathrm{erf}(\sqrt{x}). \tag{4.77}$$

Some of the properties listed above are illustrated for the three lowest order of Boys function in Figure 4.2.

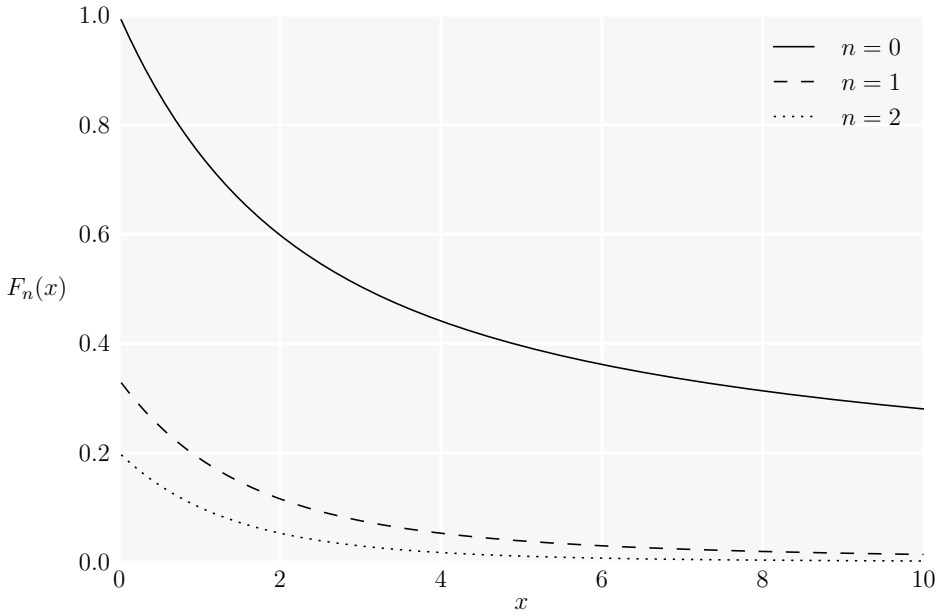

Figure 4.2: The Boys function $F_n(x)$ for $n = 0, 1, 2$.

Evaluation

The Boys function is central in evaluation of Coulomb integrals, and it is, therefore, important to calculate it efficiently. We first note that for large values of x, Eq. (4.76)

provides a good approximation for the Boys function. Unfortunately, this approximation breaks down for small x. One option for small values of x, is to construct a Taylor expansion, based on Eqs. (4.71) and (4.74);

$$F_n(x) = \sum_{k=0}^{\infty} \frac{(-x)^k}{k!(2n+2k+1)}. \tag{4.78}$$

This approximation for small values of x, together with the approximation for large values of x (Eq. (4.76)) are shown in Figure 4.3. Although these two expressions seem

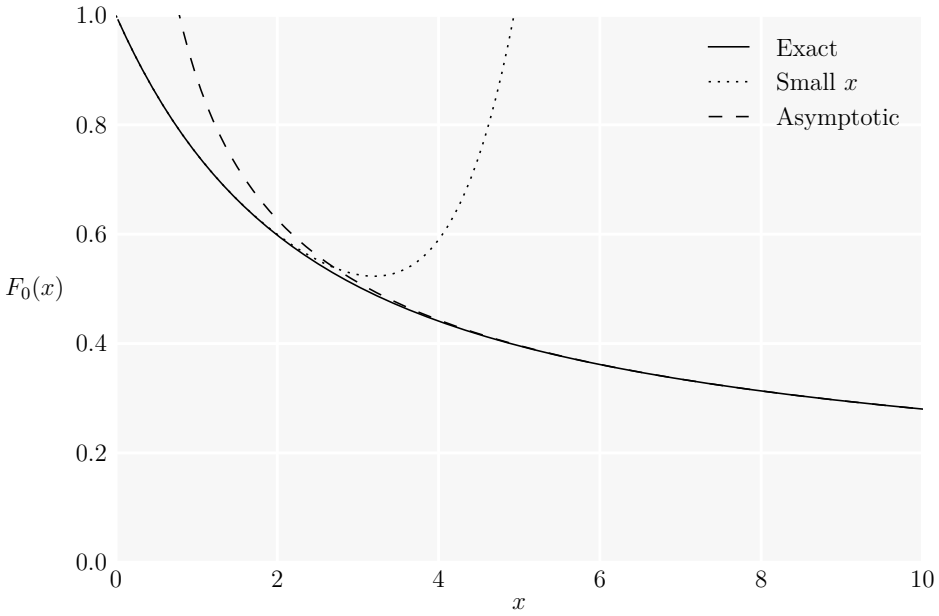

Figure 4.3: The zeroth-order Boys function $F_0(x)$ (solid line) as approximated by the long range formula (Eq. (4.76)) for large x and by a sixth-order Taylor expansion (Eq. (4.78)) around $x = 0$ for small x.

to give a reasonable approximation of the Boys function, they don't provide the desired accuracy for all values of x. We therefore need more accurate methods (with an error of order 10^{-10} or smaller) to approximate the Boys function.

A common way to approximate this function, is to numerically calculate and pretabulate the function at regular intervals x_t for small arguments. The Boys function at some point x is then expanded around the nearest tabulated point $x_t = x - \Delta x$:

$$F_n(x_t + \Delta x) = \sum_{k=0}^{\infty} \frac{F_{n+k}(x_t)(-\Delta x)^k}{k!}. \tag{4.79}$$

By using intervals of 0.1, convergence to errors smaller than 10^{-14} is obtained after six terms [7]. The tabulated values can be computed by evaluating Eq. (4.69), by some numerical integral scheme, such as the trapezoidal method [13]. For larger arguments, the Boys function is approximated by the asymptotic formula in Eq. (4.76).

The Boys functions of different orders n are related by recursion, which can be obtained by integrating the Boys function by parts. The resulting relation for upward recursion is given by [7]

$$F_{n+1} = \frac{(2n+1)F_n(x) - \exp(-x)}{2x}, \tag{4.80}$$

and for downward recursion

$$F_n = \frac{2xF_{n+1}(x) + \exp(-x)}{2n+1}. \tag{4.81}$$

By using these recurrence relations, we only need to calculate $F_n(x)$ for one value of n, obtaining the others by upward or downward recursion. However, for small x, upward recursion is numerically unstable, since it involves the difference of two almost equal numbers. Therefore, in practice the downward recursion is preferred.

4.5.3 Hermite Integrals

Having discussed the Coulomb integrals over spherical Gaussian distributions and Boys function, we are now in position to go one step further and consider Coulomb integrals over nonspherical Gaussians. Following the McMurchie-Davidson scheme, we first show how Coulomb integrals over Hermite integrals may be obtained by differentiating the Boys function, and thereafter how the corresponding integrals over Cartesian Gaussians can obtained by expansion.

The one-electron Coulomb integral can be expressed in terms of Hermite Gaussians by

$$V_{tuv}^{efg} = \int \Lambda_{tuv}(\mathbf{r})(\partial/\partial C_x)^e(\partial/\partial C_y)^f(\partial/\partial C_z)^g \, r_C^{-1} \, \mathrm{d}\mathbf{r}, \tag{4.82}$$

where for example V_{tuv}^{000} is the potential. The two-electron integral can similarly be expressed as

$$V_{tuv;\,t'u'v'} = \int\int \frac{\Lambda_{tuv}(\mathbf{r}_1)\Lambda_{t'u'v'}(\mathbf{r}_2)}{r_{12}} \, \mathrm{d}\mathbf{r}_1 \, \mathrm{d}\mathbf{r}_2, \tag{4.83}$$

where r_{12} is the separation between the electrons, Λ_{tuv} is a Hermite Gaussian of exponent p centered on $\mathbf{P}$ and $\Lambda_{t'u'v'}$ is a Hermite Gaussian of exponent q centered on $\mathbf{Q}$. Inserting the definition of Hermite Gaussians, given in Eq. (4.12), we obtain

$$\begin{aligned} V_{tuv}^{efg} = &\left(\frac{\partial}{\partial P_x}\right)^t \left(\frac{\partial}{\partial P_y}\right)^u \left(\frac{\partial}{\partial P_z}\right)^v \left(\frac{\partial}{\partial C_x}\right)^e \left(\frac{\partial}{\partial C_y}\right)^f \left(\frac{\partial}{\partial C_z}\right)^g \\ &\times \int \frac{\exp(-pr_P^2)}{r_C} \, \mathrm{d}\mathbf{r}, \end{aligned} \tag{4.84}$$

and

$$V_{tuv;\,t'u'v'} = \left(\frac{\partial}{\partial P_x}\right)^t \left(\frac{\partial}{\partial P_y}\right)^u \left(\frac{\partial}{\partial P_z}\right)^v \left(\frac{\partial}{\partial Q_x}\right)^{t'} \left(\frac{\partial}{\partial Q_y}\right)^{u'} \left(\frac{\partial}{\partial Q_z}\right)^{v'} \times \int \frac{\exp(-pr_{1P}^2)\exp(-qr_{2Q}^2)}{r_{12}}\,\mathrm{d}\mathbf{r}_1\,\mathrm{d}\mathbf{r}_2. \tag{4.85}$$

These two expressions may now be written in terms of the Boys function, by using the results from the previous sections (Eqs. (4.63) and (4.67));

$$V_{tuv}^{efg} = \frac{2\pi}{p}\left(\frac{\partial}{\partial P_x}\right)^t \left(\frac{\partial}{\partial P_y}\right)^u \left(\frac{\partial}{\partial P_z}\right)^v \left(\frac{\partial}{\partial C_x}\right)^e \left(\frac{\partial}{\partial C_y}\right)^f \left(\frac{\partial}{\partial C_z}\right)^g \times F_0(pR_{PC}^2), \tag{4.86}$$

and

$$V_{tuv;\,t'u'v'} = \frac{2\pi^{5/2}}{pq\sqrt{p+q}}\left(\frac{\partial}{\partial P_x}\right)^t \left(\frac{\partial}{\partial P_y}\right)^u \left(\frac{\partial}{\partial P_z}\right)^v \left(\frac{\partial}{\partial Q_x}\right)^{t'} \left(\frac{\partial}{\partial Q_y}\right)^{u'} \left(\frac{\partial}{\partial Q_z}\right)^{v'} \times F_0(\alpha R_{PQ}^2), \tag{4.87}$$

where the factors in front arise due to the normalization of the charge distributions given in Eq. (4.52). Thus, we have managed to express integrals over nonspherical distributions as derivatives of integrals over spherical distributions. The derivatives may be simplified even further, since the Boys function depends only on the relative separation of the two centers, leading to much more simpler expressions;

$$V_{tuv}^{efg} = (-1)^{e+f+g}\frac{2\pi}{p}R_{t+e,u+f,v+g}(p, \mathbf{R}_{PC}), \tag{4.88}$$

and

$$V_{tuv;\,t'u'v'} = (-1)^{t'+u'+v'}\frac{2\pi^{5/2}}{pq\sqrt{p+q}}R_{t+t',u+u',v+v'}(\alpha, \mathbf{R}_{PQ}), \tag{4.89}$$

where we have introduced the integrals

$$R_{tuv}(a, \mathbf{A}) = \left(\frac{\partial}{\partial A_x}\right)^t \left(\frac{\partial}{\partial A_y}\right)^u \left(\frac{\partial}{\partial A_z}\right)^v F_0(aA^2). \tag{4.90}$$

It remains now to find a way to calculate the integrals in Eq. (4.90).

Evaluation of Hermite Coulomb Integrals

The Integrals in Eq. (4.90) are often referred to as Hermite Coulomb integrals, even though the factors in front of actual Coulomb integrals (Eqs. (4.88)–(4.89)) are missing. In order to develop a scheme for evaluating these integrals, we introduce the auxiliary integrals [7]:

$$R^n_{tuv}(a,\mathbf{A}) = \left(\frac{\partial}{\partial A_x}\right)^t \left(\frac{\partial}{\partial A_y}\right)^u \left(\frac{\partial}{\partial A_z}\right)^v R^n_{000}(a,\mathbf{A}), \tag{4.91}$$

where

$$R^n_{000}(a,\mathbf{A}) = (-2a)^n F_n(aA^2). \tag{4.92}$$

By incrementing t, we obtain

$$\begin{aligned} R^n_{t+1,u,v}(a,\mathbf{A}) &= \left(\frac{\partial}{\partial A_x}\right)^t \left(\frac{\partial}{\partial A_y}\right)^u \left(\frac{\partial}{\partial A_z}\right)^v \frac{\partial R^n_{000}(a,\mathbf{A})}{\partial A_x} \\ &= \left(\frac{\partial}{\partial A_x}\right)^t A_x R^{n+1}_{0uv}(a,\mathbf{A}), \end{aligned} \tag{4.93}$$

where we have used the differentiating properties of the nth order Boys function. The operator on the last line may be written as

$$\left(\frac{\partial}{\partial A_x}\right)^t A_x = \left[\left(\frac{\partial}{\partial A_x}\right)^t, A_x\right] + A_x \left(\frac{\partial}{\partial A_x}\right)^t = t\left(\frac{\partial}{\partial A_x}\right)^{t-1} + A_x \left(\frac{\partial}{\partial A_x}\right)^t, \tag{4.94}$$

which leads to the following recurrence relation

$$R^n_{t+1,u,v} = tR^{n+1}_{t-1,u,v} + A_x R^{n+1}_{tuv}, \tag{4.95}$$

and similarly for the other indices

$$R^n_{t,u+1,v} = uR^{n+1}_{t,u-1,v} + A_y R^{n+1}_{tuv}, \tag{4.96}$$

$$R^n_{t,u,v+1} = vR^{n+1}_{t,u,v-1} + A_z R^{n+1}_{tuv}. \tag{4.97}$$

Thus, all Hermite Coulomb integrals of order $t+u+v \leq N$ can be generated from the Boys functions of order $n \leq N$ by recursion.

4.5.4 Cartesian Coulomb integrals

We are now in a position to calculate the Cartesian Coulomb integrals:

$$\begin{aligned} V^{efg}_{ab} &= \langle G_a| \left(\frac{\partial}{\partial C_x}\right)^e \left(\frac{\partial}{\partial C_y}\right)^f \left(\frac{\partial}{\partial C_z}\right)^g r_C^{-1} |G_b\rangle \\ &= \int \Omega_{ab}(\mathbf{r}) \left(\frac{\partial}{\partial C_x}\right)^e \left(\frac{\partial}{\partial C_y}\right)^f \left(\frac{\partial}{\partial C_z}\right)^g r_C^{-1}\, \mathrm{d}\mathbf{r}, \end{aligned} \tag{4.98}$$

and

$$g_{acbd} = \langle G_a(\mathbf{r}_1) G_c(\mathbf{r}_2)| \frac{1}{r_{12}} |G_b(\mathbf{r}_1) G_d(\mathbf{r}_2)\rangle$$
$$= \int \frac{\Omega_{ab}(\mathbf{r}_1)\Omega_{cd}(\mathbf{r}_2)}{r_{12}} \,\mathrm{d}\mathbf{r}_1 \,\mathrm{d}\mathbf{r}_2. \tag{4.99}$$

Earlier in this chapter we show that the overlap distribution can be expanded in terms of Hermite Gaussians (Eq. (4.25)), which we can insert into the above equations

$$V_{ab}^{efg} = \sum_{tuv} E_{tuv}^{ab} \int \Lambda_{tuv}(\mathbf{r}) \left(\frac{\partial}{\partial C_x}\right)^e \left(\frac{\partial}{\partial C_y}\right)^f \left(\frac{\partial}{\partial C_z}\right)^g r_C^{-1} \,\mathrm{d}\mathbf{r} \tag{4.100}$$

$$g_{acbd} = \sum_{tuv} E_{tuv}^{ab} \sum_{t'u'v'} E_{t'u'v'}^{cd} \int\int \frac{\Lambda_{tuv}(\mathbf{r}_1)\Lambda_{t'u'v'}(\mathbf{r}_2)}{r_{12}} \,\mathrm{d}\mathbf{r}_1 \,\mathrm{d}\mathbf{r}_2, \tag{4.101}$$

where for example

$$E_{tuv}^{ab} = E_t^{ij} E_u^{kl} E_v^{mn}. \tag{4.102}$$

The integrals in these two equations are nothing but the integrals in Eqs. (4.82)–(4.83). Thus, we can use the result from last section to obtain the final expressions for Cartesian Coulomb integrals:

$$V_{ab}^{efg} = (-1)^{e+f+g} \frac{2\pi}{p} \sum_{tuv} E_{tuv}^{ab} R_{t+e,u+f,v+g}(p, \mathbf{R}_{PC}), \tag{4.103}$$

$$g_{acbd} = \frac{2\pi^{5/2}}{pq\sqrt{p+q}} \sum_{tuv} E_{tuv}^{ab} \sum_{t'u'v'} (-1)^{t'+u'+v'} E_{t'u'v'}^{cd} R_{t+t',u+u',v+v'}(\alpha, \mathbf{R}_{PQ}), \tag{4.104}$$

where

$$p = a + b, \tag{4.105}$$
$$q = c + d, \tag{4.106}$$
$$\mathbf{P} = \frac{a\mathbf{A} + b\mathbf{B}}{p}, \tag{4.107}$$
$$\mathbf{Q} = \frac{c\mathbf{C} + d\mathbf{D}}{q}. \tag{4.108}$$

Using these expressions, in combination with the recurrence relations for Hermite coefficients E_{tuv}^{ab} and Hermite Coulomb integrals R_{tuv}, the Cartesian Coulomb integrals can be calculated straightforwardly.

4.6 Geometrical Derivative Integral

The derivatives of molecular integrals with respect to the nuclei positions, is required for studying various molecular properties, such as characterization of stationary points on molecular potential energy surfaces and magnetic properties involving an external magnetic field [7]. The former involves calculation of the derivatives of the energy, which we will focus on in the following.

We consider the (restricted) Hartree-Fock energy (see Chapter (2.5.2)):

$$E = \sum_{pq}^{M} P_{pq} h_{pq} + \frac{1}{2} \sum_{pqrs}^{M} P_{pq} P_{rs} \left(g_{prqs} - \frac{1}{2} g_{prsq} \right), \tag{4.109}$$

where the sums run over contracted Gaussian-type orbitals (CGTOs). The derivatives of this expression with respect to the nuclear coordinate N_x is given by

$$\begin{aligned} \frac{\partial E}{\partial N_x} = & \sum_{pq} P_{pq} \frac{\partial h_{pq}}{\partial N_x} + \frac{1}{2} \sum_{pqrs} P_{pq} P_{rs} \left(\frac{\partial g_{prqs}}{\partial N_x} - \frac{1}{2} \frac{\partial g_{prsq}}{\partial N_x} \right) \\ & + \sum_{pq} \frac{\partial P_{pq}}{\partial N_x} h_{pq} + \sum_{pqrs} \frac{\partial P_{pq}}{\partial N_x} P_{rs} \left(g_{prqs} - \frac{1}{2} g_{prsq} \right), \end{aligned} \tag{4.110}$$

where the two last terms arise due to implicit dependency of molecular orbital coefficients on the nuclear coordinates. As it is shown in Ref. [6], these two terms can be rewritten to give the following expression for the derivative of the energy

$$\frac{\partial E}{\partial N_x} = \sum_{pq} P_{pq} \frac{\partial h_{pq}}{\partial N_x} + \frac{1}{2} \sum_{pqrs} P_{pq} P_{cd} \left(\frac{\partial g_{prqs}}{\partial N_x} - \frac{1}{2} \frac{\partial g_{prsq}}{\partial N_x} \right) - \sum_{pq} W_{pq} \frac{\partial S_{pq}}{\partial N_x}, \tag{4.111}$$

where

$$W_{pq} = 2 \sum_{l} \epsilon_l C_{pl} C_{ql}. \tag{4.112}$$

Thus, the derivatives of the energy with respect to the nuclear positions is given by the derivatives of the one-electron integral h_{pq}, the derivatives of the two-electron integral g_{prqs} and the derivatives of the overlap integral S_{pq}. Now, since the sums over p, q, r and s run over CGTOs (which are linear combination of single Gaussian functions) the derivatives of these molecular integrals involve derivatives of integrals over primitive GTOs. This means that we need to calculate integral derivatives of the form

$$\frac{\partial S_{ab}}{\partial N_x} = \delta_{AN} \frac{\partial S_{ab}}{\partial A_x} + \delta_{BN} \frac{\partial S_{ab}}{\partial B_x}, \tag{4.113}$$

$$\begin{aligned} \frac{\partial h_{ab}}{\partial N_x} = & \delta_{AN} \frac{\partial T_{ab}}{\partial A_x} + \delta_{BN} \frac{\partial T_{ab}}{\partial B_x} - Z_N V_{ab}^{100}(\mathbf{C}_N) \\ & - \delta_{AN} \sum_{K} Z_K \frac{\partial V_{ab}^{000}(\mathbf{C}_K)}{\partial A_x} - \delta_{BN} \sum_{K} Z_K \frac{\partial V_{ab}^{000}(\mathbf{C}_K)}{\partial B_x}, \end{aligned} \tag{4.114}$$

and

$$\frac{\partial g_{acbd}}{\partial N_x} = \delta_{AN}\frac{\partial g_{acbd}}{\partial A_x} + \delta_{BN}\frac{\partial g_{acbd}}{\partial B_x} + \delta_{CN}\frac{\partial g_{acbd}}{\partial C_x} + \delta_{DN}\frac{\partial g_{acbd}}{\partial D_x}, \tag{4.115}$$

where a, b, c and d now are indices of primitive Gaussian-type orbitals (GTOs). The molecular integrals S_{ab}, T_{ab}, V_{ab}^{000} and g_{acbd} are all expressed in terms of the overlap distribution Ω_{ab} (Eqs. (4.37), (4.98) and (4.99)), so we need a method for calculating the derivatives of the overlap distribution with respect to the nuclear coordinates. Once we know the derivatives of the overlap distribution we can compute the derivatives of the molecular integrals.

To find the geometrical derivatives of the overlap distribution, we could compute the derivatives with respect to the nuclear coordinates directly. This leads to an analogous expansion like the one in Eq. (4.25), but with a higher summation range. Therefore, the amount of work required to transform from the Hermite Gaussians to the Cartesian Gaussians, is greater for the expansion of the differentiated overlap distributions, compared to the undifferentiated one. The amount of extra work increases as the order of differentiation increases. A better approach is to calculate the derivatives indirectly, as suggested in Ref. [14]. This approach is based on the fact that in the Hermite expansion:

$$\Omega_{ij} = \sum_{t=0}^{i+j} E_t^{ij}\Lambda_t, \tag{4.116}$$

the expansion coefficients E_t^{ij} are functions of $Q_x = A_x - B_x$ only (independent of P_x), and the Hermite Gaussians are functions of $P_x = \frac{aA_x+bB_x}{p}$ only (independent of Q_x). The derivatives with respect to those coordinates take a simple form and by using the notation

$$\Omega_{ij}^{mn} = \frac{\partial^{m+n}\Omega_{ij}}{\partial P_x^m \partial Q_x^n}, \tag{4.117}$$

we obtain

$$\Omega_{ij}^{mn} = \sum_{t=0}^{i+j} E_t^{ij;\,n}\Lambda_{t+m}, \tag{4.118}$$

where the differentiated coefficients are those given by Eq. (4.32). Note that the summation range is the same as for the undifferentiated expansion, and hence is the number of operations the same as the undifferentiated case. Now, these derivatives are related to the derivatives with respect to the nuclear coordinates by

$$\frac{\partial}{\partial A_x} = \frac{a}{p}\frac{\partial}{\partial P_x} + \frac{\partial}{\partial Q_x}, \tag{4.119}$$

$$\frac{\partial}{\partial B_x} = \frac{b}{p}\frac{\partial}{\partial P_x} - \frac{\partial}{\partial Q_x}, \tag{4.120}$$

and

$$\frac{\partial}{\partial P_x} = \frac{\partial}{\partial A_x} + \frac{\partial}{\partial B_x}, \tag{4.121}$$

$$\frac{\partial}{\partial Q_x} = \frac{q}{a}\frac{\partial}{\partial P_x} - \frac{q}{a}\frac{\partial}{\partial B_x}. \tag{4.122}$$

Thus, the derivatives with respect to nuclear coordinates can be found by using these relations. Higher order derivatives can be generated according to the binomial expansion [14]

$$\left(\frac{\partial}{\partial A_x}\right)^q = \sum_{k=0}^{q} \binom{q}{k} \left(\frac{a}{p}\right)^k \left(\frac{\partial}{\partial Q_x}\right)^{q-k} \left(\frac{\partial}{\partial P_x}\right)^k, \tag{4.123}$$

$$\left(\frac{\partial}{\partial B_x}\right)^r = \left(\frac{\partial}{\partial P_x}\right)^r - \sum_{k=0}^{r-1} \binom{r}{k} \left(\frac{\partial}{\partial A_x}\right)^{r-k} \left(\frac{\partial}{\partial B_x}\right)^k. \tag{4.124}$$

Note that these expansions are independent of Cartesian quantum numbers.

Chapter 5

From Quantum Mechanics to Molecular Dynamics

In quantum mechanics, the dynamics of particles is described by the Schrödinger equation. In classical mechanics, on the other hand, the evolution of a system is determined by the classical equations of motion, in particular Newton's second law. From a conceptual point of view, quantum mechanics is more fundamental than classical mechanics as it encompasses classical mechanics as a special case, in the limit of large quantum numbers. This is the essence of the correspondence principle [9]. In studies of processes at the molecular and (sub)atomic level, quantum mechanics has had a major success, but the complexity of the Schrödinger equation has limited its applications to very simple systems and very small number of particles. Macroscopic processes are therefore extremely difficult to handle quantum mechanically. However, classically these problems are simpler to solve, leading to the development of a new technique for molecular studies, namely molecular dynamics (MD) [15]. This technique involves computer simulations of systems at the atomic level, where the equations of motion are solved numerically to follow the time evolution of the system, allowing for "computer measurement" of thermodynamic properties of the system.

In this chapter the transition from quantum mechanics to MD is discussed. First, a derivation of classical MD is given, starting from the time-dependent Schrödinger equation. Then, an outlook on the methods of ab initio MD is provided. Finally, in the last part of this chapter, the interaction potentials in MD simulations are discussed. The material in this chapter is based on Refs. [5, 15, 16].

5.1 Deriving Classical Molecular Dynamics

In the upcoming sections, we will follow the route suggested by Ref. [16] to derive classical MD, starting from Schrödinger equation.

5.1.1 Decomposition of the Hamiltonian

We start with the time-dependent Schrödinger equation for a system of electrons and nuclei:

$$i\hbar\frac{\partial}{\partial t}\Psi_{\rm tot}(\{\mathbf{r}_i\},\{\mathbf{R}_n\};t) = \mathcal{H}\Psi_{\rm tot}(\{\mathbf{r}_i\},\{\mathbf{R}_n\};t), \tag{5.1}$$

where $\Psi_{\rm tot}(\{\mathbf{r}_i\},\{\mathbf{R}_n\};t)$ is the total wave function of the system, and the Hamiltonian is given by

$$\begin{aligned}\mathcal{H} = &-\sum_{n=1}^{N_n}\frac{\hbar^2}{2M_n}\nabla_n^2 - \sum_{i=1}^{N_e}\frac{\hbar^2}{2m_e}\nabla_i^2 + \frac{1}{4\pi\epsilon_0}\frac{1}{2}\sum_{\substack{i,j=1\\ i\neq j}}^{N_e}\frac{e^2}{|\mathbf{r}_i-\mathbf{r}_j|}\\ &-\frac{1}{4\pi\epsilon_0}\sum_{n=1}^{N_n}\sum_{i=1}^{N_e}\frac{Z_n e^2}{|\mathbf{r}_i-\mathbf{R}_n|} - \frac{1}{4\pi\epsilon_0}\frac{1}{2}\sum_{\substack{n,m=1\\ n\neq m}}^{N_n}\frac{Z_n Z_m e^2}{|\mathbf{R}_n-\mathbf{R}_m|}.\end{aligned} \tag{5.2}$$

The indices i and j refer to the electrons while n and m refer to the nuclei, m_e is the electron mass and M_n is the mass of nucleus n. The first two terms represent the kinetic energy of the nuclei and electrons, while the third and fourth terms represent the Coulomb repulsion between the electrons and the Coulomb attraction between the electrons and nuclei, respectively. Finally, the last term represents the Coulomb repulsion between the nuclei. For our purpose, it is convenient to decompose this Hamiltonian into

$$\mathcal{H} = -\sum_{n=1}^{N_n}\frac{\hbar^2}{2M_n}\nabla_n^2 - \sum_{i=1}^{N_e}\frac{\hbar^2}{2m_e}\nabla_i^2 + V_{\rm N}(\{\mathbf{R}_n\}) + V_{\rm e}(\{\mathbf{r}_i\},\{\mathbf{R}_n\}), \tag{5.3}$$

where $V_{\rm N}$ is the Coulomb interaction energy between the nuclei, and $V_{\rm e}$ contains the Coulomb repulsion between the electrons and the Coulomb attraction between the electrons and nuclei. The Hamiltonian can be decomposed even further by

$$\mathcal{H} = \sum_{n=1}^{N_n}\frac{\hbar^2}{2M_n}\nabla_n^2 + \mathcal{H}_{\rm Ne}(\{\mathbf{r}_i\},\{\mathbf{R}_n\}), \tag{5.4}$$

where $\mathcal{H}_{\rm Ne}$ is

$$\begin{aligned}\mathcal{H}_{\rm Ne}(\{\mathbf{r}_i\},\{\mathbf{R}_n\}) &= \sum_{i=1}^{N_e}\frac{\hbar^2}{2m_e}\nabla_i^2 + V_{\rm N}(\{\mathbf{R}_n\}) + V_{\rm e}(\{\mathbf{r}_i\},\{\mathbf{R}_n\})\\ &= \sum_{i=1}^{N_e}\frac{\hbar^2}{2m_e}\nabla_i^2 + V_{\rm Ne}(\{\mathbf{r}_i\},\{\mathbf{R}_n\}).\end{aligned} \tag{5.5}$$

To keep the notation simple we will use $\mathbf{r} = \{\mathbf{r}_i\}$ and $\mathbf{R} = \{\mathbf{R}_n\}$, for electronic and nuclear coordinates, respectively, unless otherwise specified.

5.1.2 Separation of the Wave function

As a first approximation we assume that the solution $\Psi_{\text{tot}}(\mathbf{r}, \mathbf{R}; t)$ of the full Schrödinger equation (5.2) has the form of a separated wave function with a nuclear and an electronic component:

$$\Psi_{\text{tot}}(\mathbf{r}, \mathbf{R}; t) \approx \tilde{\Psi}_{\text{tot}}(\mathbf{r}, \mathbf{R}; t) = \chi(\mathbf{R}; t)\Psi(\mathbf{r}; t) \exp\left[\frac{i}{\hbar}\int_{t_0}^{t} \tilde{E}_{\text{Ne}}(t')\,\mathrm{d}t'\right], \tag{5.6}$$

where χ and Ψ are the nuclear and electronic wave functions, respectively. Each component is assumed to be separately normalized to unity at every instant of time, i.e.

$$\langle \Psi; t | \Psi; t \rangle = \int \Psi^*(\mathbf{r}; t)\Psi(\mathbf{r}; t)\,\mathrm{d}\mathbf{r} = 1, \tag{5.7}$$

$$\langle \chi; t | \chi; t \rangle = \int \chi^*(\mathbf{R}; t)\chi(\mathbf{R}; t)\,\mathrm{d}\mathbf{R} = 1. \tag{5.8}$$

The phase factor $\tilde{E}_{\text{Ne}}$ is defined as

$$\tilde{E}_{\text{Ne}}(t) = \int \Psi^*(\mathbf{r}; t)\chi^*(\mathbf{R}; t)\mathcal{H}_{\text{Ne}}\Psi(\mathbf{r}; t)\chi(\mathbf{R}; t)\,\mathrm{d}\mathbf{R}\,\mathrm{d}\mathbf{r}, \tag{5.9}$$

which has a convenient form for the following derivation. Inserting the separation ansatz in Eq. (5.6) into the time-dependent Schrödinger equation, multiplying from the left by $\Psi^*(\mathbf{r}; t)\chi^*(\mathbf{R}; t)$ and integrating over $\mathbf{r}$ and $\mathbf{R}$, and finally imposing the energy conservation

$$\frac{\mathrm{d}}{\mathrm{d}t}\int \tilde{\Psi}^*\mathcal{H}\tilde{\Psi}\,\mathrm{d}\mathbf{R}\,\mathrm{d}\mathbf{r} = 0, \tag{5.10}$$

yields the following relations

$$i\hbar\frac{\partial\Psi}{\partial t} = -\sum_{i=1}^{N_e}\frac{\hbar^2}{2m_e}\nabla_i^2\Psi + \left(\int \chi^*(\mathbf{R}; t)V_{\text{Ne}}(\mathbf{R}, \mathbf{r})\chi(\mathbf{R}; t)\,\mathrm{d}\mathbf{R}\right)\Psi, \tag{5.11}$$

$$i\hbar\frac{\partial\chi}{\partial t} = -\sum_{n=1}^{N_n}\frac{\hbar^2}{2M_n}\nabla_n^2\chi + \left(\int \Psi^*(\mathbf{r}; t)\mathcal{H}_{\text{Ne}}(\mathbf{R}, \mathbf{r})\Psi(\mathbf{r}; t)\,\mathrm{d}\mathbf{r}\right)\chi. \tag{5.12}$$

Note that in these two equations, the phase factor doesn't arise. This is due to the chosen form for the phase of the wave function in Eq. (5.9). The obtained coupled system of equations can be solved instead of the original Schrödinger equation, whenever the explicit knowledge of the phase is of no importance. This is for example the case in expectation value calculations since all expectation values are invariant under phase shift.

In this description, both electrons and nuclei move in time-dependent effective potentials. These are obtained from appropriate expectation values over the coordinates of the other unknown. This picture is the foundation of the time-dependent self-consistent field (TDSCF) approach.

5.1.3 The Nuclear Wave function

The next step in the derivation of classical MD is to approximate the nuclei as classical point particles. In order to do this, we first rewrite $\chi(\mathbf{R};t)$ in terms of a real amplitude factor $A > 0$, and a real phase factor S (see Chapter 2.4 in Ref. [17]):

$$\chi(\mathbf{R};t) = A(\mathbf{R};t)\exp\left[\frac{i}{\hbar}S(\mathbf{R};t)\right]. \tag{5.13}$$

This rewrite to polar form can be done for any complex function of $\mathbf{R}$ and $\mathbf{t}$. By inserting the new form of $\chi(\mathbf{R};t)$ into Eq. (5.12) and separating the real and imaginary parts, we get

$$\frac{\partial S}{\partial t} + \sum_{n=1}^{N_n}\frac{1}{2M_n}(\nabla_n S)^2 + \int \Psi^*\mathcal{H}_{\mathrm{Ne}}\Psi\,\mathrm{d}\mathbf{r} = \hbar^2\sum_{n=1}^{N_n}\frac{1}{2M_n}\frac{\nabla_n^2 A}{A}, \tag{5.14a}$$

$$\frac{\partial A}{\partial t} + \sum_{n=1}^{N_n}\frac{1}{M_n}(\nabla_n A)(\nabla_n S) + \sum_{n=1}^{N_n}\frac{1}{2M_n}A(\nabla_n^2 S) = 0. \tag{5.14b}$$

This set of equations corresponds exactly to Eq. (5.12), but is expressed in the new variables A and S, and can be used to solve the time-dependent Schrödinger equation for the nuclear component.

The Relation for the Amplitude factor A

The relation for A, given in Eq. (5.14b), is nothing but a continuity equation. This relation is independent of $\hbar$ and ensures locally the conservation of the particle probability $|\chi|^2 = A^2$ associated to the nuclei. This can be shown by examining how the probability density $|\chi|^2$ changes in time, i.e.

$$\frac{\partial}{\partial t}|\chi|^2 = \chi^*\frac{\partial\chi}{\partial t} + \frac{\partial\chi^*}{\partial t}\chi. \tag{5.15}$$

Inserting the nuclear Schrödinger equation (5.12) and its complex conjugate, we obtain

$$\begin{aligned}\frac{\partial}{\partial t}|\chi|^2 &= -\sum_{n=1}^{N_n}\frac{\hbar}{2iM_n}\left(\chi^*\nabla_n^2\chi - \chi\nabla_n^2\chi^*\right)\\ &= -\sum_{n=1}^{N_n}\nabla_n\cdot\left[\frac{\hbar}{2iM_n}\left(\chi^*\nabla_n\chi - \chi\nabla_n\chi^*\right)\right]\\ &= -\sum_{n=1}^{N_n}\nabla_n\cdot\left[\frac{\hbar}{M_n}\mathrm{Im}\left(\chi^*\nabla_n\chi\right)\right],\end{aligned} \tag{5.16}$$

where the Hermiticity of the operator $\mathcal{H}_{\mathrm{Ne}}$ has been used. This equation is of the form of a standard continuity equation;

$$\frac{\partial \rho}{\partial t} = -\nabla \cdot \mathbf{j}, \tag{5.17}$$

and ensures local conservation of the particle probability.

Now, by inserting the polar form of the nuclear equation (Eq. (5.13)) into Eq. (5.16) and using the relation

$$\chi^* \nabla_n \chi = A(\nabla_n A) + \frac{i}{\hbar} A^2 (\nabla_n S), \tag{5.18}$$

we obtain

$$\frac{\partial A^2}{\partial t} = -\sum_{n=1}^{N_n} \nabla_n \cdot \left(A^2 \frac{\nabla_n S}{M_n} \right). \tag{5.19}$$

This is exactly the same expression we get by multiplying $2A$ on both sides of Eq. (5.14b). Thus, we have shown that the relation for the amplitude A, is nothing but the continuity relation for the particle density associated with the nuclei.

The Relation for the Phase Factor S

For our purpose, the relation for the phase S of the nuclear wave function is much more interesting. By considering $\hbar \to 0$ as the classical limit, Eq. (5.14a) reduces to

$$\frac{\partial S}{\partial t} + \sum_{n=1}^{N_n} \frac{1}{2M_n} (\nabla_n S)^2 + \int \Psi^* \mathcal{H}_{\mathrm{Ne}} \Psi \, \mathrm{d}\mathbf{r} = 0, \tag{5.20}$$

or, by setting $\nabla_{\mathbf{R}} S = (\nabla_1 S, \ldots, \nabla_{N_n} S)$,

$$\frac{\partial S}{\partial t} + H(\mathbf{R}, \nabla_{\mathbf{R}} S) = 0, \tag{5.21}$$

where $H(\mathbf{R}, \nabla_{\mathbf{R}} S)$ contains the two last terms on the left hand side in Eq. (5.20). We recognize the last equation as the Hamiltonian-Jacobi form of the equation of motion of classical mechanics with the classical Hamiltonian function [16]:

$$H(\mathbf{R}, \mathbf{P}) = T(\mathbf{P}) + V(\mathbf{R}). \tag{5.22}$$

This function is defined in terms of the generalized coordinates $\mathbf{R} = \{\mathbf{R}_n\}$ and their conjugated momenta $\mathbf{P} = \{\mathbf{P}_n\}$, where one puts

$$\mathbf{P}_n \equiv \nabla_n S. \tag{5.23}$$

In this description the potential is the time-dependent term $\langle \Psi | \mathcal{H}_{\mathrm{Ne}} | \Psi \rangle$. The equations of motion associated to Eq. (5.20) can then be written as

$$\frac{d\mathbf{P}_n}{dt} = -\nabla_n \left\langle \Psi | \mathcal{H}_{\mathrm{Ne}} | \Psi \right\rangle, \tag{5.24}$$

or

$$\begin{aligned} M_n \ddot{\mathbf{R}}_n &= -\nabla_n \langle \Psi | \mathcal{H}_{\mathrm{Ne}} | \Psi \rangle \\ &= -\nabla_n V^{\mathrm{Ehr}}(\mathbf{R}(t)). \end{aligned} \tag{5.25}$$

Thus, the nuclei move according to classical mechanics in an effective potential V^{Ehr} due to the electrons. This potential depends on the nuclear positions at time t while they are fixed at their instantaneous values $\{\mathbf{R}_n(t)\}$.

5.1.4 Nuclei as Classical Point Particles

As already mentioned, the nuclei are approximated as point particles in classical MD. Therefore, the nuclear wave function has to replaced by the positions of the nuclei in the electronic equations of motion. This can be done by rewriting the nuclear wave function as a product of delta functions. More precisely, we write (in the limit $\hbar \to 0$):

$$|\chi(\mathbf{R}; t)|^2 = \prod_n \delta(\mathbf{R}_n - \mathbf{R}_n(t)), \tag{5.26}$$

so that for example

$$\int \chi^*(\mathbf{R}; t) \mathbf{R}_n \chi(\mathbf{R}; t) \, \mathrm{d}\mathbf{R} \quad \xrightarrow{\hbar \to 0} \quad \mathbf{R}_n(t). \tag{5.27}$$

This leads to the following equation for the electronic degrees of freedom

$$\begin{aligned} i\hbar \frac{\partial}{\partial t} \Psi_{\mathbf{R}(t)}(\mathbf{r}; t) &= \left(-\sum_{i=1}^{N_e} \frac{\hbar^2}{2m_e} \nabla_i^2 + V_{\mathrm{Ne}}(\mathbf{R}(t), \mathbf{r}) \right) \Psi_{\mathbf{R}(t)}(\mathbf{r}; t) \\ &= \mathcal{H}_{\mathrm{Ne}}(\mathbf{r}, \mathbf{R}(t)) \Psi_{\mathbf{R}(t)}(\mathbf{r}; t), \end{aligned} \tag{5.28}$$

where the electronic wave function Ψ is indexed with $\mathbf{R}(t)$, to clearly show the implicit dependency on $\mathbf{R}$ via the coupling in the system. Note that the electronic wave function in the last equation is not equal to the wave function in Eq. (5.11), due to the approximation introduced by letting $\hbar \to 0$.

The approach relying on solving Eq. (5.25) together with Eq. (5.28) is known as Ehrenfest MD, named after Paul Ehrenfest, who was the first to show how Newtonian classical dynamics can be derived from Schrödinger wave equation [16]. This approach is a mixed approach because only the nuclei are treated classically, while the electrons are still considered as quantum mechanical particles.

5.2 Ab Initio Molecular Dynamics

The basic idea of the so-called ab initio MD, is to solve the electronic Schrödinger equation approximately to determine an effective potential for the nuclei. From the obtained potential the nuclear forces can be computed, and Newton's equations can be applied to find the motion of the nuclei. This hybrid approach in its different

variants forms the basis for the Ehrenfest MD, Born-Oppenheimer MD (BOMD) and Car-Parrinello MD (CPMD).

In the next three sections, we will give a short description of each of these ab initio methods. Our goal is not give a detailed description of these methods, but only a quick overview without discussing all the details. The reader is referred to Ref. [16] for details and more complementary description.

5.2.1 Ehrenfest Molecular Dynamics

Ehrenfest MD involves solving the following equations of motion:

$$M_n \ddot{\mathbf{R}}_n = -\nabla_n \langle \Psi | \mathcal{H}_{\mathrm{Ne}} | \Psi \rangle \,, \tag{5.29}$$

$$i\hbar \frac{\partial \Psi_{\mathbf{R}(t)}}{\partial t} = \mathcal{H}_{\mathrm{Ne}} \Psi_{\mathbf{R}(t)}, \tag{5.30}$$

where $\mathcal{H}_{\mathrm{Ne}}$ is time-dependent via the nuclear coordinates $\{\mathbf{R}_n\}$. This method is, as already mentioned, a mean field self-consistent method, where the time-dependent electronic Schrödinger equation is solved on-the-fly, i.e. for each time step of Newton's equation.

A common restriction, which normally is introduced in Ehrenfest MD, is to first expand the electronic wave function in the so-called adiabatic basis [15], and thereafter restrict the whole electronic wave function to a single state in that basis, typically the ground state. The adiabatic basis consists of the solutions of the time-independent electronic Schrödinger equation given by

$$\mathcal{H}_{\mathrm{Ne}} \Psi_k(\mathbf{r}; \mathbf{R}) = E_k(\mathbf{R}) \Psi_k(\mathbf{r}; \mathbf{R}). \tag{5.31}$$

The solutions Ψ_k of this equation are combined with complex, time-dependent coefficients to construct the electronic wave function. Mathematically, this can be stated as

$$\Psi_{\mathbf{R}(t)}(\mathbf{r}; t) = \sum_{j=0}^{\infty} c_j(t) \Psi_k(\mathbf{r}; \mathbf{R}), \tag{5.32}$$

where the coefficients describe how the occupancy of the different states evolves over time. Restricting the electronic wave function to the ground state in this basis corresponds to only include the first term in the sum. Since the time evolution of the wave function corresponds to a unitary propagation [16], the ground state wave function which minimizes the expectation value of $\mathcal{H}_{\mathrm{Ne}}$ initially, will stay in its respective minimum as the nuclei move.

In Ehrenfest MD the time scale and thus the time step to integrate the equations motion is determined by the dynamics of the electrons. As a result, since the electrons move much faster than the nuclei, the largest possible time step is the one that allows to integrate the electronic equations of motion. This is a huge disadvantage of the

Ehrenfest MD, since we are confined to work with much smaller time scales than the one given by the nuclear motion. Because of this, the Ehrenfest MD is not in widespread use, specially if the system has many active degrees of freedom, although it has been used to study collision and scattering-type problems [16].

5.2.2 Born-Oppenheimer Molecular Dynamics

The BOMD is based on the Born-Oppenheimer approximation (see Section 2.1.3), which rests on the fact that nuclei are much more massive than electrons. Because of the huge difference in mass between electrons and nuclei, the former can be considered as particles that follow the nuclear motion adiabatically. This means that the electrons respond instantaneously to the nuclear motion and relax to the instantaneous ground-state configuration. We may therefore consider the nuclei as fixed with respect to the electronic motion. This means that we can fix the nuclear configuration $\{\mathbf{R}_n\}$ at some value and solve for the electronic wave function, which only depends implicitly on $\{\mathbf{R}_n\}$.

The ansatz for the wave function in BOMD, using $\mathbf{r} = \{\mathbf{r}_i\}$ and $\mathbf{R} = \{\mathbf{R}_n\}$, is

$$\Psi_{\text{tot}}(\mathbf{r}, \mathbf{R}; t) \approx \tilde{\Psi}_{\text{BO}}(\mathbf{r}, \mathbf{R}) = \chi_{\text{BO}}(\mathbf{R}; t)\Psi_{\text{BO}}(\mathbf{r}; \mathbf{R}), \tag{5.33}$$

which is separated in a time-dependent nuclear term and an electronic term which depends parametrically on $\mathbf{R}$. We assume that both terms are separately normalized to unity at every instant of time;

$$\langle \Psi_{\text{BO}}; \mathbf{R} | \Psi_{\text{BO}}; \mathbf{R} \rangle = \int \Psi^*_{\text{BO}}(\mathbf{r}; \mathbf{R})\Psi_{\text{BO}}(\mathbf{r}; \mathbf{R})\, \mathrm{d}\mathbf{r} = 1, \tag{5.34}$$

$$\langle \chi_{\text{BO}}; t | \chi_{\text{BO}}; t \rangle = \int \chi^*_{\text{BO}}(\mathbf{R}; t)\chi_{\text{BO}}(\mathbf{R}; t)\, \mathrm{d}\mathbf{R} = 1. \tag{5.35}$$

Moreover we require the electronic wave function $\Psi_{\text{BO}}(\mathbf{r}, \mathbf{R})$ to satisfy the time-independent Schrödinger equation for the electrons with fixed nuclei:

$$\left(-\sum_{i=1}^{N_e} \frac{\hbar^2}{2m_e} \nabla_i^2 + V_{\text{Ne}}(\mathbf{r}, \mathbf{R}) \right) \Psi_{\text{BO}} = E_{\text{Ne}}(\mathbf{R})\Psi_{\text{BO}}, \tag{5.36}$$

where V_{Ne} contains the Coulomb interaction energies. This equation yields a set of normalized eigenfunctions $\Psi_{\text{BO},k}$ with corresponding eigenvalues $E_{\text{Ne},k}$.

The total time-independent Schrödinger equation for both electrons and nuclei, is given by

$$\left(-\sum_{n=1}^{N_n} \frac{\hbar^2}{2M_n} \nabla_n^2 - \sum_{i=1}^{N_e} \frac{\hbar^2}{2m_e} \nabla_i^2 + V_{\text{Ne}}(\mathbf{r}, \mathbf{R}) \right) \chi_{\text{BO}}\Psi_{\text{BO}} = E\chi_{\text{BO}}\Psi_{\text{BO}}, \tag{5.37}$$

where E must not be confused with the electronic energy $E_{\text{Ne}}(\mathbf{R})$. Multiplying both sides from left with Ψ^*_{BO} and integrating over $\mathbf{r}$ gives

$$\left(-\sum_{n=1}^{N_n}\frac{\hbar^2}{2M_n}\nabla_n^2+E_{\mathrm{Ne}}(\mathbf{R})\right)\chi_{\mathrm{BO}}$$
$$-\sum_{n=1}^{N_n}\frac{\hbar^2}{2M_n}\int\Psi_{\mathrm{BO}}^*\left(\chi_{\mathrm{BO}}\nabla_n^2\Psi_{\mathrm{BO}}+2\nabla_n\chi_{\mathrm{BO}}\cdot\nabla_n\Psi_{\mathrm{BO}}\right)\mathrm{d}\mathbf{r}=E\chi_{\mathrm{BO}}. \tag{5.38}$$

The terms in the second brackets are normally ignored since their contribution is negligible compared to the other terms, due to the mass difference between electrons and nuclei (see for example Chapter 3 in Ref. [18]). We may therefore drop these terms, to obtain

$$\left(-\sum_{n=1}^{N_n}\frac{\hbar^2}{2M_n}\nabla_n^2+E_{\mathrm{Ne}}(\mathbf{R})\right)\chi_{\mathrm{BO}}=E\chi_{\mathrm{BO}}, \tag{5.39}$$

where the electronic energy $E_{\mathrm{Ne}}(\mathbf{R})$ enters the nuclear equation as the internuclear potential. But, as already mentioned, solving the electronic equation (Eq. (5.36)) yields a *set* of eigenvalues $E_{\mathrm{Ne},k}$. This means that each electronic eigenvalue will give rise to a different internuclear potential. However, one can assume that the electronic states are at the ground state. This is because electrons move much faster than the nuclei and will be able to adjust themselves to the electronic ground state for the current nuclear positions. We can therefore use the ground-state eigenvalue $E_{Ne,0}$ to set up the *time-dependent* Schrödinger equation for the system (after multiplication of Ψ_{BO}^* from left and integrating over $\mathbf{r}$);

$$i\hbar\frac{\partial}{\partial t}\chi_{\mathrm{BO}}=\left(-\sum_{n=1}^{N_n}\frac{\hbar^2}{2M_n}\nabla_n^2+E_{Ne,0}(\mathbf{R})\right)\chi_{\mathrm{BO}}. \tag{5.40}$$

We can now perform the same steps as we did in the derivation of Ehrenfest MD: (i) approximate the nuclear wave function in terms of an amplitude factor and a phase factor, (ii) insert this form in Eq. (5.40) and separate the real and imaginary parts, (iii) neglect terms involving $\hbar$ and (iv) recognize the relation for the phase factor as the Hamiltonian-Jacobi form of the equations of motion of classical mechanics, with a potential given by

$$E_{Ne,0}(\mathbf{R})=\langle\Psi_{\mathrm{BO},0}|\mathcal{H}_{\mathrm{Ne}}|\Psi_{\mathrm{BO},0}\rangle\,. \tag{5.41}$$

By performing these steps, we find the equations of motion fro BOMD to be

$$M_n\ddot{\mathbf{R}}_n=-\nabla_n\min_{\Psi_{\mathrm{BO},0}}\left\{\langle\Psi_{\mathrm{BO},0}|\mathcal{H}_{\mathrm{Ne}}|\Psi_{\mathrm{BO},0}\rangle\right\}, \tag{5.42}$$

$$\mathcal{H}_{\mathrm{Ne}}\Psi_{\mathrm{BO},0}=E_{Ne,0}(\mathbf{R})\Psi_{\mathrm{BO},0}. \tag{5.43}$$

Thus, the computation of the electronic structure is reduced to the solution of the time-independent electronic Schrödinger equation, which is then used for computations of forces acting on the nuclei at each time step. The only time-dependency of the electrons is due to the classical motion of the nuclei. This is in contrast to Ehrenfest MD where the dynamics is determined from the time-dependent electronic Schrödinger equation. Because of this, the time step in BOMD is determined by the nuclear motion. This is a huge advantage of BOMD compared to Ehrenfest MD, where the time step is determined by the electronic motion. The disadvantage of BOMD is, however, that a minimization is required at each time step.

BOMD with Hartree-Fock

As an ending of our discussion of BOMD, we will consider the Born-Oppenheimer equations of motion for the special case when the Hartree-Fock method is used. Within the Hartree-Fock method, the electronic wave function is approximated by a single Slater determinant $\Psi_{\mathrm{SD}} = \det\{\psi_i\}$, where the one-particle orbitals ψ_i, subjected to the orthonormality constraint $\langle\psi_i|\psi_j\rangle = \delta_{ij}$, are optimized to give the variational minimum of the energy expectation value $E^{\mathrm{HF}} = \langle\Psi_{\mathrm{SD}}|\mathcal{H}_{\mathrm{Ne}}|\Psi_{\mathrm{SD}}\rangle$ (see Section 2.4)[1]. In this case, the Lagrange functional, which we wish to minimize by varying the orbitals, is given by

$$\mathcal{L}\{\psi_i\} = \langle\Psi_{\mathrm{SD}}|\mathcal{H}_{\mathrm{Ne}}|\Psi_{\mathrm{SD}}\rangle - \sum_{ij}\Lambda_{ij}\left(\langle\psi_i|\psi_j\rangle - \delta_{ij}\right), \tag{5.44}$$

leading to the well-known Hartree-Fock equations given by

$$\mathcal{F}\psi_i = \sum_j \lambda_{ij}\psi_j, \tag{5.45}$$

with $\mathcal{F}$ as the Fock operator and λ_{ij} as the Lagrange multipliers. Thus, the corresponding equations of motion to those in Eqs. (5.42)–(5.43), read

$$M_n\ddot{\mathbf{R}}_n = -\nabla_n \min_{\{\psi_i\}}\{E^{\mathrm{HF}}\}, \tag{5.46}$$

$$\mathcal{F}\psi_i = \sum_j \lambda_{ij}\psi_j, \tag{5.47}$$

for the Hartree-Fock case.

[1]Note that $\mathcal{H}_{\mathrm{Ne}}$ includes the electrostatic energy of the nuclei, but in Chapter 4 this term was not included in the derivation of the Hartree-Fock equations. However, since the nuclear coordinates are fixed during Hartree-Fock calculations, this term is a constant and the derivation will not be affected by this term.

5.2.3 Car-Parrinello Molecular Dynamics

One of the breakthrough in ab initio MD, came with the development of the Car-Parrinello method [5], which made it possible to treat large-scale problems via ab initio MD. CPMD attempts to combine the advantages of Ehrenfest MD and BOMD, and at the same time avoid their disadvantages. The advantage of Ehrenfest MD is that the wave function that minimize the energy initially, will stay in its respective minimum as the nuclei move, but has the disadvantage of having a time step determined by the fast electronic motion. In BOMD, on the other hand, the time step is determined by the nuclear motion, but a minimization is required at each time step. Ideally, one wishes to integrate the equations of motion on the large time scale set by the nuclear motion, and at the same time avoid the minimization of the energy at each time step. This is exactly what the Car-Parrinello method offers. In CPMD, the electrons are explicitly included as active degrees of freedom via a fictitious dynamic, which is used to keep the electrons near the ground state. In particular, an extended Lagrangian for the system is introduced, leading to a system of coupled equations of motion for the nuclei and the electrons. Thus, an electronic minimization is not needed in every time step, since after an initial, standard minimization, the fictitious dynamics of the electrons will keep them at (or near) the ground state as the nuclei move.

To set up the extended Lagrangian, we consider first the Ehrenfest MD and BOMD, which when restricted to the ground state, have the effective potential felt by the nuclei

$$E_0(\mathbf{R}) \equiv E_{\mathrm{Ne},0}(\mathbf{R}) = \langle \Psi_0 | \mathcal{H}_{\mathrm{Ne}} | \Psi_0 \rangle \,. \tag{5.48}$$

It is clear that the energy of the electronic ground state can be regarded as a functional of the wave function Ψ_0. If the wave function is expanded in a set of time-dependent one-particle functions $\{\psi_i(\mathbf{r}, t)\}$, E_0 can be considered as a functional of the orbitals, i.e. $E_0(\mathbf{R}, \{\psi_i\})$. Now, if we treat the orbitals as "classical particles", one can determine the forces acting on the orbitals as the functional derivatives of the extended Lagrangian with respect to the orbitals—analog to finding the forces acting on the nuclei by taking the derivative with respect to nuclei positions. Using this idea we can set up the extended Lagrangian as

$$\mathcal{L}_{\mathrm{CP}} = \sum_{n=1}^{N_n} \frac{1}{2} M_n \dot{\mathbf{R}}_n + \sum_{i=1}^{N_o} \frac{1}{2} \mu_i \int \dot{\psi}_i^* \dot{\psi}_i \, \mathrm{d}\mathbf{r} - E_0(\mathbf{R}, \{\psi_i\}) + \text{constraint}, \tag{5.49}$$

where μ_i is the fictitious mass of orbital ψ_i and the constraint can for example be the orthonormality of the orbitals;

$$\sum_{ij} \lambda_{ij} \left(\int \psi_i^* \psi_j \, \mathrm{d}\mathbf{r} - \delta_{ij} \right), \tag{5.50}$$

with λ_{ij} as the Lagrange multipliers. This extended Lagrangian consist of two kinetic energy terms, one for the nuclei and one for the electronic orbitals, followed by the potential energy term and possible appropriate constraints. Setting up the respective Euler-Lagrangian equations [19]:

$$\frac{\mathrm{d}}{\mathrm{d}t}\frac{\partial \mathcal{L}_{\mathrm{CP}}}{\partial \dot{\mathbf{R}}_n} = \frac{\partial \mathcal{L}_{\mathrm{CP}}}{\partial \mathbf{R}_n}, \qquad \frac{\mathrm{d}}{\mathrm{d}t}\frac{\partial \mathcal{L}_{\mathrm{CP}}}{\delta \dot{\psi}_k^*} = \frac{\partial \mathcal{L}_{\mathrm{CP}}}{\delta \psi_k^*}, \tag{5.51}$$

we obtain the following equations of motion

$$M_n \ddot{\mathbf{R}}_n = -\nabla_n E_0\left(\mathbf{R}, \{\psi_i\}\right) + \sum_{ij} \lambda_{ij} \nabla_n \left(\int \psi_i^* \psi_j \, \mathrm{d}\mathbf{r} \right), \tag{5.52}$$

$$\mu_k \ddot{\psi}_k = -\frac{\delta E_0}{\delta \psi_k^*} + \sum_j \lambda_{kj} \psi_j. \tag{5.53}$$

where the second term on the right hand side of Eq. (5.52) is kept, due to implicit dependency on the nuclear coordinates. Thus, we can use these two equations to evolve the nuclei and the orbitals forward in time without requiring energy minimization at each step.

The kinetic energy term for the orbitals is perhaps the most unusual and counterintuitive term in the Lagrangian. This term is a consequence of the initial idea of treating the orbitals as classical particles. Note that the mass μ should be sufficiently small to enable the orbitals to adapt reasonably to the changing nuclear configuration. Therefore, the fictitious mass is much smaller than the mass of the nuclei [11]. An extensive discussion about how to choose the fictitious mass and the Car-Parrinello method in general is given in Ref. [16].

CPMD with Hartree-Fock

As for the BOMD, we end the formal discussion of the CPMD by formulating the Car-Parrinello dynamics for the special case of the Hartree-Fock approximation. When using the Lagrangian given by

$$\mathcal{L}_{\mathrm{CP}} = \sum_{n=1}^{N_n} \frac{1}{2} M_n \dot{\mathbf{R}}_n + \sum_{i=1}^{N_o} \frac{1}{2} \mu_i \left\langle \dot{\psi}_i^* | \dot{\psi}_i \right\rangle - \left\langle \Psi_{\mathrm{SD}} | \mathcal{H}_{\mathrm{Ne}} | \Psi_{\mathrm{SD}} \right\rangle + \sum_{ij} \Lambda_{ij} \left(\left\langle \psi_i | \psi_j \right\rangle - \delta_{ij} \right), \tag{5.54}$$

the following equations of motion is obtained

$$M_n \ddot{\mathbf{R}}_n = -\nabla_n E^{\mathrm{HF}} + \sum_{ij} \lambda_{ij} \nabla_n \left\langle \psi_i | \psi_j \right\rangle, \tag{5.55}$$

$$\mu_k \ddot{\psi}_k = -\mathcal{F} \psi_k + \sum_j \lambda_{kj} \psi_j. \tag{5.56}$$

This set of equations is very similar to the one we obtained for BOMD in Eqs. (5.46)–(5.47), but in this case no minimization of the electronic total energy is required and an additional fictitious kinetic energy term is added. It is worth mentioning that in the limit $\mu_k \to 0$, the equations of motion become identical to those in Born-Oppenheimer dynamics, as discussed in Ref. [16].

Model calculation on Hydrogen Molecule

In order to illustrate some of the applications of the CPMD, we will in this section represent the results from a simple calculation on the hydrogen molecule. This example is based on several programming exercises in Ref. [11], and all expressions and basis set parameters are taken from there. The electronic wave function is constructed using the linear combination of atomic orbitals (LCAO) approach, with Gaussian basis functions. The basis set used is an STO-4G basis.

For this diatomic system an C++ code is written[2], which uses the Car-Parrinello method to compute the dynamics of two hydrogen atoms. The simulated annealing method (see Ref. [16], Sect. 2.4.6) is used to evolve the system towards the energy ground state. This is done by adding a frictional term of the form $-\gamma_e \dot{\psi}_i$ to the electronic Car-Parrinello equation of motion, where $\gamma_e \geq 0$ is the friction constant. Thus, we can start at some initial configuration which might be far away from the equilibrium, and let the wave function find its way to the minimum, given that the energy dissipation is done slowly. In Figure 5.1, the change in the electronic energy

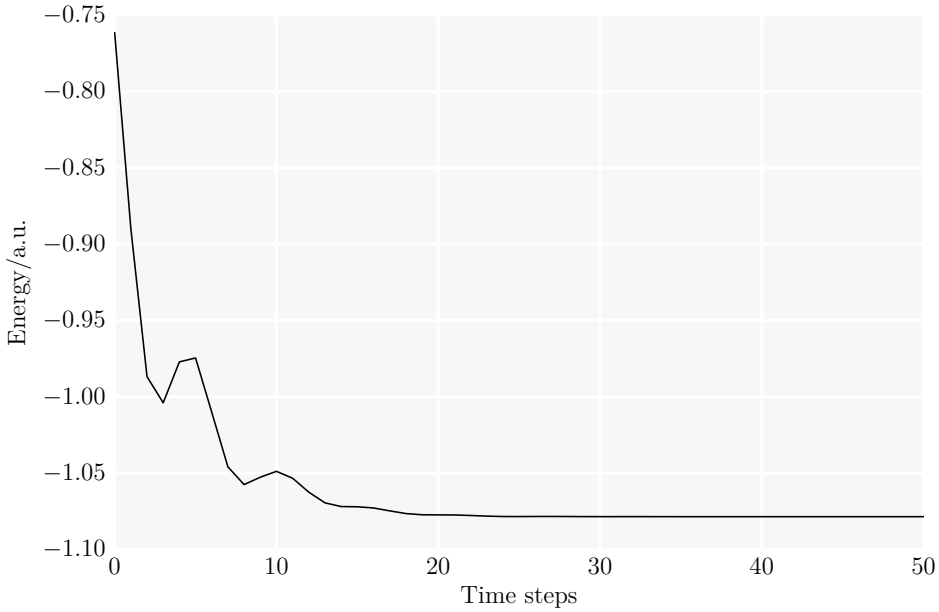

Figure 5.1: Evolution of the electronic energy in a Car-Parrinello simulation of the hydrogen molecule with bond length $X = 1\,\text{a.u.}$, and with frictional force included. The number of electronic integration steps is shown along the x-axis. The time step was set to 0.1 a.u. and the frictional constant was set to 1. The energy stabilizes at $E_{\text{H}_2} = -1.078\,5476$ a.u.

versus the number of time steps is shown. This figure illustrates how the energy evolves towards the ground state energy. The distance between the two atoms is $X = 1\,\text{a.u.}$, the electronic time step is 0.1 a.u., the fictitious mass is set to $\mu = 0.5$ and the frictional

[2] The source code for this example can be found at: https://github.com/miladh/CPMD

constant is set to one. Using these parameters, the energy tends to $E_{H_2} = -1.078\,5476$ a.u., which is the same value one gets by doing a pure Hartree-Fock calculation, with the same basis set and the same distance between the atoms [11].

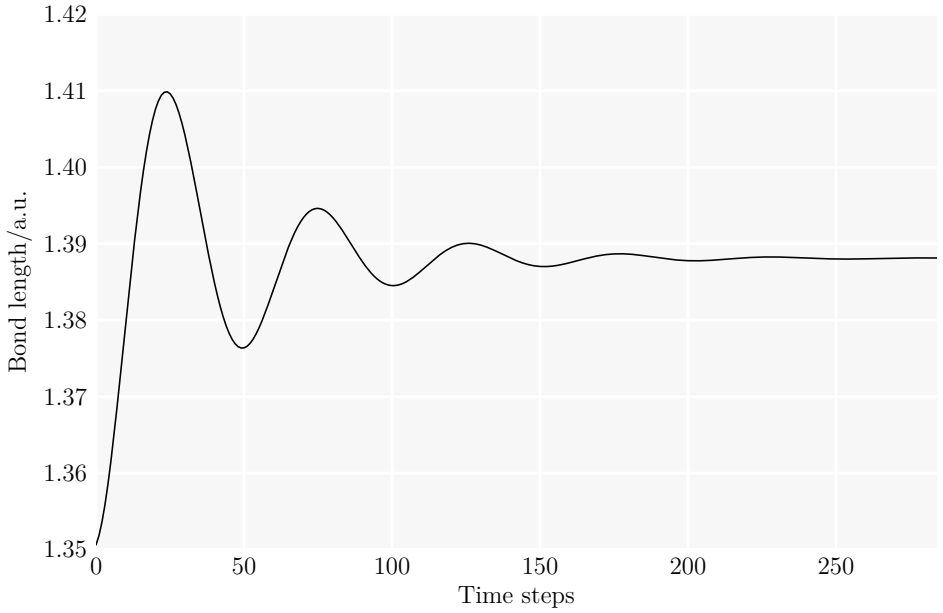

Figure 5.2: The change of the bond length in a hydrogen molecule as function of time. The number of nuclear integration steps is shown along the x-axis. The nuclear time step is 4.3 a.u., while the electronic time step is 0.1 a.u. The frictional constant for electrons is set to 1, and 5 for the nuclei. The equilibrium bond length is $X = 1.3881$ a.u.

The equation of motion for the nuclei can also be extended with a frictional term. This will slow down the nuclei and eventually make them end up with zero velocity at their equilibrium spacing. The frictional term is typically of the form $-\gamma_n \dot{X}$, where $\gamma_n \geq 0$ is the frictional constant and $\dot{X}$ is the time-derivative of the spacing between the two atoms. In Figure 5.2, the change of the bond length is shown as a function of time, with the frictional force included. In this case the nuclear mass is set to be 1000 times larger than μ, the electronic time step is, as before, 0.1 a.u., while a time step of 4.3 a.u. is used for the nuclear motion. The damping factor for nuclei is five, and one for the electrons. The equilibrium spacing becomes $X = 1.3881$ a.u., which is quite near the experimental value of 1.401 a.u.

By removing the frictional term in the equation of motion of the nuclei, the atoms will oscillate around their equilibrium spacing, as shown in Figure 5.3. In this case the mass of the nuclei is set to $M = 1836.15$ (proton mass), while the other parameters are the same as before. With an initial separation of 1.35 a.u., the frequency of the oscillations is approximately 1.359×10^{14} Hz, which is to be compared with the experimental value of 1.248×10^{14} Hz [11].

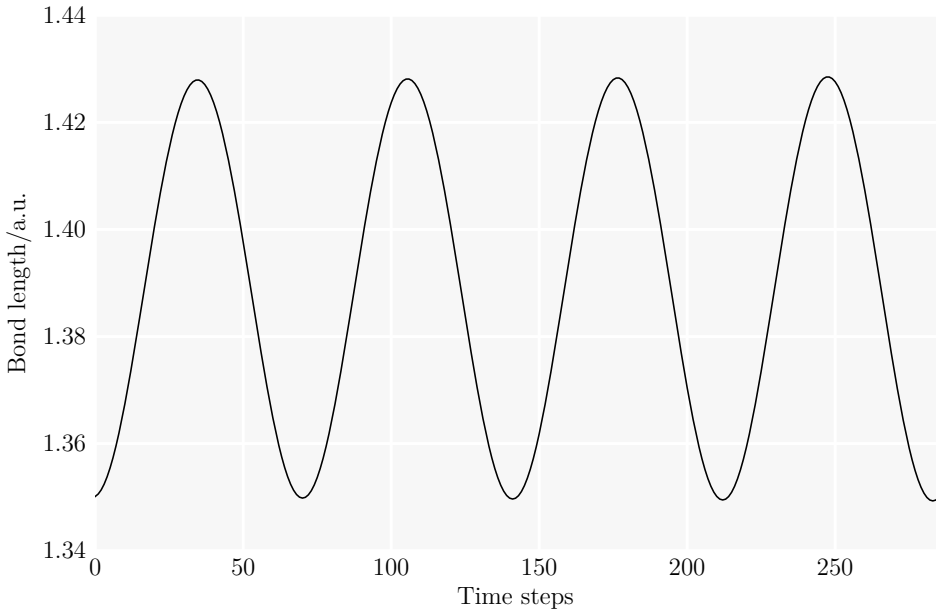

Figure 5.3: The change of the bond length in a hydrogen molecule as function of time. The number of nuclear integration steps is shown along the x-axis. The nuclear time step is 4.3 a.u., while the electronic time step is 0.1 a.u. The frictional constant for electrons is 1.

5.3 Classical Molecular Dynamics

We have so far discussed the time-evolution of molecular systems in cases where the Schrödinger equation is solved directly using certain approximations. In these cases the nuclear and electronic degrees of freedom are separated. While the electrons are treated as quantum mechanical particles, the nuclei are considered as classical point particles moving in a mean field set up by the electrons. The mean field is obtained from quantum mechanical calculations which are computationally expensive.

As a substitute for the semi-quantum mechanical approach described above, one can use an entirely classical approach, wherein the quantum mechanical mean field felt by the nuclei is replaced by a closed-form analytical potential. Assuming the stationary electronic Schrödinger equation (Eq. (5.31) or Eq. (5.36)) can be solved for a fixed nuclear configuration, we can find the potential energy surface for the system of interest by calculating the electronic energy $E_{\mathrm{Ne}} = \langle \Psi | \mathcal{H}_{\mathrm{Ne}} | \Psi \rangle$ for a sufficient number of configurations. The calculated energies can then used to construct an analytical expression for the potential. This can be done by making an expansion of the quantum mechanical potential of the form

$$E_{\mathrm{Ne}}(\mathbf{R}) \approx V_{\mathrm{CM}} = \sum_{k}^{N_n} V_1(\mathbf{R}_k) + \sum_{k<l}^{N_n} V_2(\mathbf{R}_k, \mathbf{R}_l) + \sum_{k<l<m}^{N_n} V_3(\mathbf{R}_k, \mathbf{R}_l, \mathbf{R}_m) + \ldots, \quad (5.57)$$

which is appropriately truncated. In this way, the electronic degrees of freedom are replaced by the interaction potential V_{CM} and are no longer part of the equations of motion. Thus, the semi-quantum mechanical approach in ab initio MD is reduced to a completely classical problem, with the equations of motion given by

$$M_n \ddot{\mathbf{R}}_n = -\nabla_n V_{\mathrm{CM}}(\mathbf{R}). \tag{5.58}$$

Approximating the mean field potential by an analytical function is of course a challenging and drastic approximation that needs to be justified in many respects. Perhaps the most critical problem with this approximation is the assumption that the interaction potential is represented by a sum of simple potential forms. This certainly does not include quantum mechanically effects. Even if the potential actually is represented well by this sum, we still have the problem of knowing how many and which nuclear configurations one has to consider to get a reasonably good approximation of the mean field potential. It may, for example, be that we haven't sampled specific nuclear configurations and therefore lose some of the information in the mean field potential. In addition, the truncation of the sum in Eq. (5.57) affects the quality of the approximated potential. Despite all the problems and shortcomings related to derivation of analytical potentials, classical MD simulations have been proven to be extremely useful, and their applications span over many fields of physics, including biophysics and materials science [4].

5.4 Forcefield Parameterizations

In classical MD the interaction between the particles is described by a sum of analytical functions involving bond stretching, angle bending and nonbonded interactions. These terms typically consist of adjustable parameters that can be parametrized either based on quantum mechanical calculations or experimental data, or a combination of both. Today, there are many different types of analytical potentials available for MD simulations, such as Lennard-Jones [20], Stillinger-Weber-Potential [21], Tersoff [22], ReaxFF [23], and ClayFF [24]. The "FF" stands for "force field". To illustrate how an interaction potential can be parametrized based on quantum mechanical calculations, we will in the following sections give a recipe on parameterization of the ClayFF potential for a system of water molecules (H_2O).

The ClayFF potential is given by

$$V = V_{\mathrm{Coul}} + V_{\mathrm{VDW}} + V_{\text{bond stretch}} + V_{\text{angle bend}}. \tag{5.59}$$

The Coulombic (V_{Coul}) and the van der Waals term (V_{VDW}) describe the nonbonded interactions, while the bonded interactions are represented by the bond stretch ($V_{\text{bond stretch}}$) and angle bend term ($V_{\text{angle bend}}$). In this model a molecule is considered as a collection of balls held together by springs, meaning that the bonded terms are described using the classical spring model [19]. The different terms in ClayFF are illustrated in Figure 5.4.

5.4.1 Bond Stretching

The bond stretch term in ClayFF is given by

$$V_{\text{bond stretch}} = \frac{1}{2} k_S (r_{ij} - r_0)^2, \tag{5.60}$$

where k_S is a force constant, r_{ij} is the distance between two atoms, and r_0 represents the equilibrium bond length. The force constant k_S describes the stiffness of a bond in a molecule, i.e. how much the bond resists begin stretched. The equilibrium bond length r_0 corresponds to the atomic separation that minimize the energy.

The force constant k_S and the equilibrium bond length r_0 are the two parameters that must be parameterized in the bond stretch term of ClayFF. This can be done by sampling the potential energy surface (PES) for many different atomic configurations of an H_2O molecule. The PES is thereafter fitted by the bond stretch term in Eq. (5.60) and the angle bend term in Eq. (5.61).

5.4.2 Angle Bending

The angle bend term in ClayFF is given by

$$V_{\text{angle bend}} = \frac{1}{2} k_B (\theta_{ijk} - \theta_0)^2, \tag{5.61}$$

where k_B is a force constant, θ_{ijk} is the size of the angle (HOH), and θ_0 represents the equilibrium size of the angle. The force constant k_B describes how much the bond resists begin bended and the equilibrium bond angle θ_0 corresponds to the angle between the hydrogen-oxygen-hydrogen that minimize the energy.

The parameters that needs to be parameterized in the angle bend term of ClayFF is the force constant k_B and the equilibrium bond angle θ_0. This is done as described in the last subsection; the energy of an H_2O molecule is calculated for different bond lengths (H—O) and bond angles (HOH), and the obtained energies are used to fit the potential energy surface by the bond stretch term in Eq. (5.60) and the angle bend term in Eq. (5.61).

5.4.3 Van der Waals Interaction

The van der Waals term in ClayFF is given by

$$V_{\text{VDW}} = \sum_{i \neq j} 4\epsilon_{ij} \left[\left(\frac{\sigma_{ij}}{r_{ij}} \right)^{12} - \left(\frac{\sigma_{ij}}{r_{ij}} \right)^{6} \right], \tag{5.62}$$

where ϵ_{ij} and σ_{ij} are optimized for intermolecular interactions. This term is also known as the Lennard-Jones (12-6) function and is responsible for the short-range repulsion associated with the increase in energy as two atoms approach each other, and the attractive dispersion energy [24]. Note that this term is excluded when evaluating intramolecular (bonded) interactions.

The adjustable parameters in V_{VDW} are ϵ_{ij} and σ_{ij}. These interaction parameters for atoms of different kinds are usually computed by mixing:

$$\epsilon_{ij} = \epsilon_{ji} = \sqrt{\epsilon_{ii}\epsilon_{jj}}, \tag{5.63}$$

$$\sigma_{ij} = \sigma_{ji} = \frac{1}{2}\left(\sigma_{ii} + \sigma_{jj}\right), \tag{5.64}$$

where ϵ_{ii} and σ_{ii} are the interaction parameters of two identical atoms. In H_2O, ϵ_{ii} and σ_{ii} are parameterized by individual calculations of the PES of the diatomic systems H_2 and O_2, which are fitted by their own Lenard-Jones potential. Once the interaction parameters for H_2 and O_2 are obtained, the expressions in Eq. (5.63) can be used to find the interaction parameters in the van der Waals term of ClayFF (Eq. (5.62)).

5.4.4 Coulomb Interaction

The Coulombic term in ClayFF is given by

$$V_{\text{Coul}} = \sum_{i \neq j} \frac{q_i q_j}{r_{ij}}, \tag{5.65}$$

where q_i and q_j are partial charges of atom i and j. This term describes the non-bonded, electrostatic interaction between the atoms. Thus, the Coulombic term is excluded in evaluation of intramolecular interactions, like the van der Waals term. The partial charges are derived from quantum mechanical calculations, where methods such as Mulliken population analysis can be applied (see Section 9.1.3). The simplest approach is to use the partial charges obtained from Mulliken population analysis at the equilibrium configuration.

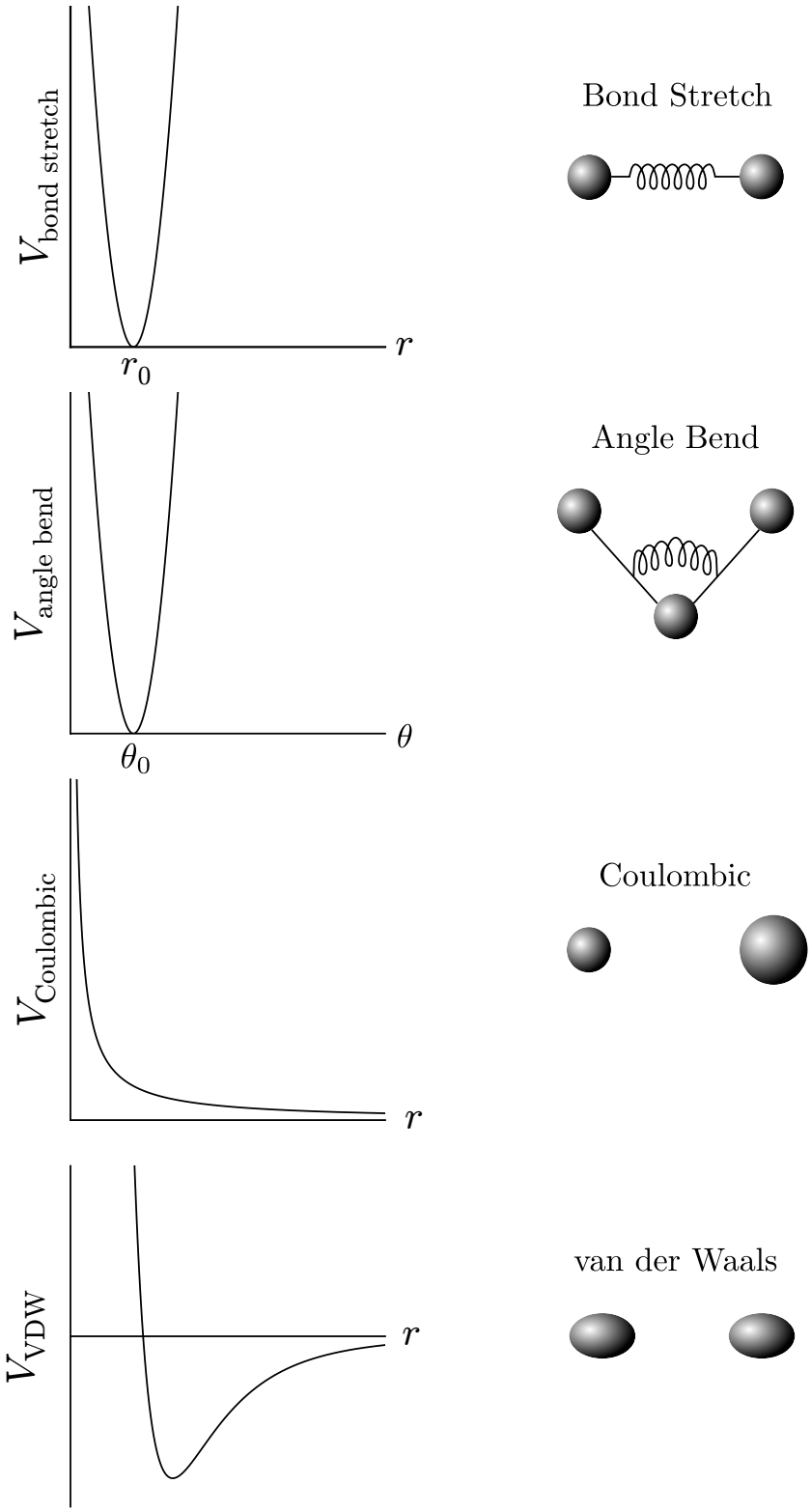

Figure 5.4: Potential energy functions in ClayFF. See text for details.

Part II

Implementation

Chapter 6

Scientific Programming

In this chapter, the concepts, methods, and tools used to develop the code for this thesis are discussed. First a short intro to essential concepts regarding object-orientation in the programming language C++ is presented. Thereafter, useful tools that has been used during the development of the code are presented and in the final part of this chapter, the concept of unit testing is discussed. The reader is assumed to have basic background in programming and familiar with the programming languages C++ and Python.

6.1 Object-Orientation

C++ is an object-oriented programming language built on the C language. The main purpose of its development was to allow for object-oriented programming, which is essential for being able to design modular and reusable software. This ability is very beneficial in science and engineering applications, allowing us to treat various forms of the same problem, without the need to write a completely new code for each instance. Below, some of the most central features of C++ are introduced. For more details about object-orientation in C++ , the reader is referred to [25].

6.1.1 Class

A class is a collection of variables and functions. By defining a class one determines what type of data and which kind of operations that can be performed on these data. The variables and functions in a class are called class members. As an example, we consider the definition of a class for primitive Gaussian-type orbitals (GTOs):

```
class PrimitiveGTO
{
public:
    PrimitiveGTO();
    ~PrimitiveGTO();
    const double &exponent() const;
    void setExponent(const double &exponent);

    const double &weight() const;
    void setWeight(const double &weight);
    ...

private:
    double m_exponent;
    double m_weight;
    ...
};
```

A class definition starts with the keyword `class` followed by the name of the class. The class body contains member variables and functions, in this example `m_exponent`, `m_weight` and their getter and setter functions[1]. The keywords `public` and `private` are access modifiers and set the accessibility of member variables and member functions. A `public` member can be assessed anywhere outside the class, while a `private` member only can be accessed within the current class.

6.1.2 Object

An instance of a class is called object. That is, a self-contained component that consist of both data and methods to manipulate the data. A `PrimitiveGTO` object can be declared by

```
PrimitiveGTO pGTO(); //or as a pointer
PrimitiveGTO* pGTO = new  PrimitiveGTO();
```

The declaration of an object calls the constructor function (`PrimitiveGTO()`) in a class, which initializes the new object. The constructor can have input parameters, used to assign values to member variables. To delete an object the destructor function (`~PrimitiveGTO()`) is called.

6.1.3 Inheritance

In object-oriented programming, objects can inherit properties and methods from existing classes. Inheritance provides the opportunity to reuse existing code. A class that is defined in terms of another class, is called a subclass or derived class, while the class used as the basis for inheritance is called a superclass or base class. The terms child class and parent class are also common to use for the subclass and superclass,

[1]The prefix `m_<memberName>` is a naming convention used for class members to distinguish them from other variables.

respectively. An example of inheritance is shown below, where the class `RHF` (restricted Hartree-Fock (RHF)) is derived from the base class `HFsolver`:

```
class HFsolver
{
public:
   HFsolver(ElectronicSystem *system);

   virtual void solveSingle() = 0;
   virtual void calculateEnergy() = 0;
   ...

protected:
   int m_nElectrons;
   ...
};

class RHF : public HFsolver
{
public:
    RHF(ElectronicSystem *system);

    void solveSingle();
    void calculateEnergy();
    ...
};
```

When an object of class `RHF` is declared, it inherits all the members of `HFsolver` beside the `private` members of `HFsolver`. Note the special deceleration of the functions in the `HFsolver` class. These functions are virtual functions whose behavior can be overridden in a derived class, allowing efficient implementation of new solvers.

6.2 Scientific Toolbox

In this section the tools used during the development of the code is presented. We will not go into the details of each of these tools, but we are including them as a recommendation for the reader.

6.2.1 Git

Git is an open source version control software, that makes it possible to have ”versions” of a project. That is, snapshots of the files in the project at certain points in time. By having different versions of a project, it is possible to see the changes that have been made to the code over time, and it is also possible to revert the project to another version. It should mentioned that when files remain unchanged from one version to another, Git simply links to the previous files, making everything fast and clean. For more details about Git the reader is referred to Ref. [26].

6.2.2 Qt Creator

Qt Creator is a cross-platform integrated development environment (IDE) and is part of the Qt Project [27]. It consist of a number of features with the aim to increase the productivity of the developer and to help organizing large projects. Some of the features included in its editor, with C++ support, are [28]:

- rapid code navigation tools,
- syntax highlighting and code completion,
- static code checking and style hints as you type,
- context sensitive help,
- code folding.

Qt Creator includes a debugger plugin, providing a simplified representation of the raw information provided by the external native debuggers to debug the C++ language. Some of the possibilities in debugging mode are [28]:

- interrupt program execution,
- step through the program line-by-line or instruction-by-instruction,
- set breakpoints,
- examine call stack contents, watchers, and local and global variables.

Qt Creator also provides useful code analysis tools for detecting memory leaks and profiling function execution. For more details see Ref. [27].

6.2.3 Armadillo

Armadillo is an open source C++ linear algebra library, with the aim to provide an intuitive interface combined with efficient calculations. Its functionalities includes efficient classes for vectors, matrices and cubes, as well as many functions which operate on the classes [29]. Some of the functionalities of Armadillo are demonstrated in the example below:

```
vec x(10);                  // column vector of length 10
rowvec y = zeros<rowvec>(10); // row vector of length 10

mat    A = randu<mat>(10,10); // random matrix of dimension 10 X 10
rowvec z = A.row(5);          // extract a row vector

cube q(4,5,6);              // cube of dimension 4 X 5 X 6
mat B = q.slice(1);         // extract a slice from the cube
                            // (each slice is a matrix)
```

One very useful class in Armadillo is `field`, where arbitrary objects in matrix-like or cube-like layouts can be stored. Each of these objects can have an arbitrary size. Here is an example of the usage of the `field` class [29]:

```
field<vec> F(3,2);       // a field of dimension 3 X 2 containing vectors

// each vector in the field can have an arbitrary size
F(0,0) = vec(5);
F(1,1) = randu<vec>(6);
F(2,0).set_size(7);

double x = F(2,0)(1);    // access element 1 of vector stored at 2,0
F.row(0) = F.row(2);     // copy a row of vectors
field<vec> G = F.row(1); // extract a row of vectors from F
```

6.2.4 IPython Notebook

IPython Notebook is a web-based interactive computational environment for Python where code execution, text, mathematics, plots and rich media can be combined into a single document [30]. Some of the main features of IPython Notebook are [31]:

- In-browser editing for code, with automatic syntax highlighting, indentation, and tab completion/introspection.
- The ability to execute code from the browser, with the results of computations attached to the code which generated them.
- Displaying the result of computation using rich media representations, such as HTML, LaTeX, PNG, SVG, etc.
- In-browser editing for rich text using the Markdown markup language, which can provide commentary for the code.
- The ability to easily include mathematical notation within markdown cells using LaTeX, and rendered natively by MathJax.

One very nice of feature of IPython Notebook documents is that they can be shared via the IPython Notebook Viewer [32], as long as they are publicly available. This service renders the notebook document, specified by an url, as a static web page. This makes it easy to share a document with other users that can read the document immediately without having to install anything.

6.2.5 SymPy

SymPy is a Python library for doing symbolic math, including features such as basic symbolic arithmetic, simplification and other methods of rewriting, algebra, differentiation and integration, discrete mathematics and even quantum physics [33]. SymPy is also able to format the result of the computations as LaTeX, ASCII, Fortran, C++ and Python code. Some of the named features of SymPy are shown below:

```
>>> from sympy import *
>>> x = Symbol('x')
>>> y = Symbol('y')
>>> x+y+x-y
2*x
>>> simplify((x+x*y)/x)
1 + y
>>> series(cos(x), x)
1 - x**2/2 + x**4/24 + O(x**6)
>>> diff(sin(x), x)
cos(x)
>>> integrate(log(x), x)
-x + x*log(x)
>>> solve([x + 5*y - 2, -3*x + 6*y - 15], [x, y])
{y: 1, x: -3}
```

For more examples and details see Ref. [33].

6.2.6 Hierarchical Data Format 5

Hierarchical Data Format 5 (HDF5) is a library and binary file format for storing and organizing large amounts of numerical data, and is supported by many software platforms including C++ and Python. The core concepts in HDF5 are datasets, groups and attributes. Datasets are array-like collections of data which can be of any size and dimension, groups are folder-like collections consisting of datasets and other groups, and attributes are metadata associated with a group or dataset, stored right next to the data it describes. This limited primary structure makes the file design simple, but provides at the same time a very structured way to store data. Here is a short list of advantages of the HDF5 format:

- open-source software,
- different data types (images, tables, arrays, etc.) can be combined in one single file,
- support for user-defined data types,
- data can be accessed independently of the platform that generated the data,
- possible to read only part of the data, not the whole file,
- source code examples for reading and writing in this format is widely available.

For HDF5 software documentation see Ref. [34], and for the documentation of the Pythonic interface to the HDF5 see Ref. [35].

6.3 Unit Testing

Unit testing is the practice of testing the smallest testable parts, called units, of an application individually and independently to determine if they behave exactly as expected. Unit tests (short code fragments) are usually written such that they can be

performed at any time during the development to continually verify the behavior of the code. In this way, possible bugs will be identified early in the development cycle, making the debugging at later stage much easier. There are many benefits associated with unit testing, such as

- It increases confidence in changing and maintaining code. Big changes can be made to the code quickly, since the tests will ensure that everything still is working properly.
- Since the code needs to be modular to make unit testing possible, the code will be easier to reuse. This improves the code design.
- Debugging is easier, since when a test fails, only the latest changes need to be debugged.
- Different parts of a project can be tested without the need to wait for the other parts to be available.
- A unit test can serve as a documentation on the functionality of a unit of the code.

The unit testing of the code for this thesis has been performed by using the framework UnitTest++ [36]. An example of this framework is shown below, where we consider the unit testing of a multiply function in a class:

```
// test.cpp
#include <unittest++/UnitTest++.h>

class MyMultiplyClass{
public:
    double multiply(double x, double y) {
        return x + y;
    }
};

TEST(MyMath) {
    MyMultiplyClass my;
    CHECK_EQUAL(56, my.multiply(7,8));
}

int main()
{
    return UnitTest::RunAllTests();
}
```

Compiling and linking to UnitTest++'s static library, and running this program will produce the following output (details may vary):

```
.\test.cpp:12: error: Failure in MyMath: Expected 56 but was 15
FAILURE: 1 out of 1 tests failed (1 failures).
Test time: 0.00 seconds.
```

By replacing the addition operator with the multiplication operator in the multiply function, and rerunning the program, we get the following output:

```
Success: 1 tests passed.
Test time: 0.00 seconds.
```

For more details about UnitTest++ see Ref. [36].

Chapter 7

Hartree-Fock Implementation

In this chapter the numerical implementation of the Hartree-Fock method is discussed[1]. We start by describing the Self-Consistent Field (SCF) procedure step by step, and thereafter specific details related to this scheme are discussed. Further, the implementation of the most central elements in molecular integral calculations are demonstrated, including the implementation of Hermite coefficients, Hermite integrals, and Boys function. The parallelization of the two-particle integral is also discussed. In the final part of this chapter the structure of the Hartree-Fock code is presented and the verification of the code is discussed.

The code developed for this thesis is written in the C++ programming language and the development is done using Qt Creator. Data-analysis is performed using several small Python scripts, written in IPython Notebook. The Hartree-Fock code developed for this thesis is publicly available at https://github.com/miladh/HF under a GPL license.

7.1 The Self-Consistent Field Procedure

The Roothaan equation in matrix form is given by (see Section 2.5.2)

$$\mathbf{FC} = \mathbf{SC}\boldsymbol{\epsilon}, \tag{7.1}$$

where $\mathbf{C}$ is the coefficient matrix, $\boldsymbol{\epsilon}$ is a rectangular diagonal matrix of the orbital energies, $\mathbf{S}$ is the overlap matrix and $\mathbf{F}$ is the Fock matrix with elements

$$F_{pq} = h_{pq} + \frac{1}{2}\sum_{rs}^{M} P_{rs}\Big(2g_{prqs} - g_{prsq}\Big), \tag{7.2}$$

$$h_{pq} = \int \varphi_p^*(\mathbf{r}) \left(-\frac{1}{2}\nabla^2 - \sum_{n=1}^{N_n}\frac{Z_n}{|\mathbf{r}-\mathbf{R}_n|}\right)\varphi_q(\mathbf{r})\,\mathrm{d}\mathbf{r}, \tag{7.3}$$

$$g_{prqs} = \int \varphi_p^*(\mathbf{r})\varphi_r^*(\mathbf{r}')\,\frac{1}{|\mathbf{r}-\mathbf{r}'|}\,\varphi_q(\mathbf{r})\varphi_s(\mathbf{r}')\,\mathrm{d}\mathbf{r}\,\mathrm{d}\mathbf{r}'. \tag{7.4}$$

[1] For the theory behind the Hartree-Fock method, see Chapter 2.

In these expressions P_{rs} is the density matrix, and $\{\varphi_p\}$ are basis functions used to expand the unknown spatial molecular orbitals (MOs) (see Section 2.5.2). Equation (7.1) cannot be solved directly because the matrix elements F_{pq} involve integrals over the Coulomb and exchange operators which themselves depend on the expansion coefficients $\mathbf{C}$. Therefore, a SCF iterative procedure must be applied. The procedure is illustrated in Figure 7.1. The first step is to specify a basis in which the unknown

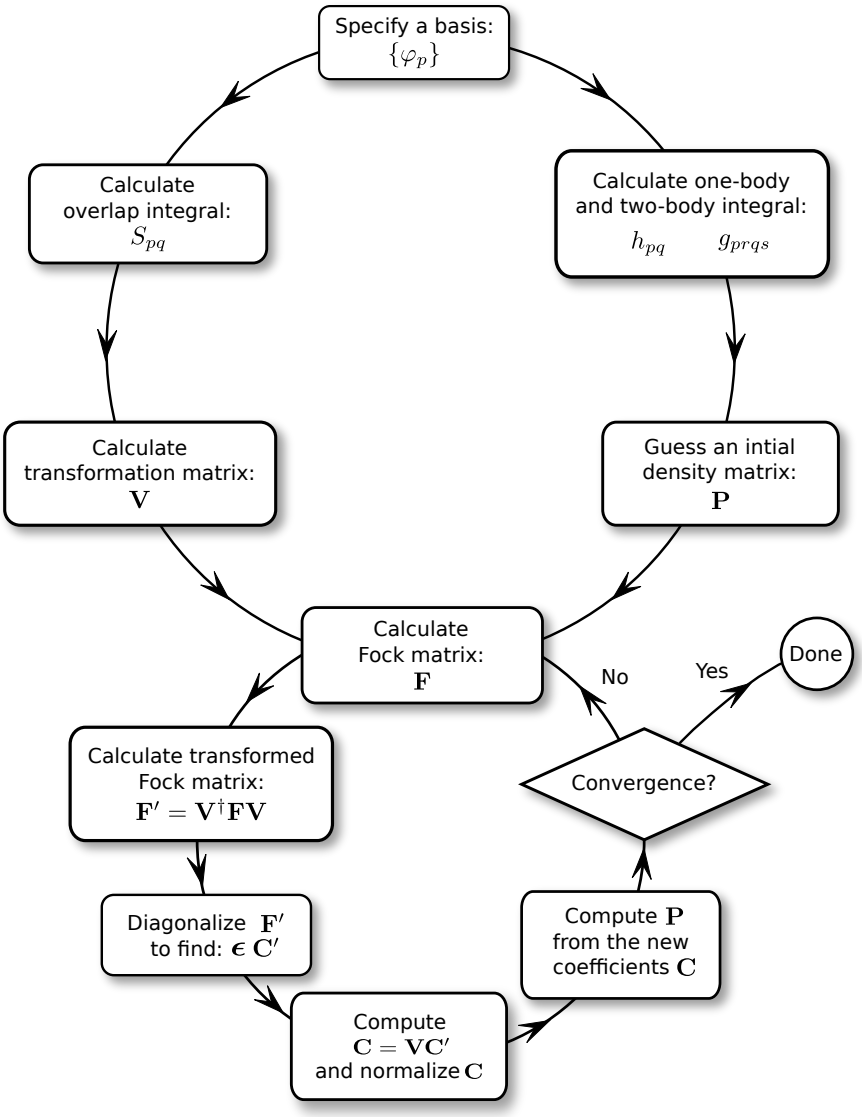

Figure 7.1: Flow-chart diagram of the SCF procedure. For details see the text.

spatial MOs are expanded. This basis can for example be a basis of Slater-type orbitals (STOs) or contracted Gaussian-type orbitals (CGTOs). After having specified the basis set, all molecular integrals can be calculated and stored in their own array. These integrals includes the overlap integral S_{pq}, the one-particle integral h_{pq}, and the two-particle integral g_{prqs}. The next step is to find the transformation matrix $\mathbf{V}$

that brings $\mathbf{S}$ to unit form (see Section 2.5.3), that is, to find the matrix $\mathbf{V}$ such that $\mathbf{V}^\dagger\mathbf{S}\mathbf{V} = \mathbf{1}$ is satisfied. Afterwards, an initial guess on the density matrix $\mathbf{P}$ is made, and used together with h_{pq} and g_{prqs} to set up the initial Fock matrix. Using the transformation matrix $\mathbf{V}$, the transformed Fock matrix $\mathbf{F}'$ can be calculated and thereafter diagonalized to find $\mathbf{C}'$ and $\boldsymbol{\epsilon}$. In the next step the transformed coefficient matrix $\mathbf{C}'$ is transformed back to the actual coefficient matrix $\mathbf{C}$, using $\mathbf{V}$, and thereafter normalized according to[2]

$$\sum_{pq}^{M} C_{pk} S_{pq} C_{qk} = 1, \qquad k = 0, 1, \ldots, N_e/2, \tag{7.5}$$

where N_e is the number of electrons and M is the number of basis functions. The normalized coefficients are used to compute a new density matrix $\mathbf{P}$. In the final step, the convergence of the solution is checked. If convergence is not obtained the new obtained density matrix $\mathbf{P}$ is used to set up a new Fock matrix, and the same steps are repeated (the small circle in Figure 7.1).

The procedure described above is also used to solve the Pople-Nesbet equations (see Section 2.5.5), but in that case there are two Fock matrices involved; $\mathbf{F}^\alpha$ and $\mathbf{F}^\beta$, for spin up and spin down electrons, respectively. These are constructed from their own density matrices and diagonalized individually.

7.1.1 Convergence

There are several ways to define a convergence criteria. A simple and not so uncommon criterion is to require that the total calculated energy of two successive iterations should not differ by more than a small value δ. For this criterion an appropriate value for δ is 10^{-6} a.u. [6]. Alternatively, one can define convergence using elements of the density matrix instead.

The convergence criterion used in our implementation is based on the convergence of the orbital energies ϵ_i. More precisely, we require

$$\frac{1}{M} \sum_{i} |\epsilon_i^n - \epsilon_i^{n-1}| \leq \delta, \tag{7.6}$$

where n specifies the iteration number, δ is a user prefixed quantity ($\delta \sim 10^{-8}$ or smaller), i runs over all calculated orbital energies, and M is the number of orbitals.

7.1.2 Damping

The initial guess on the density matrix $\mathbf{P}$ is usually a null (zero) matrix, and is equivalent to neglecting all electron-electron interaction in the first iteration step. This is a convenient way to start the iterations, but it does happen that the solution either fails to converge and ends up oscillating between two or more configurations, or diverge. This is often due to a poor initial guess on the density matrix $\mathbf{P}$. In many cases the

[2]This requirement is a consequence of the orthonormalization requirement of the MOs in Hartree-Fock.

convergence problems are solved by mixing, that is to use a weighted average of the last and the previous density matrix for the density matrix in the next iteration [11]:

$$\mathbf{P}^{\text{new}} = \alpha \mathbf{P}^{\text{last}} + (1-\alpha)\mathbf{P}^{\text{previous}}, \qquad 0 < \alpha < 1. \tag{7.7}$$

It should also be mentioned that convergence issues also arise when the atoms making up the molecule are far from the global energy minimum configuration. In these cases, it sometimes helps to start the iterations with the converged density matrix $\mathbf{P}$ corresponding to the equilibrium configuration. Alternatively, one can use the Direct Inversion in the Iterative Subspace (DIIS) procedure [7].

7.1.3 Exploiting Symmetries

The most time consuming part of the SCF procedure is the calculation of the molecular integrals, and especially the two-particle integrals. Since there are four basis functions involved in a two-particle integral, for M basis functions there will be of the order of M^4 integrals that need to be calculated. However, not all of them are unique, because of the symmetries in the two-particle integral. These symmetries arise because we have real matrix elements and the basis functions used to calculate these elements are also real. As a result we have the following symmetries in the overlap, one-particle, and two particle integral:

$$S_{pq} = S_{qp}, \tag{7.8}$$

$$h_{pq} = h_{qp}, \tag{7.9}$$

$$g_{prqs} = g_{qrps} = g_{psqr} = g_{qspr} = g_{rpsq} = g_{sprq} = g_{rqsp} = g_{sqrp} \tag{7.10}$$

Using these symmetries there are $M^4/8$ unique two-particle integrals that need to be calculated.

7.1.4 Implementation

The SCF scheme is implemented in the `HFsolver` class and its two subclasses `RHF` and `UHF`. In the parent class, all operations that are common for both the restricted Hartree-Fock (RHF) method and the unrestricted Hartree-Fock (UHF) method are performed. These operations include the calculation and storing of the overlap, one-particle and two-particle integrals. To start the calculations the `runSolver()` function in `Hfsolver` is called. The code is presented below:

```
void HFsolver::runSolver()
{
    setupOneParticleMatrix();
    setupTwoParticleMatrix();
    updateFockMatrix();
    advance();
    calculateEnergy();
}
```

The functions `updateFockMatrix()`, `advance()` and `calculateEnergy()` are virtual functions, with different implementations in the `RHF` class and the `UHF` class. The implementation of the `advance()` function in the `RHF` class is shown below:

```
void RHF::advance()
{
    ...
    while (stdDeviation  > HFSOLVERTOLERANCE){ // convergence criterion
        fockEnergyOld = m_fockEnergy;
        solveSingle();                         // perform one SCF iteration
        stdDeviation = computeStdDeviation(m_fockEnergy, fockEnergyOld);
        updateFockMatrix();
        ...
    }
}
```

In this function (and similarly in the `advance()` function in `UHF` class) the SCF iterations are performed. The diagonalization of the transformed Fock matrix and the normalization of the expansion coefficients are performed in the `solveSingle()` function. The implementation is given below:

```
void RHF::solveSingle()
{
    mat Ctilde;
    eig_sym(m_fockEnergy, Ctilde, m_V.t() * m_F * m_V); //diagonalize F'
    m_C = m_V*Ctilde;                                   //C = VC'
    normalize(m_C, m_nElectrons/2);                     //normaliziation

    // new density matrix with mixing:
    m_P = m_dampingFactor * m_P
        + (1 - m_dampingFactor) * 2.0
        * m_C.cols(0, m_nElectrons/2.0-1) * m_C.cols(0, m_nElectrons/2.0-1).t();
}
```

Note that the density matrix is constructed by using only the occupied orbitals, i.e. the $N_e/2$ lowest orbitals. These correspond to the $N_e/2$ first columns in the coefficient matrix.

7.2 Implementation of the Hermite Coefficients

Hermite coefficients are the central quantities in the molecular integral evaluation techniques presented in Chapter 4. These coefficients are needed for the computation of the overlap integral (Eq. (4.44)), the one-particle integrals (Eqs. (4.50) and (4.103)) and the two-particle integral (Eq. (4.104)). In the following we will discuss how these coefficients are calculated in the x-direction. The sets of coefficients in the y- and z-direction are found in exactly the same way.

We recall that given two Gaussian functions

$$G_{ikm}(\mathbf{r}, a, \mathbf{A}) = (x - A_x)^i (y - A_y)^k (z - A_z)^m \exp(-a r_A^2), \tag{7.11}$$
$$G_{jln}(\mathbf{r}, b, \mathbf{B}) = (x - B_x)^j (y - B_y)^l (z - B_z)^n \exp(-b r_B^2), \tag{7.12}$$

the recursion relation for the Hermite coefficients in the x-direction is expressed as (see Chapter 4):

$$E_t^{i+1,j} = \frac{1}{2p} E_{t-1}^{ij} - \frac{bQ_x}{p} E_t^{ij} + (t+1) E_{t+1}^{ij}, \tag{7.13a}$$
$$E_t^{i,j+1} = \frac{1}{2p} E_{t-1}^{ij} + \frac{aQ_x}{p} E_t^{ij} + (t+1) E_{t+1}^{ij}, \tag{7.13b}$$

with initial coefficient

$$E_0^{00} = K_{AB}^x = \exp(-q Q_x^2), \tag{7.14}$$

where

$$p = a + b, \tag{7.15}$$
$$Q_x = A_x - B_x, \tag{7.16}$$
$$q = \frac{ab}{a+b}. \tag{7.17}$$

The relations for the y- and z-direction can be expressed similarly. Additionally, the coefficients are forced to satisfy the relation

$$E_t^{ij} = 0, \qquad t < 0 \text{ or } t > i + j. \tag{7.18}$$

In the following we will show how these elements can be calculated from the relations in Eq. (7.13). An example implementation will also be given. Note that the coefficients can be calculated more efficiently than what will be presented here, but to keep things simple we have chosen to present a more intuitive implementation of the Hermite coefficients.

7.2.1 Starting Coefficient

The first step is to calculate the initial coefficient given in Eq. (7.14). This term is the only non-vanishing element in E_t^{00} for all t. All the other terms vanish due to the relation in Eq. 7.18. The code for calculating the initial coefficients is shown below:

```
for(uint cor = 0; cor < 3; cor++){
    m_E(cor)(0,0,0) = std::exp(-q*Q(cor)*Q(cor));
}
```

The calculated Hermite coefficients are stored in an Armadillo `field<cube>` object with three elements, for each Cartesian direction. For example, element `m_E(0)(0,2,1)` corresponds to Hermite coefficient $E_{t=1}^{i=0,j=2}$ in the x-direction.

7.2.2 Forward Recursion of j

From the calculated coefficients E_t^{00}, we are able to calculate E_t^{0j} for all t and j by using Eq. (7.13b). This must, however, be done in order. First E_t^{01} is found for all t. These are then used to find E_t^{02} for all t, which again is used to find E_t^{03} for all t, and so on.

```
for(uint cor=0; cor < 3; cor++){ //Loop for x,y,z

//p = previous, n = next
//E(t,i,j) = 1/(2*p) * E(t-1,i,j-1) + a*Q/p * E(t,i,j-1) + (t + 1)*E(t+1,i,j-1)
//iA = i, iB = j
  for(int iB = 1; iB < iBmax(cor); iB++){
      for(int t = 0; t < tmax(cor); t++){

          int iA = 0;
          int iBp = iB - 1;
          int tp = t - 1;
          int tn = t + 1;

          double E_iA_iBp_tp = 0.0;
          if(interiorPoint(iA, iBp, tp)){
              E_iA_iBp_tp = m_E(cor)(iA, iBp, tp);
          }

          double E_iA_iBp_t = 0;
          if(interiorPoint(iA, iBp, t)) {
              E_iA_iBp_t = m_E(cor)(iA, iBp, t);
          }

          double E_iA_iBp_tn = 0;
          if(interiorPoint(iA, iBp, tn)) {
              E_iA_iBp_tn = m_E(cor)(iA, iBp, tn);
          }

          m_E(cor)(iA,iB,t) = 1.0/(2*p) * E_iA_iBp_tp + a/p * Q(cor) *
              E_iA_iBp_t +  (t + 1)*E_iA_iBp_tn;
      }
  }
  ...
```

The `interiorPoint` function makes sure that the relation in Eq. (7.18) is satisfied. Note that in the implementation above the index j is shifted to $j-1$ compared to Eq. (7.13b).

7.2.3 Forward Recursion of i

So far we have calculated E_t^{0j} for all t and j. We can now do the exact same thing as we did in the last step to find E_t^{i0} for all t and i, but by using the recursion relation in Eq. (7.13a) instead. However, since we already know E_t^{0j} for all t and j, we can use E_t^{01} to compute E_t^{i1} for all t and i, E_t^{02} can be used to compute E_t^{i2} for all t and i, and so on. Completing this scheme enables us to calculate E_t^{ij} for all i, j and t. An implementation of this last step is shown below.

```
...
//p = previous, n = next
//E(t,i,j) = 1/(2*p) * E(t-1,i-1,j) - b*Q/p * E(t,i-1,j) + (t + 1)*E(t+1,i-1,j)
//iA = i, iB = j
for(int iB = 0; iB < iBmax(cor); iB++){
    for(int iA = 1; iA < iAmax(cor); iA++){ // iA starts at 1 since we using
        for(int t = 0; t < tmax(cor); t++) {// forward recursion relation for iA

            int iAp = iA - 1;
            int tp = t - 1;
            int tn = t + 1;

            double E_iAp_iB_tp = 0;
            if(interiorPoint(iAp, iB, tp)) {
                E_iAp_iB_tp = m_E(cor)(iAp, iB, tp);
            }

            double E_iAp_iB_t = 0;
            if(interiorPoint(iAp, iB, t)) {
                E_iAp_iB_t = m_E(cor)(iAp, iB, t);
            }

            double E_iAp_iB_tn = 0;
            if(interiorPoint(iAp, iB, tn)) {
                E_iAp_iB_tn = m_E(cor)(iAp, iB, tn);
            }

            m_E(cor)(iA,iB,t) = 1.0/(2*p) * E_iAp_iB_tp - b/p * Q(cor) *
                 E_iAp_iB_t + (t + 1)*E_iAp_iB_tn;
        }
    }
}
...
```

Note that in the implementation above the index i is shifted to $i-1$ compared to Eq. (7.13a).

7.3 Implementation of Hermite Integrals

Hermite integrals are needed for the computation of the Coulomb integrals (Eqs. (4.103) and (4.104)). In the following we will discuss how these integrals are calculated.

We start by recalling that given the following Gaussian functions

$$G_a(\mathbf{r}, a, \mathbf{A}) = (x - A_x)^i (y - A_y)^k (z - A_z)^m \exp(-ar_A^2), \tag{7.19}$$

$$G_b(\mathbf{r}, b, \mathbf{B}) = (x - B_x)^j (y - B_y)^l (z - B_z)^n \exp(-br_B^2), \tag{7.20}$$

$$G_c(\mathbf{r}, c, \mathbf{C}) = (x - C_x)^{i'} (y - C_y)^{k'} (z - C_z)^{m'} \exp(-cr_C^2), \tag{7.21}$$

$$G_d(\mathbf{r}, d, \mathbf{D}) = (x - D_x)^{j'} (y - D_y)^{l'} (z - D_z)^{n'} \exp(-dr_D^2), \tag{7.22}$$

the expressions for Cartesian Coulomb integrals in terms of Hermite coefficients and Hermite integrals can be written as (see Section 4.5.4):

$$V_{ab}^{NA} = \frac{2\pi}{p} \sum_{tuv} E_{tuv}^{ab} R_{t+e,u+f,v+g}(p, \mathbf{R}_{PN}) \tag{7.23}$$

$$g_{acbd} = \frac{2\pi^{5/2}}{pq\sqrt{p+q}} \sum_{tuv} E_{tuv}^{ab} \sum_{t'u'v'} (-1)^{t'+u'+v'} E_{t'u'v'}^{cd} R_{t+t',u+u',v+v'}(\alpha, \mathbf{R}_{PQ}) \tag{7.24}$$

where for example

$$E_{tuv}^{ab} = E_t^{ij} E_u^{kl} E_v^{mn}, \tag{7.25}$$

and

$$p = a + b, \quad q = c + d, \quad \alpha = \frac{pq}{p+q}, \tag{7.26}$$

$$\mathbf{P} = \frac{a\mathbf{A} + b\mathbf{B}}{p}, \quad \mathbf{Q} = \frac{c\mathbf{C} + d\mathbf{D}}{q}, \tag{7.27}$$

$$\mathbf{R}_{PN} = \mathbf{P} - \mathbf{N}, \quad \mathbf{R}_{PQ} = \mathbf{P} - \mathbf{Q}, \tag{7.28}$$

with $\mathbf{N}$ as the position vector of the interacting nucleus in the nuclear attraction integral. The Hermite integrals R_{tuv} are defined as

$$R_{tuv}^n(a, \mathbf{A}) = (-2a)^n \left(\frac{\partial}{\partial A_x}\right)^t \left(\frac{\partial}{\partial A_y}\right)^u \left(\frac{\partial}{\partial A_z}\right)^v F_n(aA^2), \tag{7.29}$$

where F_n is the n-th order Boys function. Also recall that $t_{\max} = i + j$, $u_{\max} = k + l$, $v_{\max} = m + n$, and so on. The Hermite integral R_{tuv} for all t, u and v can be calculated by using the recursion relations:

$$R_{t+1,u,v}^n = tR_{t-1,u,v}^{n+1} + A_x R_{tuv}^{n+1}, \tag{7.30a}$$

$$R_{t,u+1,v}^n = uR_{t,u-1,v}^{n+1} + A_y R_{tuv}^{n+1}, \tag{7.30b}$$

$$R_{t,u,v+1}^n = vR_{t,u,v-1}^{n+1} + A_z R_{tuv}^{n+1}, \tag{7.30c}$$

where n goes from 0 up to $n_{\max} = t_{\max} + u_{\max} + v_{\max}$. Note that only the elements R_{tuv}^0 for all t, u and v, are needed in the computation of Coulomb integrals, but finding these requires that also elements with $n > 0$ are known.

7.3.1 Starting Integrals

The first step is to calculate the starting integrals with $t = u = v = 0$ for all n. These elements are simply different orders of Boys function. An implementation of this is shown below:

```
m_boys->evaluateBoysFunctions(a*dot(A,A));
for(int n = 0; n < nMax+1; n++){
    m_R(n)(0,0,0) = std::pow(-2*a,n)*m_boys->getBoysFunctions(n);
}
```

The calculated Hermite integrals are stored in an Armadillo `field<cube>` object with $n_{\max}$ elements. For example, element `m_R(2)(0,3,1)` corresponds to Hermite integral $R^2_{t=0,u=3,v=1}$.

7.3.2 Forward Recursion of v

Having calculated $R^n_{0,0,0}$ for all n, we are now able to calculate $R^n_{0,0,v}$ for all v and $n \leq n_{\max} - v$, using Eq. (7.30c). Note that $n + v \leq n_{\max}$ at all iterations. An example implementation of this step is shown below

```
// p = previous
// R(n,t,u,v+1) = v * R(n+1,t,u,v-1) + Az * R(n+1,t,u,v)
for(int v = 0; v < vMax; v++){//not including vMax -> v+1 in formula
  for(int n = 0; n < nMax-v; n++){//not including nMax -> n+1 in formula
      int t = 0.0; int u = 0.0;
      int vp = v - 1.0;

      double R_t_u_vp = 0.0;
      if(!(vp < 0)){
          R_t_u_vp = m_R(n+1)(t,u,vp);
      }

      double R_t_u_v = m_R(n+1)(t,u,v);

      m_R(n)(t,u,v+1) = v * R_t_u_vp + A(2) * R_t_u_v;
  }
}
```

7.3.3 Forward Recursion of u

So far we have calculated $R^0_{0,0,v}$ for all v. The next step is to calculate $R^n_{0,u,0}$ for all u and $n \leq n_{\max} - u$, using Eq. (7.30b). However, since we already have calculated $R^0_{0,0,v}$ for all v, we can calculate $R^n_{0,u,0}$ not only for the case where $v = 0$, but for all v. Doing so, will modify the loop over n which now goes up to $n_{\max} - u - v$. This means that the relation $n + u + v \leq n_{\max}$ is satisfied at all iterations. An example implementation of this step is shown below

```
// p = previous
// R(n,t,u+1,v) = u * R(n+1,t,u-1,v) + Ay * R(n+1,t,u,v)
for(int v = 0; v < vMax+1; v++) { // including vMax -> v in formula (not v+1)
    for(int u = 0; u < uMax; u++) { // excluding uMax -> u+1 in formula
        for(int n = 0; n < nMax-u-v; n++) { // excluding nMax -> n+1 in formula
            int t = 0.0;
            int up = u - 1.0;

            double R_t_up_v = 0.0;
            if(!(up < 0)){
                R_t_up_v = m_R(n+1)(t,up,v);
            }

            double R_t_u_v = m_R(n+1)(t,u,v);
            m_R(n)(t,u+1,v) = u * R_t_up_v + A(1) * R_t_u_v;
        }
    }
}
```

7.3.4 Forward Recursion of t

In the previous steps we have calculated $R^0_{0,u,v}$ for all u and v. The remaining integrals are those with $t < 0$. These integrals can be calculated doing similar calculations, as in the last step. But now we know $R^0_{0,u,v}$ for all u and v. Thus, we can calculate all $R^0_{t,u,v}$ for all t, u and v. The loop over n goes up to $n_{\max} - t - u - v$ and the relation $n + t + u + v \leq n_{\max}$ is satisfied at all iterations. An example implementation of this final step is shown below:

```
// p = previous
// R(n,t+1,u,v) = t * R(n+1,t-1,u,v) + Ax * R(n+1,t,u,v)
for(int u = 0; u < uMax+1; u++) { // including uMax -> u in formula (not u+1)
   for(int v = 0; v < vMax+1; v++) { // including vMax ->  v in formula (not v+1)
      for(int t = 0; t < tMax; t++) { // excluding tMax -> t+1 in formula
         for(int n = 0; n < nMax-t-u-v; n++) { // excluding nMax->n+1 in formula
                int tp = t - 1.0;

                double R_tp_u_v = 0.0;
                if(!(tp < 0)){
                    R_tp_u_v = m_R(n+1)(tp,u,v);
                }

                double R_t_u_v = m_R(n+1)(t,u,v);

                m_R(n)(t+1,u,v) = t * R_tp_u_v + A(0) * R_t_u_v;
            }
        }
    }
}
```

7.4 Calculating the Boys Function

The Boys function of order n is defined as (see Section 4.5.2):

$$F_n(x) = \int_0^1 \exp\left(-xt^2\right) t^{2n} dt \tag{7.31}$$

This function is central in the computation of Coulomb integrals, and hence it is important to calculate it efficiently. The order n depends on the powers of primitive Gaussian-type orbitals (GTOs), with a maximum value $n_{\max}$ equal to the sum of the powers of the primitive GTOs involved in the Coulomb integral (see Eqs. (7.23)–(7.24)). For a given argument x the Boys function is calculated as follows:

- The highest order $n_{\max}$ is determined.
- For $n = n_{\max}$ the Boys function function is evaluated by

$$F_n(x) = \begin{cases} \dfrac{(2n-1)!!}{2^{n+1}}\sqrt{\dfrac{\pi}{x^{2n+1}}} & \text{if } x > 50, \\ \displaystyle\sum_{k=0}^{6} \frac{F_{n+k}(x_t)(-\Delta x)^k}{k!} & \text{if } x \leq 50, \end{cases} \tag{7.32}$$

  where $F_{n+k}(x_t)$ are tabulated values at x_t which is the nearest tabulated value to x, and $\Delta x = x - x_t$. The tabulated values are found by numerical integration of Eq. (7.31), using the trapezoidal method [13] with $1.0 \cdot 10^6$ points. The numerical integration were performed at 1000 equally spaced points between $[0, 50]$[3].
- In the last step, the Boys function function for all $n < n_{\max}$ are calculated by downward recursion:

$$F_n(x) = \frac{2xF_{n+1}(x) + \exp(-x)}{2n+1}. \tag{7.33}$$

7.5 Parallelization of the Two-Particle Integral

The most time-consuming part in SCF calculations is by far the computation of the two-particle integral g_{prqs}. This part of the code has therefore been parallelized, using the Boost MPI library [37]. Since each two-particle integral involves four basis functions, four for-loops are required (over p, q, r and s), where the two outermost loops are parallelized (p and q). For M basis functions there are $\frac{M}{2}(M+1)$ unique pairs of p and q (when taking the symmetries in the two-particle integral into account), that can distributed among the processes. An implementation on how tasks (i.e. pairs of p and q) are distributed among the processes is shown below. In this example all processes have a vector (`m_myPQIndices`) filled with their own p, q pairs that they are going to calculate. The Armadillo matrix `m_pqIndicesToProcsMap` registers which process is responsible for calculating which pair of p, q.

[3] The tabulated values used in the Hartree-Fock code are taken from calculations done by Henrik M. Eiding [2].

```
int nPQElements = 0.5 * m_nBasisFunctions * (m_nBasisFunctions + 1);
int procs = 0;
int s = 0;

for (int p = 0; p < m_nBasisFunctions; p++) {
    for (int q = p; q < m_nBasisFunctions; q++) {
        if (m_rank == procs){
            m_myPQIndices.push_back(pair<int, int>(p,q));
        }
        m_pqIndicesToProcsMap(p,q) = procs;
        s++;
        if(s >= BLOCK_SIZE(procs, m_nProcs, nPQElements)){
            s = 0;
            procs++;
        }
    }
}
```

The vector `m_myPQIndices` is filled with new pairs of p, q, until the variable `s` is larger or equal the output of the `BLOCK_SIZE` function. This function returns the number of tasks each process should have for a given number of processes and tasks:

```
#define BLOCK_SIZE(id,p,n) (BLOCK_HIGH(id,p,n) - BLOCK_LOW(id,p,n)+1)
#define BLOCK_LOW(id,p,n) (((id)*(n))/(p))
#define BLOCK_HIGH(id,p,n) (BLOCK_LOW((id)+1,p,n)-1)
```

Having distributed the tasks, each process calculates its own set of integrals. Afterwards the calculated integrals are broadcasted between the processes by using the Boost MPI's broadcast function:

```
boost::mpi::communicator m_world;
for (int p = 0; p < m_nBasisFunctions; p++) {
    for(int q = p; q < m_nBasisFunctions; q++){

        boost::mpi::broadcast(m_world, m_Q(p,q).memptr(), m_Q(p,q).n_elem,
            m_pqIndicesToProcsMap(p,q));
        ...
```

The variable `m_Q` is an Armadillo `field<mat>` object that stores the calculated two-particle integral values. `m_pqIndicesToProcsMap` tells which process that will be transmitting data. Note that whole matrices are broadcasted. To read more about the broadcast function in Boost MPI library see Ref. [37].

7.6 Code Structure

The Hartree-Fock code for this thesis is implemented in such way that it can be used as a library by other functions. For example, Hartree-Fock calculations are often combined with other many-body theory methods and it would be beneficial to be able to

use the Hartree-Fock implementation as a library in the implementation of these other methods. Other examples where it would be relevant to use the Hartree-Fock implementation as a library is in the implementation of ab initio molecular dynamics (MD) codes. Furthermore, writing a code with the aim to use it as a library eases the process of writing modular code, and thereby improves the quality of the implementation. One essential point when writing a library is to separate the source code from the rest of the project. In a sense, it corresponds to an implementation without a `main` function, where we a have header file that includes everything necessary to use the library. To read about project structuring with Qt Creator and how a program can be separated into its own library see Ref. [1].

The structure of the Hartree-Fock project in Qt Creator is shown below:

```
HF
├── hf.pro
├── defaults.pri
├── include/
│   └── hf.h
├── infiles/
│   ├── turbomole/
│   │   └── ...
│   └── tabulatedBoys.dat
├── apps/
│   ├── apps.pro
│   ├── default/
│   │   ├── default.pro
│   │   └── defaultmain.cpp
│   └── tests/
│       ├── tests.pro
│       └── testsmain.cpp
└── src/
    ├── src.pro/
    ├── hfSolver/
    │   └── ...
    └── ...
```

The main project file is `hf.pro` and `defaults.pri` is a helper project file [1]. In `turbomole` directory the input basis files are found. All header includes are in `hf.h`. The `apps` directory consists of the app (`.cpp` file that uses the functions in the source code) itself (`default/defaultmain.cpp`) and unit tests. The source code including all classes is found in the `src` directory.

In Figure 7.2, an overview of the class hierarchy of the code is given. Note that, in order to keep the diagram clean and simple, only the most essential relations between the classes are shown. Here is a short description of the central elements:

- `TurbomoleParser`: Reads input basis file to construct the CGTOs associated with an `Atom` object, in addition to atom type, mass and core charge.
- `Atom`: Consist of various atom properties (type, mass, charge, position) and a vector of CGTOs.
- `ElectronicSystem`: Has a vector of atoms and an `Integrator` object. The summation of integrals over primitive GTOs is done in this class.
- `Integrator`: Consist of different integral-type classes (kinetic, overlap, nuclear,

etc.), including their geometric derivatives. All operations in this class and the integral-classes it consist of, is on primitive GTOs.

- `HFsolver`: Has an `ElectronicSystem` object. When setting up the molecular integral matrices the indices of CGTOs are send to `ElectronicSystem` class.
- `Analyzer`: Computes different quantities such as partial charge, dipole moment and densities based on the results from the solver.
- `OutputManager`: Responsible for writing the results from the computation to file.

7.6.1 Basis Set Exchange

The input basis files read by the code are in the Turbomole format with file extension `.tm`. These files are taken from the website Basis Set Exchange [38], which is a web-accessible environment where different basis sets can be downloaded in various formats [39]. Here is an example of an input file for the oxygen atom with the 3-21G basis:

```
#...
$basis
*
O   3-21G
*
    3  s
    322.0370000              0.0592394
     48.4308000              0.3515000
     10.4206000              0.7076580
    2  s
      7.4029400             -0.4044530
      1.5762000              1.2215600
    1  s
      0.3736840              1.0000000
    2  p
      7.4029400              0.2445860
      1.5762000              0.8539550
    1  p
      0.3736840              1.0000000
*
$end
```

The first line starting with # is ignored (comment). The first column is a list of exponents for the primitive GTOs, while the numbers in the second column are the corresponding coefficients. The contracted basis functions are marked with a heading of type `3 s`, `2 s`, etc., which are indicating the number of primitives in the contracted basis function. In the 3-21G basis set the core orbitals consist of three primitive GTOs, while the valence orbitals are split into two CGTOs with two and one primitive GTOs, respectively. In oxygen there is only one core orbital (1s), and the contraction parameters (exponents and coefficients) of this orbital is under the heading `3 s`. The values below the next two headings, `2 s` and `1 s`, are the contraction parameters corresponding to the 2s valence orbital. The last two groups of parameters with headings `2 p` and `1 p` are the parameters for the valence p-orbitals ($2p_x$, $2p_y$ and $2p_z$).

Note that the coefficients read from the file should be rescaled by the normalization factor of the individual primitive GTOs, before they are used in calculations. For a general Gaussian function

$$G_{ijk}(x, y, x) = G_i(x)G_j(y)G_k(z) \tag{7.34}$$

with

$$G_i(x) = x^i \exp(-\alpha x^2) \tag{7.35}$$

and similar for the components in the y- and z-direction, the normalization factor is given by

$$\left(\frac{2\alpha}{\pi}\right)^{(3/4)} \sqrt{\frac{(4\alpha)^{i+j+k}}{(2i-1)!!(2j-1)!!(2k-1)!!}}. \tag{7.36}$$

7.7 Verification

The implementation of the Hartree-Fock method consists of many different elements that are designed to be individually tested before they are incorporated in SCF calculations. The integrator forms a large part of the code, but is very separable making it possible to carefully test and verify each element separately. In the following sections we show how the different parts of the integrator are verified through unit tests.

7.7.1 Overlap Integral

The overlap integral is the integral over all space of the product of two primitive GTO:

$$S_{ab} = \int G_{ikm}(\mathbf{r}, a, \mathbf{A})G_{jln}(\mathbf{r}, b, \mathbf{B})\, \mathrm{d}\mathbf{r}. \tag{7.37}$$

To verify the calculations of the overlap integral we have used Python to generate unit tests by calculating the overlap integral for different primitive GTOs. The integrals have been calculated in Python by using the library SymPy. Here is an example:

```
from numpy import array, dot
from sympy import symbols, exp, integrate, oo

x, y, z = symbols('x, y, z')

a = 0.2; b = 0.3
Ax =  1.2;  Ay = 2.3; Az =  3.4
Bx = -1.3;  By = 1.4; Bz = -2.4
i, k, m = 1, 0, 0
j, l, n = 0, 0, 2

rA = array([x - Ax, y - Ay, z - Az])
rB = array([x - Bx, y - By, z - Bz])

Ga = rA[0]**i * rA[1]**k * rA[2]**m * exp(-a*dot(rA,rA))
Gb = rB[0]**j * rB[1]**l * rB[2]**n * exp(-b*dot(rB,rB))

Sab = integrate(Ga * Gb, (x, -oo, oo), (y, -oo, oo), (z, -oo, oo))
```

The obtained values are used as a benchmark to verify the calculated integrals in the Hartree-Fock code, by using the `CHECK_CLOSE` macro found in the UnitTest++library:

```
CHECK_CLOSE(1.191723635809e-01, integrator.overlapIntegral(), 1e-5);
```

The last number (`1e-5`) is a threshold for how close the two numbers should be.

Unit tests for the geometric derivatives of the overlap integral are generated similarly. In the example below the coordinates of $\mathbf{B}$ are first defined as symbols, so the derivatives of the Gaussian product with respect to B_x, B_y and B_z can be calculated, using SymPy's `diff` function, and thereafter the symbols B_x, B_y and B_z are substituted with actual numbers in the differentiated product. In the final step, the integrals in each of the Cartesian directions are evaluated.

```
Bx_sym, By_sym, Bz_sym = symbols('B_x, B_y, B_z')
Ax =  1.2;  Ay = 2.3; Az =  3.4
Bx = -1.3;  By = 1.4; Bz = -2.4

rA = array([x - Ax, y - Ay, z - Az])
rB = array([x - Bx_sym, y - By_sym, z - Bz_sym])
Ga = rA[0]**i * rA[1]**k * rA[2]**m * exp(-a*dot(rA,rA))
Gb = rB[0]**j * rB[1]**l * rB[2]**n * exp(-b*dot(rB,rB))

O = Ga * Gb

dOBx = diff(O,Bx_sym)
...

dOBx =dOBx.subs(Bx_sym,  Bx).subs(By_sym,  By).subs(Bz_sym,  Bz)
...

dSBx = integrate(dOBx, (x, -oo, oo), (y, -oo, oo), (z, -oo, oo)).evalf()
...
```

7.7.2 Kinetic Integral

The kinetic integral of two primitive GTOs is given by

$$T_{ab} = \int G_{ikm}(\mathbf{r}, a, \mathbf{A}) \nabla^2 G_{jln}(\mathbf{r}, b, \mathbf{B}) \ \mathrm{d}\mathbf{r}. \tag{7.38}$$

This integral can be evaluated exactly like the overlap integral above. The only difference is that $G_{jln}(\mathbf{r}, b, \mathbf{B})$ is first differentiated twice in each Cartesian direction before the integral is evaluated:

```
Gbxx = diff(Gb, x, x)
Gbyy = diff(Gb, y, y)
Gbzz = diff(Gb, z, z)
Tab = -0.5*integrate(Ga*(Gbxx + Gbyy + Gbzz), (x,-oo,oo), (y,-oo,oo), (z,-oo,oo))
```

The geometric derivatives of the kinetic integral can be evaluated in the same way as for the overlap integral.

7.7.3 Nuclear Attraction Integral

The nuclear-attraction integral of two primitive GTOs is given by

$$V_{ab}^{NA} = \int \frac{G_{ikm}(\mathbf{r}, a, \mathbf{A}) G_{jln}(\mathbf{r}, b, \mathbf{B})}{|\mathbf{r} - \mathbf{C}|} \ \mathrm{d}\mathbf{r} \tag{7.39}$$

In order to generate unit tests for this integral, we have used Python's `tplquad` function. This function is able to compute triple (definite) integrals. An example of the calculation of this integral using Python is shown below:

```
from scipy.integrate import tplquad
from numpy import array, exp, sqrt

class gaussian():
    def __init__(self,R,alpha):
        self.R = R
        self.alpha = alpha
        self.i, self.j, self.k = 0, 0, 0

    def __call__(self,x,y,z):
        i, j, k = self.i, self.j, self.k
        R = self.R
        alpha = self.alpha

        coef = (x-R[0])**i * (y-R[1])**j * (z-R[2])**k
        R = (x-R[0])**2 + (y-R[1])**2 + (z-R[2])**2

        return coef * exp(-alpha*R)

upLim =   10.
lowLim = -10.
a = 0.2;  b = 0.3

A = array(( 1.2, 2.3,  3.4))
B = array((-1.3, 1.4, -2.4))
C = array(( 2.3, 0.9,  3.2))

Ga = gaussian(A,a)
Gb = gaussian(B,b)
Ga.i, Ga.j, Ga.k  = 0, 1, 0
Gb.i, Gb.j, Gb.k  = 2, 0, 0

I = tplquad(lambda x,y,z:
            Ga(x,y,z)*Gb(x,y,z)/sqrt((x-C[0])**2 + (y-C[1])**2 + (z-C[2])**2),
            upLim, lowLim, lambda y: upLim, lambda y: lowLim, lambda x,y: upLim,
                lambda x,y: lowLim)
```

Note that the integration limits are given explicitly (`upLim` and `lowLim`), in this example -10 and 10, although the integral is supposed to be evaluated over all space. However, since the integrand falls quick to zero, the contributions at large distances from the origin can be neglected.

7.7.4 Electron Repulsion Integral

Evaluation of the electron repulsion integral with Python is very time-consuming using the same functions that have been used to evaluate the other integrals. These tests have therefore been skipped for the electron repulsion integral. However, this integral is calculated in the Hartree-Fock code by using Hermite coefficients and Hermite integrals which have been throughly tested. It is therefore easier to debug this part of the code since the elements used to calculate this integral have been already tested thoroughly.

7.7.5 Verification of the Solver

The Hartree-Fock solver has been tested by calculating the ground state energy of a few simple systems with different basis sets, and checking against the expected values found in the literature. Here is an example, where the calculated ground state energy of H_2 is checked against the value given in Ref. [40]:

```
TEST(H2_431G)
{
  /*
  * test case:   H2
  * basis:       4-31G
  * bondlength:  1.380
  * energy:      -1.127
  *
  * source:
  *      Molecular Quantum Mechanics
  *      Peter Atkins
  * */

  vector<Atom *> atoms;
  atoms.push_back(new Atom("infiles/turbomole/atom_1_basis_4-31G.tm",{-0.69,
      0.0, 0.0}));
  atoms.push_back(new Atom("infiles/turbomole/atom_1_basis_4-31G.tm",{ 0.69,
      0.0, 0.0}));

  ElectronicSystem *system = new ElectronicSystem ();
  system->addAtoms(atoms);

  RHF *solver = new RHF(system);
  solver->runSolver();

  CHECK_CLOSE(-1.127, solver->energy(), 1e-3);
}
```

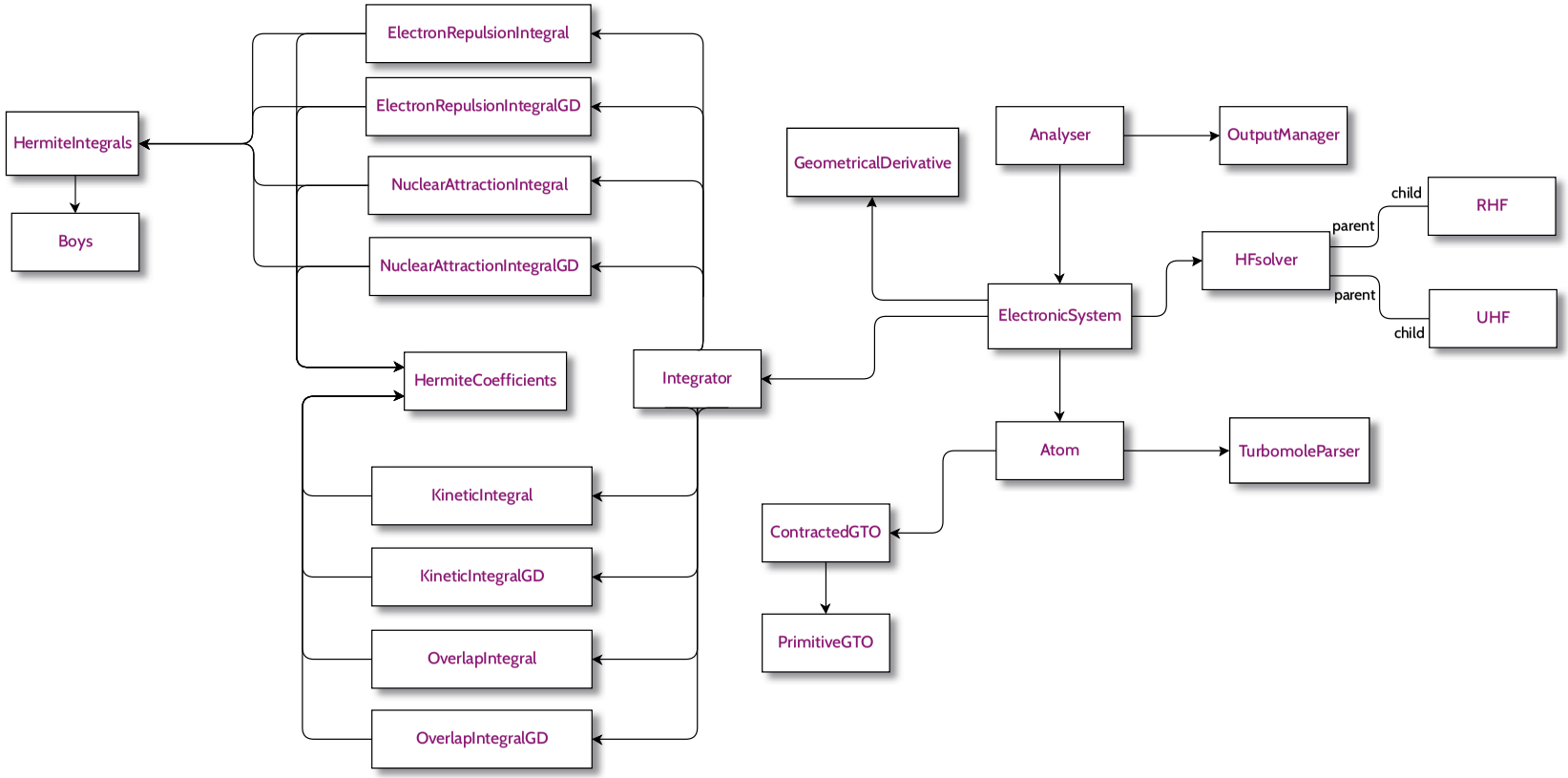

Figure 7.2: Chart diagram of the class hierarchy of the Hartree-Fock code. The direction of the arrows is from owner to member. Note that not all relations are included in this diagram.

Chapter 8

Ab initio Molecular Dynamics Implementation

In this chapter, the numerical implementation of the molecular dynamics (MD) code is discussed. The velocity Verlet algorithm, used to integrate the equations of motions, is presented, followed by a disscusion on various boundary conditions used in MD simulations. In the final part of this chapter, the structure of the Born-Oppenheimer MD (BOMD) code is described.

The code is written in C++ programming language and the development is done using Qt Creator. The data-analysis is performed using several small Python scripts, written in IPython Notebook. The BOMD code developed for this thesis is publicly available at https://github.com/miladh/BOMD under a GPL license.

8.1 Velocity-Verlet Discretization

In ab initio MD, the electronic and nuclear degrees of freedom are separated (see Chapter 5). At this level of theory the electrons are treated quantum mechanically, while the nuclei are considered as classical point particles. Within the Hartree-Fock theory, the nuclear equations of motion in BOMD is given by (see Section 5.2.2)

$$\mathbf{F}_n = M_n \ddot{\mathbf{R}}_n = -\nabla_n E^{\mathrm{HF}}, \tag{8.1}$$

where $\mathbf{R}_n$ is the position vector of nucleus n with mass M_n and E^{HF} is the Hartree-Fock energy. This equation is time discretized in the BOMD code by using the Velocity Verlet algorithm. The basic formula for this algorithm can be derived from the Taylor expansions of the positions $\mathbf{R}_n$ [15]. The resulting formula for position and velocity is given by:

$$\mathbf{R}_n(t+\Delta t) = \mathbf{R}_n(t) + \Delta t\, \mathbf{V}_n(t) + \frac{\Delta t^2}{2M_n}\mathbf{F}_n(t), \tag{8.2}$$

$$\mathbf{V}_n(t+\Delta t) = \mathbf{V}_n(t) + \frac{\Delta t}{2M_n}\left(\mathbf{F}_n(t) + \mathbf{F}_n(t+\Delta t)\right), \tag{8.3}$$

where $\mathbf{V}_n = \dot{\mathbf{R}}_n$. This algorithm is very common in MD simulations, due to its stability with respect to rounding errors and long-term energy conservation. Furthermore, the positions and velocities are available at the same time without additional computations, in contrast to methods such as leapfrog [15].

The Velocity Verlet algorithm is implemented in the code as follows:

1. Half kick in velocity:

$$\mathbf{V}_n\left(t + \frac{\Delta t}{2}\right) = \mathbf{V}_n(t + \Delta t) + \frac{\Delta t}{2M_n}\mathbf{F}_n(t).$$

2. New position:

$$\mathbf{R}_n(t + \Delta t) = \mathbf{R}_n(t) + \Delta t\, \mathbf{V}_n\left(t + \frac{\Delta t}{2}\right).$$

3. Force calculation at the new position: $\mathbf{F}_n(t + \Delta t)$.

4. New half kick in velocity:

$$\mathbf{V}_n\left(t + \Delta t\right) = \mathbf{V}_n\left(t + \frac{\Delta t}{2}\right) + \frac{\Delta t}{2M_n}\mathbf{F}_n(t + \Delta t).$$

8.2 Boundary Condition

In MD simulations, atoms move around in a simulation box with certain conditions imposed on the boundaries depending on the problem at hand. The simplest case is free boundaries or no boundaries, which is appropriate for processes where the effect of boundaries is not important due to the short time-scale of the involved processes. Alternatively one can have reflecting boundaries where atoms hitting the boundary of the box are reflected (see Figure 8.1a). This type of boundary condition is however in most cases unphysical and can introduce artifacts into the simulation results.

A widely used condition in MD simulations is periodic boundary conditions, wherein atoms that leave the simulation box at one side reenter the box at the opposite side. This condition has the advantages of removing surface effects and is a compensation for the limited size of a numerical simulation box [15]. When using periodic boundary conditions, one assumes that the simulation box is surrounded by an infinite number of identical copies forming an infinite lattice. Thus, as an atom leaves the central box, one of its images will enter the box on the other side (see Figure 8.1b).

When using periodic boundary conditions, the interactions between the atoms are usually described by applying the so-called minimum image convention. In this technique each atom only interacts with the nearest image of all the other atoms. This means in practice that the interaction range is limited to half the box size. As an example consider a one-dimensional domain of length L with two atoms placed at x_i and x_j with $\Delta x = x_j - x_i$. The convention dictates that atom i interacts only with the nearest image of atom j, and therefore the shortest separation between atom i and atom j (including its images) has to be found. This can be expressed as

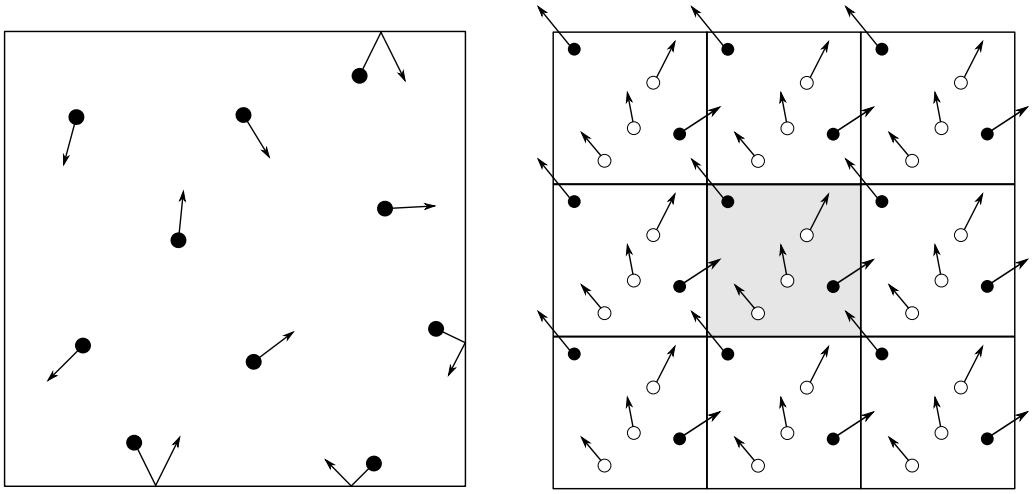

(a) Reflecting: atoms hitting the boundaries are reflected.

(b) Periodic: as an atom leaves the central box (gray), one of its images will enter the box on the other side.

Figure 8.1: Examples of boundary conditions in MD simulations.

$$\Delta x_{\min} = \Delta x - L \,\text{Round}\left(\frac{\Delta x}{L}\right), \tag{8.4}$$

where Round(y) returns to nearest integer value to y. Thus, the nearest image of atom j relative to atom i is placed at $x_i + \Delta x_{\min}$.

Periodic boundary conditions are introduced in BOMD code as follows.

- For each atom:
  - find the nearest image of all the other atoms by using the rule in Eq. (8.4).
  - Perform electronic structure calculations for this atomic configuration and determine the forces acting on the central atom.
- Integrate one-step forward in time.
- Repeat from top.

As it should be clear from the steps described above, at each time step one needs to perform N_n electronic structure calculations, where N_n is the number of nuclei.

In Figure 8.2, a snapshot from a simulation of hydrogen atoms with periodic boundary conditions is shown. In this simulation all the atoms are part of a bound pair, forming hydrogen molecules. At each time step twelve electronic structure calculations has been performed, making such simulations quite expensive.

8.3 Code Structure

The structure of the BOMD code is very much like the Hartree-Fock code developed for this thesis (see Section 7.6), and is implemented such that it can be used as a library

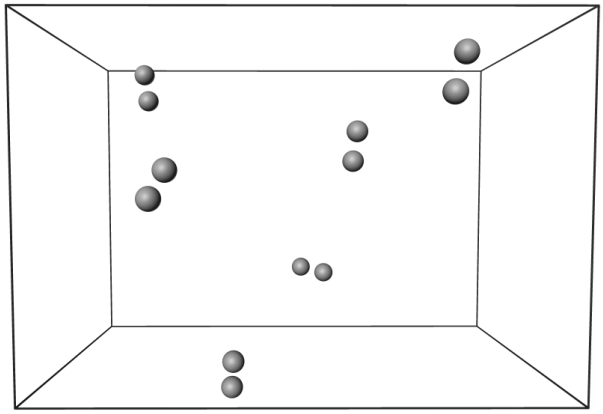

Figure 8.2: Snapshot from a simulation of twelve hydrogen atoms, with periodic boundary conditions.

in other softwares. The BOMD code itself uses the Hartree-Fock code as a library for electronic structure and force calculations. The structure of the BOMD project in Qt Creator is shown below:

```
BOMD
├── HF/
│   └── ...
├── bomd.pro
├── defaults.pri
├── include/
│   └── bomd.h
├── apps/
│   ├── apps.pro
│   ├── default/
│   │   ├── default.pro
│   │   └── defaultmain.cpp
│   └── tests/
│       ├── tests.pro
│       └── testsmain.cpp
└── src/
    ├── src.pro/
    ├── molecularSystem/
    │   └── ...
    └── ...
```

The main project file is `bomd.pro` and `defaults.pri` is a helper project file [1]. All header includes are in `bomd.h`. The `apps` directory consist of the app (`.cpp` file that uses the functions in the source code) itself (`default/defaultmain.cpp`) and unit tests. The source code including all classes is found in the `src` directory, which consists of the following classes `generator`, `molecularSystem`, `modifier` and `fileManager`. Here is a short description of the classes in the BOMD code:

- `generator`: generates initial structure and velocities of the atoms.

- `molecularSystem`: consists of an integrator to evolve the system forward in time, and computes different system properties.
- `modifier`: a class for system modifiers such as thermostats [15] and velocity rescaling operations.
- `fileManager`: responsible for witting the results to file. The outputs are written both in Hierarchical Data Format 5 (HDF5) and lammps format.

8.4 Parallel Computing

The most time-consuming part in BOMD calculations is by far the force calculations, and specially the evaluation of the geometric derivatives of the two-particle integral. This part of the computations is therefore coded to run in parallel. This is done by using the same procedure used to parallelize the two-particle integral. For details see Section 7.5.

Part III

Computational Results and Analysis

Chapter 9

Hartree-Fock Results

In this chapter, the numerical results from the Hartree-Fock calculations, are represented, analyzed and discussed. The first part of this chapter provides some illustrative results for a few simple molecules that are used for benchmarking of the Hartree-Fock code. These results involve ground state energies, ionization potentials, population analysis, and dipole moments. Thereafter, we will discuss graphical models applied on a few selected molecules.

9.1 Illustrative Restricted Calculations

For benchmarking the code and illustrating some of the applications of the Hartree-Fock method, we will in the following sections present some results for the following molecules: H_2, CO, N_2, CH_4, NH_3, H_2O, and FH. The molecular geometries used in the calculations are given in Table 9.1.

Basis set	Bond length (a.u.)	Bond angle
H_2	1.400	
CO	2.132	
N_2	2.074	
CH_4	2.050	109.47°
NH_3	1.913	106.67°
H_2O	1.809	104.52°
FH	1.733	

Table 9.1: Standard geometries used in calculations.

The calculations carried out for each of these molecules, are based on some of the model calculations given in Ref. [6]. The results in the upcoming sections have been, unless otherwise indicated, successfully benchmarked against the values given in Chapter 3.7 in Ref. [6].

9.1.1 Total Energy

The total energy of a system, defined as the electronic energy plus the nuclear repulsion energy, is one of the most central quantities in quantum chemistry calculations. Within the Hartree-Fock approximation, the electronic energy is variational and becomes lower as the quality of the basis improves. In the limit of an infinite basis, the energy approaches the Hartree-Fock limit, which is, however, still above the exact energy due to the variational principle.

Tables 9.2 and 9.3 show the total energies for the molecules of Table 9.1, using the following Gaussian basis sets: STO-3G, 4-31G, 6-31G*, and 6-31G**. Note that the 4-31G basis and 6-31G* basis for H_2 are equivalent since this molecule neither have inner shells or p-orbitals to be polarized with d-type orbitals. For N_2 and CO, the 6-31G* and 6-31G** basis sets are equivalent since they don't have hydrogen atoms to add p-type polarizations to.

Table 9.2: SCF total energies (a.u.) of H_2, N_2 and CO with the standard basis sets.

Basis set	H_2	N_2	CO
STO-3G	-1.117	-107.496	-111.225
4-31G	-1.127	-108.754	-112.552
6-31G**	-1.131	-108.942	-112.737
HF limit[a]	-1.134	-108.997	-112.791

[a]Estimated HF limit limits are from Ref. [41].

Table 9.3: SCF total energies (a.u.) of for then ten-electron series with the standard basis sets.

Basis set	CH_4	NH_3	H_2O	FH
STO-3G	-39.727	-55.454	-74.963	-98.571
4-31G	-40.140	-56.102	-75.907	-99.887
6-31G*	-40.195	-56.184	-76.011	-100.003
6-31G**	-40.202	-56.195	-76.023	-100.011
HF limit[a]	-40.225	-56.225	-76.065	-100.071

[a]Estimated Hartree-Fock limits are from Ref. [41].

For all molecules, we see that even for the crudest basis set, the obtained energy is quite near the Hartree-Fock limit (HF limit) energy, and becomes lower as the basis size is increased. In all cases, the obtained energy with the STO-3G basis is approximately 98% of the HF limit energy. This estimate is good enough for a first approximation of the energy.

9.1.2 Ionization Potential

In Section 2.4.2, we saw that solving the Hartree-Fock equation

$$\mathcal{F}\psi_k = \epsilon_k \psi_k, \tag{9.1}$$

yields an infinite set $\{\psi_k\}$ of orthonormal spin orbitals with orbital energies $\{\epsilon_k\}$. For a system consisting of N_e electrons, the ground state is approximated by using the N_e lowest eigenstates to construct the Slater determinant $|^{N_e}\Psi_0\rangle$. The corresponding orbital energies are given physical significance through Koopmans' theorem. This theorem states that when using the same set of spin orbitals as the one used to construct $|^{N_e}\Psi_0\rangle$, the ionization potential to produce an (N_e-1)-electron determinant $|^{N_e-1}\Psi_n\rangle$, obtained by removing an electron from spin orbital ψ_n, is just the negative of the corresponding eigenvalue ϵ_n [6]. Mathematically, we can write the ionization potential E_{IP} as

$$E_{\text{IP}} = {}^{N_e}E_0 \; - \; {}^{N_e-1}E_n = -\epsilon_n, \tag{9.2}$$

where ${}^{N_e}E_0$ and ${}^{N_e-1}E_n$ are the expectation values of the energy of the two relevant determinants. The ionization potential of removing an electron from the highest occupied spin orbital, is commonly called the first ionization potential.

In restricted Hartree-Fock, all (spatial) orbitals are doubly occupied. This means that for H_2 there is only one occupied orbital. The negative of the corresponding eigenvalue of this orbital is the ionization potential of H_2. In Table 9.1b, the ionization energy for H_2 is shown for various basis sets, and in Figure 9.1a all orbitals in H_2 are shown. From the table we see that beyond the minimal basis STO-3G, the ionization energy remains fixed at -0.595 a.u., which is only in error by $\sim$2% from the experimental value. This remarkable agreement in ionization potential, is, however, due to a fortuitous cancellation of errors introduced by the Hartree-Fock approximation and the approximation in Koopmans' theorem. First, we note that the exact energy of H_2 is lower than the Hartree-Fock energy due to correlations which are not fully described by the Hartree-Fock method. The H_2^+ system is, on the other hand, unaffected by correlations. Second, the orbitals in $|^{N_e}\Psi_0\rangle$ that minimize the energy of the N_e-electron system, do not necessarily minimize the energy of the (N_e-1)-electron system. To "relax" the orbitals for the ionized system, a separate Hartree-Fock calculation must be performed. The effect of these two approximations nearly cancel each other, leading to an ionization potential close to the experimental value [6].

A case where we don't have the same fortunate cancellation of errors, is the nitrogen molecule. To study the problems arising in using the Koopmans' theorem to interpret the ionization spectra of N_2, we consider Figure 9.2, which shows all the occupied orbitals of N_2, in addition to the lowest unoccupied orbitals. Furthermore, Table 9.2b shows the ionization potential for two different ion symmetries (Σ and Π) of N_2 for various basis sets. The values near the HF limit and the experimental values are also included. The lowest experimental ionization potential corresponds to the production of an ion with Σ symmetry, and the second lowest corresponds to the production of an ion with Π symmetry.

Figure 9.1: Orbital energies and ionization potential of H_2 for various basis sets.

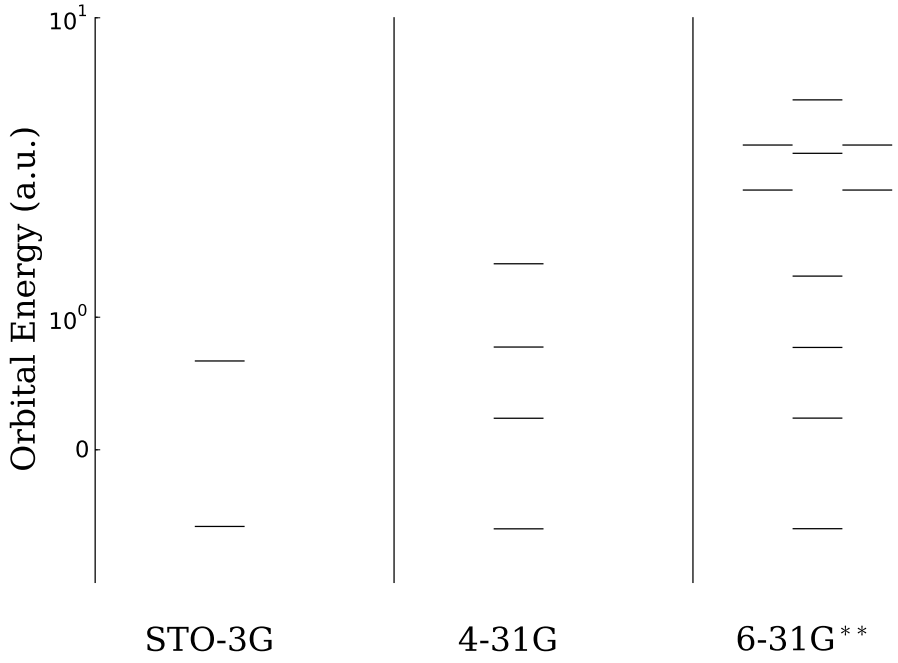

(a) Orbital energies

Basis set	Ionization potential
STO-3G	0.578
4-31G	0.596
6-31G**	0.595
Near-HF limit[a]	0.595
Experiment[b]	0.584

(b) Ionization potential (a.u.)

Estimated HF limits from [a]Ref. [42]. Experimental values from [b]Ref. [6].

The first thing we notice is that the minimal basis calculations are in disagreement with calculations using better basis sets. More specifically, we see that the STO-3G basis has a different highest occupied orbital, than the other basis sets. Furthermore, we notice that the highest occupied orbital in STO-3G calculations, is the second highest orbital for the other basis sets, and vice versa. Since the Hartree-Fock results should improve as the quality of the basis sets is improved, we conclude that the highest occupied orbital is the one suggested by the basis sets beyond the minimal basis set, leading to Π ion symmetry when an electron is removed from this orbital. By comparing the "correct" Hartree-Fock results with the experimental values, however,

we realize that the former are in qualitative disagreement with the experimental values. The experimental values indicate that the lowest ionization potential corresponds to the production of an ion with Σ symmetry.

Figure 9.2: Orbital energies and ionization potential of N_2 for various basis sets. Note that the two lowest orbitals are very close in energy, and therefore indistinguishable in the energy ladder plot.

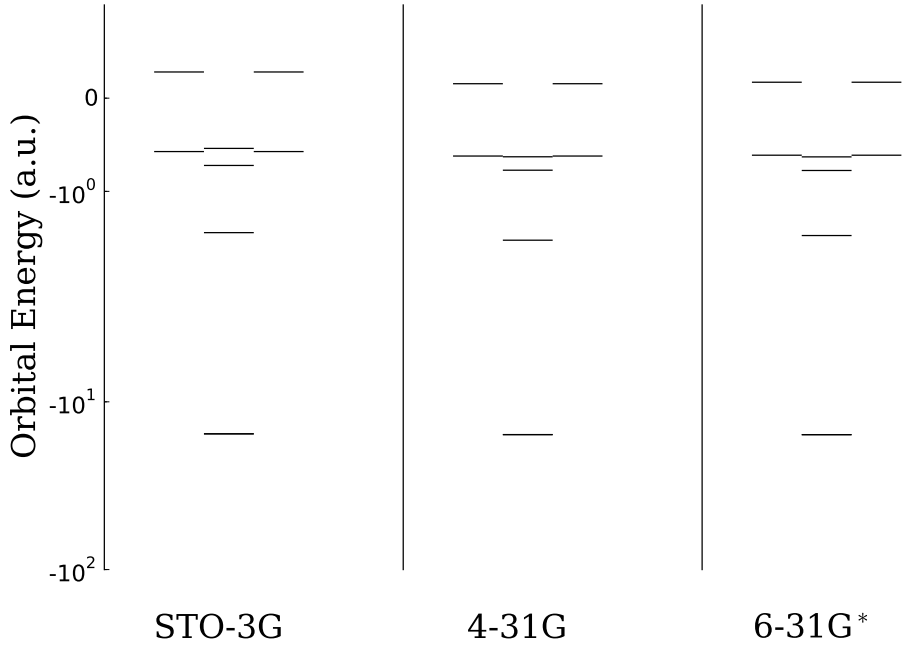

(a) Orbital energies

	Ion symmetry	
Basis set	Σ	Π
STO-3G	0.540	0.573
4-31G	0.629	0.621
6-31G*	0.630	0.612
Near-HF limit[a]	0.635	0.616
Experiment[b]	0.573	0.624

(b) Ionization potential (a.u.)

Estimated HF limits from [a]Ref. [43]. Experimental values from [b]Ref. [6].

This is an example of breakdown of the simple orbital picture of ionization. The Hartree-Fock approximation is simply not sufficiently accurate enough for even qualitative studies of the ionization spectra of N_2. By using more sophisticated many-body theories the theoretical calculations and experimental values ultimately agree on the ionization spectra of N_2 [44].

For the sake of illustrating the code's ability to reproduce typical Hartree-Fock results, we also include the first ionization potential of CH_4, NH_3, H_2O, and FH, and their ionization spectra, shown in Figure 9.3. The orbital energies given in Figure 9.3a, include all the occupied orbitals in addition to the first virtual orbital (lowest unoccupied orbital) of the relevant molecules.

Figure 9.3: Orbital energies and ionization potential of the ten-electron series

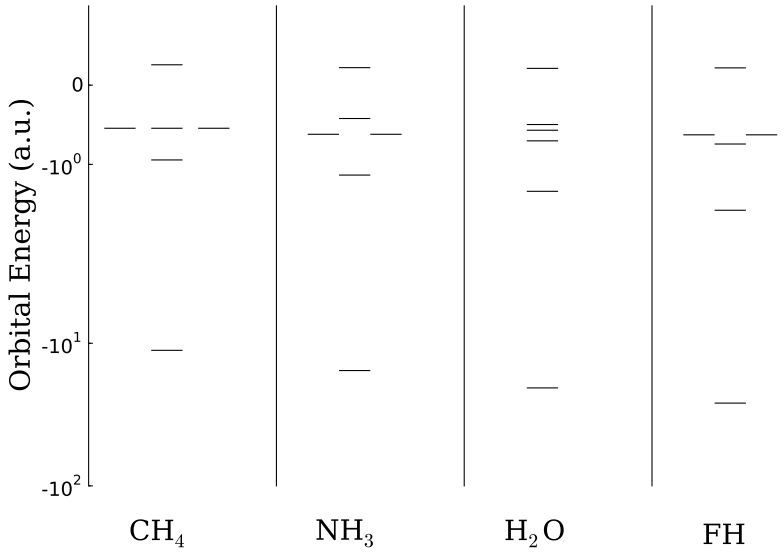

(a) 6-31G** orbital energies

Basis set	CH_4	NH_3	H_2O	FH
STO-3G	0.518	0.353	0.391	0.464
4-31G	0.543	0.414	0.500	0.628
6-31G*	0.545	0.421	0.498	0.628
6-31G**	0.543	0.421	0.497	0.627
Near-HF limit	0.546[a]	0.428[b]	0.507[c]	0.650[d]
Experiment[e]	0.529	0.400	0.463	0.581

(b) Ionization potential (a.u.)

Estimated HF limits from [a]Ref. [45], [b]Ref. [46], [c]Ref. [47], and [d]Ref. [48]. [e]Experimental values are from Ref. [6].

The experimental values indicate the following ordering of the ionization potentials; FH > CH_4 > H_2O > NH_3. This ordering is reproduced for all basis sets beyond the minimal basis. For all molecules, the largest basis set gives an ionization potential slightly over the experimental value. This is expected since Koopmans' theorem tends to produce too positive ionization potential, because of the neglect of relaxation. Furthermore, we observe that the average energy of the three highest occupied orbitals decreases as one moves to the right in the periodic table, when considering the heavy atom (C, N, O and F). The individual energies are determined by the symmetry of the system [6].

9.1.3 Population Analysis

In a closed-shell molecule described by a single determinant wave function with doubly occupied molecular orbitals (MOs), the electron density is given by

$$\rho(\mathbf{r}) = 2\sum_{k=1}^{N_e/2} |\phi_k(\mathbf{r})|^2, \tag{9.3}$$

where N_e is the number of electrons and ϕ_k is MO k. The electron density is defined such that $\rho(\mathbf{r})\mathrm{d}\mathbf{r}$ is the probability of finding an electron in a small volume $\mathrm{d}\mathbf{r}$. The integral of the electron density is just the number of electrons N_e;

$$\int \rho(\mathbf{r})\mathrm{d}\mathbf{r} = 2\sum_{k=1}^{N_e/2} \int \mathrm{d}\mathbf{r}|\phi_k(\mathbf{r})|^2 = 2\sum_{k=1}^{N_e/2} 1 = N_e. \tag{9.4}$$

Taking the linear combination of atomic orbitals (LCAO) approach (see Section 2.2.2), we expand the molecular orbitals in some known basis $\{\varphi_p\}$:

$$\phi_k(\mathbf{r}) = \sum_{p=1}^{M} C_{pk}\varphi_p(\mathbf{r}), \tag{9.5}$$

where M is the number of basis functions in the new basis. Inserting this to the definition of the electron density we obtain

$$\begin{aligned}\rho(\mathbf{r}) &= 2\sum_{k=1}^{N_e/2}\sum_{q=1}^{M} C_{qk}^*\varphi_q^*(\mathbf{r})\sum_{p=1}^{M} C_{pk}\varphi_p(\mathbf{r}) \\ &= \sum_{p,q=1}^{M}\left[2\sum_{k=1}^{N_e/2} C_{pk}C_{qk}^*\right]\varphi_p(\mathbf{r})\varphi_q^*(\mathbf{r}) \\ &= \sum_{p,q=1}^{M} P_{pq}\varphi_p(\mathbf{r})\varphi_q^*(\mathbf{r}),\end{aligned} \tag{9.6}$$

where we have used the definition of the density matrix. Now, using this new form of $\rho(\mathbf{r})$ we can express the number of electrons as

$$N_e = \sum_{p,q=1}^{M} P_{pq} S_{pq} = \sum_{p=1}^{M} (\mathbf{PS})_{pp}, \tag{9.7}$$

where $\mathbf{P}$ and $\mathbf{S}$ are the density and overlap matrix, respectively. It is common to interpret $(\mathbf{PS})_{pp}$ as the number of electrons associated with φ_p. This is the idea behind *Mulliken population analysis*. As an attempt to get an estimate on the number of electrons to be associated with a given atom in a molecule, we use the sum of all basis functions centered on that atom. That is, the number of electrons associated with atom A is given by

$$N_A = \sum_{p \in A}^{M} (\mathbf{PS})_{pp}, \tag{9.8}$$

where the sum goes only over functions which are centered at atom A. The net charge associated with a given atom in a molecule is then given by

$$q_A = Z_A - \sum_{p \in A}^{M} (\mathbf{PS})_{pp}, \tag{9.9}$$

where Z_A is the nuclear charge of that atom.

The Mulliken population analysis may sometimes be useful for interpretative purposes, and gives chemically intuitive charge sign on atoms in a molecule. However, it is important not to over interpret the results, since partial charges are artificial and do not represent an observable property of atoms and molecules. As an illustration of the population analysis, Table 9.4 contain the net positive charge on each of the hydrogen atoms in the ten-electron series.

Basis set	CH_4	NH_3	H_2O	FH
STO-3G	0.06	0.16	0.18	0.21
4-31G	0.15	0.30	0.39	0.48
6-31G*	0.16	0.33	0.43	0.52
6-31G**	0.12	0.26	0.34	0.40

Table 9.4: Mulliken SCF population analysis for the ten-electrons series. The entries are the net charges on the hydrogens.

For all basis sets, the net positive charge increases as one goes to the right in the periodic table. This is due to the increasing electronegativity of the heavy atom. In all cases the partial charge decreases as one goes from the 6-31G* basis to the 6-31G** basis. This is due to the addition of orbitals to the hydrogen atoms, leading to a less positive charge. In general, the 6-31G** basis set always assign more electrons to the

hydrogen atoms, than the 6-31G* basis set does since the only difference between these two sets is the addition of orbitals to the hydrogen atoms.

The partial charge varies significantly with respect to the basis sets, and it is difficult to say much about the absolute magnitude of these charges. In fact one of the disadvantages of Mulliken population analysis is that the results vary significantly for the same system when different basis sets are used, making the comparison of the results from different basis sets impossible [10].

9.1.4 Dipole Moments

The classical definition of the dipole moment of a collection of charges q_i with position vectors $\mathbf{r}_i$ is

$$\boldsymbol{\mu} = \sum_i q_i \mathbf{r}_i. \tag{9.10}$$

The corresponding quantum mechanical definition, within the single determinant approximation and using LCAO, is given by

$$\boldsymbol{\mu} = -\sum_{p,q=1}^{M} P_{pq} \int \varphi_q^*(\mathbf{r}) \mathbf{r} \varphi_p(\mathbf{r}) \mathrm{d}\mathbf{r} + \sum_n Z_n \mathbf{R}_n, \tag{9.11}$$

where the first term is the quantum mechanical contribution of the electrons of charge -1, and the second term is the classical contribution of the nuclei of charge Z_n, to the dipole moment.

An interesting case for dipole moment calculations is the CO molecule. In Table 9.5, the calculated dipole moment using different basis sets is shown, in addition to the value near the HF limit and the experimental value. Since dipole moment is a vector, pointing from the positive end of the molecule to the negative end of the molecule, the values in table are given with sign, where positive sign corresponds to C^-O^+, that is when carbon is the negative end of the molecule, which is also the correct experimental result.

Table 9.5: SCF dipole moments (a.u.) of CO with the standard basis sets. A positive dipole moment corresponds to C^-O^+.

Basis set	Dipole moment
STO-3G	0.066
4-31G	-0.237
6-31G*	-0.131
Near-HF limit[a]	-0.110
Experiment[b]	0.044

Estimated HF limit from [a]Ref. [49]. Experimental values from [b]Ref. [6].

The minimal basis set is the only set that gives the right sign, while all the other sets and the "correct" Hartree-Fock result (near-HF limit) predict wrong sign. The reason for this disagreement is due to cancellation of two large and opposite contributions to the dipole moment. On one hand the electronegativity arguments suggest oxygen to be the negative end, since it is the most electronegative atom in CO. On the other hand, the lone pair of electrons on carbon, directed away from the bond, has a contribution to the dipole moment, which is opposite to the contribution of net charge. The sum of these two contributions leads to a small dipole moment, with carbon as the negative end. Because of the small magnitude of this dipole moment, SCF calculations are simply not accurate enough to reproduce the right sign. The disagreement in sign, as mentioned in Ref. [6], disappears when more sophisticated many-body theories are used.

Table 9.6 contains the calculated dipole moments for NH_3, H_2O and FH, using our standard basis sets. Comparing the values from various basis sets with the experimental values, we see that the correct trend $H_2O > FH > NH_3$, is reproduced only for the 6-31G* basis set and beyond, reflecting the importance of polarization for correct qualitative results.

Table 9.6: SCF dipole moments (a.u.) for then ten-electron series with the standard basis sets.

Basis set	NH_3	H_2O	FH
STO-3G	0.703	0.679	0.507
4-31G	0.905	1.026	0.897
6-31G*	0.768	0.876	0.780
6-31G**	0.744	0.860	0.776
Near-HF limit	0.653[a]	0.785[b]	0.764[c]
Experiment[d]	0.579	0.728	0.716

Estimated HF limits from [a]Ref. [50], [b]Ref. [47] and [c]Ref. [51]. Experimental values from [d]Ref. [6].

9.2 Illustrative Unrestricted Calculations

In the next two subsections we will discuss the application of unrestricted Hartree-Fock (UHF) on two well-known systems; H_2 and O_2. These two cases illustrate very clearly the shortcomings of restricted Hartree-Fock (RHF) and the advantage of using UHF.

9.2.1 Unrestricted Hartree-Fock Description of the Ground State of O_2

It is well-known that the oxygen molecule is paramagnetic. This means that it must have unpaired electrons. This is the case even though the number of electrons is even

and we might expect complete pairing of electrons. As it turns out, the ground state of an oxygen molecule consist of two unpaired electrons, each occupying their own orbital, meaning that the unrestricted formulation should be used instead of RHF. In Figure 9.4, the unrestricted occupied MOs of O_2 is shown for the 6-31G* basis set, where nine of total sixteen electrons have spin α, while the rest have spin β.

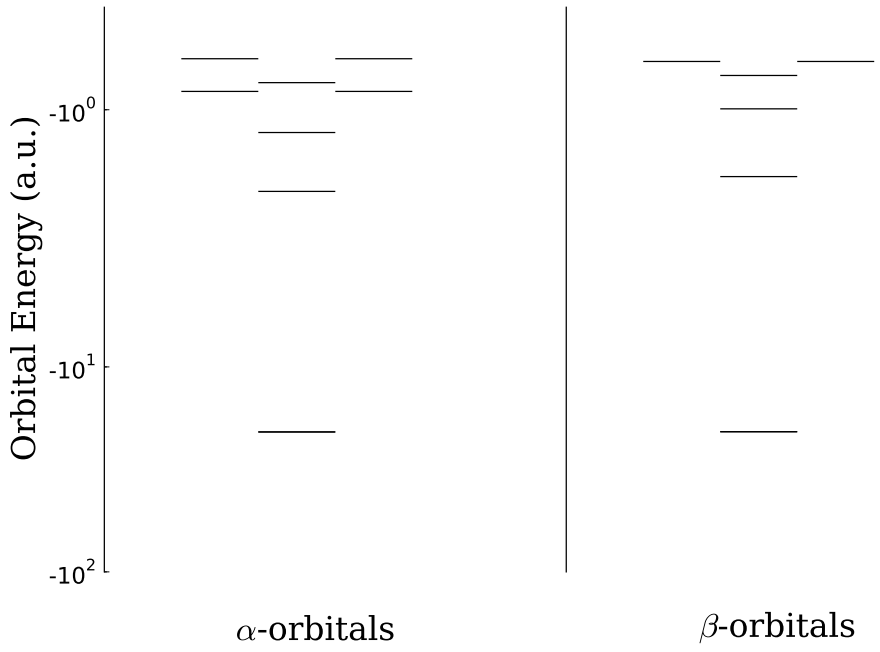

Figure 9.4: Unrestricted occupied MOs of O_2 with nine spin α-electrons and seven spin β-electrons, using the 6-31G* basis set. Note that the two lowest orbitals are very close in energy, and therefore indistinguishable in the energy ladder plot.

The ground state configuration of O_2 is the one shown in Figure 9.4, where two of the electrons goes into the degenerate highest occupied molecular orbital. According to Hund's rule (see Griffiths [12]) these two electrons will go into separate orbitals with their spin parallel, resulting in negative exchange interaction, which lowers the total energy. As it is clear in the energy ladder plot given in Figure 9.4, the orbital energies of α-electrons are pushed down relative to β-electrons due to the exchange interactions that are present only between electrons of the same spin. In a restricted description all the electrons would be constrained to be paired, leading to a higher energy.

9.2.2 Dissociation Problem

The ground state of a molecule like H_2 is normally described by the restricted formalism, where both electrons are described by the same spatial wave function. This restricted formulation of the system usually works fine, but under certain circumstances this description becomes problematic. In particular, at large bond lengths the restricted

formalism tends to overestimate the energy of the system, which is now a system of more or less two individual hydrogen atoms. In Figure 9.5, the potential curve of H_2 is shown, together with the corresponding curve from high accurate calculations. This figure clearly shows the energy overestimation of RHF. For large R we expect the energy of the system to go towards twice the energy of a single hydrogen atom, since the atoms "feel" each other less. At large bond lengths, a proper description of

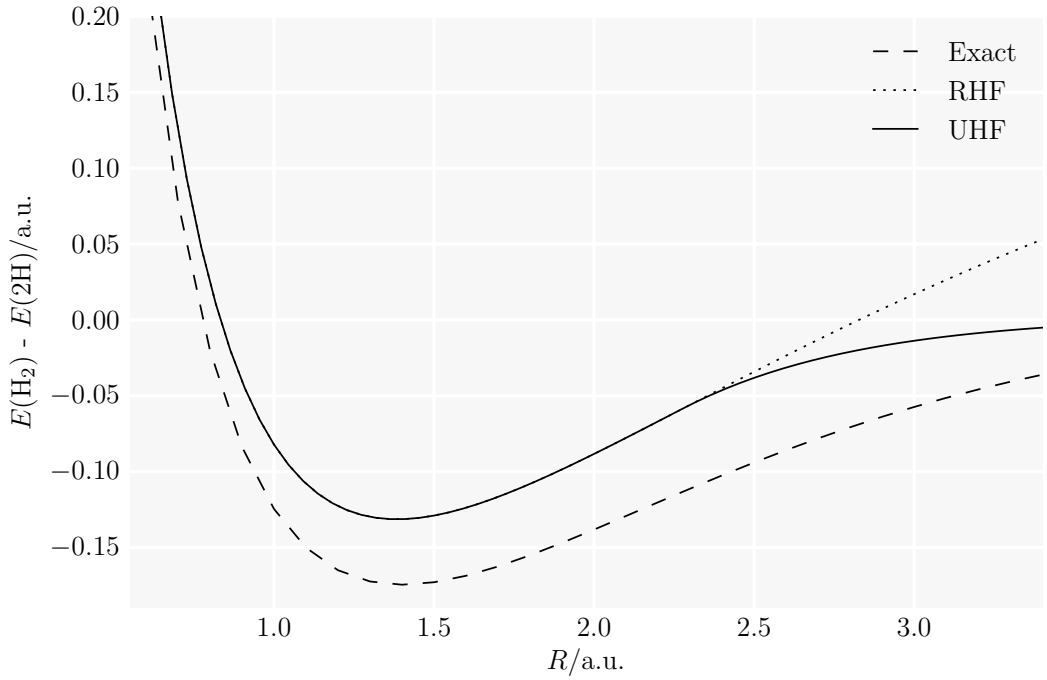

Figure 9.5: Potential energy curve for H_2 with the 6-31G** basis set. The hydrogen atom energy used is $E(H) = -0.498$ a.u., obtained from Hartree-Fock calculation on a single hydrogen atom with the 6-31G** basis set, and $E_e(H) = -0.5$ a.u. for the exact solution. The exact data are from Ref.[52].

the system have one electron on each of the hydrogen atoms with not necessarily the same spatial distributions. Therefore, the restricted formulation is unfortunate since the spatial distributions are confined to be identical for the two electrons. An unrestricted formulation, on the other hand, seems much more appropriate for the system at large bond lengths. Figure 9.5 shows the potential curve obtained from unrestricted calculations, which is much more promising than the restricted potential curve. At distance near the ground state bond length the restricted and unrestricted curves fully overlap, but at large distances they differ significantly. The unrestricted energy goes towards twice the energy of a single hydrogen atom, which is the correct behavior.

This model presented in this subsection, is an example of applications of the unrestricted formalism on a closed-shell system. Note that the effects shown for H_2 also occur for other closed-shell systems when a bond is stretched [6].

9.3 Graphical Models

Physical properties and the chemical reactivity of atoms and molecules are closely linked to their structure, which are usually represented by graphical models showing the atomic geometry and the electronic distribution. These models are used to assist in interpreting the results from quantum chemistry calculations, and in most cases give, at least, a qualitative description of the chemical structure of the system.

In the following the graphical models for some selected molecules are represented and used to study molecular size, shape and molecular charge distributions[1]. The central quantity in the graphical models represented here is the isosurface, which is a three-dimensional surface of constant value. The graphics are created by `cubeViz` (see Appendix B.1), using the results from Hartree-Fock calculations. The molecular configuration used in the calculations are given in Appendix B.2.

It should be mentioned that the results we are going to present on graphical models are obtained from minimal basis calculations and are only illustrative, without any attempt to give a very detail description of the systems studied. Our main objective is to give an overview of the most common graphical models and how they can give us valuable knowledge about the system of interest, by relatively low-cost calculations.

9.3.1 Electron Density

Visualization of the total electron density is perhaps the most common one among the graphical models. The electron density in the RHF is defined as

$$\rho(\mathbf{r}) = \sum_{p,q=1}^{M} P_{pq}\varphi_p(\mathbf{r})\varphi_q^*(\mathbf{r}), \tag{9.12}$$

or if we are dealing with the unrestricted case, the same quantity is defined as

$$\rho(\mathbf{r}) = \rho^{\alpha}(\mathbf{r}) + \rho^{\beta}(\mathbf{r}) = \sum_{p,q=1}^{M} (P_{pq}^{\alpha} + P_{pq}^{\beta})\varphi_p(\mathbf{r})\varphi_q^*(\mathbf{r}). \tag{9.13}$$

In these expressions the sums goes over the basis functions φ and $\mathbf{P}$, $\mathbf{P}^{\alpha}$ and $\mathbf{P}^{\beta}$ are density matrices. The two last ones are the density matrices for spin α and spin β electrons, respectively.

The electron density may be represented by an isosurface (isodensity surface). Depending on the value of the isosurface, the electron density may either serve to locate atoms, delineate chemical bonds, or to indicate overall molecular size and shape. In Figure 9.6, the isodensity of benzene is shown for two different values. An isodensity surface of value 0.002 electrons/a.u.^{3}, as shown in Figure 9.6a, indicates the overall size and shape of the molecule, while an isosurface of value 0.1 electrons/a.u.^{3} (Figure 9.6b) depicts the locations of bonds[2]. The lower density surface is often referred

[1]The studied systems are inspired from some of the models given in Ref. [53].
[2]The density values for the isosurfaces are the same as the one used in Ref. [53].

to as a size surface, while the higher density surface is known as the bond surface. It should be emphasized that there are no definite ways to choose the value for these two surfaces. The electron density decays rapidly with distance from the nuclei, but it is difficult to determine where exactly the electron density has fallen to zero—if it does reach zero at all. The best we can do is to pick some value as a limit for the minimum density and connect together all the points that have this value, enclosing a certain amount of space, indicating the size of the molecule. It is similarly difficult to know how large the electron density should be to indicate a bonding. In general, it is often most useful to study the isodensities for a range of values. In our discussion, the values 0.002 electrons/a.u.^{3} and 0.1 electrons/a.u.^{3} for the size density and the bond density, respectively, give a good illustration of the quantities of interest, and we will use these values in the following discussions, regardless of the system.

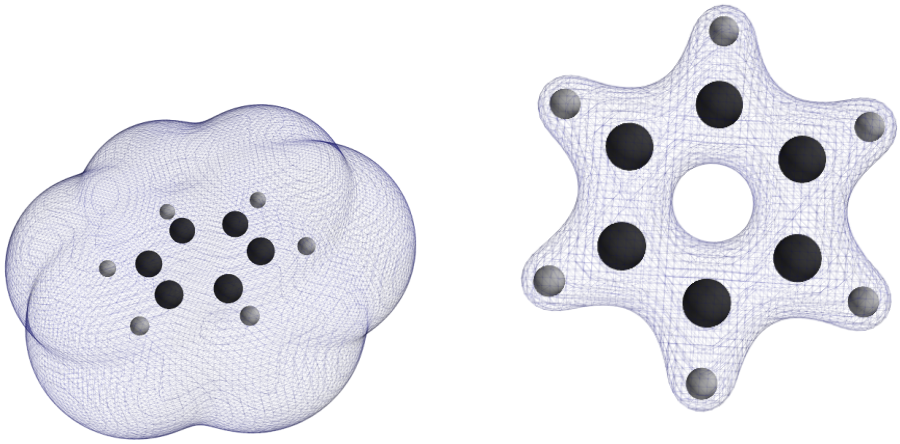

(a) Size surface **(b)** Bond surface

Figure 9.6: Isodensity surface of benzene for two different values. The size surface has value 0.002 electrons/a.u.^{3}, while the bond surface has value 0.1 electrons/a.u.^{3}. Black spheres are carbon atoms and gray spheres are hydrogen atoms.

The size surface density (Figure 9.6a) shows the expected planar six-sided structure of benzene. For lower electron densities the size surface becomes more ”cylindrical” with rounded edges and the ”bumps” slightly visible. The bond density surface in Figure 9.6b clearly shows the ring structure of benzene where each carbon atom is bonded to two other carbon atoms in addition to a hydrogen atom. There is no electron density concentrated in the middle of the ring, indicating that there are no bonds between the carbon atoms across the ring. Higher values of electron density lead to almost spherical regions of electron density around the carbon atoms. This serves to locate the positions of theses atoms.

As a second example we consider the dibroane molecule, consisting of two boron atoms and six hydrogen atoms. Figure 9.7 shows the bond density surface of this molecule, indicating low electron density between the two boron atoms and therefore lack of bonding between these two atoms.

The boron atom has three valence electrons and needs five more to obtain octet,

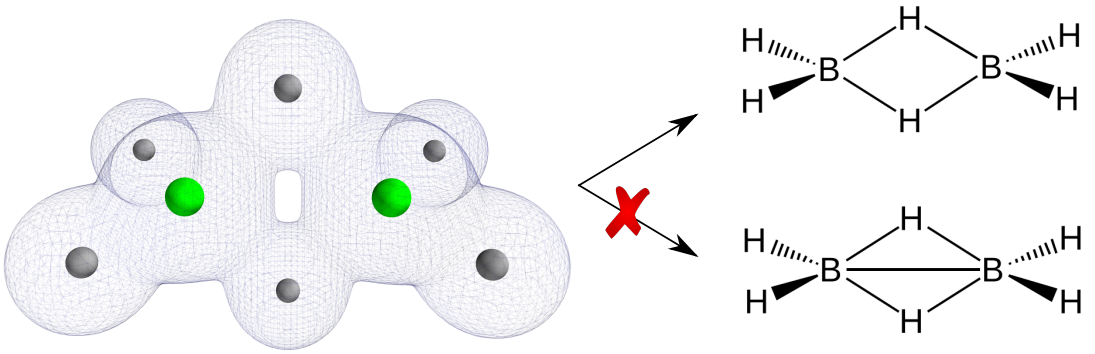

Figure 9.7: Bond density surface of dibroane. The value of the isodensity surface is 0.1 electrons/a.u.^{3}. The green spheres are boron atoms and the gray ones are hydrogen atoms. The correct Lewis structure of this molecule is also shown, in addition to a wrong Lewis model of the structure.

while each hydrogen atom has one valence electron and needs one more to fill their valence shell. There are therefore in total twelve valence electrons in B_2H_6 for chemical bonding. By having three hydrogen atoms bonded to each boron atom, we will get two BH_3 molecules, which are, however, not stable since the boron atoms are surrounded by only six valence electrons. Instead, the two boron atoms share two hydrogen atoms with each other, forming a 3-center-2-electron bond. In this way will the boron atoms combine to form a stable electron configuration closer to octet. The Lewis structure[3] of this molecule is shown on the upper right hand side in Figure 9.7. The location of the bonds agrees with the bond density surface. This example clearly shows the usefulness of the bond density surface, in cases where the bondings are perhaps not so obvious.

Electron density surfaces can also be used to qualitative describe trends that may exist among molecules. As an example the size surfaces of methyl anion, ammonia and hydronium cation are shown in Figure 9.8.

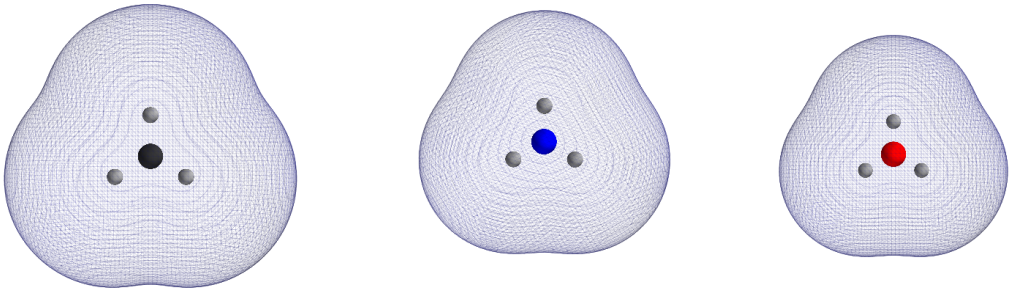

(a) Methyl anion **(b)** Ammonia **(c)** Hydronium cation

Figure 9.8: Electron density surfaces for three different molecules. The black sphere is carbon, the blue sphere is nitrogen, the red sphere is oxygen and the gray spheres are hydrogen. The value of the isodensity surface is 0.002 electrons/a.u.^{3}.

[3]Lewis structures are diagrams that show the bonding between atoms of a molecule.

These molecules have a very similar structure with ten electrons each and a heavy atom in middle surrounded by three hydrogen atoms. It is clear from the figure that there is a marked decrease in overall size from the methyl anion to the hydronium cation. This trend can simply be explained by the increasing electronegativity of the heavy atom as one moves to the right in the periodic table, resulting in more tightly bonded electrons and reduction in the overall size.

9.3.2 Electrostatic Potential

Another common quantity in graphical models is the visualization of the electrostatic potential, defined as the energy of interaction of a positive point charge located at some point $\mathbf{C}$, with the nuclei and electrons of a molecule [53]. Mathematically, it can be written as (in the restricted formulation)

$$E_p = \sum_{n=1}^{N_n} \frac{Z_n}{|\mathbf{R}_n - \mathbf{C}|} - \sum_{p,q=1}^{M} P_{pq} \int \frac{\varphi_p(\mathbf{r})\varphi_q^*(\mathbf{r})}{|\mathbf{r} - \mathbf{C}|} \mathrm{d}\mathbf{r}, \tag{9.14}$$

where the first summation is over the nuclei, located at $\mathbf{R}_n$ with charge Z_n, while the second summation is over basis functions φ, and reflects the Coulombic interactions between the electrons and the point charge. The density matrix is as always $\mathbf{P}$. The electrostatic potential is a function of the location of the point charge, which will have a positive value if it is placed in electron poor regions, leading to repulsive interaction, and negative value if it is placed at electron rich regions, leading to attractive interaction between the point charge and the molecule. The electrostatic potential can as electron density be represented by isosurfaces; points in space with the same value for the electrostatic potential.

In Figure 9.9, the negative and positive electrostatic potential surface (isosurface where the electrostatic potential is negative/positive) of benzene shown. There are two isosurfaces with negative electrostatic potential, one above the face of the ring and one below. This is reasonable because of the symmetry of benzene. A negative charge will therefore be repelled in these regions, while positive charges are attracted. The positive isosurface, on the other hand, has a completely different shape and is similar to the bond density surface; disk-shaped and wrapped fairly tightly around the nuclei. Negative charges will be attached in these regions.

The electrostatic potential surfaces suggest that a positive charge will be attracted by the top and bottom face of a benzene molecule. From this observation we may therefore conclude that a dimer—a chemical component consisting of structurally similar molecules—consisting of benzene molecules, will probably not prefer a geometry where the rings are ”stacked” upon each other, due to the repulsive interaction which will occur between the benzene rings. In fact, it turns out that the benzene rings are perpendicular to each other (T-shaped geometry), as it is shown in figure 9.10 [53]. The reason for this is because in a T-shaped geometry the negative regions of the electrostatic potential meet positive regions of electrostatic potential, leading to attractive interaction between the molecules and lower energy for the system, making it the favorable geometry.

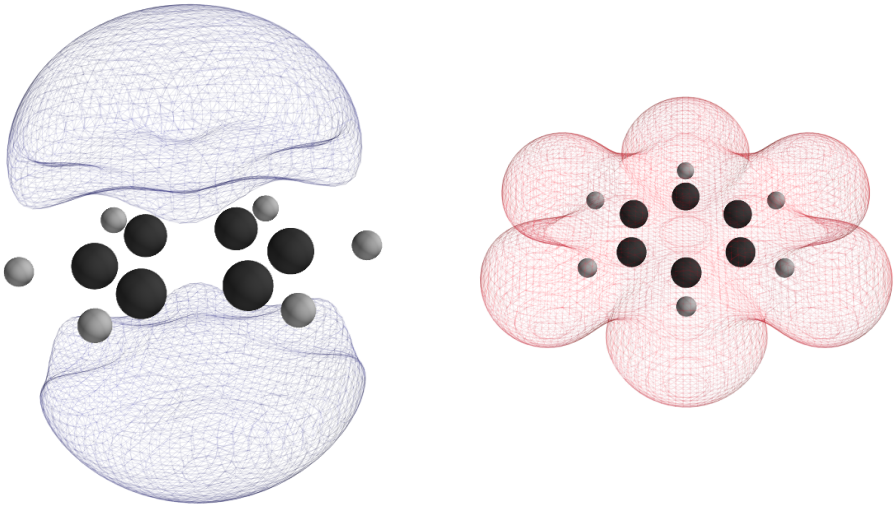

(a) Negative **(b)** Positive

Figure 9.9: Negative and positive electrostatic potential surfaces for benzene. The black spheres are carbon atoms and the gray spheres are hydrogen atoms.

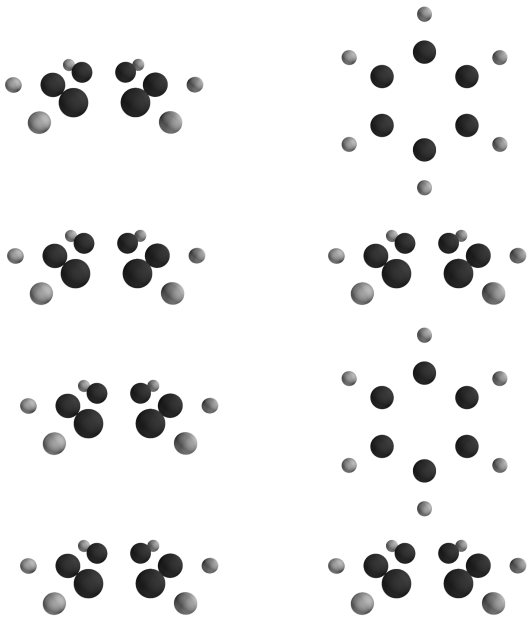

Figure 9.10: Two different geometries for the benzene dimer. The geometry on the right hand side is the favorable geometry because of the attractive interaction which occurs between the rings.

As a final example we consider the pyridine molecule, where one of the carbon atoms and one of the hydrogen atoms in benzene are replaced with a nitrogen atom. The positive electrostatic potential surface of pyridine, as shown in Figure 9.11b, is very

similar to the corresponding surface in benzene, but a marked cut is observed around the nitrogen atom compared to benzene. The symmetry in the isosurface is therefore lost. Beside this, the surface is quite similar to the one seen in benzene. The negative electrostatic potential surface (Figure 9.11a), on the other hand, has a completely different shape compared to benzene. In this case the negative isosurface is in the ring plane above the nitrogen atom, which is due to the higher electronegativity of the nitrogen atom relative to carbon and the electron lone-pair in nitrogen which makes the region around the nitrogen atom electron rich, leading to a negative electrostatic potential in these regions.

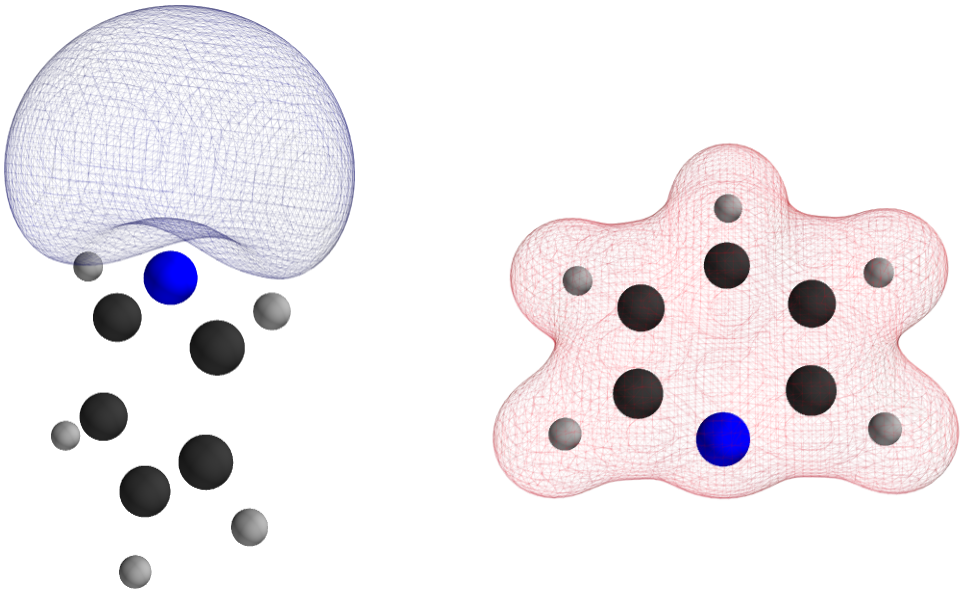

(a) Benzene **(b)** Pyridine

Figure 9.11: Negative and positive electrostatic potential surfaces for pyridine. The blue sphere is nitrogen, the black spheres are carbon atoms and the gray spheres are hydrogen atoms.

Chapter 10

Molecular Dynamics Results

In this chapter, the numerical results from the molecular dynamics (MD) simulations are presented, analyzed and discussed. These results include equilibrium bond length and vibration frequencies of selected diatomic molecules (H_2, N_2, F_2, FH, and CO).

10.1 Bond lengths

The optimized bond lengths of H_2, N_2, F_2, FH, and CO, obtained from the Born-Oppenheimer MD (BOMD) calculations, for various basis sets are given in Table 10.1. These bond lengths are found by letting the diatomic system evolve in time from an initial configuration and by rescaling the velocities of the nuclei by a factor of 0.95 at each time step. This slows down the motion of the nuclei and eventually makes them end up with zero velocity at their equilibrium spacing (see Figure 10.1). The equilibrium bond lengths obtained from Car-Parrinello MD (CPMD) simulations are also included in Table 10.1, in addition to the Hartree-Fock results from the minimization of the energy with respect to the atomic spacing [54].

The BOMD calculations were done using a time step $\Delta t = 0.1$ a.u. and the proton mass was set equal to one. The restricted Hartree-Fock (RHF) method was used for the electronic structure calculations at each time step.

The obtained bond lengths from the BOMD calculations are in very good agreement with the Hartree-Fock results, with a maximum discrepancy less than $\sim$0.1%. The correct ordering of the bond lengths with respect to the experimental values (H_2 < FH < N_2 < CO < F_2) is reproduced for all basis sets. The calculated bond length for the hydrogen molecule becomes closer to the experimental value as the size of the basis set is increased, with the largest improvement when going from the STO-3G to the 6-31G basis set. For all the other molecules the 6-31G basis set gives bond lengths closest to the experimental values, while the more "correct" 6-31G** basis set underestimate the equilibrium spacing between the atoms. This underestimation is very common i Hartree-Fock calculation and is due to the neglect of electron correlations [10]. The magnitude of the error relative to the experimental value for the largest basis set increases as the elements involved in the bond move from left to right in the periodic table. The largest error is in F_2, followed by N_2, FH, CO, and H_2. The only molecule that seems to deviate from this trend is the CO molecule, which has a smaller error

Table 10.1: Bond length values of the diatomic molecules in atomic units.

		Bond length (a.u.)				
Method	Basis set	H_2	N_2	F_2	FH	CO
BOMD	STO-3G	1.346	2.143	2.484	1.806	2.165
	6-31G	1.379	2.058	2.668	1.740	2.137
	6-31G**	1.384	2.038	2.541	1.702	2.105
Hartree-Fock[a]	STO-3G	1.345	2.143	2.485	1.805	2.164
	6-31G	1.379	2.058	2.670	1.740	2.137
	6-31G**	1.385	2.037	2.542	1.701	2.105
CPMD[a]	Plane wave	1.453	2.084	2.627	1.759	2.152
Experiment[b]		1.402	2.075	2.668	1.733	2.132

Hartree-Fock and Car-Parrinello values from [a]Ref. [54]. Experimental data from [b]Ref. [55].

than FH even though it consist of two heavy elements (atoms on the right side of the periodic table), in contrast to FH with only one heavy element.

The equilibrium bond lengths, obtained by the BOMD method with the largest basis set, are shorter than the corresponding values obtained by the CPMD method, except for the hydrogen molecule. However, since the CPMD results are found by using a plane wave basis set (see Ref. [54]), a direct comparison of the CPMD results and the BOMD results, without considering the basis sets used in these calculations, is not simple. This is because both methods are very sensitive to the choice of the basis set. More importantly, the underlying many body theory in the CPMD calculations is Density functional theory [11], in contrast to the BOMD calculations where the Hartree-Fock method has been used to calculate the nuclear forces. The difference between the CPMD and BOMD results are therefore not only due to the differences between these two methods, but also the underlying many-body theory and the basis set used in calculations.

10.2 Vibrational frequencies

Molecular vibrations occur when atoms in a molecule are in periodic motion while the molecule as a whole experiences constant translational and rotational motion. The frequency of the periodic motion is known as a vibration frequency, with typical values within the IR range of the frequency spectrum. Knowledge about the vibrational frequencies of a molecule provides useful information about the structure of the molecule,

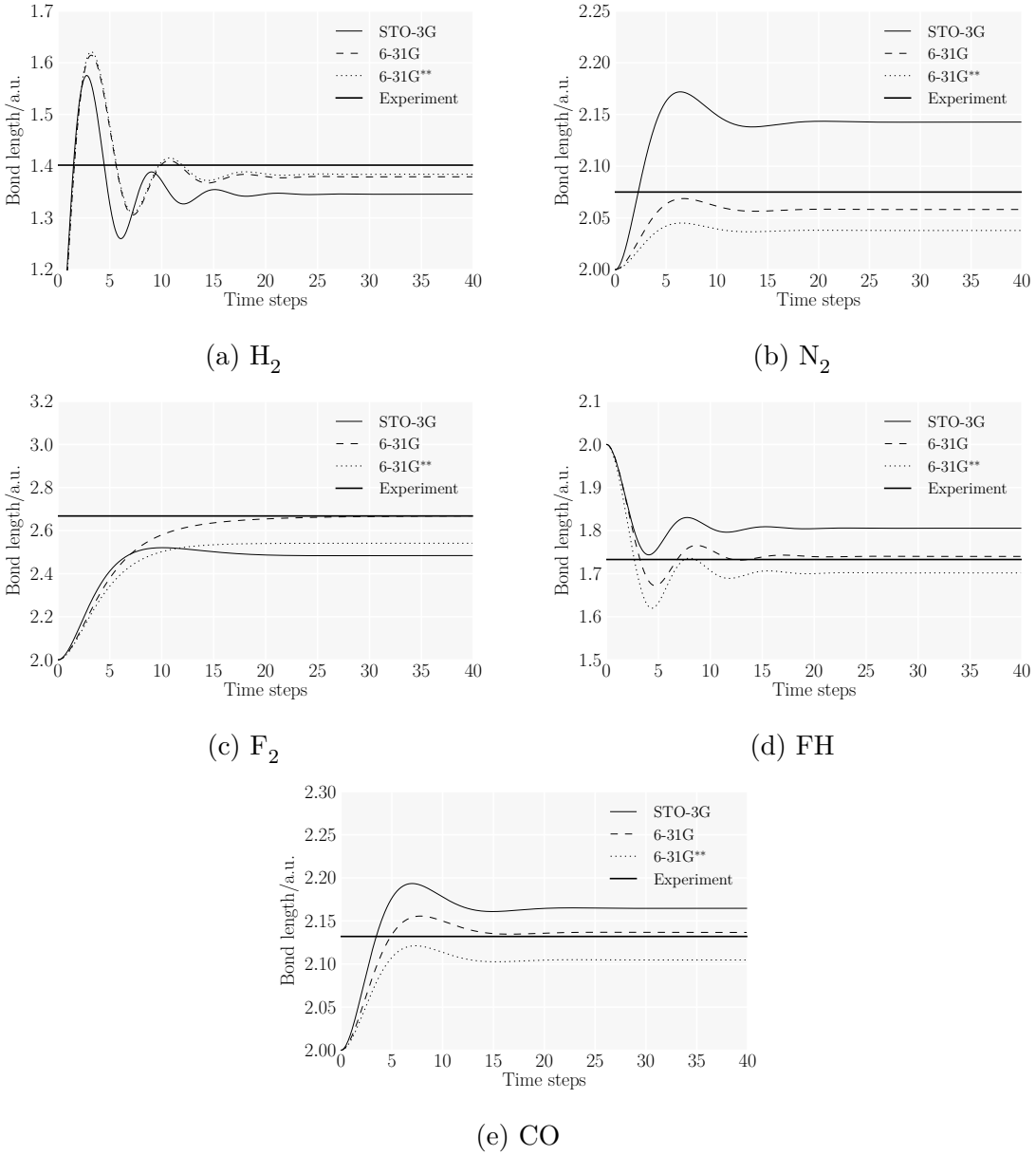

(a) H_2 (b) N_2

(c) F_2 (d) FH

(e) CO

Figure 10.1: Damped bond length oscillations obtained from the BOMD simulations. The velocity of each atom is rescaled by 0.95 at every time step. The thick straight lines indicate the experimental bond lengths (see Table 10.1). The x-axis is the number of time steps. A time step $\Delta t = 0.1$ a.u. is used and the proton mass is set equal to 1.

and methods such as IR spectroscopy and Raman spectroscopy have a long history of use in structure determination [10]. To a first approximation, the vibrational motion for small perturbations from the equilibrium configuration can be described as a simple harmonic motion. Within this approximation, the vibrational frequency of a diatomic

molecule is proportional to the square root of the force constant k (the second derivative of the energy with respect to the interatomic distance) divided by the reduced mass μ of the system:

$$\text{frequency} \propto \sqrt{\frac{\text{force constant}}{\text{reduced mass}}}. \tag{10.1}$$

This assumes that the first derivative of the energy with respect to the intermolecular distance is zero, i.e. the molecule is at a stationary point. Another way to determine the vibrational frequency of a diatomic system is to perform molecular dynamics simulations where the atoms are allowed to oscillate freely around their equilibrium spacing. From the Fourier spectrum or the period of bond oscillations, it is then possible to estimate the vibrational frequency of the diatomic system.

In Table 10.2, the obtained vibrational frequencies of H_2, N_2, F_2, FH, and CO from the BOMD calculations for various basis sets are shown. The results from Ref. [54], obtained by the CPMD method and the Hartree-Fock method are also included. The Hartree-Fock results are found using the harmonic oscillator approximation. In the BOMD calculations the proton mass was set equal to 1836.15 a.u., and a time step $\Delta t = 10$ a.u. was used. With this time step, the energy of the systems was conserved better than 10^{-5} a.u. throughout the dynamical simulations. The atoms were slightly displaced from their equilibrium spacing in the initial step of the simulations, and for the electronic structure calculations at each time step, the RHF method was used. The Fourier spectrum of the bond oscillations for various basis sets are also included and are shown in Figure 10.2. Due to the finite duration of the simulations, a smoothing procedure like the one described in Appendix A.3 is used. Also the obtained frequencies from the least squares (LS) trigonometric fitting of the bond oscillations is included[1].

The obtained frequencies from the Fourier transform of bond oscillations are in some cases the same for two different basis sets. This is however only due to the resolution we have in the frequency spectrum. In cases where the frequencies for two different basis sets are close to each other, we simply don't have good enough resolution in the frequency spectrum to distinguish these from each other. To obtain better resolution in the frequency spectrum, the dynamical simulation has to be performed over a longer period of time.

The vibrational frequencies obtained from LS fitting of bond oscillations are slightly lower than the corresponding Hartree-Fock results. This is the case even though the electronic structure calculations in the BOMD simulations and thereby the forces acting on the nuclei were based on the Hartree-Fock method. This disagreement can be explained by the fact that the Hartree-Fock results are based on the harmonic oscillator approximation, while the molecular vibrations are not entirely harmonic. The harmonic oscillator approximation assumes a parabolic form for the potential energy surface, and therefore do not allow the molecule to dissociate into its component atoms. Thus, this description breaks down at large intermolecular distances. However, even at very short distances beyond the equilibrium bond length, the true potential energy surface differs from the parabolic potential of the harmonic approximation (see Ref. [10]). This leads to a systematic error in the Hartree-Fock results, and is most likely responsible for the

[1]The least squares fitting of the bond oscillations has been done using the `scipy.optimize.curve_fit` function in Python [56].

Table 10.2: Vibrational frequencies of the diatomic molecules in cm^{-1}. The BOMD results are obtained from Fourier analysis and trigonometric fitting (least squares (LS)) of the bond oscillations. A time step $\Delta t = 10$ a.u. was used and 800 time steps were simulated. This gives a resolution $\Delta f = 172.3$ cm^{-1} in the frequency spectrum. The standard deviations in the trigonometric fits are of order 10^{-8}.

			Vibrational frequency (cm^{-1})				
Method	Basis set		H_2	N_2	F_2	FH	CO
BOMD	STO-3G	Fourier	5512	2584	1723	4479	2412
		LS fitting	5472	2660	1671	4463	2453
	6-31G	Fourier	4651	2584	1206	4134	2239
		LS fitting	4635	2651	1137	4124	2277
	6-31G**	Fourier	4651	2756	1206	4479	2412
		LS fitting	4624	2748	1240	4481	2429
Hartree-Fock[a]	STO-3G		5481	2670	1677	4474	2463
	6-31G		4644	2661	1141	4135	2286
	6-31G**		4635	2758	1245	4493	2439
CPMD[a]	Plane wave		4118	2282	1106	3999	2040
Experiment[b]			4160	2331	891	3962	2143

Hartree-Fock and Car-Parrinello values from [a]Ref. [54]. Experimental data from [b]Ref. [57].

deviation from the BOMD frequencies.

It is not only the Hartree-Fock frequencies that suffer from systematic errors. The calculated frequencies from the BOMD simulations also suffer from a systematic error due to the non-self-consistency that exists in the electronic structure calculations. This gives raise to a correction term in the force expression that is not included in our calculations. Within a given incomplete basis set, this correction term vanishes only when self-consistency has been reached [16]. In practice, by requiring very high accuracy, we can make this term arbitrarily small but it can never be suppressed completely.

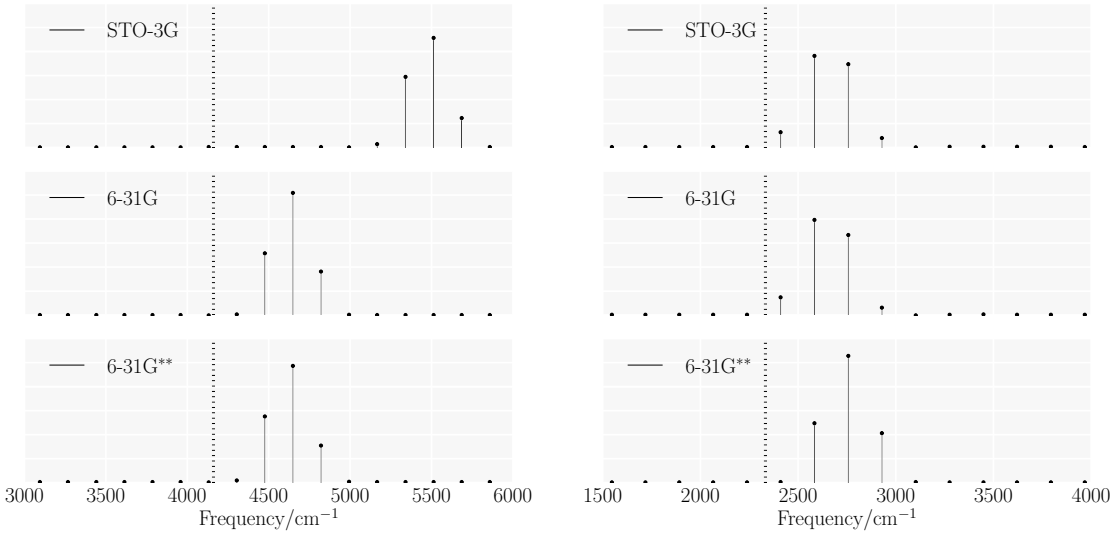

(a) H_2

(b) N_2

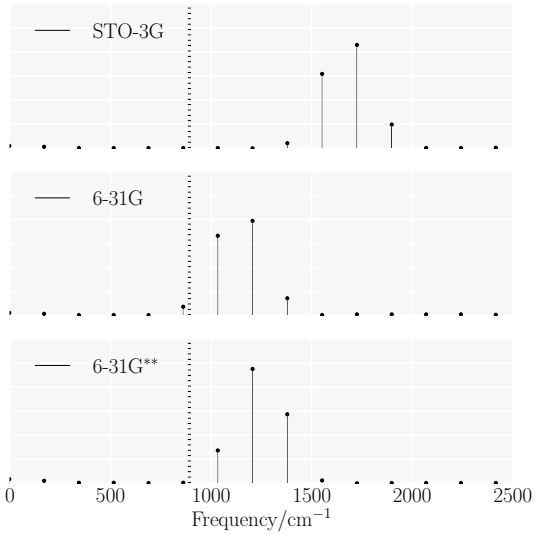

(c) F_2

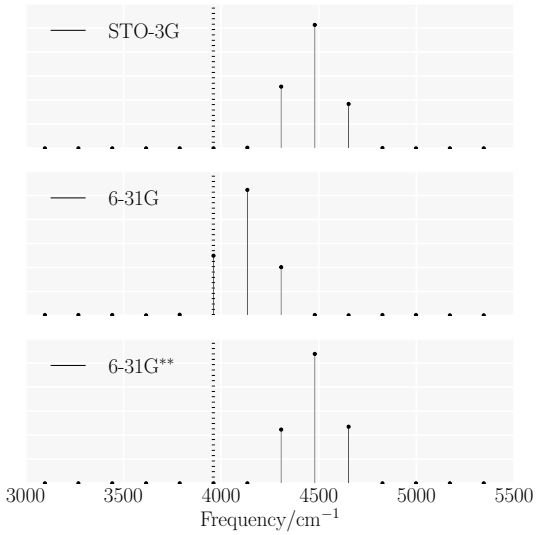

(d) FH

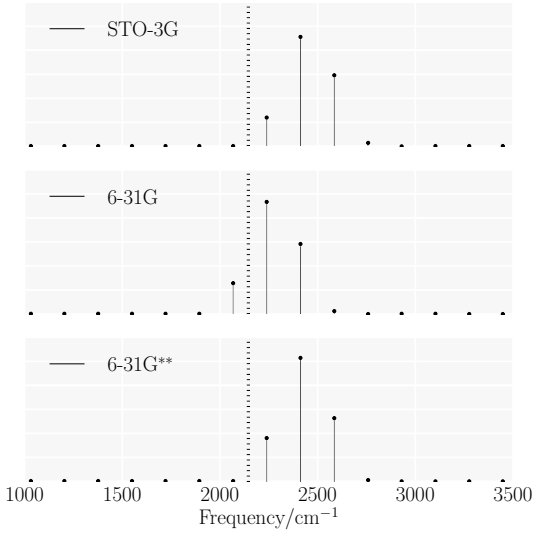

(e) CO

Figure 10.2: Vibrational frequency distribution spectrum obtained from BOMD simulations. The dashed lines indicate the experimental vibration frequencies.

All basis sets overestimate the vibrational frequencies relative to the experimental values. This is common in calculations based on the Hartree-Fock method [10]. The reason for this overestimation is due to the neglect of electron correlations and basis set truncation effects. However the overestimation of the vibrational frequencies turns out to be systematic within Hartree-Fock theory. A lot of work has been done to estimate an empirical, constant scaling factor for the different basis sets to improve the Hartree-Fock frequencies [58]. For example, the frequencies obtained by the 6-31G** basis set are usually scaled by a factor of 0.8992 [58], giving frequencies in much more agreement with experiments. Multiplying the BOMD results with this factor brings the frequencies from the range of 11-18% of the experimental values to a range of 0.5-1.9% of the experimental values, except for the F_2 molecule where the frequency is still overestimated by 25% (initially overestimated by 39%). It should be noted that the scaling factor we have scaled the BOMD frequencies with is optimized for the Hartree-Fock frequencies within the harmonic oscillator approximation, while no such approximation is assumed in the BOMD simulations. We see however that this factor improves our results significantly.

The frequencies obtained by the CPMD method are for all molecules closer to the experimental values compared to the BOMD frequencies with the largest basis set. The CPMD calculations are however based on density functional theory within the local density approximation where plane wave basis functions have been used [54]. It is therefore difficult to make a fair comparison of the obtained frequencies from the BOMD and the CPMD method, since their underlying many-body method is different.

10.3 The Nucleophilic Substitution Reaction $H^- + CH_4 \rightarrow CH_4 + H^-$

Nucleophilic substitution reactions are a class of reactions that involve the interaction of electron-rich species (nucleophile) with electron-poor species (electrophile). In these reactions the electron-rich nucleophile attacks the electron-poor electrophile forming a new bond, leading to detachment of an atom or group (leaving group) in the electrophile species [59]. An example of this type of reaction is the S_N2[2] reaction $H^- + CH_4 \longrightarrow CH_4 + H^-$, where the nucleophilic hydrogen anion attacks the electrophilic carbon atom in the methane molecule at 180° to the leaving negatively charged hydrogen atom. The S_N2 mechanism of this reaction is shown in Figure 10.3. The breaking of the C–H bond and the formation of the new bond occur simultaneously through a transition state [53] in which the carbon atom is partially attached to both the incoming and the leaving atom. As the leaving atom is pushed off, the initial tetrahedron is inverted, much like an umbrella turning inside out in the wind.

[2]In the term S_N2, S stands for substitution, N for nucleophilic and the number 2 refers to the fact that two species are involved in the initial stage of the reaction.

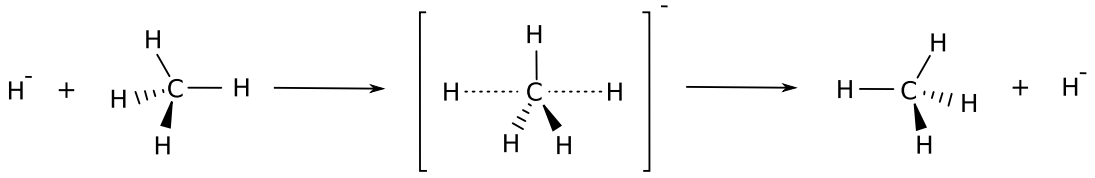

Figure 10.3: S_N2 nucleophile substitution reaction of methane with hydrogen anion. The structure in the middle corresponds to the transition state [53] structure.

To investigate the dynamics of this reaction, BOMD calculations has been carried out, where the classical trajectories of the atoms, starting from two separate reactants ($H^- + CH_4$), has been computed. A time step $\Delta t = 10$ a.u. was used, and a total of 200 time steps were simulated. For the electronic structure and force calculations, the unrestricted Hartree-Fock (UHF) method has been used with the STO-3G basis set. The initial configuration corresponds to the one where the methane molecule is in rest in its equilibrium geometry with bond length 2.047 a.u. and bond angle 104°[3]. The hydrogen anion is initially at a distance 8.66 a.u. from the carbon atom with start velocity 0.017 a.u., directed towards the carbon atom and the leaving group.

In Figure 10.4, a sequence of structures observed during the dynamical simulation is shown, illustrating the formation of the carbon-nucleophile bond and the breaking of the carbon-leaving group bond. Note that some of the kinetic energy of the nucleophilic hydrogen anion after the collision is transformed into vibrational energy in the methane molecule. In Figure 10.5a, the negative electrostatic potential isosurface corresponding to -0.25 a.u. for four different instances in time is shown, illustrating how the electron-rich regions are relocated during the dynamical simulation. The configurations at 400 a.u. and 500 a.u. are near the transition state configuration and clearly show the relocation of the electron-rich regions from the attacked side to the opposite side. The relocation of charges becomes more clear by considering the change in the net charge of the atoms, as shown in Figure 10.5b. The net charge of the incoming hydrogen anion goes from being negative to slightly positive while the leaving atom undergoes a nearly opposite transformation. The net charge of the three non-reacting hydrogen atoms exhibits very little change in the first 30 integration steps when the interaction with the incoming hydrogen anion is small, but starts to oscillate weakly afterwards due to the vibration in the methane molecule. The incoming atom follows these oscillations fairly closely, after the departure of the leaving atom. The net charge of the carbon atom exhibits also very little change before the non-reacting hydrogen atoms are inverted, but it increases and becomes slightly positive as the distances to the incoming and leaving atom are close to each other. As the leaving atom is pushed off and the initial tetrahedron is inverted, the net charge of the carbon atom oscillates around its initial value before the collision with the hydrogen anion.

[3]The equilibrium structure of methane was found by the same method used to find the equilibrium bond lengths of the diatomic systems in Section 10.1 and successfully benchmarked against the values given in [6].

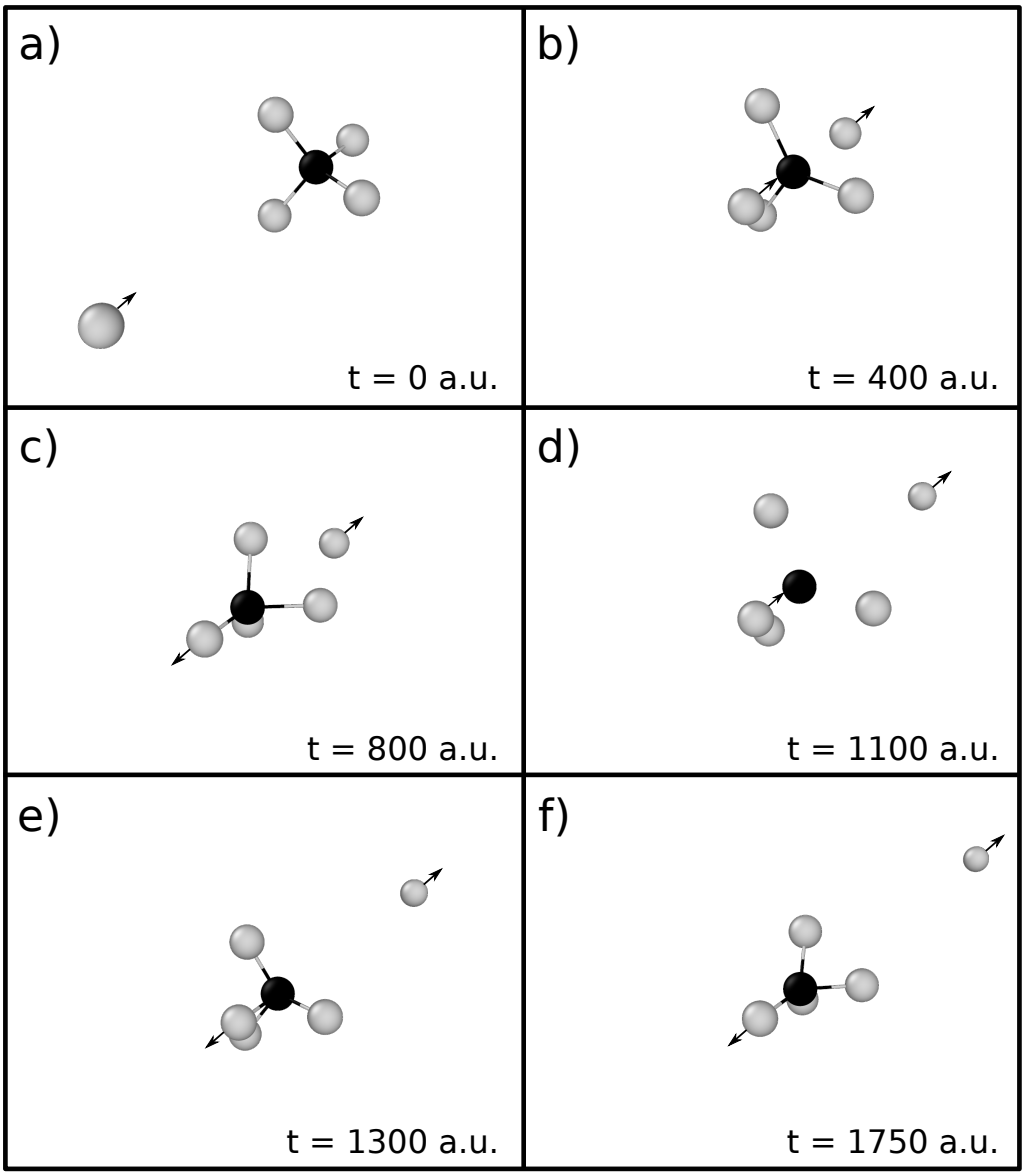

Figure 10.4: Sequence of structures observed during the dynamical simulation. The black sphere is the carbon atom, while the gray spheres are hydrogen atoms. The arrows indicates the direction of the velocity of the atom at that instance of time. The bonds between the carbon atom and the hydrogen atoms are only shown when the distance C-H is equal or less than the equilibrium bond length in methane (2.047 a.u.).

Figure 10.5

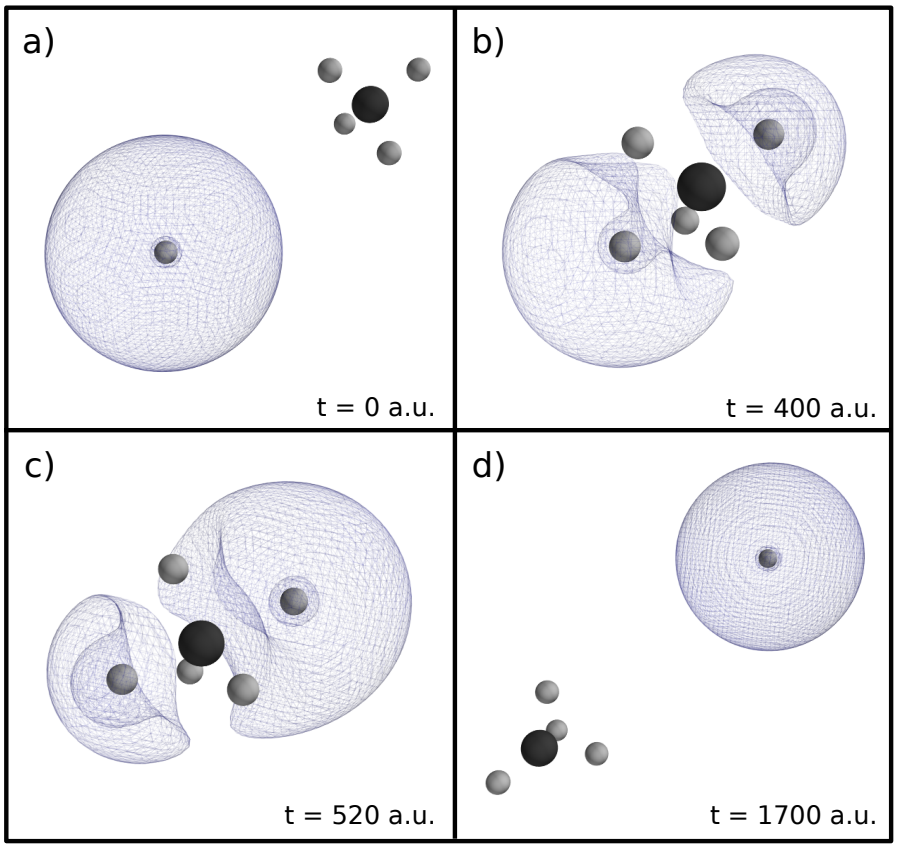

(a) Sequence of structures with negative electrostatic potential isosurface observed during the dynamical simulation. The electrostatic potential surface corresponds to a value of -0.25 a.u. in all figures. The black sphere is the carbon atom, while the gray spheres are hydrogen atoms.

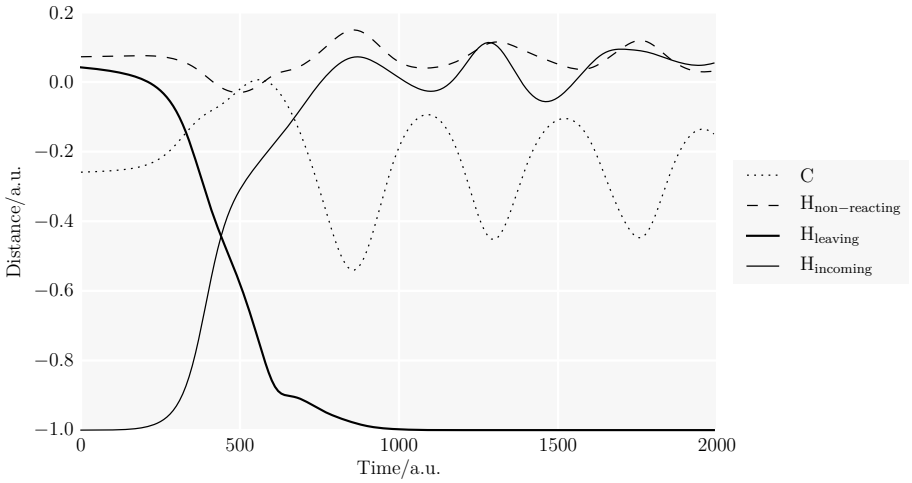

(b) Variation of the net charge of the atoms. The charges are calculated using the Mulliken SCF population analysis (see Section 9.1.3).

10.3.1 The Effect of Different Basis Sets

The calculations presented in the last section were done using the minimal basis set STO-3G. This basis set has no flexibility to allow for weakly bound electrons (as we have in the hydrogen anion) and can lead to serious errors in energy and other molecular properties. As it turns out, the same calculations as the ones we have done so far, but with larger basis sets such as the 6-31++G** basis set, show that the reaction does not occur. The incoming hydrogen anion is pushed back and no inversion of the tetrahedron occurs. Simulations with higher initial translational energy led to even faster repulsion of the incoming hydrogen anion.

To investigate the effect of basis set on the dynamics of the reaction, the trajectories of the atoms has been, starting from the transition state configuration, computed for the minimal basis set and the 6-31++G** basis set[4]. The geometry of the transition state is shown in Figure 10.6b with the distances R_1 and R_2 equal to each other and $\theta = 90°$. The calculations has been performed with a time step $\Delta t = 10$ a.u. and the UHF method is used for electronic structure and force calculations. The initial translational energy of the hydrogen anion was set to 0.05 kcal/mol.

To illustrate the effect of basis set on the atomic trajectories, the energy barrier $E_{barrier}$, the collision energy $E_{collision}$ and the vibrational energy $E_{vibration}$ of the methane molecule are computed for both basis sets. The energy barrier corresponds to the difference in (potential) energies between reactants ($CH_4 + H^-$) in equilibrium configuration and transition state. The collision energy is the sum of the translational energy of the leaving atom and the methane molecule. The calculated values are shown in Table 10.6a, where also the ratio $\tau = E_{vibration}/E_{collision}$ is shown. The change in various energy forms and the atomic distance changes between the carbon atom and the incoming and leaving hydrogen atom during the dynamical simulation, are shown in Figure 10.7.

The first thing to notice is the significant underestimation of the energy barrier with the STO-3G basis set compared to the 6-31++G** basis set and other high quality calculations [61]. This underestimation is a consequence of a poor description of the weakly bound electron in the hydrogen anion, and can be improved with the addition of diffuse functions in the basis set. This improvement is apparent in the obtained ground state energy of the hydrogen anion with the 6-31++G** basis set, with a value of -0.487 a.u., close to the Hartree-Fock limit (HF limit) of -0.488 a.u. [60]. The ratio $E_{vibration}/E_{collision}$ is also significantly underestimated by the minimal basis set and is less than a half of the ratio found with the largest basis set. The smaller amount of collision energy with the largest basis set is a consequence of a higher energy barrier, pushing the leaving atom faster out of the interaction region between H^- and CH_4 while the geometry of the methane molecule still corresponds to a high potential energy [60]. As a result, after the departure of the leaving atom, the methane molecule will have a larger amount of vibrational energy, mainly concentrated in the stretching (R_1) and bending (θ) modes[5]. With a lower energy barrier the detachment of the hydrogen

[4]The calculations and analysis represented in this section are similar to the ones done in Ref. [60], but with a larger basis set.

[5]The R_0 parameter which represent the bond length of the three non-reacting hydrogen atoms exhibits very little change during the dynamical simulation for both basis sets.

Figure 10.6

		Distances[a] (a.u.)			Energy (kcal/mol)			
System	Basis set	R_0	R_1	R_2	$E_{barrier}$	$E_{collision}$	$E_{vibration}$	τ
CH_4H^-	STO-3G	2.06	2.80	2.80	46.859	30.896	16.011	0.52
	6-31++G**	2.02[b]	3.21[b]	3.21[b]	62.987	28.216	34.839	1.24
CH_4D^-	6-31++G**	2.02[b]	3.21[b]	3.21[b]	62.987	30.442	30.937	1.02
CD_4H^-	6-31++G**	2.02[b]	3.21[b]	3.21[b]	62.987	21.761	41.283	1.89

(a) Geometry of the transition state and the calculated energy barrier, collision energy and vibrational energy for the reactions $H^- + CH_4$, $D^- + CH_4$ and $H^- + CD_4$. τ corresponds to the ratio $E_{vibration}/E_{collision}$.

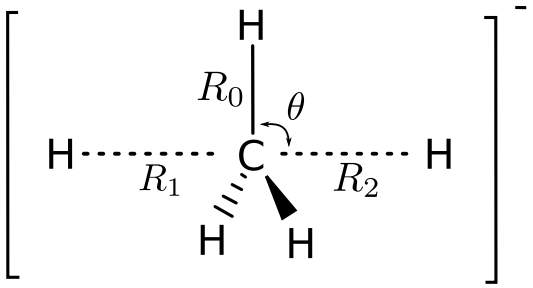

(b) Transition state geometry. R_1 is initially equal to R_2 and θ is equal to 90°.

[a]The transition state geometries are from Ref. [54].
[b]These values are the optimal values for the largest basis used in Ref. [54] and are assumed to be near the optimal values for the 6-31++G** basis set.

atom occurs more slowly, allowing the methane molecule to more efficiently release its potential energy to translational energy. The faster departure of the leaving atom with the largest basis set is clear in Figure 10.7b, where we see the R_2 parameter starting to increase earlier with the largest basis set. The higher vibrational energy with this basis is also indicated by the higher oscillations in R_1.

Similar effect in the ratio of vibrational and kinetic energy can also be observed in calculations of two similar systems $D^- + CH_4$ and $H^- + CD_4$, using the 6-31++G** basis set. The only difference between these systems and the original system we have been discussing so far ($H^- + CH_4$) is the higher mass of the deuterium atoms. In Figure 10.8, the results from these calculations are shown and the calculated energies after the detachment of the leaving group is shown in Table 10.6a. In these results we saw the same effect as obtained in the calculations with different basis sets. The CH_4D^- system has a lower ratio $E_{vibration}/E_{collision}$ compared to the CD_4H^- system,

Figure 10.7: Simulation of the reaction $H^- + CH_4$, starting from the transition state, with the minimal basis set and the 6-31++G** basis set.

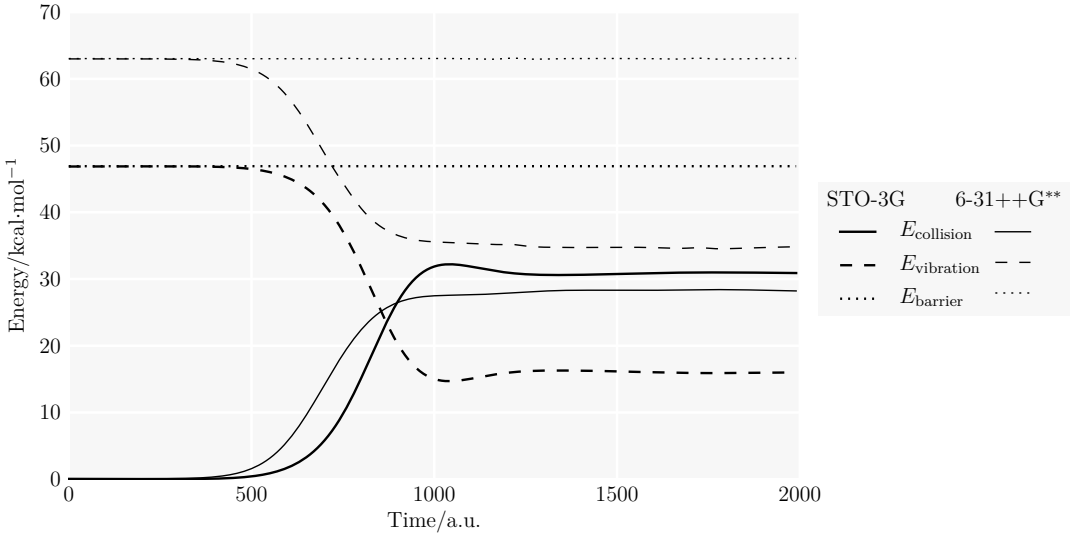

(a) The change in different energy forms during the dynamical simulation. The sum of the vibrational and collision energy is equal to the energy barrier minus the initial translational energy.

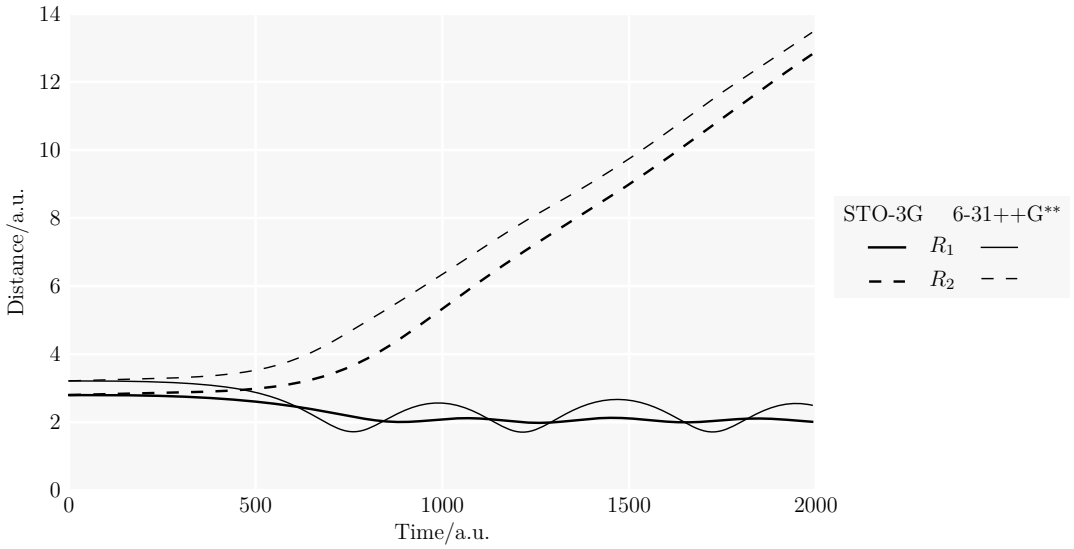

(b) The atomic distance changes between C and the incoming and leaving hydrogen atom.

due to the slower departure of the deuterium atom in the former system because of the higher mass of deuterium atom compared to the hydrogen atom. In the former system the methane molecule is in a more stable configuration when the deuterium atom is out of the interaction range, leading to less vibrational motion. In the CD_4H^- system, on the other hand, the motion of the hydrogen atom is faster than the heavier

deuterium atoms, resulting in faster departure of the hydrogen atom and higher amount of vibrational energy in the methane molecule.

Figure 10.8: Simulations of the reactions $D^- + CH_4$ and $H^- + CD_4$, starting from the transition state, with the 6-31++G** basis set.

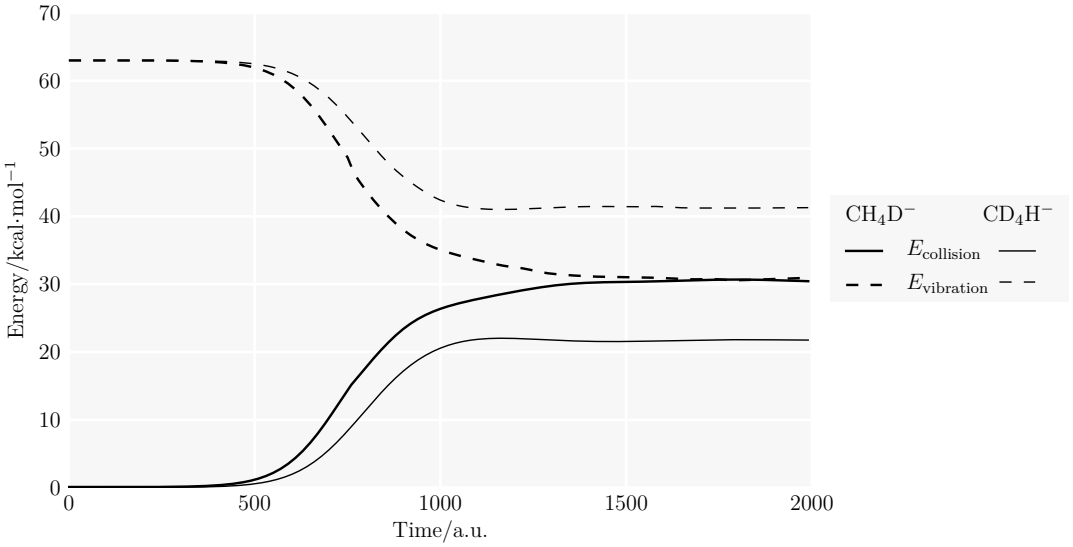

(a) The change in different energy forms during the dynamical simulation. The sum of the vibrational and collision energy is equal to the energy barrier minus the initial translational energy.

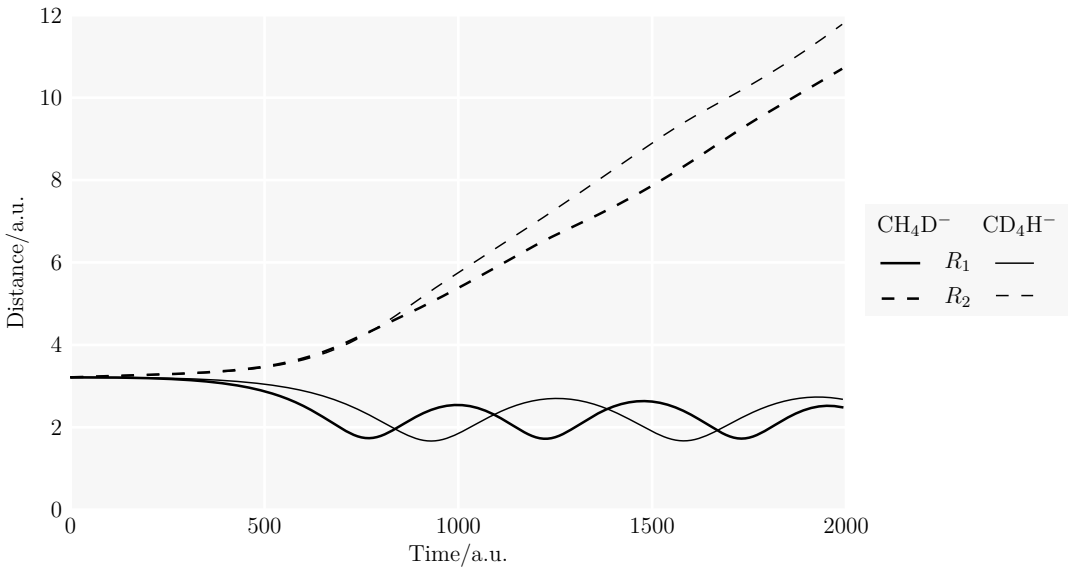

(b) The atomic distance changes between C and the incoming and leaving hydrogen atom.

10.3.2 Final comments

The importance of diffuse functions in systems with weakly bonded electrons is evident in our simulations. Calculations with the minimal basis set underestimates the energy barrier in the reaction $H^- + CH_4 \longrightarrow CH_4 + H^-$ significantly, and the importance of the initial vibrational energy of the methane molecule is not apparent. The latter turns out to be essential for the reaction to occur. Simulations with initially separated reactants using the 6-31++G** basis set, show that the incoming atom is not able to invert the tetrahedron, due to the larger inertia of the umbrella relative to the motion of the incoming atom. Therefore, for the reaction to occur there must be a sufficient amount of vibrational motion in the methane molecule. Furthermore, the vibrations should be in phase with the arrival of the incoming nucleophile [60].

Part IV

Summary and Outlook

Chapter 11

Conclusion

The aim of this thesis has been to investigate the gap between quantum mechanical calculations and molecular dynamics (MD) simulations. This has been done by linking first principle calculations on molecules to atomic simulations in MD. The main objective of this thesis has been to develop an efficient and modular many-body quantum mechanics code, with the intent to be used in ab initio MD calculations and/or parameterization of predefined potentials. In particular, the focus has been on the Hartree-Fock method because of its ability to handle large molecular systems compared to other more sophisticated many-body methods. The implementation of the Hartree-Fock method has been based on molecular integral evaluation techniques, provided by the McMurchie-Davidson scheme [7].

The Hartree-Fock code has been thoroughly tested by running numerous verification tests on the different parts of the code. These tests include unit testing of the integrator and ground state energy benchmarking of a few simple systems. Furthermore, the results from calculations on the ground state energy, dipole moment, ionization potential, and population analysis of H_2, N_2, FH, CO, NH_3, H_2O, and CH_4 have been checked and verified against the literature. The size of the basis set has an obvious influence in these calculations. The best results are obtained with the largest basis sets. However, for some quantities, such as the ionization potential of N_2 and the dipole moment of O_2 molecule, the minimal basis set was closest to the experimental values. These results can, however, not be trusted because of the small size of the minimal basis set. All in all, the "correct" Hartree-Fock results are obtained with the largest basis sets. The disagreement of these results with experiments or high quality calculations is due to the breakdown of the simple orbital picture in the Hartree-Fock method. In these cases the Hartree-Fock method is simply not accurate enough, and one needs to take correlations into account [6].

As a next step, we aimed at incorporating the first principle calculations into MD simulations. An MD code was therefore implemented. This code uses the Hartree-Fock implementation as a library, making it possible to compute the forces acting on the nuclei on-the-fly based on electronic structure calculations. The MD code has been used to study the vibrational frequency of the diatomic systems H_2, N_2, F_2, FH, and CO. The obtained frequencies are slightly better than the ones obtained by the harmonic oscillator approximation, but there are still overestimated frequency values,

compared to experimental data. This is common in calculations based on the Hartree-Fock method, and is caused by the neglect of electron correlations. The overestimations are, however, very systematic. The calculated frequencies can be brought closer to experimental data by multiplying them by a constant factor that only depends on the basis set [10]. This brought the frequencies from the range of 11-18% of the experimental values to a range of 0.5-1.9% of the experimental values, except for the F_2 molecule, where the frequency was still overestimated by 25% (initially overestimated by 39%).

Ab initio MD calculations, on the reaction dynamics of $H^- + CH_4 \longrightarrow CH_4 + H^-$, similar those of Ref. [60], have also been performed. These results show the importance of diffuse basis functions in studies of systems with weakly bound electrons. The minimal basis set underestimates the energy barrier of this reaction significantly, and neglects the importance of the initial vibrational energy of the methane molecule. Calculations with the 6-31++G** basis set, however, show that the initial vibrational motion of the methane molecule is crucial for the reaction to occur.

Future Prospects

Although the focus in this thesis has been on the transition from quantum mechanics to MD, the Hartree-Fock code is written in a general way such that it can easily be used for pre-calculations in pure quantum mechanical studies. For example, in quantum Monte-Carlo calculations it is necessary to have optimized single-particle wave functions in order to maintain a reasonable precision for larger atomic and molecular systems [8]. These optimized single-particle wave functions can be found by performing Hartree-Fock calculations. One of the future goals is to combine Hartree-Fock calculations with quantum Monte-Carlo calculations.

Another extension of this thesis project would be to use the integration scheme with other solver methods, such as density functional theory. This is possible because of the similarities between the Hartree-Fock equations and the Kohn-Sham equations [11]. The first principle calculations based on density functional theory can then be linked to MD simulations, which would be of great interest.

The integration scheme implemented in the Hartree-Fock code can also be used as basis in Car-Parrinello MD (CPMD) simulations. A general implementation of this method will allow us to study large systems, since no energy minimization is required at each nuclear time step, in contrast to Born-Oppenheimer MD (BOMD) [16]. This reduces the gap between quantum mechanics and molecular dynamics.

Appendices

Appendix A

Mathematics

A.1 Atomic units

Atomic units are designed to simplify the appearance of fundamental equations in quantum mechanics, which in their original form consist of many small valued constants. Beside the aesthetic aspect, use of atomic units is important from a programming point of view as well, to avoid the effects of round off errors.

We define atomic units by setting the following fundamental constants to one, namely

- Electron mass: $m_e = 1$.
- Elementary charge : $e = 1$.
- Reduced Planck's constant: $\hbar = 1$.
- Coulomb's constant: $\frac{1}{4\pi\epsilon_0} = 1$.

By using these constraints, we can derive the atomic units of some of the most important physical quantities [62]:

- **Unit of lenght**: $a_0 \equiv \frac{4\pi\epsilon_0\hbar^2}{m_e e^2} = 0.529\,177\,219\,2(17)$ Å.
- **Unit of energy**: $E_h \equiv \frac{m_e e^4}{(4\pi\epsilon_0\hbar)^2} = 27.211\,\text{eV}$.
- **Unit of time**: $\tau_0 \equiv \frac{\hbar}{E_h} = 2.418\,884\,326\,505(16) \times 10^{-17}\,\text{s}$.
- **Unit of velocity**: $v_0 \equiv \frac{a_0 E_h}{\hbar} = 2.187\,691\,263\,3(73) \times 10^6\,\text{m/s}$.

These quantities are the conversion factors for their respective physical quantity, such that the SI value, Q, of each of them is related to the their value in atomic units Q' by

$$Q = XQ', \tag{A.1}$$

where X is the conversion factor.

The electronic Hamiltonian is in its original form (in SI units) given as

$$\mathcal{H} = -\sum_{i=1}^{N_e} \frac{\hbar^2}{2m_e}\nabla_i^2 + \frac{1}{4\pi\epsilon_0}\sum_{i<j}^{N_e}\frac{e^2}{|\mathbf{r}_i - \mathbf{r}_j|} - \frac{1}{4\pi\epsilon_0}\sum_{n=1}^{N_n}\sum_{i=1}^{N_e}\frac{Z_n e^2}{|\mathbf{r}_i - \mathbf{R}_n|}. \tag{A.2}$$

This expression can be brought to dimensionless form, by introducing the following relations;

$$\mathcal{H}' = \mathcal{H}/E_h, \qquad \nabla' = \nabla/a_0, \qquad \mathbf{r}' = \mathbf{r}/a_0, \qquad \mathbf{R}' = \mathbf{R}/a_0. \tag{A.3}$$

By using these relations in Eq. (A.2), we obtain

$$\begin{aligned}\mathcal{H} &= -\frac{\hbar^2}{2m_e a_0^2}\sum_{i}^{N_e}(\nabla_i')^2 - \frac{e^2}{4\pi\epsilon_0 a_0}\left[\sum_{n=1}^{N_n}\sum_{i=1}^{N_e}\frac{Z_n}{|\mathbf{r}_i' - \mathbf{R}_n'|} + \frac{1}{2}\sum_{\substack{i,j=1\\ i\neq j}}^{N_e}\frac{1}{|\mathbf{r}_i' - \mathbf{r}_j'|}\right] \\ &= E_h\left(-\frac{1}{2}\sum_{i}^{N_e}(\nabla_i')^2 - \sum_{n=1}^{N_n}\sum_{i=1}^{N_e}\frac{Z_n}{|\mathbf{r}_i' - \mathbf{R}_n'|} + \frac{1}{2}\sum_{\substack{i,j=1\\ i\neq j}}^{N_e}\frac{1}{|\mathbf{r}_i - \mathbf{r}_j|}\right) \\ &= E_h\mathcal{H}'. \end{aligned} \tag{A.4}$$

The electronic Schrödinger equation can therefor be written as

$$\mathcal{H}'\Psi\left(\{\mathbf{r}_i'\};\{\mathbf{R}_n'\}\right) = E'\Psi\left(\{\mathbf{r}_i'\};\{\mathbf{R}_n'\}\right), \quad \text{where} \quad E' = \frac{E}{E_h}. \tag{A.5}$$

In this dimensionless form of Schrödinger equation, the energy will be measured in the units of Hartree (or a.u.), where $1E_h = 2 \cdot 13.6\,\text{eV}$ is twice the ground state energy of the hydrogen atom.

A.2 Antisymmetrizer

The antisymmetrizer operator $\mathcal{A}$ is a linear operator, defined as

$$\mathcal{A} \equiv \frac{1}{N!}\sum_{P}(-1)^{P_n}\mathcal{P}, \tag{A.6}$$

where $\mathcal{P}$ is the permutation operator and P_n is the parity of the permutation. By applying this operator on a wave function on the form

$$\Psi_{\text{H}} = \psi_1(\mathbf{q}_1)\psi_2(\mathbf{q}_2)\ldots\psi_N(\mathbf{q}_N), \tag{A.7}$$

the wave function will be antisymmetric with respect to exchange of coordinates of any pair of electrons, i.e.

$$\begin{aligned}
&\mathcal{P}_{ij}\Psi\left(\mathbf{q}_1,\ldots,\mathbf{q}_i,\ldots,\mathbf{q}_j,\ldots,\mathbf{q}_N\right)\\
&\quad=\mathcal{P}_{ij}\left[\sqrt{N!}\,\mathcal{A}\Psi_{\mathrm{H}}\left(\mathbf{q}_1,\ldots,\mathbf{q}_i,\ldots,\mathbf{q}_j,\ldots,\mathbf{q}_N\right)\right]\\
&\quad=-\sqrt{N!}\,\mathcal{A}\Psi_{\mathrm{H}}\left(\mathbf{q}_1,\ldots,\mathbf{q}_i,\ldots,\mathbf{q}_j,\ldots,\mathbf{q}_N\right)\\
&\quad=-\Psi\left(\mathbf{q}_1,\ldots,\mathbf{q}_i,\ldots,\mathbf{q}_j,\ldots,\mathbf{q}_N\right).
\end{aligned}\tag{A.8}$$

where $\sqrt{N!}$ is included to ensure normalization of the wave function. The antisymmetrizer operator has several interesting properties[1]:

- **Idempotent:**

  The square of the operator is itself, i.e. $\mathcal{A}^2=\mathcal{A}$.

  Proof:

$$\mathcal{A}\mathcal{A}=\left(\frac{1}{N!}\right)^2\sum_P\sum_Q(-1)^{P_n+Q_n}\mathcal{P}\mathcal{Q}\tag{A.9}$$

  For a given $\mathcal{P}$, the product $\mathcal{R}=\mathcal{P}\mathcal{Q}$ runs over all $N!$ permutations, so that

$$\mathcal{A}\mathcal{A}=\left(\frac{1}{N!}\right)^2\sum_P\underbrace{\left[\sum_R(-1)^{R_n}\mathcal{R}\right]}_{N!\mathcal{A}}=\left(\frac{1}{N!}\right)^2N!^2\mathcal{A}=\mathcal{A}\tag{A.10}$$

- **Hermitian:**

  Antisymmetrizer is self-adjoint, i.e. $\mathcal{A}^\dagger=\mathcal{A}$.

  Proof:

  Permutations of identical particles are unitary, i.e. $\mathcal{P}^\dagger=\mathcal{P}^{-1}$. By taking the adjoint of $\mathcal{A}$, we obtain

$$\mathcal{A}^\dagger=\frac{1}{N!}\sum_{P^\dagger}(-1)^{P_n}\mathcal{P}^\dagger=\frac{1}{N!}\sum_{P^{-1}}(-1)^{P_n}\mathcal{P}^{-1}\tag{A.11}$$

  Now, $\mathcal{P}$ and $\mathcal{P}^{-1}$ perform the same operations, only in inverse order, and therefore will their parity be the same. This means that $\mathcal{A}$ and $\mathcal{A}^\dagger$ have the same action, so $\mathcal{A}=\mathcal{A}^\dagger$.

- **Commutation relation with $\mathcal{H}$:**

  The antisymmetrizer commutes with the Hamiltonian, i.e. $[\mathcal{A},\mathcal{H}]=0$

  Proof: Since $\mathcal{H}$ is symmetric in the system coordinates, it will commute with each individual permutation, and therefore also with sums of such permutations. So $[\mathcal{A},\mathcal{H}]=0$.

[1] The proofs are based on the discussion in Chapter 7 in Ref. [63].

A.3 Discrete Fourier Transform

The discrete Fourier transform y of a signal x of length N is defined as [64]:

$$y_k = \sum_{n=0}^{N-1} x_n e^{-i2\pi\, k\, n/N}, \quad k = 0, 1, 2, \ldots, N-1. \tag{A.12}$$

By assuming that the data in vector x are separated by a constant interval Δt in time, we can define the sampling frequency as $f_s = 1/\Delta t$. The discrete Fourier transform y is complex-valued, and the absolute value of it at index k measures the amount of the frequency $f = k(f_s/N)$ present in the data. The resolution of the frequencies in the spectrum is given by

$$\Delta f = \frac{f_s}{N} = \frac{1}{N\Delta t}, \tag{A.13}$$

indicating that better frequency resolutions can be obtained either by more sample data (higher N) or larger time step.

A.3.1 Leakage

The computation of the discrete Fourier transform assumes that a signal x is periodic in the sampling period. If this assumption is violated, the frequency spectrum will suffer from leakage [65]. This effect will result in the signal energy smearing out over a wide range of frequency range in cases where it should be a narrow frequency range. To illustrate this effect we consider the frequency spectrum of a cosine signal:

$$x(t) = \cos(2\pi \cdot 2t), \tag{A.14}$$

which has an integer number of periods within the time window $[0, 6\text{s}]$. The frequency spectrum of this signal (Figure A.1), has only one spike at $f = 2$ Hz, which is the frequency of the cosine signal. However, if the signal instead is

$$x(t) = \cos(2\pi \cdot 2.2t), \tag{A.15}$$

which is not periodic within the time window, we see from the upper part of Figure A.2 that the frequency spectrum contains more than one spike, with the highest one at $f = 2.33$ Hz. This is the case even though the signal is a single cosine function with frequency $f = 2.2$ Hz. This effect is called leaking, and makes it difficult to identify the frequency content of the measured signal.

The leakage in the frequency spectrum is usually reduced by applying windowing [65]. That is, by multiplying the original signal with a window function before taking the Fourier transform of the signal. The window functions are typically chosen so that the resulting signal starts at zero at the beginning of the time window and then rises to some maximum and decays again to zero before the end of the time window. The resulting signal will then satisfy the periodicity requirement. There are a lot of different window functions available for spectral analysis, suitability for different applications (see Ref. [66]). We will focus on one of the most common window functions, namely the Hanning window function, defined as [64]:

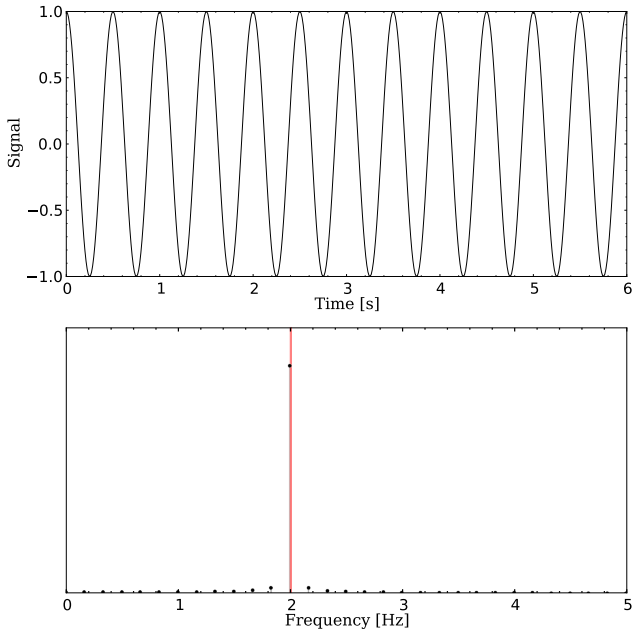

Figure A.1: Periodic cosine signal and its frequency spectrum. The signal is sampled at $N = 512$ points. Within the sampling period $t = [0, 6\text{s}]$, the signal has an integer number of periods, giving raise to only one spike in the frequency spectrum. This spike overlaps completely with the correct frequency (red line) of the signal.

$$w(t) = 0.5 \left(1 - \cos\left(\frac{2\pi t}{N-1}\right)\right). \tag{A.16}$$

By multiplying the signal in Eq. (A.15) with this function, the resulting signal will have the same character as the one described above; zero at the beginning and the end of the time window, with a maximum in the middle (see Figure A.2). Taking the discrete Fourier transform of this new signal will result in a much more narrow frequency range. This makes it easier to identify the frequency content of the measured signal.

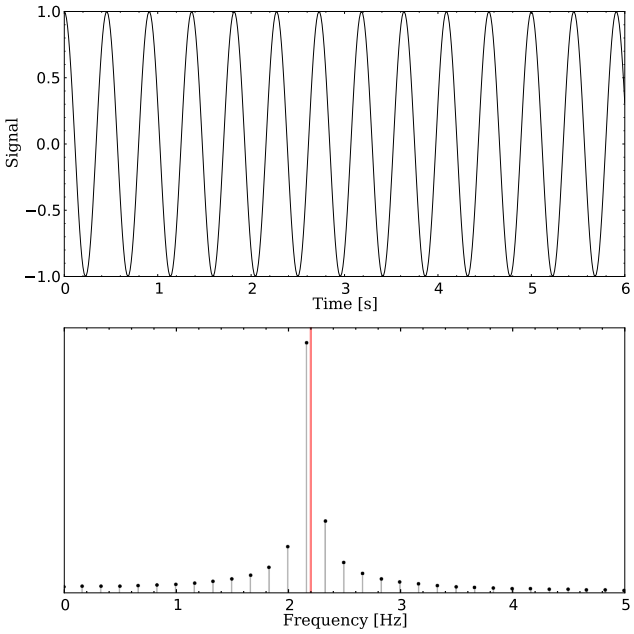

(a) Non periodic signal

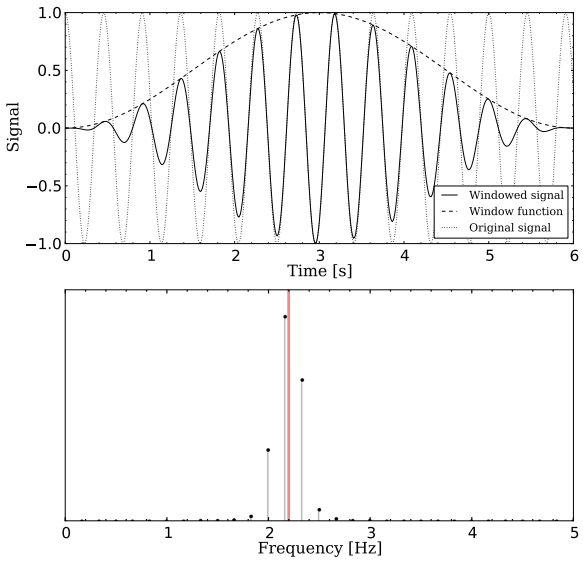

(b) Windowed signal

Figure A.2: Comparison of the non periodic (within the time window) cosine signal and frequency spectrum with leakage (a) to the windowed cosine signal and frequency spectrum showing much less leakage (b). The red lines indicate the correct frequency of the cosine function. The signal is sampled at $N = 512$ points.

Appendix B

Visualization

B.1 `cubeViz`

By solving the Hartree-Fock equation for an atomic or molecular system we find an ansatz for the total wave function. From the wave function we can compute the electron density, which gives the probability of finding an electron at a specific location. This quantity is a key concept for structure and reactivity studies. It is also the fundamental variable of density functional theory.

In order to visualize the electron density obtained from the Hartree-Fock calculations, a script named `cubeViz`[1] is written in the programming language Python. This script provides different opportunities for visualization of volumetric data such as iso-surface representation with surfaces, wireframes or points, plane view of cut planes on volumetric data, and representation based on volume rendering (see Figures B.1 and B.2). `cubeViz` is also capable of making animations of a set of dataset for different configurations of atoms, including the movement of the nuclei.

`cubeViz` is based on the Python library Mayavi [67], which is a data visualizer for interactive scientific data visualization and 3D plotting in Python. For plotting nuclei, the function `points3d()` is used, which plots glyphs at the position of supplied data. The contour plots are created using the function `contour3d()`, which takes a three-dimensional array as input and plots iso-surfaces based on the supplied data. The volume plots are created using volume rendering, based on the example in [68]. The slicer plots are created by inspiration from the example in [69].

The input files read by `cubeViz` are binary files with the extension `.cube` and consist of a header followed by the volumetric data. The header consists of the number of atoms, their type, charge and position, the position of the origin of the volumetric data, number of points in x, y and z direction and finally the limits in each Cartesian direction. The volumetric data is represented with a floating point number (value of the density function) for each volumetric element, that is for each grid point.

We will now show how the `.cube` files can be generated in C++ . The first step is to create an `ofstream` object for the output file:

[1] The source code can be found at https://github.com/miladh/cubeViz.

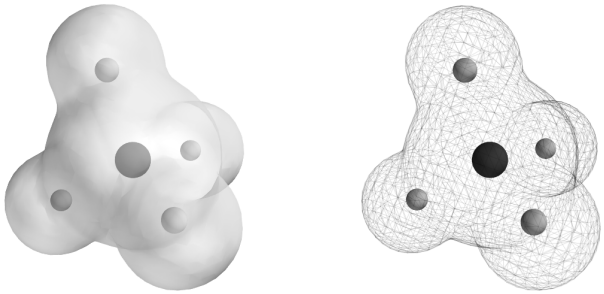

(a) Surface **(b)** Wireframe

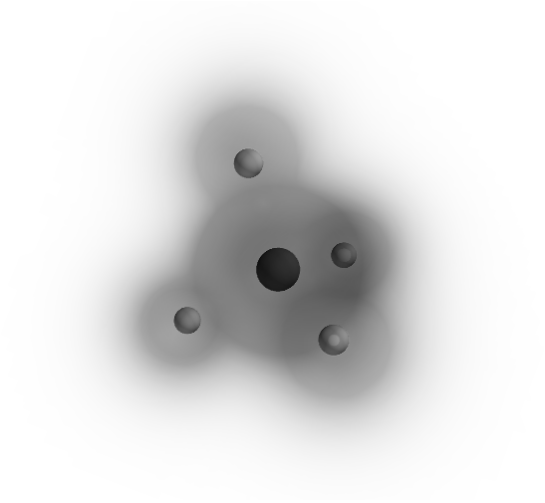

(c) Volume

Figure B.1: Different representations of the electron density for CH_4. The largest sphere (black) is the carbon nucleus, while the small spheres (gray) are the hydrogen nuclei.

```
stringstream filename << "output.cube";
ofstream cubefile(filename.str(), ios::out | ios::binary);
```

where the second line specifies that the file is open for writing and the operations are performed in binary mode. In order to write to this file one can use

```
double numCores = 2;
cubefile.write(reinterpret_cast<const char*>(&numCores), sizeof(double));
```

where the number of cores is written to file. Note that the variable `numCores` is a `double`. The other header parameters can be written to file in the same manner, in the following order:

- Origin of the data in x-, y-, and z-direction.

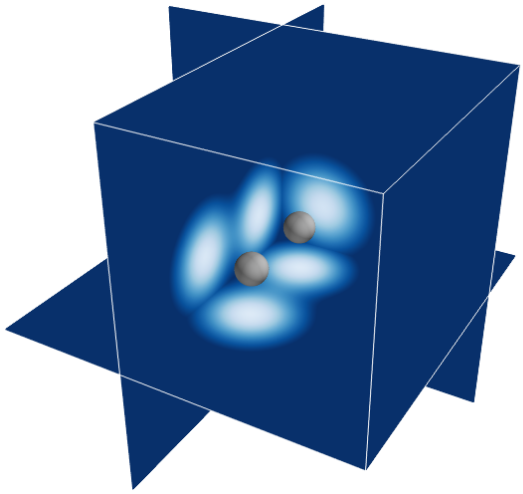

Figure B.2: Representation of electron density for H_2 with moveable slicer in each direction.

- Number of grid points in x-, y-, and z-direction.
- Value of the first and the last grid point in x-direction.
- Number of grid points in x-direction.
- Value of the first and the last grid point in y-direction.
- Number of grid points in y-direction.
- Value of the first and the last grid point in z-direction.
- Number of grid points in z-direction.
- For each atom: atom type, atom charge, and their position coordinates in x, y, and z-direction.

When the density data are stored in an Armadillo `cube` object, the data can be written to file in the following way:

```
for(uint k = 0; k < numZpoints; k++){
  for(uint i = 0; i < numXpoints; i++){
    for(uint j = 0; j < numYpoints; j++){

        cubeFile.write(reinterpret_cast<const char*>(&densitydata(i,j,k)),
          sizeof(double));
    }
  }
}
```

Note the order in which the data is written to the file on.

B.2 Supplementary Data for Graphical Models

The atomic configurations and basis sets used in graphical model calculations are listed in the tables below. Most of these atomic configurations are taken from Refs. [70] and [71].

Table B.1: Atomic configuration and basis set used in graphical model calculations of methyl anion. The atomic coordinates are given in atomic units.

Atom	Basis set	x	y	z
C	STO-3G	0.0	0.0	0.0
H	STO-3G	-1.74	0.85	0.66
H	STO-3G	1.55	1.18	-0.62
H	STO-3G	0.19	-2.04	-0.04

Table B.2: Atomic configuration and basis set used in graphical model calculations of ammonia. The atomic coordinates are given in atomic units.

Atom	Basis set	x	y	z
N	STO-3G	0.0	0.0	0.0
H	STO-3G	-1.77	0.0	0.72
H	STO-3G	0.89	1.53	0.72
H	STO-3G	0.89	-1.53	0.72

Table B.3: Atomic configuration and basis set used in graphical model calculations of Hydronium cation. The atomic coordinates are given in atomic units.

Atom	Basis set	x	y	z
O	STO-3G	0.0	0.0	0.12
H	STO-3G	0.0	1.76	-0.32
H	STO-3G	1.52	-0.88	-0.32
H	STO-3G	-1.52	-0.88	-0.32

Table B.4: Atomic configuration and basis set used in graphical model calculations of dibroane molecule. The atomic coordinates are given in atomic units.

Atom	Basis set	x	y	z
B	STO-3G	-3.17	0.0	0.0
B	STO-3G	3.17	0.0	0.0
H	STO-3G	-5.22	3.70	0.0
H	STO-3G	-5.22	-3.70	0.0
H	STO-3G	0.0	0.0	3.46
H	STO-3G	0.0	0.0	3.46
H	STO-3G	5.22	3.703	0.0
H	STO-3G	5.22	-3.703	0.0

Table B.5: Atomic configuration and basis set used in graphical model calculations of benzene. The atomic coordinates are given in atomic units.

Atom	Basis set	x	y	z
C	STO-3G	0.0	2.64	0.0
C	STO-3G	2.28	1.32	0.0
C	STO-3G	2.28	-1.32	0.0
C	STO-3G	0.0	-2.64	0.0
C	STO-3G	-2.28	-1.32	0.0
C	STO-3G	-2.28	1.32	0.0
H	STO-3G	0.0	4.68	0.0
H	STO-3G	4.06	2.34	0.0
H	STO-3G	4.06	-2.34	0.0
H	STO-3G	0.0	-4.68	0.06
H	STO-3G	-4.06	-2.34	0.0
H	STO-3G	-4.06	2.34	0.0

Table B.6: Atomic configuration and basis set used in graphical model calculations of pyridine. The atomic coordinates are given in atomic units.

Atom	Basis set	x	y	z
C	STO-3G	0.00	2.16	1.36
C	STO-3G	0.00	2.26	-1.27
C	STO-3G	0.00	0.00	-2.61
C	STO-3G	0.00	-2.26	-1.27
C	STO-3G	0.00	-2.16	1.36
N	STO-3G	0.00	0.00	2.68
H	STO-3G	0.00	0.00	-4.66
H	STO-3G	0.00	3.89	2.47
H	STO-3G	0.00	4.07	-2.23
H	STO-3G	0.00	-4.07	-2.23
H	STO-3G	0.00	-3.89	2.47

Glossary

3-21G

A split-valence Gaussian basis set. 54, 55, 58

4-31G

A split-valence Gaussian basis set. 142, 144–146, 148–150

6-31G

A split-valence Gaussian basis set. 159, 160, 163

6-31G*

A split-valence Gaussian basis set with polarization functions. 56, 142, 145, 146, 148–150

6-31G**

A split-valence Gaussian basis set with polarization functions. 56, 142, 144, 146, 148, 150, 152, 159, 160, 163, 165

ab initio MD

Molecular dynamics simulations where the forces acting on the nuclei are computed on-the-fly as the molecular dynamics trajectory is generated. 3, 4, 9, 81, 86, 91, 96, 124, 133, 177, 178

AO

Atomic orbital. A mathematical function describing the wave-like behavior of either one or pair of electrons in an atom. 14–16, 18, 44–47, 52–55, 57, 58

Armadillo

An open source C++ linear algebra library. 106, 107, 116, 120, 122, 123, 189

atomic units

A system of natural units, suitable in atomic physics calculations. 49, 181, 190–192

BOMD

Born-Oppenheimer molecular dynamics. An ab initio molecular dynamics method. 87–92, 133, 135–137, 159–166, 178

Boost

A set of libraries for the C++ programming language. 122, 123

Born-Oppenheimer approximation

Born-Oppenheimer approximation. An approximation in quantum many-body calculations, where the electronic motion and the nuclear motion in molecules are separated. 3, 13, 14, 44, 88

Boys function

Also known as the Incomplete Gamma Function. Used in calculations of Coulomb integrals. 59, 67–75, 111, 119, 122

C++

An object-oriented programming language. 4, 93, 103, 106–108, 111, 133, 187

CGTO

Contracted Gaussian-type orbital. Linear combination of primitive Gaussian-type orbitals. 52–55, 57, 58, 77, 112, 124, 125

class

A collection of variables and functions. 103–105

classical MD

Molecular dynamics simulations based on a predefined interaction potential. 3, 4, 81, 84, 86, 96

ClayFF

A force field for molecular dynamics simulations. 96–99

CPMD

Car-Parrinello molecular dynamics. An ab initio molecular dynamics method. 87, 91–93, 159, 160, 162, 163, 165, 178

density functional theory

A quantum many-body method where the main idea is to describe an interacting system via its electron density, instead of the wave function of the system. 160, 165, 178, 187

Ehrenfest MD

An ab initio molecular dynamics method. 86–91

Git

An open source version control software. 105

GTO

Gaussian-type orbital. Mathematical functions used as atomic orbitals in the linear combination of atomic orbitals method. 50–53

Hartree-Fock

Hartree-Fock. A quantum many-body method where the wave function of an N-body system is approximated by a single Slater determinant. 3–5, 7, 9, 10, 15, 24, 29–32, 35, 37, 39, 40, 43, 52, 90, 92, 94, 111, 113, 122–124, 126, 127, 129–131, 133, 135, 136, 141–144, 146, 150, 152, 153, 159, 160, 162, 163, 165, 177, 178, 187

HDF5

A library and file format for storing and organizing large amounts of numerical data. 108, 137

Hermite coefficient

Expansion coefficients of Hermite polynomials. These are used in calculations of molecular integrals. 64–67, 76, 111, 115, 116, 118, 129

Hermite integral

Set of integrals used in calculations of Coulomb integrals. 65, 73, 111, 118–120, 129

HF limit

Hartree-Fock limit. The limit of the Hartree–Fock energy as the basis set approaches completeness. 43, 44, 142–146, 149, 150, 169

IDE

Integrated development environment. Programming environment, packaged as an application program. 106

inheritance

When an class (subclass) is based on another class (superclass). 104

IPython Notebook

A web-based interactive computational environment where code execution, text, mathematics, plots and rich media can be combined into a single document [30]. 107, 111, 133

IPython Notebook Viewer

A webservice that makes it possible to share static HTML versions of publicly available notebook files. 107

LCAO

Linear combination of atomic orbitals. A technique for calculating molecular orbitals. 15, 35, 45, 93, 147, 149

library

A collection of precompiled routines, exposed for use by other programs. 123, 124, 135, 177

MD

Molecular dynamics. A computer simulation technique of complex systems, modeled at atomic level, in which the time evolution of the system is followed using numerical integration of the equations of motion. 3–5, 9, 81, 84, 86–91, 96, 124, 133–135, 159, 177, 178, 193, 194

MO

Molecular orbital. A mathematical function describing the wave-like behavior of either one or pair of electrons in a molecule. 14–18, 21, 35–37, 45, 46, 54, 55, 59, 112, 113, 147, 151

object

An instance of a class. 104, 105

PES

Potential energy surface. A multidimensional surface that gives the energy of a molecule as a function of its geometry. 13, 97, 98

Pople-Nesbet equation

Representation of unrestricted Hartree-Fock equations in a non-orthonormal basis. 41, 113

primitive GTO

Primitive Gaussian-type orbital. Single Gaussian function used in Contracted Gaussian-type orbitals. 52–54, 77, 78, 103, 122, 124–126, 128

Python

A widely used object-oriented, high-level programming language. 4, 103, 107, 108, 126, 128, 129, 187

Qt Creator

A cross-platform integrated development environment. 106, 111, 124, 133, 136

RHF

Restricted Hartree-Fock. A variant of Hartree-Fock method where the molecular orbitals are doubly occupied. 9, 32, 105, 114, 150–153, 159, 162

Roothaan equation

Representation of restricted Hartree-Fock equation in a non-orthonormal basis. 36, 40, 111

SCF

Self-Consistent Field. See Hartree-Fock. 20, 24, 29, 37, 44, 46, 50–53, 66, 111, 112, 114, 115, 122, 126

Slater determinant

An antisymmetric wave function. 21–24, 27, 29, 30, 43, 90, 143

STO

Slater-type orbital. Mathematical functions used as atomic orbitals in the linear combination of atomic orbitals method. 48–55, 57, 112

STO-3G

A minimal Gaussian basis set. 53, 55, 57, 142–146, 148–150, 159, 160, 163, 166, 169, 170, 190–192

SymPy

A Python library for symbolic math. 107, 126, 127

UHF

Unrestricted Hartree-Fock. A variant of Hartree-Fock method where different molecular orbitals are used for different spins. 9, 32, 114, 150, 166, 169

unit testing

The practice of testing the smallest testable parts of an application individually and independently to determine if they behave exactly as expected. 108, 109, 177

UnitTest++

A unit testing framework for C++. 109, 110, 127

variational principle

States that the ground state energy is always less than or equal to the expectation value of the Hamiltonian calculated with some trail wave function. 11, 12

Velocity Verlet

A numerical method used to integrate Newton's equations of motion. 133, 134

virtual function

A function that can be redefined in derived class. 105, 115

Bibliography

[1] S.-A. Dragly. "Bridging Quantum Mechanics and Molecular Dynamics with Artifical Neural Networks". MA thesis. University of Oslo, In preparation, 2014.

[2] H. M. Eiding. "Ab Initio Studies of Molecules". MA thesis. University of Oslo, In preparation, 2014.

[3] B. Rizzuti and V. Daggett. "Using simulations to provide the framework for experimental protein folding studies". In: *Archives of Biochemistry and Biophysics* 531. (2013). Protein Folding and Stability, 128. DOI: 10.1016/j.abb.2012.12.015.

[4] S. Reddy and V. K. Kuppa. "Molecular dynamics simulations of organic photovoltaic materials: Investigating the formation of -stacked thiophene clusters in oligothiophene/fullerene blends". In: *Synthetic Metals* 162. (2012), 2117. DOI: 10.1016/j.synthmet.2012.09.020.

[5] D. Marx and J. Hutter. *Ab Initio Molecular Dynamics: Basic Theory and Advanced Methods*. Cambridge University Press, 2009.

[6] A. Szabo and N. Ostlund. *Modern Quantum Chemistry: Introduction to Advanced Electronic Structure Theory*. Dover Books on Chemistry Series. Dover Publications, 1996.

[7] T. Helgaker, P. Jørgensen, and J. Olsen. *Molecular electronic-structure theory*. Wiley, 2000.

[8] J. Høgberget. "Quantum Monte-Carlo Studies of Generalized Many-body Systems". MA thesis. University of Oslo, 2013. http://urn.nb.no/URN:NBN:no-38645.

[9] R. Shankar. *Principles of Quantum Mechanics*. Springer, 1994.

[10] C. Cramer. *Essentials of Computational Chemistry: Theories and Models*. Wiley, 2005.

[11] J. Thijssen. *Computational Physics*. Cambridge University Press, 2007.

[12] D. Griffiths. *Introduction to Quantum Mechanics*. 2nd Edition. Pearson, 2005.

[13] M. Hjorth-Jensen. *Computational Physics*. University of Oslo, 2011. http://www.uio.no/studier/emner/matnat/fys/FYS3150.

[14] D. Yarkony. *Modern Electronic Structure Theory*. Advanced series in physical chemistry poeng 1. World Scientific, 1995.

[15] M. Griebel, S. Knapek, and G. Zumbusch. *Numerical Simulation in Molecular Dynamics: Numerics, Algorithms, Parallelization, Applications*. Texts in Computational Science and Engineering. Springer, 2007.

[16] D. Marx and J. Hutter. "Ab initio molecular dynamics: Theory and implementation". In: *Modern methods and algorithms of quantum chemistry, John Von Neumann institute for computing, Forschungszentrum Julich, 2000*. 2000, 329.

[17] J. J. Sakurai. *Modern Quantum Mechanics*. Revised. Reading, MA: Addison-Wesley Publishing Company, 1994.

[18] J. Steinfeld. *Molecules and Radiation: An Introduction to Modern Molecular Spectroscopy. Second Edition*. Dover Books on Chemistry. Dover Publications, 2012.

[19] J. Taylor. *Classical Mechanics*. University Science Books, 2005.

[20] J. E. Jones. "On the Determination of Molecular Fields. II. From the Equation of State of a Gas". In: *Proceedings of the Royal Society of London. Series A* 106. (1924), 463. DOI: 10.1098/rspa.1924.0082. http://rspa.royalsocietypublishing.org/content/106/738/463.short.

[21] F. H. Stillinger and T. A. Weber. "Computer simulation of local order in condensed phases of silicon". In: *Physical Review B* 31 (1985), 5262. DOI: 10.1103/PhysRevB.31.5262.

[22] J. Tersoff. "New empirical approach for the structure and energy of covalent systems". In: *Physical Review B* 37 (1988), 6991. DOI: 10.1103/PhysRevB.37.6991.

[23] A. C. T. van Duin, S. Dasgupta, F. Lorant, and W. A. Goddard. "ReaxFF: A Reactive Force Field for Hydrocarbons". In: *The Journal of Physical Chemistry A* 105. (2001), 9396. DOI: 10.1021/jp004368u.

[24] R. T. Cygan, J.-J. Liang, and A. G. Kalinichev. "Molecular Models of Hydroxide, Oxyhydroxide, and Clay Phases and the Development of a General Force Field". In: *The Journal of Physical Chemistry B* 108. (2004), 1255. DOI: 10.1021/jp0363287.

[25] D. Yevick. *A First Course in Computational Physics and Object-Oriented Programming with C++ Hardback with CD-ROM*. A First Course in Computational Physics and Object-oriented Programming with C++. Cambridge University Press, 2005.

[26] Git. *Documentation*. 2014. http://git-scm.com/doc.

[27] Qt Project. *Qt Creator Manual*. 2014. http://qt-project.org/doc/qtcreator-2.8/.

[28] Qt Project. *Qt Creator*. 2014. http://qt-project.org/wiki/category:tools::qtcreator.

[29] Armadillo. *API Reference for Armadillo 4.300*. 2014. http://arma.sourceforge.net/docs.html.

[30] IPython: Interactive Computing, *The IPython Notebook*. 2014. http://ipython.org/notebook.html.

[31] IPython: Interactive Computing, *Documentation: The IPython Notebook*. 2014. http://ipython.org/ipython-doc/stable/notebook/notebook.html.

[32] *nbviewer: A simple way to share IPython Notebooks*. 2014. http://nbviewer.ipython.org/.

[33] SymPy Development Team, *Welcome to SymPy's documentation!* 2014. http://docs.sympy.org/latest/index.html.

[34] The HDF Group, *HDF5 Software Documentation*. 2014. http://www.hdfgroup.org/HDF5/doc/index.html.

[35] Andrew Collette and contributors, *HDF5 for Python*. 2014. http://docs.h5py.org/en/latest/.

[36] N. Llopis and C. Nicholson. *UnitTest++ in brief*. 2014. http://unittest-cpp.sourceforge.net/UnitTest++.html.

[37] D. Gregor and M. Troyer. *Chapter 20. Boost.MPI*. 2014. http://www.boost.org/doc/libs/1_55_0/doc/html/mpi.html.

[38] Basis Set Exchange. *Basis Set Exchange*. 2014. https://bse.pnl.gov/bse/portal.

[39] K. L. Schuchardt, B. T. Didier, T. Elsethagen, L. Sun, V. Gurumoorthi, J. Chase, J. Li, and T. L. Windus. "Basis Set Exchange: A Community Database for Computational Sciences". In: *Journal of Chemical Information and Modeling* 47. (2007). PMID: 17428029, 1045. DOI: 10.1021/ci600510j.

[40] P. W. Atkins and R. Friedman. *Molecular Quantum Mechanics*.

[41] P. Hariharan and J. Pople. "The influence of polarization functions on molecular orbital hydrogenation energies". In: *Theoretica chimica acta* 28. (1973), 213. DOI: 10.1007/BF00533485.

[42] J. M. Schulman and D. N. Kaufman. "Application of Many-Body Perturbation Theory to the Hydrogen Molecule". In: *The Journal of Chemical Physics* 53. (1970), 477. DOI: 10.1063/1.1674013.

[43] P. E. Cade, K. D. Sales, and A. C. Wahl. "Electronic Structure of Diatomic Molecules. III. A. Hartree—Fock Wavefunctions and Energy Quantities for $N_2(X^1\Sigma g^+)$ and $N_2^+(X^2\Sigma g^+, A^2\prod_u, B^2\Sigma_u^+)$ Molecular Ions". In: *The Journal of Chemical Physics* 44. (1966), 1973. DOI: 10.1063/1.1726972.

[44] W. C. Ermler and A. D. McLean. "The effects of basis set quality and configuration mixing in abinitio calculations of the ionization potentials of the nitrogen molecule". In: *The Journal of Chemical Physics* 73. (1980), 2297. DOI: 10.1063/1.440379.

[45] W. Meyer. “PNO–CI Studies of electron correlation effects. I. Configuration expansion by means of nonorthogonal orbitals, and application to the ground state and ionized states of methane”. In: *The Journal of Chemical Physics* 58. (1973), 1017. DOI: 10.1063/1.1679283.

[46] A. Rauk, L. C. Allen, and E. Clementi. “Electronic Structure and Inversion Barrier of Ammonia”. In: *The Journal of Chemical Physics* 52. (1970), 4133. DOI: 10.1063/1.1673621.

[47] B. J. Rosenberg and I. Shavitt. “Ab initio SCF and CI studies on the ground state of the water molecule. I. Comparison of CGTO and STO basis sets near the Hartree–Fock limit”. In: *The Journal of Chemical Physics* 63. (1975), 2162. DOI: 10.1063/1.431596.

[48] P. E. Cade and W. M. Huo. “Electronic Structure of Diatomic Molecules. VI.A. Hartree—Fock Wavefunctions and Energy Quantities for the Ground States of the First-Row Hydrides, AH”. In: *The Journal of Chemical Physics* 47. (1967), 614. DOI: 10.1063/1.1711938.

[49] M. Yoshimine and A. D. Mclean. “Ground states of linear molecules: Dissociation energies and dipole moments in the hartree–fock approximation”. In: *International Journal of Quantum Chemistry* 1. (1967), 313. DOI: 10.1002/qua.560010637.

[50] A. Rauk, L. C. Allen, and E. Clementi. “Electronic Structure and Inversion Barrier of Ammonia”. In: *The Journal of Chemical Physics* 52. (1970), 4133. DOI: 10.1063/1.1673621.

[51] P. E. Cade and W. M. Huo. “Electric Dipole Moment for First- and Second-Row Diatomic Hydride Molecules, AH”. In: *The Journal of Chemical Physics* 45. (1966), 1063. DOI: 10.1063/1.1727659.

[52] J. S. Sims and S. A. Hagstrom. “High precision variational calculations for the Born-Oppenheimer energies of the ground state of the hydrogen molecule”. In: *The Journal of Chemical Physics* 124., 094101 (2006), DOI: 10.1063/1.2173250.

[53] W. Hehre. *A Guide to Molecular Mechanics and Quantum Chemical Calculations*. Wavefunction, 2003.

[54] V. Wathelet, B. Champagne, D. H. Mosley, J. André, and S. Massidda. “Vibrational frequencies of diatomic molecules from Car and Parrinello molecular dynamics”. In: *Chemical Physics Letters* 275. (1997), 506. DOI: 10.1016/S0009-2614(97)00753-7.

[55] W. Hehre, L. Radom, P. Schleyer, and J. Pople. *Ab initio molecular orbital theory*. Wiley-interscience publication. Wiley, 1986.

[56] *SciPy, scipy.optimize.curve_fit*. 2013. http://docs.scipy.org/doc/scipy-0.13.0/reference/generated/scipy.optimize.curve_fit.html.

[57] G. Herzberg and K. Huber. *Molecular spectra and molecular structure*. Molecular Spectra and Molecular Structure v. 4. Van Nostrand, 1979.

[58] A. P. Scott and L. Radom. "Harmonic Vibrational Frequencies: An Evaluation of Hartree−Fock, Møller−Plesset, Quadratic Configuration Interaction, Density Functional Theory, and Semiempirical Scale Factors". In: *The Journal of Physical Chemistry* 100. (1996), 16502. DOI: 10.1021/jp960976r.

[59] F. Carey and R. Sundberg. *Advanced Organic Chemistry: Part B: Reaction and Synthesis*. Springer, 2007.

[60] C. Leforestier. "Classical trajectories using the full abinitio potential energy surface $H^- + CH_4 \rightarrow CH_4 + H^-$". In: *The Journal of Chemical Physics* 68. (1978), 4406.

[61] M. Swart and F. M. Bickelhaupt. "Benchmark Study on the Smallest Bimolecular Nucleophilic Substitution Reaction: $H^- + CH_4 \rightarrow CH_4 + H^-$". In: *Molecules* 18. (2013), 7726. DOI: 10.3390/molecules18077726.

[62] Shull, H. and Hall, G. G. "Atomic Units". In: *Nature* 184. (1959), 1559. DOI: 10.1038/1841559a0.

[63] F. Pilar. *Elementary quantum chemistry*. Schaum's outline series in science v. 1. McGraw-Hill, 1990.

[64] Ø. Ryan. *Linear algebra, signal processing, and wavelets. A unified approach*. University of Oslo, 2014.

[65] *APPLICATION NOTE AN014, Understanding FFT Windows*. 2014. http://www.physik.uni-wuerzburg.de/~praktiku/Anleitung/Fremde/ANO14.pdf.

[66] *Windowing: Optimizing FFTs Using Window Functions*. 2011. http://www.ni.com/white-paper/4844/en/.

[67] Mayavi. *Mayavi: 3D scientific data visualization and plotting in Python*. 2014. http://docs.enthought.com/mayavi/mayavi/.

[68] Mayavi. *Chemistry example*. 2014. http://docs.enthought.com/mayavi/mayavi/auto/example_chemistry.html#example-chemistry.

[69] Mayavi. *Volume slicer example*. 2014. http://docs.enthought.com/mayavi/mayavi/auto/example_volume_slicer.html.

[70] *PubChem*. 2014. http://pubchem.ncbi.nlm.nih.gov/.

[71] *NIST Chemistry WebBook*. 2014. http://webbook.nist.gov/chemistry/form-ser.html.